LONDON'S GLOBAL UNIVERSITY

UCL

Topical Ocular Delivery to Posterior Eye Tissues

A thesis submitted in partial fulfilment of the requirements for the degree of Doctor of Philosophy

At the

School of Pharmacy

University College London

Moutaz Yahya A Badr

April 2021

Supervisors:

Professor Ijeoma Uchegbu

Professor Andreas Schätzlein

Declaration

I, Moutaz Yahya A Badr confirm that the work presented in this thesis is my own. Where information has been derived from other sources, I confirm that this has been indicated in the thesis.

Moutaz Yahya A Badr

Date:

27 April 2021

Abstract

Treatment of diseases affecting the posterior segment of the eye with intravitreal injections of drugs are effective yet invasive and associated with side effects such as retinal detachment and endophthalmitis. Rapamycin (RAP) was explored in eye research for chronic inflammatory disorders such as posterior uveitis. Tacrolimus (TAC) suspension is used to treat moderate to severe atopic keratoconjunctivitis (AKC) and vernal keratoconjunctivitis (VKC). This study's objectives were to formulate the hydrophobic compounds: RAP and TAC in aqueous eye drop formulations, with the overall aim of using these formulations to treat posterior uveitis, AKC and VKC, respectively. A thin-film hydration method was used to encapsulate RAP and TAC within the chitosan-based amphiphile: N-palmitoyl-N-monomethyl-N,N-dimethyl-N,N,N-trimethyl-6-O-glycolchitosan (GCPQ). The formulations were characterised, and their stability studied under three storage conditions for one month. The biocompatibility of GCPQ was assessed by measuring the IC50 value in a standard MTT assay. Experimental autoimmune uveitis (EAU) was used as a mice model to explore how RAP would clinically function on retinal disease. The ocular biodistribution of the formulations was studied in healthy rabbits, and LC-MS/MS analysed the ocular tissues. Nanoparticles formulations (GCPQ: RAP, 0.2% w/v) and (GCPQ: TAC, 0.1% w/v) were produced with characteristics within the ocular comfort range. The formulations were stable on refrigeration for one month. GCPQ demonstrates good biocompatibility *in*

vitro with IC50 ranging from 0.44–4.5 mg/mL. On topical application *in vivo*, GCPQ delivered RAP to the rabbit choroid-retina one-hour post-dosing at concentration 145±49 ng/g of tissue. The topical application of GCPQ: RAP 0.2% w/v on EAU mice model suppressed the disease progression. The TAC concentrations in rabbit cornea and conjunctiva one-hour post-dosing were 4452±2289 and 516±180 ng/g of tissue, respectively. A topical ocular aqueous RAP and TAC eye drop formulations have been prepared with the ability to deliver sufficient drugs to the relevant ocular surface tissues.

Impact statement

Topical ocular drug delivery with eye drops is commonly used in the treatment of anterior segment disorders, such as allergic conjunctivitis. Severe allergic conjunctivitis, i.e., atopic and vernal keratoconjunctivitis, is a sight-threatening disease with no overall gold standard form of therapy. Patients with severe disease are treated with anti-allergy drugs and corticosteroids. Prolonged steroid use is associated with glaucoma and hence is not ideal. Therefore, the development of alternate medications to improve patient compliance and avoid the side effects of current treatment is necessary. Tacrolimus ointment has been shown to be effective for patients with severe ocular allergic conditions. However, ointment dosage form to the eye is not well tolerated by many patients. Hence, a simple aqueous eye drops formulation of tacrolimus with sufficient eye exposure to cornea and conjunctiva would circumvent steroids' side effects and improve patients' compliance.

Efficient topical ocular drug delivery to the eye's posterior segment remains challenging due to the eye anatomical and physiological barriers. Posterior segment disorders, such as age-related macular degeneration and posterior uveitis, require immediate clinical intervention to prevent vision loss. Patients presenting with posterior eye diseases are offered injections into the eyeballs. These intravitreal injections are effective but invasive and associated with ocular complications, such as retinal detachment and increased intraocular pressure. Intravitreal injections are associated with a significant burden on the patient’s

psychological health as well. Treatment-related anxiety is shared among the patients before the injection. Other considerations include; the financial and travel issues associated with the treatment. Therefore, developing non-invasive topical eye drops would overcome most of these problems and enhance patient compliance.

We used a known non-irritant, mucoadhesive, ocular penetration enhancer -N-palmitoyl-N-monomethyl-N,N-dimethyl-N,N,N-trimethyl-6-O-glycolchitosan to formulate the hydrophobic drugs, i.e., tacrolimus and rapamycin within positively charged amphiphiles. This nanotechnology-based project seeks to uncover a new drug delivery approach in a bid to target varied conditions such as allergic conjunctivitis and posterior uveitis. We demonstrated the delivery of two novel eye drops formulations containing tacrolimus and rapamycin to the anterior and posterior segment of the eye upon single instillation to healthy rabbits, respectively. Experimental autoimmune uveitis is being used as a mice model to study the pre-clinical impact of GCPQ: RAP formulation. GCPQ: RAP as an aqueous-based eye drop formulation has been shown to suppress retinal inflammatory diseases. Thus, this formulation may be used in the future as an alternative to invasive intravitreal injection.

Acknowledgement

First and foremost, I would like to thank my supervisor, Prof. Ijeoma Uchegbu, for entrusting me with this project. Your knowledge and guidance are fundamental to the success of my PhD. Be it your encouragement, applause, or criticism, it all helped me strive towards achieving perfection in my research and helped me develop self-confidence. I would like to thank my second supervisor Prof. Andreas Schatzlein, whose keen analysis helped me in my critical thinking. I thank my supervisors for their tremendous support during my time at the group, and during the Covid-19 pandemic. I could not have completed the project if not for such support.

I want to thank my sponsor Umm Al-Qura University – College of Pharmacy and the Saudi Arabia Cultural Bureau in London for supporting my scholarship.

I am also very grateful to my colleagues in Lab 326 and 105, past and present. Dr Abdulrahman, Dr Uchechukwu, Dr Rui, Dr Asya, Dr Gang, Dr Alex, Dr Manuel, Dr David, Dr Xian, Ryan, Akunnaya, Liisa, all other lab members, thank you all for being a great community of friends and scientists. I am also grateful to the Master students whom I supervised: Sonali, Ali, Louis, and Nurul, for helping out on some of the projects in this work.

I would also like to thank: Mark Neal, Steve Coppard, and all the staff at the Animal Unit in the Royal Free Hospital; thank you for your support and assistance. I want to express my sincere appreciation to Dr Virginia L. Calder and Dr Malihe

Eskandarpour from UCL Institute of Ophthalmology to contribute to the pharmacodynamic work in this project.

To:

My father Yahya Badr (1955 – 2010)

My mother Kawakeb Derar (1960 – 2014)

My brother Captain Pilot: Ehab Badr

My brother Captain Pilot: Hassan Badr

All my family.

Dedicated to:

My wife – the one and only – Chef Turkan Sharawi

My son – the firefighter – Mohammed M. Badr.

Table of contents

List of Figures

List of Tables

List of Abbreviations

^{1}H-NMR	Proton NMR
MTT	3-(4,5-Dimethyl-2-thiazolyl)-2,5-diphenyl-2H-tetrazolium bromide
HEPES	(4-(2-hydroxyethyl)-1-piperazineethanesulfonic acid)
COSY	^{1}H-^{1}H Correlated Spectroscopy
ACN	Acetonitrile
AMD	Age related macular degeneration
ANOVA	Analysis of variance
AP	Apical
Papp	Apparent permeability coefficient
AUC	Area under the curve
ASC	Ascomycin
AKC	Atopic keratoconjunctivitis
BL	Basolateral
BAB	Blood-aqueous barrier
BRB	Blood-retinal barrier
MCF-7	Breast cancer epithelial cell line
δ	Chemical shifts
CV	Coefficient of variation
Caco-2	Colon adenocarcinoma cell line
CI	Confidence interval
CMC	Critical micelle concentration
CDs	Cyclodextrins
Da	Dalton
dGC	degraded GC
DP	Degree of palmitoylation

DQ	Degree of quaternisation
MeOD	Deuterated methanol
D_2O	Deuterium oxide
DEX	Dexamethasone
DME	Diabetic macular oedema
DR	Diabetic retinopathy
dRI	Differential refractive index
DMSO	Dimethyl sulfoxide
DL	Drug loading
DPBS	Dulbecco's phosphate buffered saline
DLS	Dynamic light scattering
ESI	Electrospray ionisation
EE	Encapsulation efficiency
MDA-MB-231	Epithelial human breast cancer cell line
EAU	Experimental autoimmune uveitis
FD-4	FITC dextran 4 kDa
FKBP12	FK binding protein
FACS	Fluorescence-activated cell sorting
FDA	Food and drug administration
FA	Formic acid
GPC-MALLS	Gel Permeation Chromatography with Multi-Angle Laser Light Scattering
GC	Glycol Chitosan
HBSS	Hank's balanced salt solution
HPLC	High performance liquid chromatography
HPH	High pressure homogenisation
HK	Human keratocyte cell line
HLA	Human leukocyte antigen

ARPE-19	Human retinal pigmented epithelial cell line
Y79	Human retinoblastoma cell line
HA	Hyaluronic acid
HCL	Hydrochloric acid
C0	Initial donor concentration
IFN	Interferon
IL	Interleukin
IS	Internal standard
ICH	International Conference on Harmonisation
IRBP	Interphotoreceptor retinoid-binding protein
Ivitr	Intravitreal injection
IV	Intravenous
kDa	Kilo Daltons
LOD	limit of detection
LOQ	Limit of quantification
LCMS	Liquid chromatography–mass spectrometry
LLOQ	Lower limit of quantification
MDCK	Madin-Darby Canine Kidney cell line
mTOR	Mammalian target of rapamycin
MeOH	Methanol
MEM	Minimum Essential Medium Eagle
MET	Molecular envelope technology
MWCO	Molecular weight cut off
MRM	Multiple reaction monitoring
NMP	N-methyl-2-pyrrolidone
GCPQ	N-palmitoyl-N-monomethyl-N, N-dimethyl-N, N, N-trimethyl-6-O-glycol-chitosan

NFAT	Nuclear factors of activated T-lymphocytes
NMR	Nuclear magnetic resonance
Mn	Number averaged molecular weight
Ω	Ohm
QD	Once a day
OChiPEG	O-octanoyl-chitosan-polyethylene glycol
PNS	Palmitic acid N-hydroxysuccinimide ester
pGC	palmitoylated GC
P-gp	Permeability glycoprotein
PTX	Pertussis toxin
PK	Pharmacokinetics
FBS	Fetal bovine serum
PBS	Phosphate buffer saline
PVA	Poly vinyl alcohol
PLGA	Poly(lactic-co-glycolic acid)
PDI	Polydispersity index
PEG	Polyethene glycol
PES	Polyethersulfone
PTFE	Polytetrafluoroethylene
QELS	Quasielastic light scattering
RAP	Rapamycin
QPR	Ratio of quaternary ammonium to palmitoyl groups
RI	Refractive index
ROR	Related orphan receptor
RH	Relative humidity
RT	Retention time
RPE	Retinal pigment epithelium

RP-HPLC	Reversed phase HPLC
SMEDDS	Self-emulsifying drug delivery system
SNR	Signal to noise ratio
SEC	Size exclusion chromatography
C10	Sodium caprate
NaOH	Sodium hydroxide
SNP	Solubilising nanoparticle technology
SD	Standard deviation
SE	Standard error
SIRC	Statens Seruminstitut Rabbit Cornea
STK	Stock solution
TAC	Tacrolimus
IC50	The half maximal inhibitory concentration
TID	Three times a day
TJ	Tight junction
TEER	Transepithelial electrical resistance
TEM	Transmission electron microscopy
TEA	Triethylamine
TMC	Trimethyl chitosan
BID	Two times a day
UV	Ultraviolet
UK	United Kingdom
USA	United States of America
VEGF	Vascular endothelial growth factor
VKC	Vernal keratoconjunctivitis
Mw	Weight averaged molecular weight
WS	Working standards

Stks	Working stocks solutions
XRD	X-ray diffraction
ZO	Zonula occludens

1. Introduction

The eyes are a unique organ in contrast to other parts of the central nervous system; the external eye is readily accessible for drug administration because it is located outside the cranium [1]. Conditions that affect the front of the eye may be treated with topical eye drops [2]. However, back of the eye diseases are commonly treated as an entirely separate ocular region, and advanced delivery systems have been designed for the back of the eye [2].

The eyes are one of the most critical and complex sensory organs; they act as a gateway to collect external images and transmit them to the brain as signals through the optic nerve [3]. As a result, mechanisms exist for the clearance of foreign materials from the cornea to maintain visual acuity. These clearance mechanisms create difficulties in the development of formulations for ophthalmic therapy [4]. Three factors may have to be considered when attempting drug delivery to the eyes; how the blood-eye barrier (systemic to ocular) or cornea (external to ocular) is crossed to reach the site of action, how to localise the pharmacodynamic action at the eye and minimise drug action on other tissues, and how to prolong the duration of drug action such that the frequency of drug administration can be reduced [4].

The complexity surrounding the physiology and anatomy of the eyes renders them highly impervious to drugs and treatments [3]. The natural anatomical and physiological ocular barriers to drug bioavailability have an impact on the ocular pharmacokinetics [2]. The ocular bioavailability is poor after eye drop administration

(< 5 %); this could be attributed to a relatively short contact time of the drug (< 1 minute) [5] and rapid drug elimination from the eye [6]. Thus, higher drug dosing frequencies may be necessary; for example, pilocarpine eyedrops (1.0% w/v) are administered 3-6 times daily, which may increase the risk of ocular side effects [7]. The increased risk of systemic side effects following oral and systemic administration of a drug to treat targeted ocular tissues could limit the utility of these routes of administration which necessitate high dosage to observe significant therapeutic efficacy [4,8].

Conventionally, two significant segments govern the anatomy of the human eye; the anterior segment and the posterior segment [9]. Figure 1-1 shows the anterior segment consists of the cornea, conjunctiva, aqueous humour, iris, ciliary body and the lens, whereas the posterior segment comprises sclera, choroid, retina and vitreous humour [10].

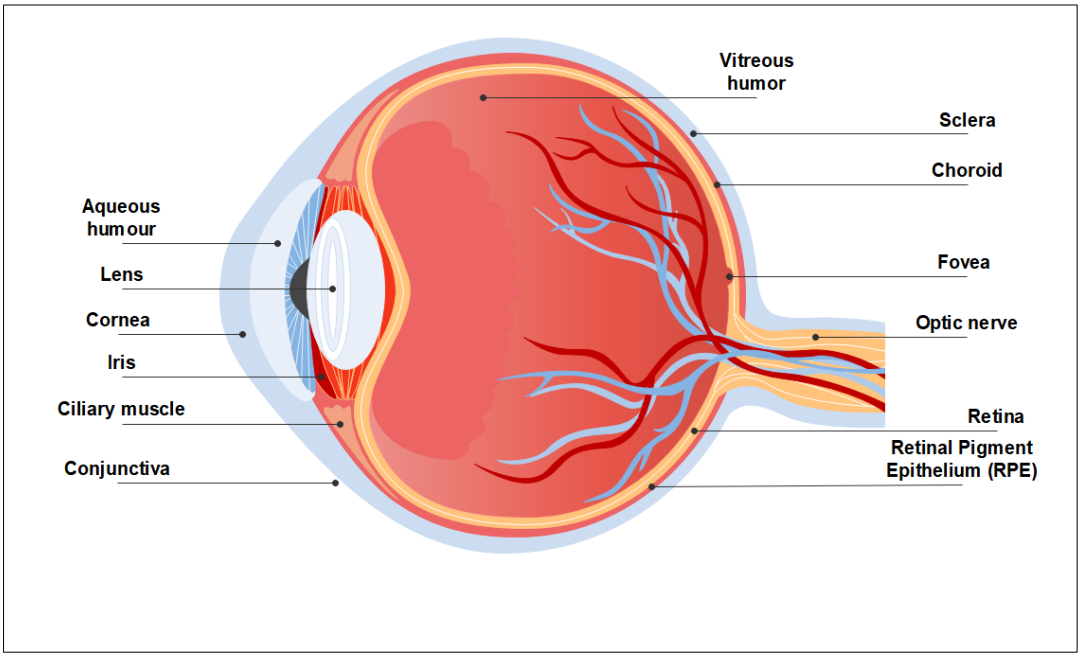

Figure 1-1: Schematic diagram of the human eye.

The figure was drawn with Edraw Max software.

1.1. Ocular drug delivery barriers

Drug delivery to the eye is challenging due to the presence of biological barriers [11]. Overcoming these ocular barriers and delivering drugs efficiently to the targeted ocular tissues is not trivial. Drugs are prevented from reaching targeted ocular tissues by static and dynamic ocular barriers [3]. In general, these barriers may be classified based on their anatomical location and functional properties as anterior and posterior segment barriers [3].

1.1.1. Anterior segment barriers

Static and dynamic barriers are the main anterior segment barriers. The static barriers mainly include the cornea, conjunctiva, and blood-aqueous barrier (BAB). The dynamic barriers mainly involve the production and drainage of tear and the opposite directional flow of the aqueous humour [3].

1.1.1.1. Anterior segment static barriers

Cornea

The cornea is the outermost part of the anterior of the eye. It refracts and transmits light to the lens and retina [2], and protects the eye against exogenous substances, including topically applied drugs from penetrating deeper ocular tissues [3]. The ocular surface is coated with a mucus film layer of glycoproteins (mucins) [12]. The cornea has five distinct layers in which the stroma makes up to 90% of its thickness [4]. The corneal epithelium is the outer layer of the cornea, made of five to six layers

of epithelial cells [3], acts as a barrier to drug absorption because they are held together and tightly bound by tight junction's proteins such as zonula occludins-1 (ZO-1) [13]. Due to the lipophilic nature of the corneal epithelium, it is considered as the rate-limiting barrier for hydrophilic drugs [5], whereas the hydrophilic stroma may act as a rate-limiting barrier for lipophilic drugs [3]. The corneal endothelium monolayer has leaky tight junctions (200 times more permeable than the corneal epithelium) that allow water and nutrients into the stroma from the anterior chamber [14]. Thus, the corneal endothelium represents a weaker barrier for drug delivery as compared to the corneal epithelium [4].

Conjunctiva

Conjunctival tissue may act as a permeability barrier to topically applied drugs. The conjunctiva expresses efflux protein such as permeability glycoprotein (P-gp) on the cell membrane providing a primary barrier for drug delivery into ocular tissues [5]. The presence of the conjunctival blood capillaries can cause a significant drug loss into the systemic circulation, thereby lowering the ocular bioavailability [8]. However, the conjunctiva is more permeable compared to the cornea; this is mainly because of the larger paracellular pore diameter (3 nm ± 1.6) for the conjunctiva and (2 nm ± 0.2) for the corneal epithelium [15]. The conjunctiva has approximately 230 times greater paracellular space than the cornea [15], due to the conjunctiva larger surface area (17 cm^2) as compared to the cornea (1 cm^2) [16,17].

Blood-aqueous barrier

Following systemic administration, drug delivery to the anterior segment of the eye is limited by the presence of the BAB [5]. This barrier is located in the uvea and is composed mainly of the endothelial cells of iris-ciliary blood vessels and the non-pigmented ciliary epithelium [18].

1.1.1.2. Anterior segment dynamic barriers

Tear drainage

The tear film is considered as one of the physiological obstacles against topically applied drugs [11]. It is produced by the lacrimal glands [2] and protects the eyes from exposure to the external environment [2]. The tear film is composed of three layers; an aqueous layer, a superficial lipid layer, and a mucus layer adhering to the corneal epithelium [2]. Typically, the average tear volume in human is 7 µL [4] and the average tear pH is 7.0 - 7.4 [4]. Thus, eye drops instilled with a pH lower than 6.6 and higher than 9.0 are commonly associated with irritation, reflex tears, and rapid blinking [4], thus reducing the ocular bioavailability.

A dynamic equilibrium exists in the pre-corneal tear film as it goes through a continuous cycle of production (0.5 - 2.2 µL/min), evaporation, and drainage [5]. Following topical ocular administration, the drug is primarily accumulated in a conjunctival cul-de-sac and mixed with the lacrimal fluid [5]. Most of the topically administered solutions are washed away within just 15 - 30 seconds after instillation [8]. Hence, the majority of the administered drug is lost (~ 95 %) [8] as a

result of tear drainage into nasolacrimal ducts, tear dilution, and drug binding to tear proteins [3], therefore reducing the ocular bioavailability [5].

Aqueous humour

The aqueous humour is an ocular fluid that is continuously formed in humans at the rate of (2.5 µL/min) from epithelial cells of the ciliary body [19]. If topically applied eye drops traverse the corneal barrier, they may encounter the flow of the aqueous humour. The aqueous humour flows towards the cornea and may cause drugs to be drained out through the trabecular meshwork into the canal of Schlemm [20].

1.1.2. Posterior segment barriers

Static and dynamic barriers are the main posterior segment barriers. The static barriers include the sclera, Bruch's membrane, blood-retinal barrier (BRB), and efflux pumps, whereas the dynamic barriers include choroidal blood supply and lymph circulation [3].

1.1.2.1. Posterior segment static barriers

Sclera

The sclera is a tough fibrous tissue that protects the eye and maintains the eyes' shape [2]. Drug permeability through the sclera is mainly dependant on lipophilicity, molecular weight, and surface charge of the particles [3]. With increasing lipophilicity and molecular weight, the permeability through aqueous scleral pores may be decreased [3,5] A study conducted on human sclera, utilising different molecular

weight compounds, found that the smallest molecular weight compound, 5-fluorouracil (MW = 130 Da) had the highest permeability. In contrast, dextran 70 kDa (MW = 70,000 Da) had the lowest permeability [21]. The charge of the particles may have an effect on drugs to permeate the sclera [22]. Positively charged particles may exhibit high retention in the sclera presumably due to their binding to the negatively charged proteoglycan matrix [8]. Elsaid et al. reported that the positively charged amphiphilic chitosan derivative, O-octanoyl-chitosan-polyethylene glycol graft copolymer allows for strong electrostatic interaction between the micelles and the negatively charged proteoglycan matrix of the sclera [23]. This resulted in higher scleral retention of the micelles which could prolong the sclera residence time of the drug [23].

Bruch's membrane

The Bruch's membrane regulates the exchange of nutrients, fluids, metabolic waste, oxygen and biomolecules between the choroidal blood circulation and the retina [24]. It is located between the retinal pigment epithelium (RPE) and the choroid [24]. During disease states such as age-related macular degeneration (AMD), the thickness of the Bruch's membrane increases, resulting in the accumulation of extracellular debris [3] and subtherapeutic drug concentrations in retinal tissues [25].

Blood-retinal barrier

BRB may be divided into the inner and outer BRB. The inner BRB comprises retinal capillary endothelial cells, whereas the outer BRB comprises tight junctions of the RPE cells [26]. The BRB limits the drug from accessing the posterior segment of the eye from the blood [8]. It primarily regulates the transfer of drugs from the eye after intravitreal injection and into the eye following systemic and topical administration [27].

Efflux pumps

Efflux pumps such as P-gp that are expressed on the apical and basal sides of human RPE have been reported [28]. At the cellular level, these efflux pumps are actively involved in reducing the intracellular drug concentrations and act as a significant barrier to drug delivery [3].

1.1.2.2. Posterior segment dynamic barriers

Choroidal blood supply and lymph circulation

Since the choroid is a highly vascularised tissue containing ~ 80% of the total ocular blood supply and supplied with lymph vessels [3], topically applied drugs may be drained into the systemic circulation leading to subtherapeutic drug concentrations in retinal tissues [3].

1.2. Factors affecting ocular drug permeation

1.2.1. Ionisation and pH

The aqueous solubility of a drug depends on the extent of its ionisation, and in general, drugs in an ionised state are more readily soluble than the unionised drugs [29]. To be effectively absorbed across the cornea, the drug must exhibit differential solubility, i.e. ionised and unionised forms coexist [30]. The unionised form is required to partition into and diffuse across the corneal epithelium. The stroma is predominantly aqueous, and therefore ionisation of the drug must occur to enable partitioning into this phase [30]. Following diffusion to the interface between the stroma and the endothelial layer, the absorption of the unionised form occurs [30]. Hence, for drugs to be well absorbed through the cornea, they may need to have a mixed hydrophilic/lipophilic nature with an intermediate partition coefficient [4].

The eye can tolerate topical ophthalmic preparations at a pH range of 6.6 - 9. Formulations close to the physiological tear pH (7.0 - 7.4) 4 are preferable to avoid discomfort and increased lacrimation [2].

1.2.2. Osmolarity

The tonicity of human tears may influence ocular drug delivery. Osmosis occurs as the particles traverse the semipermeable membrane from an area of high solute concentration to an area of low solute concentration until equilibrium is reached, and the pressure responsible for this movement is called osmotic pressure [31]. The

normal tear film osmolarity is between (288 - 293 mOsmo/L) [4], and the body fluids, including blood and tears, have an osmotic pressure corresponding to that of 0.9% w/v sodium chloride [31]. Eye drops should be isotonic to minimise cell damage and maximise drug efficacy [32]. Thus, solutions with a lower osmotic pressure than body fluids are commonly called hypotonic, whereas hypertonic solutions have a higher osmotic pressure than body fluids [31]. Theoretically, when a hypertonic solution is applied to the eye, it may encourage the passage of water from the site of an ophthalmic application through the tissues of the eye, which may result in dehydrating effect on the corneal epithelium [2]. Conversely, a hypotonic solution tends to draw water from surrounding tissues toward the site of the topical application causing oedema [31].

1.2.3. Viscosity

An optimum viscosity value is necessary for topical eye drops formulations. Viscosity enhancing materials may be used in ophthalmic solutions to improve the precorneal residence time and enhance drug absorption [2]. This increased precorneal residence time may be due to a reduction in tear drainage rate [2]. A high viscosity value was reported to have an impact on the rate of tear drainage [33]. A viscosity value of ~ 2.0 mPa.s was reported for topical ophthalmic application [34]. As compared to water's viscosity at room temperature (0.89 mPa.s) [35], a viscosity value of ~ 2.0 mPa.s may enhance the precorneal residence time.

1.3. Ocular drug distribution

The ultimate goal of topical ocular drug delivery systems is to maximise the ocular drug absorption with minimum systemic absorption [5]. The concentration of drugs reaching the intraocular tissues is determined by the rate of drug uptake by the cornea and the rate of drug loss from the precorneal area [4]. Drug diffusion and distribution into the posterior tissues of the eye after topical administration may occur via several pathways as following [36] (Figure 1-2):

- Diffusion across the conjunctiva and the sclera followed by penetration into the Bruch's membrane and the RPE.
- Direct entry through the cornea to the intraocular tissues.
- Absorption into the systemic circulation either through the conjunctival vessels or via nasolacrimal duct and eventually systemic delivery to the retinal vessels.

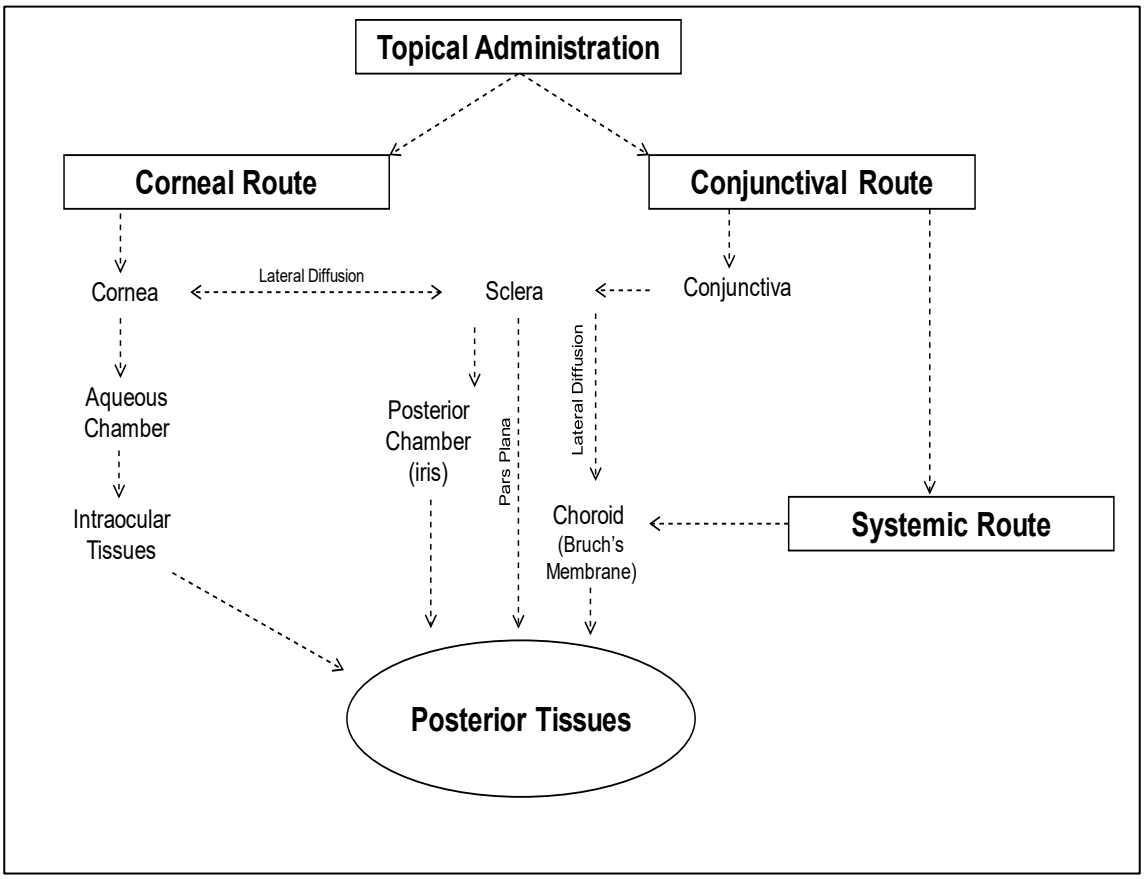

Figure 1-2: Drug distribution pathways to the back of the eye following topical administration.

1.4. Routes of ocular drug administration

Diverse ocular routes of administration have been utilised to achieve successful drug delivery to the eye, reduce side effects, and enhance patient compliance. Typically, there are four modalities exploited to deliver drugs to the eye: topical, systemic, periocular/transscleral, and intraocular injection [37]. Table 1-1 summarises various routes of ocular drug administration.

Topical ocular administration is the most common route for eye delivery, and the majority of ophthalmic drug formulations are in the form of eye drops [4]. It is the preferred route for complications associated with the anterior segment, owing to its ease of access and patient compliance. The inability to sustain high local drug concentration of drugs and the relatively short contact time with the eye are significant problems with eye drop formulations [4].

The systemic administration of drugs to treat ocular disorders mainly involves conditions affecting the optic nerve, retina, and uveal tract [4]. However, drug delivery to the anterior and posterior segment of the eye following systemic administration is limited due to the presence of BAB and BRB [38]. Less than 2% of plasma drug concentrations are present in the vitreous humour; thus, frequent high doses are generally required with a risk of systemic side effects [5].

Periocular or transscleral ocular drug delivery involve; retrobulbar, sub-tenon, sub-conjunctival, and posterior juxtascleral administration [39]. Furthermore, intraocular administration is intended to deliver drugs to the eye either anteriorly via intracameral or posteriorly through intravitreal and suprachoroidal injections.

Table 1-1: Comparison of different properties of ocular routes of administration.

Routes of administration		Benefits	Challenges	Adverse events	Duration	Ref.
Topical		○ High patient compliance. ○ Non-invasive.	• High tear dilution and turnover rate. • Cornea, conjunctiva, sclera, choroid, RPE act as barriers. • Involve the presence of efflux pumps. • Bioavailibiltiy (< 5%).	- Conjunctival redness and irritation.	30 min – 4 hr.	[4,37]
Systemic		○ Patient compliance. ○ Non-invasive.	• Involve the presence of BAB, BRB. • High dosing causes toxicity. • Bioavailibiltiy (< 2%).	- Minimum local exposure. - High systemic exposure.	< 30 min.	[4,5,37,38]
Peri-ocular	*Sub-conjunctival*	○ Delivery to the anterior and posterior segment. ○ The site for depot formulations.	• Conjunctival and choroidal circulation.	- Haemorrhage.	3 months.	[37,39]
	Sub-tenon	○ High vitreal drug level. ○ Mild systemic exposure.	• RPE acts as a barrier. • Injection risk.	- Haemorrhage.	Six hr – 1 month.	[37,39]
	Retro-bulbar	○ High local dose of anaesthetic. ○ Minimum influence on intraocular pressure.	• Injection risk.	- Retro-bulbar haemorrhage. - Globe perforation.	Up to 3 hours.	[37,39]
	Posterior-juxtascleral	○ The site for depot formulations. ○ Sustain drug in macula for up to 6 months.	• Surgery.	- Increase in intraocular pressure	6 months.	[37,39,40]
Intra-ocular	*Intravitreal*	○ Comprise the direct delivery to vitreous and retina. ○ Sustain the drug level. ○ Evades BRB. ○ Bioavailability (100%)	• Invasive. • Poor patient compliance. • Expensive.	- Retinal detachment. - Haemorrhage. - Cataract. - Endophthalmitis.	21 hr – 7 weeks.	[37,39]
	Intracameral	○ High drug level in the anterior chamber. ○ Used for anaesthetic agents.	• Injection risk.	- Toxic anterior segment syndrome. - Toxic endothelial cell destruction syndrome.	Up to 3 hours.	[37,39]
	Supra-choroidal	○ Reduced exposure to the vitreous and anterior segment. ○ High exposure to choroid and retina. ○ Mild systemic exposure.	• Pressure from injection on the ocular surface. • Patient discomfort.	- Associated with the steroids drugs. - Ocular pain.	4 – 6 months.	[37,39,41]

1.4.1. Topical eye drops for the back of the eye diseases

Up to date, there are no eye drops formulations on the market to target the back of the eye diseases. Few candidates in clinical trials (Table 1-2) have been tested for the feasibility of using eye drops to manage back of the eye diseases. Briefly, regorafenib (30 mg/mL) and pazopanib (5, 10 mg/mL) are multikinase inhibitors formulated as eye drops suspensions that are being developed by Bayer (Leverkusen, DE) and GlaxoSmithKline (Middlesex, UK), respectively. Abruptly, both drug entities were terminated after phase II trials due to insufficient exposure in the back of the eye [42,43]. Phase II clinical trials were conducted in 2010, for studying the efficacy of topical mecamylamine solution (10 mg/mL), a nicotinic acid receptor antagonist developed by CoMentis, Inc., (San Francisco, USA), in patients of diabetic macular oedema (DME) receiving maintenance injections of either ranibizumab or bevacizumab. There were no serious adverse events and no drug-related adverse events, but only 38% of the patients showed visual improvement [44].

PAN-90806 is a small molecule selective VEGF receptor antagonist that has been developed in clinical trials. This cyclodextrin-based PAN-90806 (2, 6, 10 mg/mL) was developed by PanOptica, Inc. (New Jersey, USA) to treat wet AMD. Phase I clinical trial was completed in 2016 with an advance to Phase II. In pre-clinical studies, PAN-90806 showed comparable performance to intravitreal anti-VEGF [45]. However, there is no news on the progress of this formulation.

Table 1-2: List of topical eyes drops in clinical trials for the back of the eye diseases.

Drug	Formulation	Model	Method	Results	Comments	Ref.
Regorafenib	- Monohydrate oil suspension. - 30 mg/mL.	Phase II terminated.	- One drop (25 µL) TID for 12 weeks	- The study was terminated after completion of Phase II because efficacy was not sufficient. - There were no drug-related safety concerns.	- Multikinase inhibitor - For wet AMD - Developed by Bayer - It terminated in 2016.	42,43
Squalamine (OHR-102)	- Lactate solution. - 2 mg/mL.	Phase III failed.	- One drop BID for nine months in combination with Lucentis® injection. - Initial results after ten weeks.	- Patients receive a combination of topical OHR-102, and Lucentis® achieved better visual acuity than the control group who received Lucentis® only. - Retrospective subgroup analysis failed on phase III.	- Aminosterol that binds intracellular calmodulin to inhibit angiogenesis - For wet AMD - Developed by OHR Pharmaceuticals.	46,47
Pazopanib	- Eye drops suspension - 5, 10 mg/mL	Phase II terminated.	Different concentrations and frequencies are utilised in comparison to intravitreal ranibizumab.	- Lack of efficacy identified during preliminary analysis. - Pazopanib treatment did not reduce as needed ranibizumab injections by ≥ 50% (prespecified efficacy criterion).	- Multikinase inhibitor - For wet AMD - Developed by GlaxoSmithKline - Phase II terminated in 2014.	43
Mecamylamine HCL (ATG-003)	- An ophthalmic solution containing benzalkonium chloride - 10 mg/mL.	Phase II completed.	- Twice a day for 48 weeks. - Two trials; one with (ranibizumab or bevacizumab) in wet AMD, and the other with DME.	- 8/21 patients showed improvement in wet AMD. - 38% of patients with DME showed spontaneous improvement. - 4/21 patients showed progression of DME.	- Nicotinic acetylcholine receptor antagonist. - For wet AMD, and DME. - Developed by CoMentis. - Phase II completed in 2010.	44
PAN-90806	- Cyclodextrin-based eye drops solution. 2, 6, 10 mg/mL	Phase I completed.	Different concentrations and frequencies are utilised	- Pharmacokinetics data showed that drug concentration continued up to 17 hours after dosing. - Animal studies showed comparable performance to intravitreal VEGF.	- Small-molecule selective VEGF receptor antagonist - For wet AMD, diabetic retinopathy. - Developed by Pan-Optica - Phase I completed 2016.	45

AMD: age-related macular degeneration, **QD**: once a day, **BID**: two times a day, **TID:** three times a day, **VEGF**: vascular endothelial growth factor.

1.4.2. Intravitreal injections for the back of the eye diseases

Current therapeutic approaches to treat back of the eye diseases are mainly by invasive intravitreal injections [48]. Nevertheless, it is still the only efficient route of administration owing to its 100% bioavailability at the site of action [49]. Table 1-3 shows the intravitreal injections that are currently on the market.

Pegaptanib sodium (Macugen®) is the first antiangiogenic medication that has been approved in 2004 to treat wet AMD [50]. It is a PEGylated aptamer that binds to extracellular vascular endothelial growth factor. Macugen® was developed by Eyetech Pharmaceuticals (New York, USA) and is administered once every six weeks [50]. Bevacizumab (Avastin®) is an anti-VEGF humanised full-length monoclonal antibody utilised as an off-label medication to treat wet AMD [51]. Avastin® has first received the approval to treat colon cancer in 2004, and it was developed by Genentech Inc. (San Francisco, USA) [51]. The markedly lower cost of bevacizumab as compared to similarly effective drugs such as ranibizumab has led to its adoption for the treatment of exudative AMD. Ranibizumab (Lucentis®), developed by Genentech Inc. (San Francisco, USA) is an anti-VEGF humanised fragment monoclonal antibody that received the FDA approval in 2006 to treat wet AMD and DME [52]. Aflibercept (Eylea®) is a recombinant fusion protein that has been approved in 2011 for wet AMD, and this drug was developed by Regeneron Pharmaceuticals, Inc. (New York, USA) [53]. Recently, brolucizumab (Beovu®) developed by Novartis (Basel, Switzerland), approved by the FDA in October 2019,

was followed by European Commission approval for use in the European Union in February 2020, for the treatment of wet AMD [54].

Table 1-3: Current intravitreal medications available on the market to treat back of the eye diseases.

Drug	MOA	Formulation	Dose	Cost/ dose	Comments	Ref.
Pegaptanib Sodium (Macugen®)	Anti-VEGF that binds to extracellular VEGF.	PEGylated pegaptanib sodium aptamer	- 0.3 mg/90 µL. - Once every 6 weeks.	£514	- Approved in 2004. - For wet AMD. - 50 kDa.	[50]
Bevacizumab (Avastin®)	Anti-VEGF humanised monoclonal antibody.	Full-length antibody	- 1.25 mg/50 µL. - Once every month	£50	- Approved in 2004 for colon cancer. - Off-label in wet AMD. - 148 kDa.	[51]
Ranibizumab (Lucentis®)	Anti-VEGF humanised fragment monoclonal antibody.	Antibody fragment	- 0.5 mg/50 µL. - Once every month.	£742	- Approved in 2006. - For wet AMD. - 48 kDa.	[52]
Aflibercept (Eylea®)	Anti-VEGF	Recombinant fusion protein	- 2 mg/50 µL - Once per month for three months, followed by one dose every two months.	£816	- Approved in 2011. - For wet AMD, macular oedema. - VEGF trap-eye. - 115 kDa.	[53,55]
Brolucizumab (Beovu®)	Anti-VEGF	Humanised single-chain antibody fragment	- 6 mg/50 µL - Once every 8-12 week	£1360	- Approved in 2019. - For wet AMD	[54]

However, despite encouraging outcomes in halting the disease and improving the vision, intravitreal injection of anti-VEGF agents may be associated with devastating ocular complications and systemic adverse events [56]. Table 1-4 describes the adverse events and complications associated with intravitreal injection [56].

The mainstream ocular complications that are shared among patients receiving intravitreal injections and are not related to underlying ocular diseases are; ocular haemorrhage (10% of patients), intraocular inflammation (up to 2.9% of patients), endophthalmitis (1.6% of patients), and injections related intraocular pressure elevation [56]. However, within specific ocular diseases such as AMD and diabetic retinopathy (DR), tear in RPE (up to 27%) and retinal detachment (5.2%) were observed in patients receiving intravitreal injections [56].

Although anti-VEGF therapies are highly effective in treating wet AMD and diabetic macular oedema, a monthly intraocular injection is not an ideal drug delivery platform, and it is hard to maintain patient compliance [57]. Intravitreal injections are associated with a significant burden on the patient's psychological health as well. Treatment-related anxiety is shared among the patients before the injection [58]. Other considerations include; the financial and travel issues associated with the treatment [58].

Table 1-4: Adverse events and complications associated with intravitreal injection. Adopted from [56].

Adverse events and complications associated with intravitreal injection				
Unrelated to the underlying ocular disease		***Related to specific ocular disease***		
Adverse event	***Observation***	***Disease***	***Adverse event***	***Observation***
Endophthalmitis	In multicentre clinical trial (0.019% - 1.6 %).	Diabetic retinopathy, retinal vascular occlusion	Tractional retinal detachment	(5.2%) majority within 5 days
Intraocular inflammation	With ranibizumab (1.4% -2.9%). With bevacizumab (0.09% - 0.4%).	AMD	Tear of retinal pigment epithelium	(0.06% - 27%)
Rhegmatogenous retinal detachment	(0%-0.67%).			
Intraocular pressure elevation	Injection procedure-related and develops in a few hours.			
Ocular haemorrhage	Subconjunctival haemorrhage (10%).			
Systemic safety	Out of 1173 patient receiving bevacizumab for 12 months, 18 (1.5%) showed the following: - Blood pressure elevation (0.59%). - Cerebrovascular accidents (0.5%). - Myocardial infarction (0.4%). - Deaths (0.4%). - Iliac artery aneurysm (0.17%)			

1.5. Common back of the eye diseases

Globally, the estimated number of people visually impaired in the world is 285 million, 39 million blind and 246 million having low vision. According to the World Health Organization statistics, 65 % of people are visually impaired, and 82% of all blind patients are aged 50 years and older [59].

Ocular disorders are commonly classified by whether they affect the anterior or posterior segment. The most prevalent disorders that can affect the posterior or back of the eye are; age-related macular degeneration, diabetic macular oedema, diabetic retinopathy [5], and noninfectious posterior uveitis [60].

There is a substantial global public health burden of AMD. Generally, AMD is the leading cause of blindness, with 8.7% of individuals over the age of 60 years suffering from the disease [61]. Over 600,000 people in the United Kingdom are affected by AMD, and the number may increase as the population ages [62]. A systemic analysis projected the number of people globally that will be suffering from AMD in 2020 would be around 196 million, increasing to 288 million in 2040 [61]. AMD is defined as an abnormality of the retinal pigment epithelium that leads to degeneration of the overlying photoreceptor cells in the macula and consequent loss of central vision [1]. The disease is characterised by the accumulation of membranous debris underneath the RPE basement membrane, which forms drusen. Drusen are small, yellowish extracellular deposits of lipid, cellular debris and protein, including complement components, anaphylatoxins, modulators, and high-temperature requirement A serine peptidase 1. The formation of drusen can be

caused by RPE dysfunction or by a change in the composition or permeability (to nutrients) of Bruch's membrane [1]. There are two major categories of AMD: early "dry or non-exudative", and an advanced "wet or exudative". Dry AMD is not associated with loss of vision and accounts for 85% of the AMD cases. It is characterised by the presence of drusen, and hyper- or hypo-pigmentation of the RPE [1]. In contrast, advanced AMD is usually associated with loss of vision and accounts for 15% of the AMD cases. It can be further classified into geographic atrophy, which is characterised by atrophy of the RPE and photoreceptor cells, or choroidal neovascularisation [1]. Wet AMD is associated with the growth of abnormal blood vessels into the subretinal space [1,63]. Vascular endothelial growth factor A has been implicated in choroidal neovascularisation and increased vascular permeability, resulting in loss of vision. It is produced by many ocular cell types in response to hypoxia and has multiple functions in the eye. It stimulates endothelial cell growth, promotes vascular permeability and induces dissociation of tight junction components [1].

Diabetic retinopathy is a microvascular complication of diabetes that is characterised by increased vascular permeability in the initial stages of the disease and a consequent loss of vision [64]. Diabetic retinopathy is the leading cause of blindness and visual impairment in working-age individuals over the 30 years [1]. A meta-analysis study was conducted to estimate the prevalence of blind people or visually impaired because of DR from 1990 to 2010. Globally in 2010, out of overall 32.4 million blind and 191 million visually impaired people, 0.8 million were blind, and 3.7 million were visually impaired because of DR, respectively [65]. A pooled analysis of

studies (35 studies, 22,869 patients) from 1980-2008 provided a global estimate of the prevalence of the stages of DR. Among all diabetic patients, the overall prevalence of DR is estimated to be 34.6%, 6.96% for the proliferative DR, 6.81% for the diabetic macular oedema, and 10.2% for the vision-threatening diabetic retinopathy [66].

Uveitis is a condition that involves inflammation of the uveal tract [67]. It is mainly categorised based on the site of the inflammation into anterior, intermediate, posterior, and panuveitis. Anterior uveitis is the most common encountered class, and posterior uveitis constitutes 15% – 22% of all cases of uveitis [60]. Posterior uveitis is an intraocular inflammatory disease that affects the retina and choroid. It is classified as an autoimmune disease because of the involvement of effector $CD4^+$T cells [68]. Some uveitis conditions are associated with specific Human Leukocyte Antigen associations and common responses to retinal antigens [69–71]. Uveitis is the fifth most common cause of visual loss in the developed world [72]. Uveitis accounts for 10% to 25% of all cases of total blindness in the developing world, with significant vision loss occurring in up to 35% of children and adults [41,73]. The incidence of uveitis has been estimated between 17 and 52 per 100,000 of the population annually, and the prevalence as 38 – 714 cases per 100,000 of the population [73].

1.6. Common front of the eye diseases

Common anterior or front of the eye diseases include; cataract, dry eye, glaucoma, and allergic conjunctivitis [10]. Cataracts have been reported to be responsible for 51% of world blindness [74]. Cataract is defined as an opacity of the lens that deteriorates the vision [75]. The oxidative stress is a significant factor in the genesis of senile cataract (the commonest cataract type). The oxidative processes upsurge with age in the human lens and concentration of proteins found is significantly higher in opaque lenses. This leads to breaking down and aggregation of protein and culminates in damage to fiber cell membranes. Advanced that in the ageing eye, barriers develop that prevent glutathione and other protective antioxidants from reaching the nucleus in the lens, making it susceptible to oxidation [76]. Cataract surgery is the most common approach to manage the disease [77], but this approach might be not available in many countries [78].

Dry eye disease is a multifactorial disease of the ocular surface with loss of homeostasis of the tear film [79]. Dry eye disease is characterised by instability of the tear film that can be due to an insufficient amount of tear production, which results in increased evaporation of the tears. Therefore, the dry eye can be divided into two groups: aqueous production deficient, and evaporative dry eye disease [80]. Tear-deficient dry eye due to the poor production of tears by the tear glands is found in older patients, postmenopausal women, and patients with autoimmune diseases such as Sjogren's syndrome and rheumatoid arthritis [80]. Also, the dysfunction of the lacrimal functional unit causes changes in the composition of the tear fluid and tear

film stability leading to inflammation of ocular surface [80]. Therefore, the eye does not produce adequate tears as an anti-inflammatory component of the eye is lacking, and irritation of the eye is not controlled. This causes activation of inflammatory cells, including T-lymphocytes by the immune system of the body. T-cells release cytokines, which causes inflammation of ocular surface and glands, thereby resulting in abnormal tears and dry eye symptom [80]. Evaporative loss of tear fluid and dry eyes are usually associated with inadequate lipid layer. The lipid layer stabilises and retards evaporation of the underlying aqueous layer [80]. Also, environmental factors such as; contact lens wear, or reduced blinking because of driving, and computer work are associated with evaporative dry eyes disease [80]. In epidemiological studies performed globally, dry eye disease prevalence ranges from 5 - 50 % [81]. Inflammation on the surface of the eye may be controlled with prescription eye drops that contain cyclosporine (Restasis®) or corticosteroids [82]. However, prolonged steroid use is associated with glaucoma [83] and hence is not ideal.

Glaucoma is a common eye condition where the optic nerve becomes damaged. It is caused by fluid building up in the front part of the eye, which increases pressure inside the eye [84]. Glaucomas can be classified into two broad categories: open-angle and angle-closure glaucoma [85]. In patients with open-angle glaucoma, there is increased resistance to aqueous outflow through the trabecular meshwork. In contrast, access to the drainage pathways is obstructed by apposition of the iris in patients with angle-closure glaucoma [85]. Glaucoma is the leading cause of irreversible vision loss worldwide [86]. The global prevalence of glaucoma for populations aged 40 - 80 years is 3.54%. In 2013, the number of people (aged 40 -

80 years) with glaucoma worldwide was estimated to be 64.3 million, increasing to 76.0 million in 2020 and 111.8 million in 2040 [87].

Allergic conjunctivitis is caused by an allergen-induced inflammatory response in which allergens interact with IgE bound to sensitized mast cells resulting in the clinical ocular allergic expression. The pathogenesis of allergic conjunctivitis is predominantly an IgE-mediated hypersensitivity reaction. Activation of mast cells induces enhanced tear levels of histamine, tryptase, prostaglandins and leukotrienes [88]. Allergic conjunctivitis affects 6 – 30% of the general population in Europe, with 25% of cases involving severe and persistent disease [89]. Vernal keratoconjunctivitis (VKC) and atopic keratoconjunctivitis (AKC) represents two severe forms of ocular allergies [90] that affect 4 – 39% of allergic conjunctivitis patients, depending on geographical location [89] and age [91]. VKC is a sight-threatening disease with no overall gold standard form of therapy [92]. AKC is also a sight-threatening condition which affects adults mostly and is usually present as a co-morbidity with atopic dermatitis [93]. Patients with severe disease are treated with anti-allergy drugs, and corticosteroids and treatment are frequently inappropriate [89]. Prolonged steroid use is associated with glaucoma [83] and hence is not ideal, especially with the younger patients.

1.7. Ocular drug delivery systems in the development

Novel drug delivery systems are required to overcome the eye's anatomical and physiological barriers and, most importantly, improve patient safety and compliance. Despite the challenges in manufacturing efficient ocular drug delivery systems, many innovative approaches are being developed. Table 1-5 briefly describes the various ocular drug delivery system technologies and devices currently in progress [94]. These technologies target anterior and posterior eye diseases and are focused on overcoming the inherent shortcomings of existing therapies, such as short ocular contact time, low ocular bioavailability, high dosing frequency, limited drug penetration and invasiveness of treatments [94].

Lacrimal puncta are natural openings located in the inner part of the top and bottom eyelids. A punctual plug developed by Angiotech Pharmaceuticals Inc. (Vancouver, CA) is an FDA approved medical device inserted into the puncta to block tear drainage. Ocular Therapeutix Inc. (Massachusetts, US), developed OTX-TP that delivers travoprost to the ocular surface for open-angle glaucoma and ocular hypertension via an intracanalicular punctual plug for up to 3 months. It consists of a PEG-based hydrogel with embedded travoprost–loaded PLA microspheres [95]. Mati Therapeutics, Inc., (Texas, US), also developed (Evolute® latanoprost) to treat open-angle glaucoma and ocular hypertension [94,95]. However, foreign body sensation post-placement may be a significant deterrent in some patients [95].

Ocular inserts are sterile drug-loaded micro-devices placed in or around the eye to release therapeutic drugs over a prolonged duration. Di-(ethylhexyl)phthalate,

ethylene-vinyl acetate formulated-pilocarpine (Ocusert®), and bimatoprost-loaded silicon matrix inserts are two examples to treat glaucoma [95]. Patient education and age continue to be a significant challenge for successful use of the inserts as it requires a refined manual technique to place the insert with weekly replacement. The difficulty of device insertion, irritation during insertion, and ejection of the device from the eye are other challenges in ocular inserts [95].

The ease of availability and application of contact lenses make them an ideal drug delivery system for anterior segment diseases such as glaucoma. Vinyl pyrrolidone loaded-pilocarpine and vitamin E loaded-timolol are examples of ocular contact lenses. However, the decreased ion and oxygen permeability and lens-related infections due to continuous wear significantly limit the application of contact lenses for drug delivery [95].

Ozurdex is a degradable PLGA-dexamethasone intravitreal implant produced by Allergan plc (Dublin, IR) [96]. This implant was approved in 2010 to treat macular oedema and noninfectious uveitis [97]. Refillable intraocular implants are placed in the pars plana beneath the conjunctiva using standard surgical procedures. Ranibizumab is a refillable implant (every 6 months), being investigated in clinical trials for neovascular age-related macular degeneration [98]. In phase II clinical trial, > 80% of patients could go beyond 6 months without needing a refill [98]. The authors concluded that the implant had similar efficacy to the monthly dosing regimen of intravitreal ranibizumab [98]. However, these implants are invasive and require a procedure for implantation in the eye. Following injection, patients may be at risk for potential complications, including the development of severe eye infection or

increased eye pressure. The subsequent surgical procedures to remove the refillable implants make them a less favourable choice for drug delivery [95].

Gene therapy has been explored as a potential treatment for retinal conditions ranging from AMD to rare hereditary diseases, such as Leber's congenital amaurosis. Luxturna® (voretigene neparvovec) is a prescription gene therapy product used for the treatment of patients with inherited retinal disease due to mutations in both copies of the *RPE65* gene [99]. Luxturna®, developed by Spark Therapeutics (Pennsylvania, US), has received FDA approval in 2018. It is given as a surgical injection beneath the retina of each eye. After the first eye is treated, the second eye will be treated at least 6 days later [100].

Table 1-5: Summary of ocular drug delivery technologies in development.

Target Segment	Technology		Description	Indication	Example
Anterior	Punctual plug [94,95]		- Drug loaded polymeric medical device - Reside in puncta to release the drug over time - Biodegradable - Non-invasive	- Glaucoma - Allergic conjunctivitis	- OTX-TP - Evolute latanoprost
	Topical inserts [95]		- Rests under the eyelids over the sclera to release the drug over time - Non-degradable - Non-invasive	- Glaucoma	- Ocusert
	Contact lenses [95]		- Drug-containing soft contact lens - Function as a contact lens and drug reservoir to release the drug over time. - Non-degradable - Non-invasive	- Glaucoma	- Vinyl pyrrolidone loaded-pilocarpine - Vitmine E loaded-timolol
	Iontophoresis [101]		- A wearable electrical device. - Low-amplitude electrical current to promote the migration of a charged drug substance across the biological membrane - Non-invasive - Can deliver to posterior as well.	- Dry eye - Anterior uveitis	- Charged formulation of dexamethasone phosphate (Eygate II)
Posterior	Implants	Polymeric [96,97]	- Drug-containing polymer - Implanted in various ocular compartments (subconjunctival or intravitreal) to release the drug over time - Biodegradable - Posterior and interior - Invasive	- Posterior uveitis - Retinitis pigmentosa - Glaucoma	- PLGA-dexamethasone (Ozurdex)
		Refillable [98]	- Refillable drug containing a reservoir - Placed in the subconjunctival to release the drug over time - Non-degradable - Initial implantation is invasive, but refills are minimally invasive	- Wet AMD	- Ranibizumab
		Encapsulated cells [102]	- Cells containing reservoir - *In vivo* production of therapeutic protein over time - Invasive	- Wet AMD - Retinitis pigmentosa - Glaucoma	- ARPE-19 cells
	Gene therapy [99,100]		- The viral vector-based delivery system - Injected into ocular compartments to deliver genetic material - Invasive	- Leber's congenital amaurosis.	- Luxturna® (voretigene neparvovec)
	Particulate system [103–107]		- Various drugs containing particulates (polymeric, liposomes) - Biodegradable - Posterior and interior - Topical or injectable	- Ocular inflammation - Dry eye - Glaucoma - Wet AMD	- Dexamethasone/ cyclodextrin complexes (OCS-01) - Hyaluronic acid-based (OBG) - NM134 (MET)

1.7.1. Strategies for improving eye drops ocular drug bioavailability

The main inconvenience of conventional eye drops is the rapid washout of the drugs due to nasolacrimal drainage or ophthalmic barriers [108]. The ocular drug bioavailability can be improved by either prolonging retention time in the cul-de-sac using viscosity enhancers and mucoadhesive agents, or by increasing the ocular permeability by using penetration enhancers, prodrugs and colloidal systems such as nanoparticles [108].

Nanotechnology may have an impact on topical ocular drug delivery in the future. Due to nanotechnology, it may be added to control the drug release at the target site, prolong the drug residence time on the precorneal area and enhance corneal permeation, and be amenable to surface modification that may enhance the targeting to a specific receptor [5,109,110].

Cyclodextrins (CDs) are natural cyclic oligosaccharides that are formed by bacterial digestion of starch [103]. CDs are cone-shaped with a hydrophilic outer surface and a lipophilic central cavity [103]. CDs can form hydrophilic inclusion complexes, guest/host complexes where the lipophilic drug is the guest, and the CDs is the host [103]. The complex is kept together as the drug sits in the hydrophobic core of the cyclodextrin molecule. Oculis Pharmaceuticals (Lausanne, CH) has developed a new technology called solubilising nanoparticle (SNP) technology. The SNP technology uses a novel formulation approach incorporating drug/cyclodextrin complexes to address: the limited solubility of drugs in eye drop formulations, the quick removal by tear flow, and the inability to deliver drugs to the retina [104]. One of the leading compounds

developed by Oculis is OCS-01 that is investigated for diabetic macular oedema. The OCS-01 comprises dexamethasone/cyclodextrin complexes that reached Phase II according to the company pipeline [104,111]. Another candidate developed by Oculis is a single-chain antibody fragment technology designed explicitly for topical delivery to the anterior segment. OCS-02 is a novel topical anti-TNF alpha antibody in advanced Phase II that has shown efficacy in the anterior inflammatory eye, including uveitis and dry eye disease and was in-licensed from Novartis [104,111].

Pharmaceutical approaches based on nanotechnologies and the development of eye drops composed of mucoadhesive polymers such as hyaluronic acid (HA) and chitosan are emerging strategies for the efficient treatment of ocular diseases to increase the drug's bioavailability at the ocular surface [105].

Eyegate pharma (Massachusetts, US) is developing an eye gel formulation based on hyaluronic acid (OBG), whereby the HA is modified and then cross-linked according to the company's pipeline. The cross-linking slows the degradation of the HA and provides a matrix for incorporating therapeutic agents [107]. The cross-linking allows the product's viscosity to be increased, and with the mucoadhesive properties of HA, the residence time in the tear film is improved [107]. OBG is an eye gel that provides a thin coating to the surface of the eye, serving as a protectant to facilitate and accelerate corneal re-epithelisation. It is intended for the management of corneal epithelial defects and the re-epithelisation of the ocular surface following surgery, injection, traumatic, and non-traumatic conditions [107].

Nanomerics (London, UK) has developed a modified glycol chitosan-based molecular envelope technology (MET) [106]. Nanomerics received supportive pIND

guidance from the US FDA on the development of NM134. NM134 is indicated for the treatment of potentially sight-threatening eye disease. Nanomerics' MET delivers drugs across biological barriers and significantly increases drug bioavailability. Nanomerics' MET is non-irritant on topical application to the eye, enables the formulation of hydrophobic drugs in aqueous media and is an ocular penetration enhancer [106].

Developing a novel and convenient approach that can deliver the drug to the front and back of the eye after topical instillation with the aid of nanotechnology will be our chosen area of research.

1.8. Rationale, aims, and objectives

From an ophthalmic drug delivery perspective, adequately formulated and investigated nanoparticles are reported to be based on polysaccharides; this is due to their favourable characteristics such as low cost and non-toxicity biodegradability, biocompatibility, and stability [112]. It is imperative to design a novel topical ocular delivery system using adhesive materials to enhance the retention time on the eye's surface. Without adhesion properties, nanoparticles can be eliminated as quickly as solutions from the precorneal site [113].

Chitosan is a cationic polymer and natural polysaccharides derived from chitin that is found in the exoskeleton of crustaceans [114]. Chitosan is a suitable candidate in ophthalmic formulations due to its biocompatibility and biodegradability properties [115]. Chitosan has a mucoadhesive property resulting from the cationic behaviour and the presence of free hydroxyl and amino groups, allowing the polymer to interact with a negatively charged mucin in an acidic environment by hydrogen and electrostatic bonding [116].

Intravitreal injection is considered the primary therapeutic approach to treat the back of the eye diseases [117]. However, these invasive injections are associated with adverse events, devastating ocular complications, and poor patient compliance [56]. A case study of exudative AMD patients associated with loss of vision undergoing intravitreal injections showed the following [118]: before intravitreal injections, patients showed choroidal neovascularisation with a turbid RPE. After intravitreal injection, patients developed a tear in the RPE [118]. These results highlight the importance of

developing alternative approaches to intravitreal injections for the back of the eye diseases.

Application of lipophilic compounds for an ophthalmic preparation is potentially not trivial because of their low aqueous solubility [114]. Hence, the principle for this work is to develop a nanoparticulate drug delivery system for ophthalmic applications that is based on the possible encapsulation of lipophilic drugs in a polymeric nanoparticle matrix, which may lead to potential entrapment of the polymeric nanoparticles in the ocular mucus layer and thus to a prolonged drug residence time and slow formulation drainage. Therefore, the work aims to design and formulate an aqueous-based lipophilic drug-loaded polymeric nanoparticle intended for topical ocular delivery to the anterior and posterior segments of the eye.

We hypothesise that by utilising an amphiphilic glycol chitosan-based polymer, the residence time of a lipophilic drug in the corneal epithelium will be enhanced, leading to possible delivery of the drug to the anterior and posterior segments of the eye.

Specific objectives of this work include:

1. Synthesise an amphiphilic glycol chitosan-based polymer as a novel penetration enhancer vehicle for lipophilic drugs.

2. Formulate an aqueous-based (lipophilic drug) loaded polymeric nanoparticles for topical ophthalmic delivery.

3. Optimise and characterise the formulation such that it is suitable for topical delivery to the eye.

4. Study the short-term stability of the formulation.

5. Inspect the toxicity profile and the permeability of the synthesised polymer and the formulation *in vitro*.

6. Examine the pharmacokinetic properties of the formulations *in vivo*.

7. Study the pharmacodynamic effect of the formulation on a diseased model *in vivo*.

The experimental plan for this project is shown in Figure 1-3.

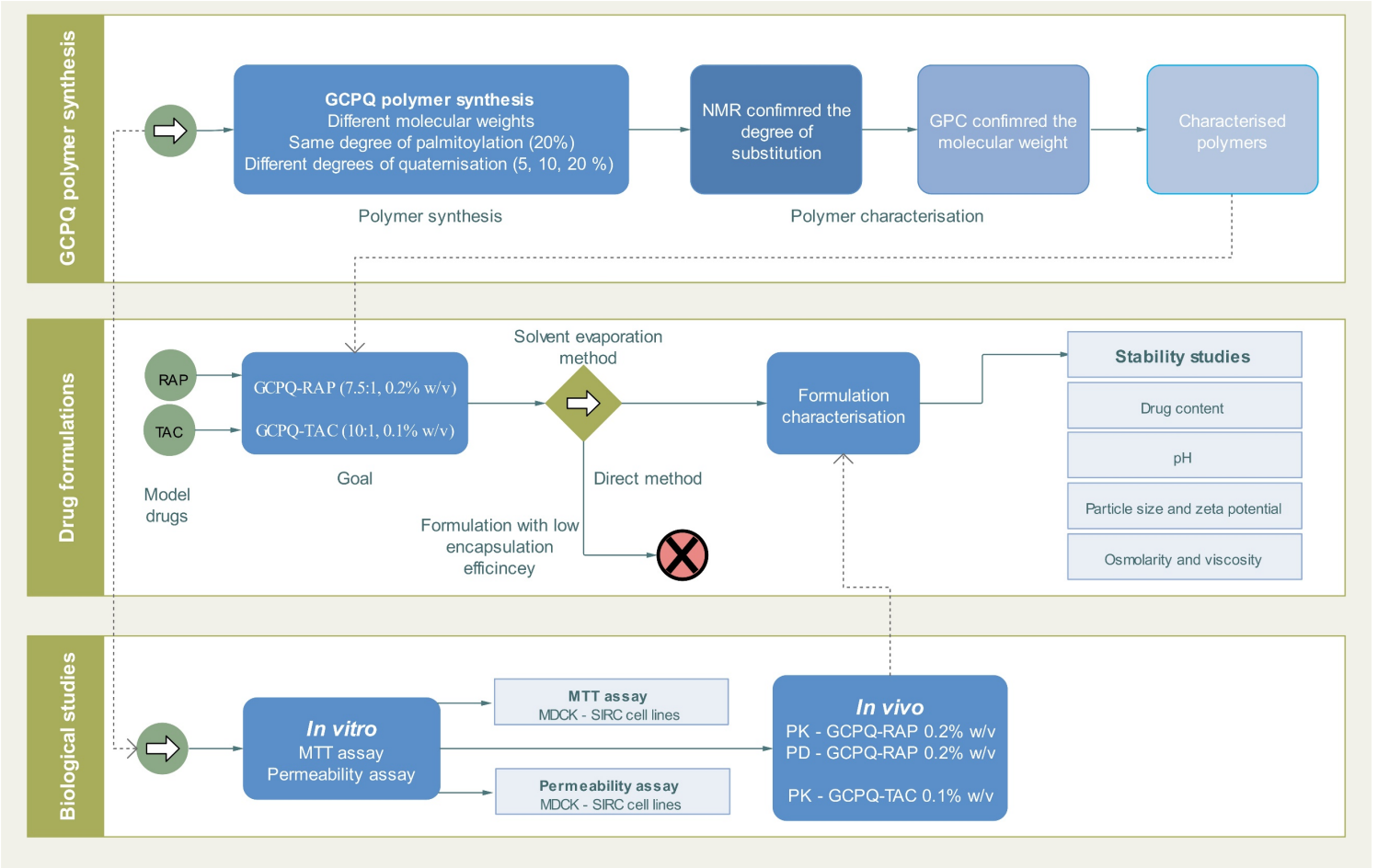

Figure 1-3: Flowchart of the experimental plan of the project.

2. Amphiphile synthesis and characterisation

2.1. Introduction

The main challenge associated with ocular drug delivery is to maintain an optimum drug concentration at the site of action in order to achieve an optimum therapeutic response [119]. For topical ocular formulations, highly hydrophobic compounds are difficult to formulate and to access the back of the eye. Also, the use of intravitreal injections is problematic and complicated [120]. Such limitations can be overcome by utilising a novel drug delivery system such as polymeric micelles.

Most of the polymeric micelles used in drug delivery consist of amphiphilic di-block (hydrophilic-hydrophobic) polymers, tri-block (hydrophilic-hydrophobic-hydrophilic) polymers, and ionic (hydrophilic-ionic) copolymers [120]. Amphiphiles are compounds possessing both hydrophilic and lipophilic components (Figure 2-1) [121]. At low concentrations of amphiphiles in water, amphiphiles orient themselves at the air-water interface, and they exist as monomers in bulk disperse phase [122]. As the concentration of the amphiphiles increases, the amphiphile molecules aggregate above their critical micelle concentration (CMC); this property gives amphiphiles a unique character of self-assembly in an aqueous environment forming colloidal particles called micelles [122]. The driving force for micelle formation in an aqueous environment is due to the hydrophobic interactions, and the entropy gained due to the release of water of solvation [122]. Amphiphiles have surface-active properties and have a wide range of applications in the field of drug delivery [122].

The use of polymeric amphiphiles for ocular drug delivery has gained attention in recent years [123]. The potential for these systems to aid in drug delivery has been researched extensively [123]. Polymeric micelles generate clear aqueous liquids which allow easy application in the form of eye drops without any visual interference. Enhanced stability, larger cargo capacity, non-toxicity, ease of surface modification and controlled drug release are additional advantages with polymeric micelles. Finally, simple and cost-effective fabrication techniques render their industrial acceptance relatively high [120].

Chitosan is a natural, non-toxic biopolymer, consisting of glucosamine and N-acetylglucosamine units produced by the deacetylation of chitin, a major component of the shells of crustaceans [124]. Chitosan is insoluble at neutral and at alkaline pH and forms salts with organic and inorganic acids, and is known to swell when in solution [125]. These limitations necessitated the search for chemical modifications that improve the chitosan properties in drug delivery. Several chemical modifications such as oligomerisation, alkylation, acylation, quaternisation, hydroxyalkylation, carboxyalkylation, thiolation, sulfation, phosphorylation, enzymatic modifications and graft copolymerisation along with many modifications have been carried out [126]. These modifications are based on substitutions and grafting at the free $–NH_2$ of chitosan to improve the drug release and the solubility at a broad pH range [126].

The trimethyl chitosan has attracted attention in ocular drug delivery due to its mucoadhesive property [127,128]. The mucoadhesive properties of trimethyl chitosan result from the interactions taking place between its positively charged quaternary ammonium groups and the negatively charged sulfate and sialic acid groups of

mucosa [128]. Hence, it is regarded as a suitable excipient to prepare buccal, nasal, ocular, and vaginal dosage forms [129].

Glycol chitosan is a water-soluble chitosan derivative with hydrophilic ethylene glycol branches and reactive functional groups for facile chemical modifications [130]. Thus, modifications with groups having amphiphilic properties allow for the encapsulation of hydrophobic substances, thus expanding the utility of chitosan in drug formulation. It should be stated that the amino group of chitosan has a pKa value of about 6.5; hence, chitosan is positively charged and soluble in acidic solutions with a charge density dependent on the pH and the degree of deacetylation [131]. Chitosan has been reported to be fully protonated at pH = 3, 50% protonated at pH = 6.5, and completely deprotonated at pH = 8.5 [132]. The deprotonation of amine groups of chitosan in an elevated pH environment could result in chitosan not interact electrostatically with negatively charged mucin on the eye surface [132]. However, a study was conducted by Rodriguez et al. utilising a fluorescently labelled chitosan on *ex vivo* bovine corneas to determine the polymer retention and the mucoadhesive properties [133]. They found that the chitosan polymer was retained significantly longer on the corneas as compared to FITC-dextran (18.6±2.06 %, remaining fluorescent (%) after washing, $p < 0.05$), suggesting that chitosan bear specific mucoadhesive properties with the corneal epithelium, and this mucoadhesion is predominantly due to an electrostatic attraction and the hydrogen bonding [133]. This could suggest that chitosan may enhance a residence time in the corneal epithelium when in contact with the tear fluids.

This chapter covers the synthesis and characterisation of glycol chitosan-based polymeric amphiphiles, specifically N-palmitoyl-N-monomethyl-N, N-dimethyl-N, N, N-trimethyl-6-O-glycol-chitosan (GCPQ). An illustration of the polymers' synthesis experimental plan is shown in Figure 2-2.

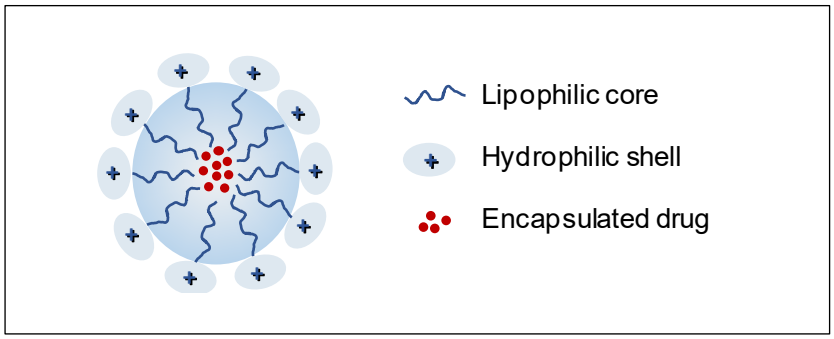

Figure 2-1: Schematic representation of an amphiphilic micelle.

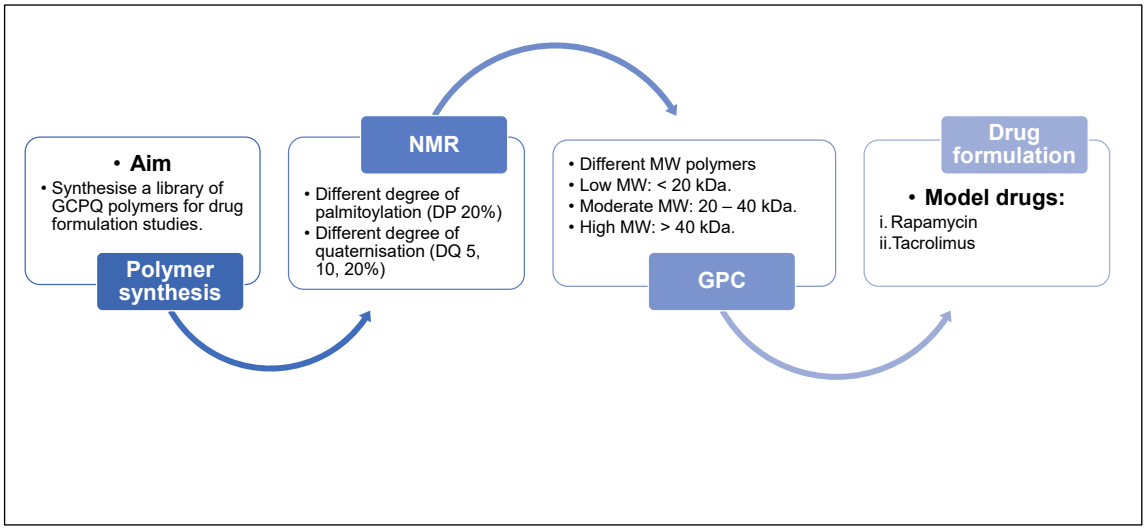

Figure 2-2: Illustration of the experimental plan for the GCPQ polymer synthesis.

2.2. Synthesis of glycol chitosan-based amphiphiles

GCPQ (Figure 2-3) is a glycol chitosan-based amphiphilic polymer, with a hydrophobic palmitic acid molecule that is covalently linked to a hydrophilic sugar backbone [134]. GCPQ is a polycationic polymer that has positive charge quaternary ammonium groups that increase the water dispersibility of the molecule [135]. It has been shown that the GCPQ enhanced the bioavailability of drugs to the systemic circulation and in the aqueous humour via oral [135], and the ocular route [136], respectively. GCPQ forms micelles in an aqueous environment and the micelles are formed at CMC values range from 6 to 100 μM [135]. GCPQ acts in formulations by increasing the aqueous level of hydrophobic drugs and enhancing transport mechanisms [135,137]. GCPQ is mucoadhesive and is likely to bind with negatively charged sialic acid residues of mucin in the eye surface [135,137].

2.2.1. Materials

Chemical	Supplier
Glycol Chitosan (GC)	Wako Pure Chemicals (Shanghai, CN)
Palmitic acid N-hydroxysuccinimide ester (PNS)	Toronto Research Chemical Inc., (North York, CA)
Visking cellulose dialysis tubing molecular weight cut off (MWCO) 3500 daltons	Medicell Membranes Ltd. (London, UK).
N-methyl-2-pyrrolidone (NMP)	Acros Organics (New Jersey, US)
Triethylamine (TEA)	Sigma-Aldrich (Gillingham, UK)
Iodomethane	Sigma-Aldrich (Gillingham, UK)
Glacial acetic acid	VWR (Leicestershire, UK)
Hydrochloric acid (HCL)	Fisher Scientific (Loughborough, UK)
Amberlite IRA-410	Sigma-Aldrich (Gillingham, UK)
Methanol-d4	Sigma-Aldrich (Gillingham, UK)
Deuterium oxide	Sigma-Aldrich (Gillingham, UK)
Deuterium chloride	Sigma-Aldrich (Gillingham, UK)
Diethyl ether	Sigma-Aldrich (Gillingham, UK)
Acetone	Sigma-Aldrich (Gillingham, UK)
Polyethersulfone (PES) filters 0.22 µm	VWR (Leicestershire, UK)
Sodium hydroxide	Sigma-Aldrich (Gillingham, UK)
Sodium iodide	Sigma-Aldrich (Gillingham, UK)
Dimethyl sulfoxide (DMSO)	Acros Organics (New Jersey, US)
Polyethene glycol (PEG, 20 kDa)	Sigma-Aldrich (Gillingham, UK)
Water double deionised	Merck Millipore (Hertfordshire, UK)

2.2.2. Methods

GCPQ was synthesised and characterised according to a protocol set up in the lab and previously described [134,135,137,138]. Briefly, glycol chitosan was degraded, followed by palmitoylation step, and a final quaternisation step, as shown in Figure 2-3. These steps are outlined in this section:

2.2.2.1. Acid degradation of glycol chitosan

GC (Molecular weight ~ 120 kDa, 10 g) was suspended in HCL (4 M, 760 mL) in a borosilicate glass vessel and allowed to dissolve under magnetic stirring for 20 min at room temperature. The GC solution was then placed in a pre-heated water bath at 50 °C and degraded for predetermined time points (2, 6, 24, and 48 hours) with continuous stirring to obtain high, moderate, and low molecular weights polymers. The degraded GC (dGC) was purified by exhaustive dialysis against distilled water (5 L) using a dialysis membrane of MWCO 3.5 kDa with six changes of water over 24 hours. The resulting dialysate was then snap frozen and freeze-dried to obtain a white fibrous solid yielded 60 – 80%, and the structure was studied using nuclear magnetic resonance (NMR).

2.2.2.2. Palmitoylation of degraded glycol chitosan

Degraded GC (dGC, 6 g) was dissolved in dimethyl sulfoxide (DMSO, 180 mL) using a clean, dry flask and the mixture magnetically stirred at room temperature for 16 hours protected from light. TEA (6.9 mL) was added to the mixture, and the mixture stirred until complete dissolution of the dGC. PNS was added to the mixture according to the target degree of palmitoylation. PNS (2.19 g) was added to obtain a level of palmitoylation of ~ 20%. The reaction was left to proceed with magnetic stirring, protected from light for at least 15 hours at room temperature. Subsequently, the mixture was precipitated by adding acetone, diethyl ether (1: 2, 900 mL) and the palmitoylated GC (pGC) was left to precipitate in a fume hood overnight. After settling of the precipitate, the supernatant was decanted, and the solid product was washed three times with acetone (300 mL), and three times with diethyl ether (300 mL). The pGC product was filtered using a glass sintered filter (porosity 3) and dried under vacuum for at least 24 hours. The pGC appeared as small white solid granules yielded 70 – 100%.

2.2.2.3. Quaternisation of palmitoyl glycol chitosan

Palmitoylated glycol chitosan (3 g) was dispersed in NMP (240 mL) in a borosilicate glass vessel for a minimum of 2 hours. Powdered sodium hydroxide (390 mg) was added to the pGC dispersion with continuous stirring at room temperature for 40 minutes, after which sodium iodide (462 mg) was added while saturating the vessel with nitrogen gas. Finally, methyl iodide was added (density = 2.28 g/cm^3, 4.5 mL)

to the pGC suspension and the reaction stirred under a nitrogen atmosphere in a pre-heated oil-bath at 36 °C. The reaction was stopped after 1.5, 4.5 and 24 hours to obtain a level of quaternisation of <10%, ~10%, and ~20%, respectively. Subsequently, the product was precipitated with diethyl ether (1.2 L) and left to settle overnight. The supernatant was then decanted, and the product washed with diethyl ether (300 mL) and subsequently decanted. Afterwards, the crude residue was solubilised in methanol (50 mL) and dialysed extensively against distilled water (5 L) using a dialysis membrane of MWCO 3.5 kDa with a minimum of six changes over 48 hours. Subsequently, to remove the iodide ions in solution, the dialysate was treated with an ion exchange resin amberlite IRA-410 (6 g resin / 1 g polymer) and stirred for a minimum of 15 minutes. The resin mixture was filtered into a clean flask using a glass sintered filter (porosity 3). The filtered solution was then snap frozen and freeze-dried to obtain a white fibrous solid.

Gel Permeation Chromatography with Multi-Angle Laser Light Scattering (GPC-MALLS) determined the molecular weight of the synthesised GCPQ, and the structure was studied using NMR spectrometry. The degree of palmitoylation (DP) was determined using the (Equation 2-1), and the degree of quaternisation (DQ) was determined using the (Equation 2-2). Proton NMR (^{1}H-NMR) spectra were used to compare the ratio of the integrals from the palmitoyl methyl protons signal (δ = 0.86 ppm) or quaternary ammonium methyl groups (δ = 3.4 ppm), to that of the integrals from the sugar ring/ethylene glycol (δ = 3.5 – 4.5 ppm). As the sugar ring protons are constant in every repeating unit, this allows us to calculate the percentage of sugar units which contain palmitoyl or quaternary groups.

Equation 2-1

$$\boldsymbol{DP}\ (\%) = \left[\frac{integral\ at\ \delta\ 0.86\ ppm}{3} \div \frac{integral\ at\ \delta\ 3.5 - 4.5\ ppm}{9}\right]$$

Equation 2-2

$$\boldsymbol{DQ}\ (\%) = \left[\frac{integral\ at\ \delta\ 3.4\ ppm}{9} \div \frac{integral\ at\ \delta\ 3.5 - 4.5\ ppm}{9}\right]$$

The ratio of quaternary ammonium to palmitoyl groups (QPR) was calculated as follows:

Equation 2-3

$$\boldsymbol{QPR} = \left[\frac{DQ\ (\%)}{DP\ (\%)}\right]$$

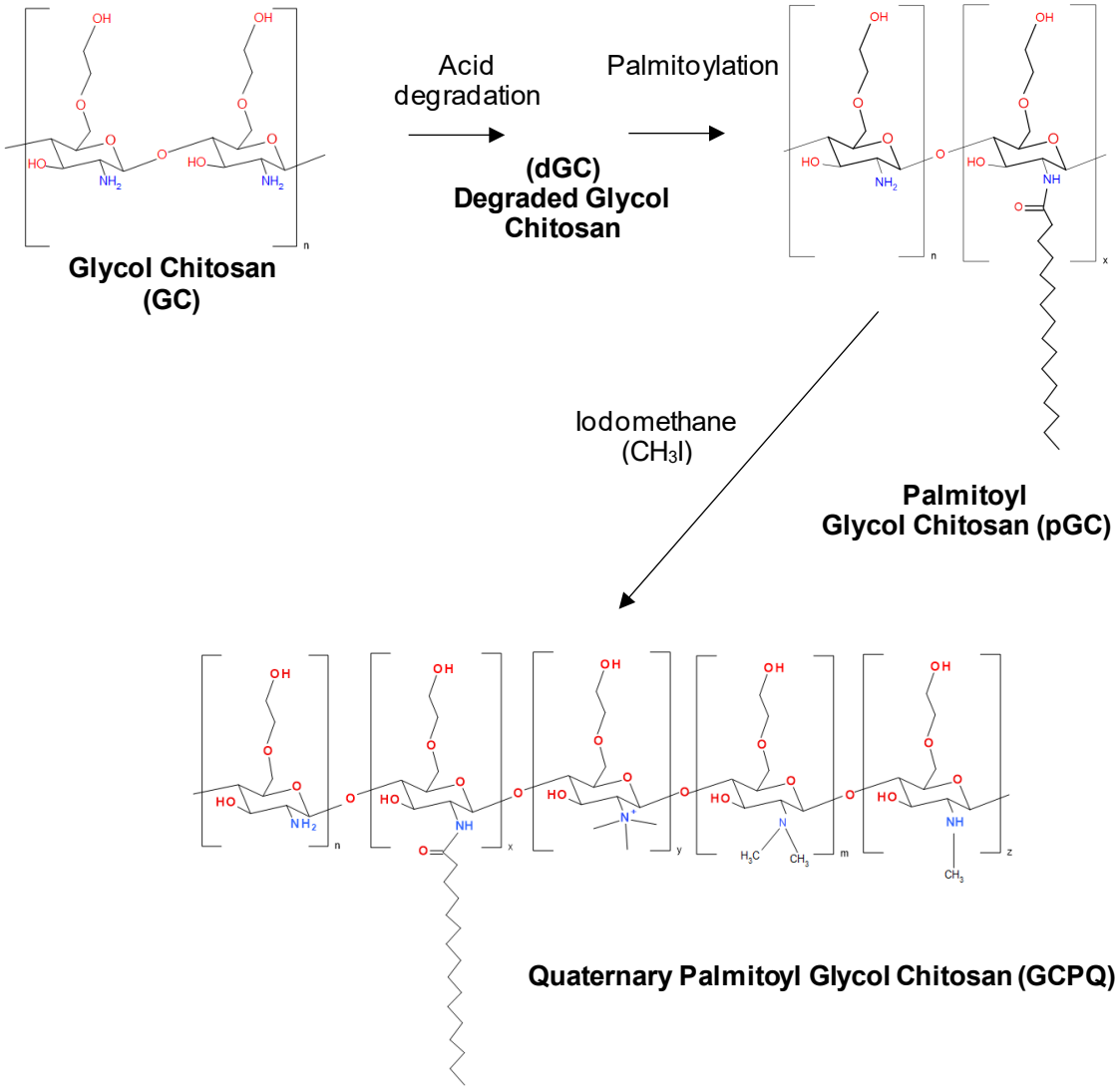

Figure 2-3: Schematic representation of the synthesis of GCPQ.

Structure of GCPQ, n = unmodified GC units, x = GC units with hydrophobic palmitoyl group, y = GC units with trimethyl ammonium group (quaternary ammonium), m = dimethyl and z = monomethyl ammonium groups formed during quaternisation.

2.3. Polymer characterisation techniques

2.3.1. Nuclear magnetic resonance

Nuclear magnetic resonance is a spectroscopic technique that allows for structure elucidation and quantification [139]. The principle of NMR is based on the fact that the signal is produced by the excitation of the nuclei in the sample that can absorb energy when the sample is placed in an external magnetic field, and subjected to a radio frequency that depends on the type of nucleus (e.g. proton ^{1}H or carbon-13 ^{13}C), and the chemical environment of the nucleus [140]. The characteristics of the chemical structure of the molecule are obtained from the signal patterns produced when the excited nucleus relaxes to the lower energy state [141].

The presence of electron-withdrawing atoms will have an impact on the resonance frequency and will result in different chemical shifts (δ). The chemical shift of an atom is the difference between the resonance frequency of the atom being analysed and that of a reference standard [142]. These chemical shifts are generally recorded as peaks in the NMR spectrum and the relative area under these peaks are directly proportional to the number of protons giving rise to the signal [143]. Protons that are surrounded by electron-donating groups are shielded protons, and the chemical shift will appear to the right of the ^{1}H-NMR. In contrast, protons that are close to high electron-withdrawing groups will require a less applied magnetic field to change the direction of their spin and are known as de-shielded protons, and the chemical shift will appear to the left of the ^{1}H-NMR. Moreover, ^{1}H-^{1}H Correlated Spectroscopy

(COSY) is used as a two-dimensional tool that shows the interaction between neighbouring protons [144].

^{1}H and COSY NMR were performed on dGC, pGC and GCPQ. In a glass vial, each compound (10 mg) was dissolved in a suitable solvent (1 mL). One mL of deuterium oxide (D_2O) was used to dissolve dGC, pGC was dissolved in a mixture of deuterated methanol (MeOD): D_2O: deuterated acetic acid (CD_3CO_2D) (8:4:1), and GCPQ was dissolved in MeOD with a drop of deuterium chloride. Subsequently, each solution (700 µL) was transferred to a clean NMR tube and analysed using Bruker AMX 500 MHz spectrometer (Bruker Ltd., Coventry, UK). The spectra obtained were processed using Topspin software for windows.

2.3.2. Gel Permeation Chromatography-Multi-Angle Laser Light Scattering (GPC-MALLS)

Gel Permeation Chromatography coupled with Multi-Angle Laser Light Scattering detector, and a differential Refractive Index (dRI) detector was used to measure the molecular weight of the polymer produced [145]. GPC is a size exclusion chromatography (SEC) technique which separates macromolecules based on the size of the molecules. SEC technique involves the use of column filled with beads that contain pores of different sizes which make up the stationary phase and the solvent for the samples that is the mobile phase. In SEC, the polymer is dissolved in the mobile phase and injected into a column packed with porous particles of defined pore size [146]. The high molecular weight material elutes first, while the low molecular weight material elutes later from the SEC column [146]. This is because small-sized molecules get trapped in the pores and therefore move through the column slowly. In contrast, larger-sized molecules move faster through the column because they do not fit into the pores of the gel [146].

Simultaneous measurement of light scattering intensity and concentration allows direct determination of the weight-average molecular weight of the eluted fraction [147], therefore, the multi-angle laser light scattering detector, which measures the intensity of light scattered by the polymer was used. The eluting compound is characterised for molecular weight by measuring changes in the refractive index of the sample, with changes in concentration (dn/dc).

The molecular weights of the GCPQ polymers were determined using a Wyatt gel permeation chromatography multi-angle laser light scattering instrument equipped with Dawn Heleos II MALLS, Optilab rEX interferometric refractometer (λ= 690 nm) and quasielastic light scattering (QELS) detectors (Wyatt Technology Corporation, Santa Barbara, USA). The mobile phase used was filtered acetate buffer (0.25 M sodium acetate, 0.2 M glacial acetic acid, pH = 4.0) and methanol (35: 65 v/v) for GCPQ.

Polyethene glycol (PEG) analytical standard for GPC (MW 20,000 Da) was used as a reference standard before the measurements. PEG samples were prepared and filtered at a concentration (1 mg/mL) in the mobile phase. Primary polymer samples were dissolved on running buffer (10 mg/mL) and filtered using 0.2 µm PTFE syringe filter. Samples (1 mg/mL, 200 µL) were injected using an Agilent 1200 series autosampler (Agilent Technologies Ltd., Cheshire, UK) on to a POLYSEP-GFC-P guard column (35 × 7.8 mm) attached to a POLYSEP-GFC-P 4000 column (300 × 7.8 mm) from (Phenomenex, Torrance, UK). The measurements were performed at room temperature with a mobile phase flow rate of 0.7 mL/min and a run time of 20 minutes.

Following injection of the polymer, the specific refractive index increments over-concentration (dn/dc) were measured by manually injecting six different concentrations ranging from 1.0 – 6.0 mg/mL prepared as shown in (Table 2-1). Samples were dissolved in the mobile phase, passed through the dRI detector set at 25°C and wavelength of 690 nm. The pump flow rate was 0.7 mL/min. The data

obtained from both dn/dc and GPC-MALLS experiment were analysed using the ASTRA software for Windows, supplied by Wyatt Technologies.

Table 2-1: Preparation of samples using a stock solution (primary sample°ontaining 10 mg/mL polymer) for dn/dc measurements.

Sample #	Running buffer (µL)	Primary sample (µL)	Final Volume (µL)	Polymer Conc. (mg/mL)
1	1350	150	1500	1
2	800	200	1000	2
3	700	300	1000	3
4	600	400	1000	4
5	500	500	1000	5
6	400	600	1000	6

2.4. Results and discussion

2.4.1. NMR

Proton- and COSY NMR confirmed the chemical structure of the synthesised polymers, the degree of palmitoylation, and the degree of quaternisation. The two-dimensional correlation spectroscopy NMR was used to identify the cross-correlation between protons on the spectrum [148].

Figure 2-4 and Figure 2-5 showed the NMR spectrum of the degraded glycol chitosan, and the protons assignments are given in Table 2-2. The reactions yield of the degradation of GCs were ~ 60 – 80% from the undegraded GC used.

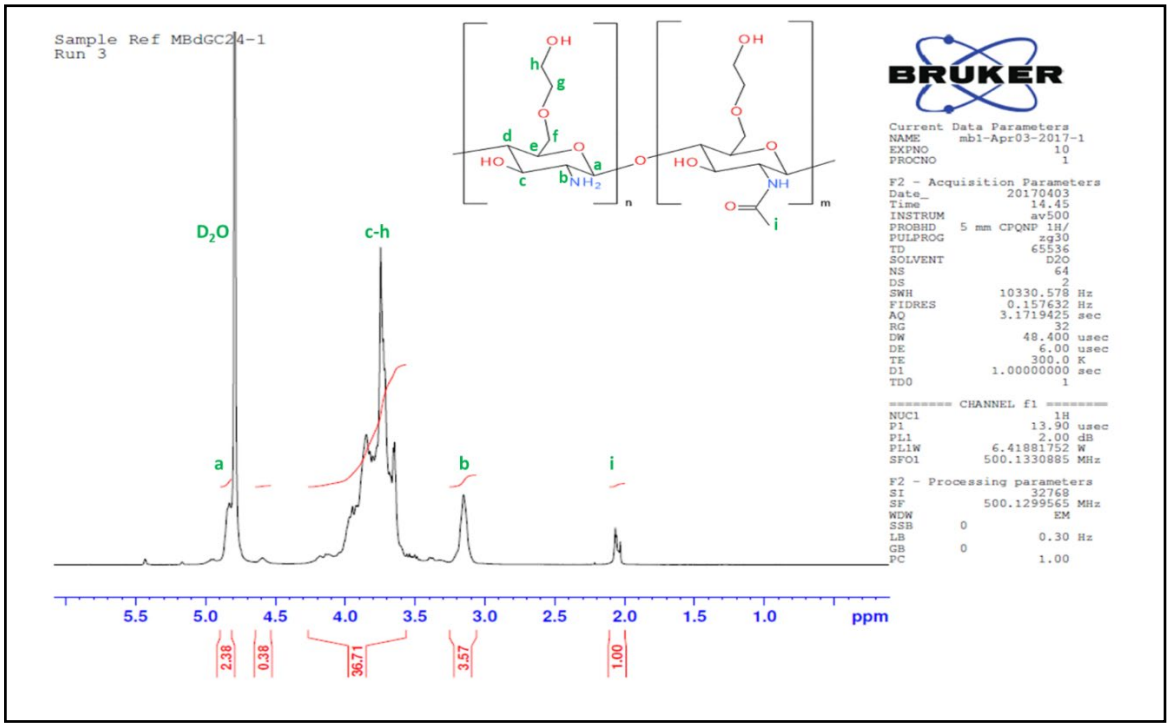

Figure 2-4: Proton NMR for degraded glycol chitosan.

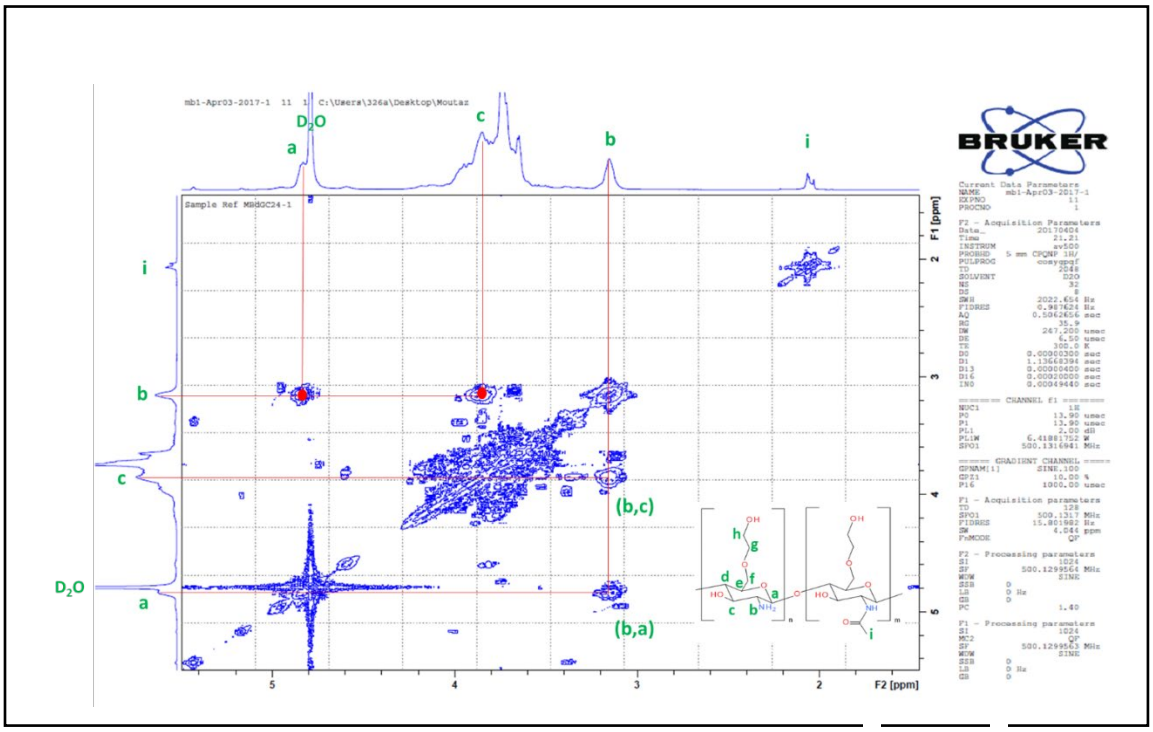

Figure 2-5: COSY NMR for degraded glycol chitosan (dGC).

Table 2-2: Proton assignments for degraded glycol chitosan (dGC).

Item	NMR chemical shift (ppm)	Corresponding proton on the structure
i	2.09	CH3 (acetyl group)
b	3.1-3.2	CH (Carbon 2)
c-h	3.5-4.5	CH (sugar ring/ethylene glycol
D_2O	4.7	Water protons
a	4.8	CH (Carbon 1)

Following the degradation of the glycol chitosan, the palmitoylation step was carried out. Figure 2-6 and Figure 2-7 showed the generated spectrum of the palmitoylated glycol chitosan (pGC). The multiple peaks appeared in (δ = 2.04-2.09) is due to the presence of deuterated acetic acid in the solvent used to dissolve pGC. The protons assignments for palmitoylated GC are given in Table 2-3.

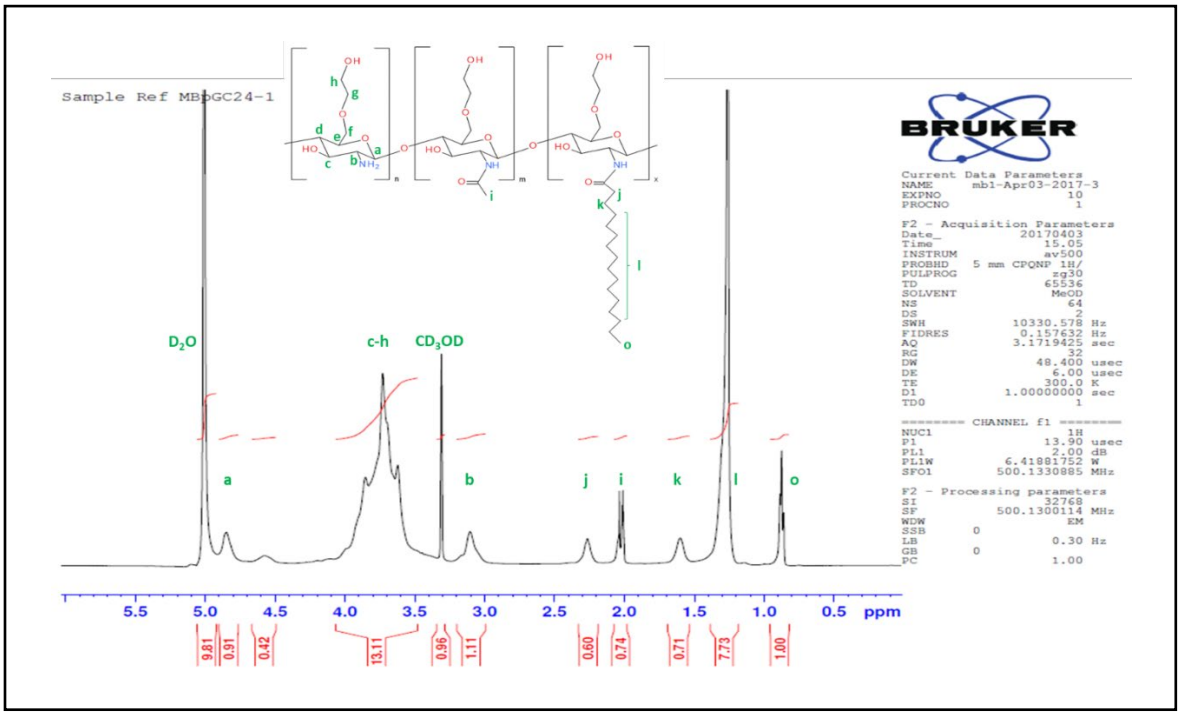

Figure 2-6: ^{1}H-NMR for palmitoylated glycol chitosan (pGC).

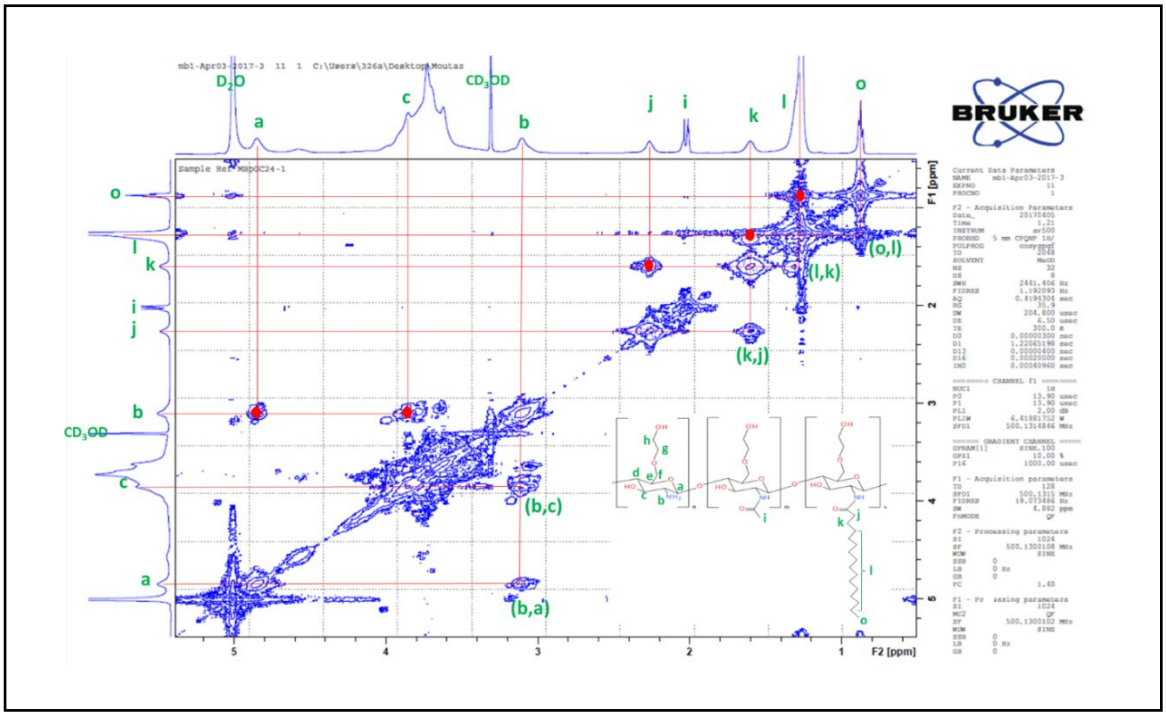

Figure 2-7: COSY NMR for palmitoylated glycol chitosan (pGC).

Table 2-3: Proton assignments for palmitoylated glycol chitosan (pGC).

Item	NMR chemical shift (ppm)	Corresponding proton on the structure
o	0.86	CH3 (Palmitoyl group)
l	1.2-1.4	CH2 (Palmitoyl chain)
k	1.6	-**CH2**-CH2-(CO)- of Palmitoyl chain
i	2.04-2.09	CH3 (acetyl group), multiple peaks is due to deuterated acetic acid
j	2.2-2.3	-CH2-**CH2**-(CO)- of Palmitoyl chain
b	3.1-3.2	CH (Carbon 2)
CD_3OD	3.31	Methanol protons
c-h	3.5-4.5	CH (sugar ring/ethylene glycol)
D_2O	5.0	Water protons
a	4.8	CH (Carbon 1)

Following the palmitoylation of the degraded glycol chitosan, the quaternisation step was carried out. Figure 2-8 and Figure 2-9 showed the generated spectrum of the GCPQ. The protons assignments for GCPQ are given in Table 2-4.

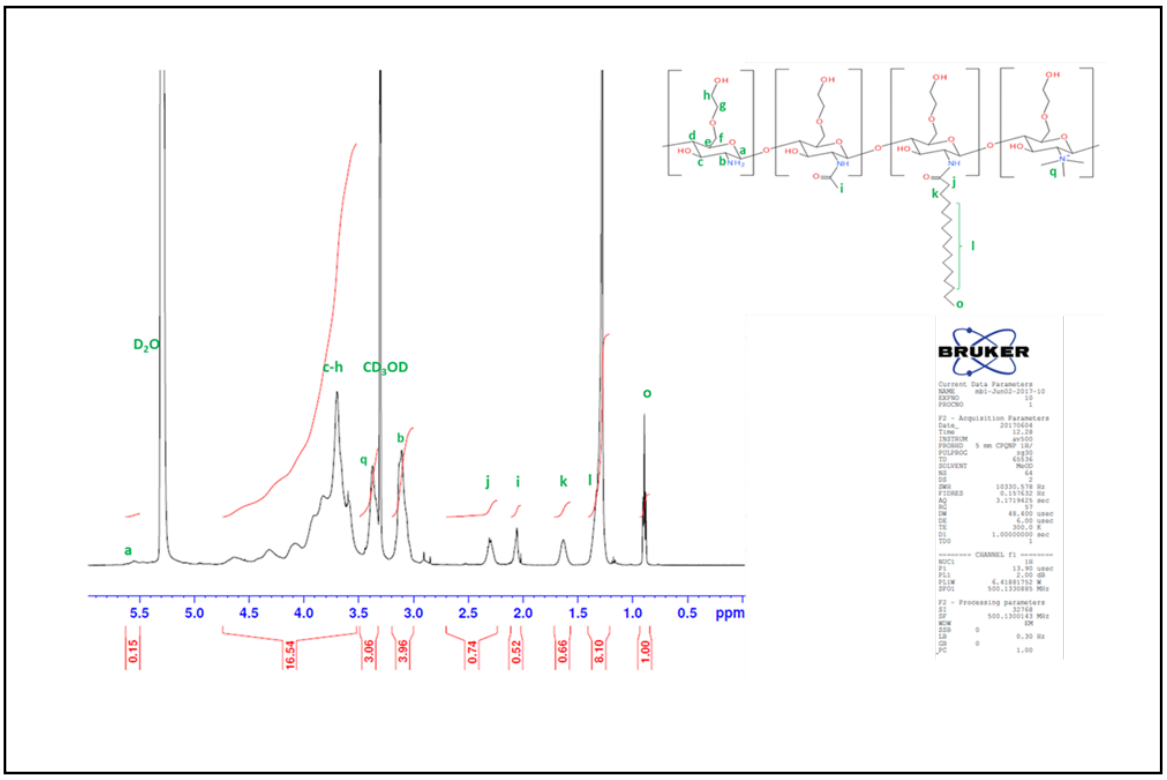

Figure 2-8: ^{1}H-NMR for quaternary ammonium palmitoyl glycol chitosan (GCPQ) with a nominal palmitoylation of 20 mole%.

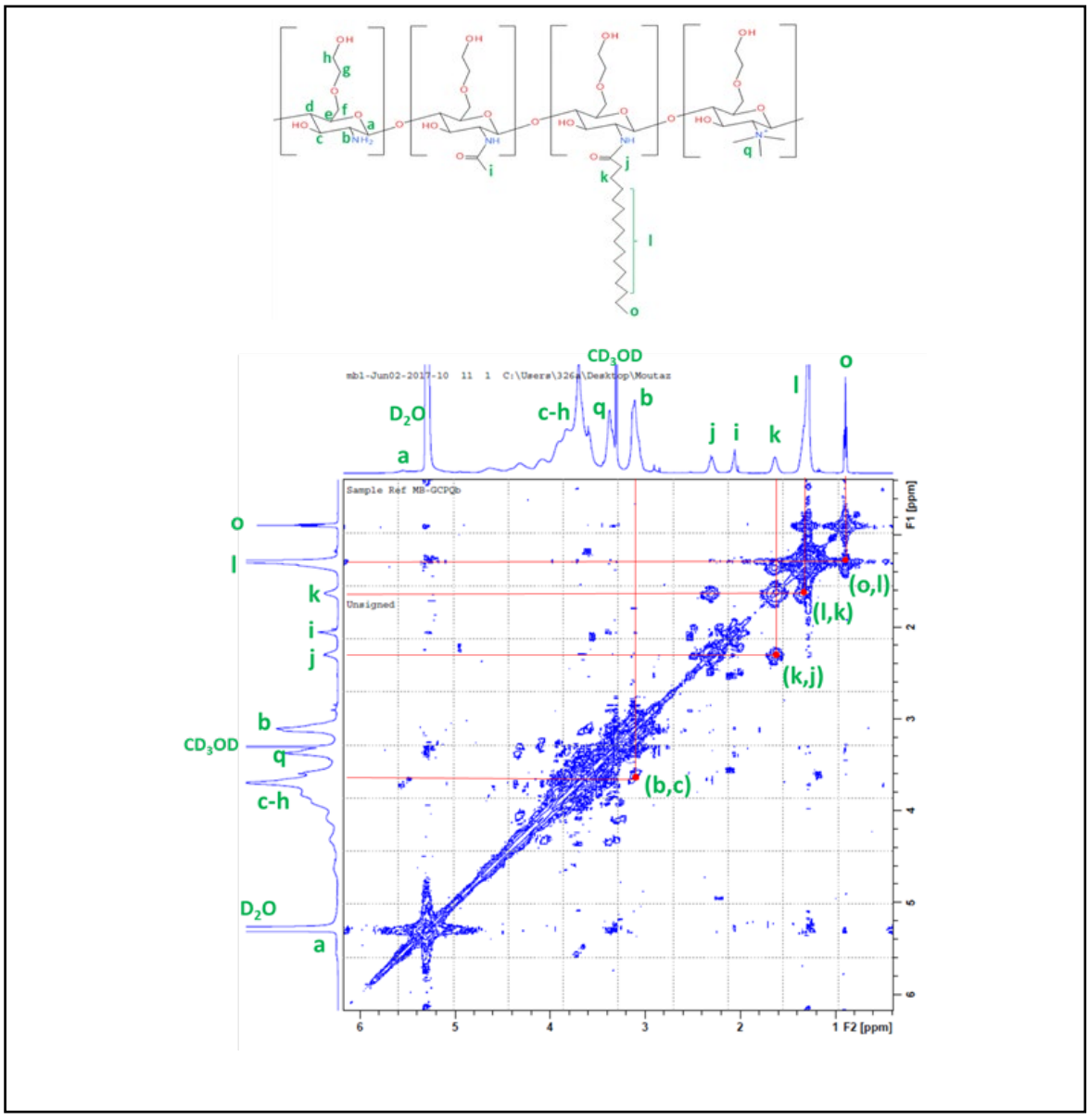

Figure 2-9: COSY NMR for quaternary ammonium palmitoyl glycol chitosan (GCPQ).

Table 2-4: Proton assignments for quaternary ammonium palmitoyl glycol chitosan (GCPQ).

Item	NMR chemical shift (ppm)	Corresponding proton on the structure
o	0.86	CH3 (Palmitoyl group)
l	1.2-1.4	CH2 (Palmitoyl chain)
k	1.6	-**CH2**-CH2-(CO)- of Palmitoyl chain
i	2.09	CH3 (acetyl group),
j	2.2-2.3	-CH2-**CH2**-(CO)- of Palmitoyl chain
b	3.1-3.2	CH (Carbon 2)
CD_3OD	3.31	Methanol protons
q	3.4	Quaternary protons
c-h	3.5-4.5	CH (sugar ring/ethylene glycol)
D_2O	5.3	Water protons
a	5.6	CH (Carbon 1)

The degree of palmitoylation (DP%), the degree of quaternisation (DQ%), and the ratio of quaternisation to a palmitoylation (QPR) of the synthesised polymers are summarised in Table 2-5. The various GCPQ polymers were named according to the order of manufacturing. For example, GCPQ01 was synthesised first followed by GCPQ02.

The level of palmitoylation was calculated by comparing the ratio of palmitoyl methyl protons (δ = 0.86 ppm) to sugar protons (δ = 3.5 – 4.5 ppm) and the level of quaternisation by comparing the ratio of quaternary ammonium (δ = 3.4 ppm) to sugar protons as described in Equation 2-1 and 2-2, respectively.

Polymers were synthesised to obtain a similar level of palmitoylation ~ 20%, and different levels of quaternisation of <10%, ~ 10%, and ~ 20%. As shown in Table 2-5, all polymers possess a degree of palmitoylation ranging from 18% to 28%, with a reaction yield ~ 70 – 100% from the mass of dGC used. The reproducibility of synthesis, as well as the level of substitution, are essential. Reproducible substituent specifications are important for GCPQ as both the CMC and drug encapsulation levels are dependent on the hydrophobicity of the polymer [138]. Apart from the first two polymers synthesised, i.e., GCPQ01 (level of palmitoylation 25%) and GCPQ02 (level of palmitoylation 28%), the remaining polymers synthesised showed a consistent and reproducible level of palmitoylation ~ 20%. The marginal higher level of palmitoylation observed in GCPQ01 and GCPQ02 is mainly attributed to the lack of experience when these polymers were initially synthesised.

The hydrophobicity of the polymer is one of the essential factors affecting the characteristics of materials. A higher level of palmitoyl substitution produces a more

hydrophobic polymer and results in more efficient hydrophobic drug encapsulation [138]. Martin et al. investigated the various degree of palmitoylation in controlling the release of a model hydrophilic drug dextran. The most hydrophobic palmitoyl glycol chitosan gel (20.31±2.22 mol% palmitoylation) resulted in the slowest controlled release of dextran compared to the degree of palmitoylation of 12 and 11% [149]. Le et al. showed that the polymer hydrophobicity affects drug encapsulation and oral drug delivery of cyclosporine A using amphiphilic poly(ethylenimine) [150]. They showed that the level of hydrophobic derivatisation was determined as (high > 12 mole%, medium = 7-12 mole% and low < 7 mole%) [150], in which the drug loading is promoted by an increase in polymer hydrophobicity [150]. Therefore, a level of palmitoylation of ~ 20% was chosen to synthesise all the polymers and will be used for the drug encapsulations studies.

GCPQ polymers were methylated to obtain a level of quaternisation of <10%, ~10%, and ~20%, as shown in (Table 2-5). Quaternary chitosan derivatives are characterised by their permanent cationic charge resulting in an increase of chitosan solubility in water and keeping it soluble over a wide range of pH values [151]. It has been reported that the water solubility of *N*-trimethyl chitosan is highly dependent on the degree of methylation [152]. Different levels of quaternisation were chosen to study the effect of this modification on the drug encapsulation and in the *in vitro* permeability assay, which will be described in Chapter three and Chapter four, respectively.

Table 2-5: General characterisation of the synthesised polymers.

Polymer	Degradation time (hr)	dGC:PNS mass ratio*	DP (%)	pGC:CH_3I mass ratio#	DQ (%)	QPR
MB-GCPQ01	24	1: 0.37	25	1: 3.42	5	0.187
MB-GCPQ02	24	(w/w)	28	(w/w)	10	0.350
MB-GCPQ03	48		21		5	0.237
MB-GCPQ04	48		20		9	0.463
MB-GCPQ05	2		19		8	0.433
MB-GCPQ06	2		18		13	0.753
MB-GCPQ07	24		22		10	0.483
MB-GCPQ08	48		21		14	0.640
MB-GCPQ09	2		18		16	0.913
MB-GCPQ10	24		18		19	1.020
MB-GCPQ11	24		21		10	0.490
MB-GCPQ12	24		22		16	0.753
MB-GCPQ13	6		22		15	0.697
MB-GCPQ14	6		19		19	1.000
MB-GCPQ15	24		18		20	1,083
MB-GCPQ16	48		18		18	1.000

* dGC:PNS mass ratio; 1 g of dGC: 0.37 g of PNS to obtain ~20% DP.

pGC:CH_3I mass ratio; 1 g of pGC: 3.42 g of CH_3I (1.5 mL). DQ% depends on the reaction time.

2.4.2. GPC-MALLS

Finally, the GCPQs were named using the following nomenclature: GC(MW in kDa), P(Mole% palmitoyl groups), and Q(Mole% quaternary ammonium groups). For example, GCPQ02 with a molecular weight of 15 kDa and containing 28 mole% palmitoyl groups and 10 mole% quaternary ammonium groups would be named as follows: GC15P28Q10.

The molecular weight results were expressed as the number averaged molecular weight (Mn), and the weight averaged molecular weight (Mw). The polydispersity (PDI) was calculated as a ratio of Mw/Mn, and the dn/dc was measured. The absence of the molecular weight data for other polymers and dGC is due to the unavailability of the instrument.

Table 2-6 shows the characteristics of the analysed polymers. The PEG reference standard (20 kDa) was measured before each measurement. The MW of the PEG standard was 21 kDa, and the Mn was 20, while the PDI was reported as 1.056. This value demonstrates the applicability of the instrument and represents a valid measure for further analysis.

Glycol chitosan was degraded for (2, 6, 24, and 48 hours) to obtain high, moderate and low molecular weight polymers. Synthesised GCPQ polymers with molecular weights lower than 20 kDa were considered low molecular weight polymers. The molecular weights of polymers from 20 to 40 kDa were considered moderate, and polymers with molecular weights higher than 40 kDa were considered high molecular weight polymers. Therefore, these polymers were synthesised to

investigate the effect of the polymer molecular weight on the drug encapsulation studies and the *in vitro* permeability assay, which will be described in chapter three and chapter four, respectively.

The PDI of the polymers, calculated as the ratio of the weight average molecular weight to the number average molecular weight, ranged between 1.08 to 1.34 for all the GCPQs synthesised, suggesting a narrow molecular weight distribution of each batch of GCPQ polymer produced.

Table 2-6: GPC-MALLS data obtained for the analysed polymers.

Polymer	Category for MW	dn/dc (mL/g)	Mw (kDa)	Mn (kDa)	PDI (Mw/Mn)
PEG	-	0.130	20.94	19.84	1.056
MB-GCPQ02	Low	0.150	14.83	11.94	1.242
MB-GCPQ06	High	0.154	53.33	39.97	1.334
MB-GCPQ07	Low	0.155	15.90	12.62	1.260
MB-GCPQ08	Low	0.155	11.87	10.13	1.172
MB-GCPQ09	High	0.140	60.12	45.62	1.318
MB-GCPQ10	Low	0.145	16.05	12.74	1.260
MB-GCPQ11	Low	0.147	14.69	12.63	1.163
MB-GCPQ12	Low	0.155	18.16	15.05	1.207
MB-GCPQ13	Moderate	0.137	27.02	21.95	1.231
MB-GCPQ14	Moderate	0.133	29.87	25.31	1.180
MB-GCPQ15	Low	0.140	15.03	13.24	1.135
MB-GCPQ16	Low	0.139	10.15	9.36	1.085

The GPC-MALLS for the reference standard (PEG, 20 kDa) is shown in (Figure 2-10). The chromatogram shows an elution time of 12 minutes corresponding to 20.94 kDa with a polydispersity of 1.056 The dn/dc value used for the PEG was 0.134 mL/g, as reported in the literature [153]. The refractive index shows a peak at about 16 minutes which is likely from the mobile phase.

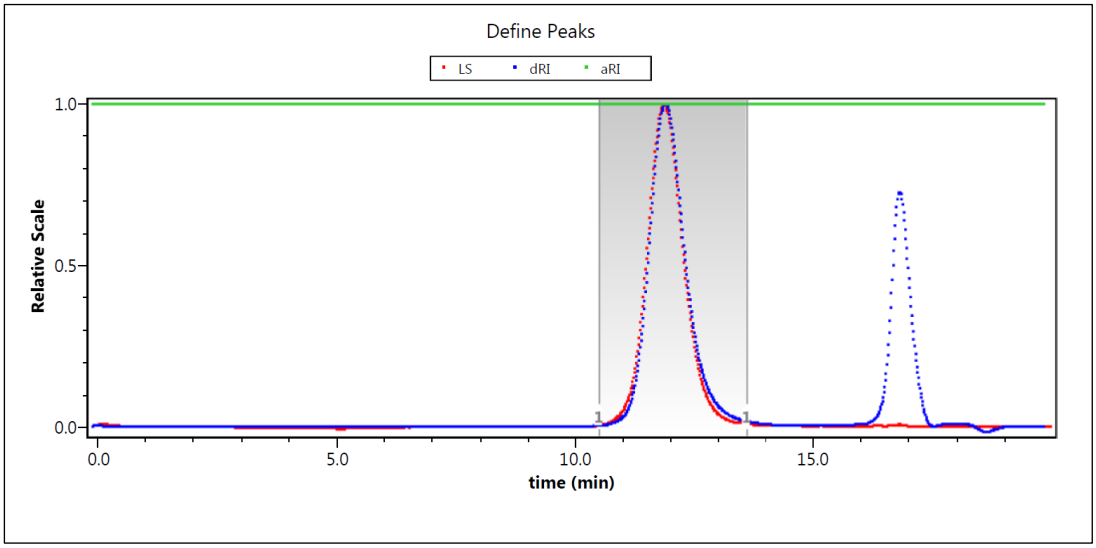

Figure 2-10: GPC-MALLS chromatogram of the reference standard PEG.

Red-line; Light scattering, Blue-line; Refractive index.

The GPC-MALLS for the analysed GCPQ is shown in (Figure 2-11). The chromatogram shows an elution time of 12 minutes, corresponding to the molecular weight as described in (Table 2-6). The dn/dc obtained for the GCPQ ranged from 0.133 to 0.155 mL/g. The refractive index shows a small peak at about 16 minutes, which is likely a ghost peak due to the salts in the mobile phase.

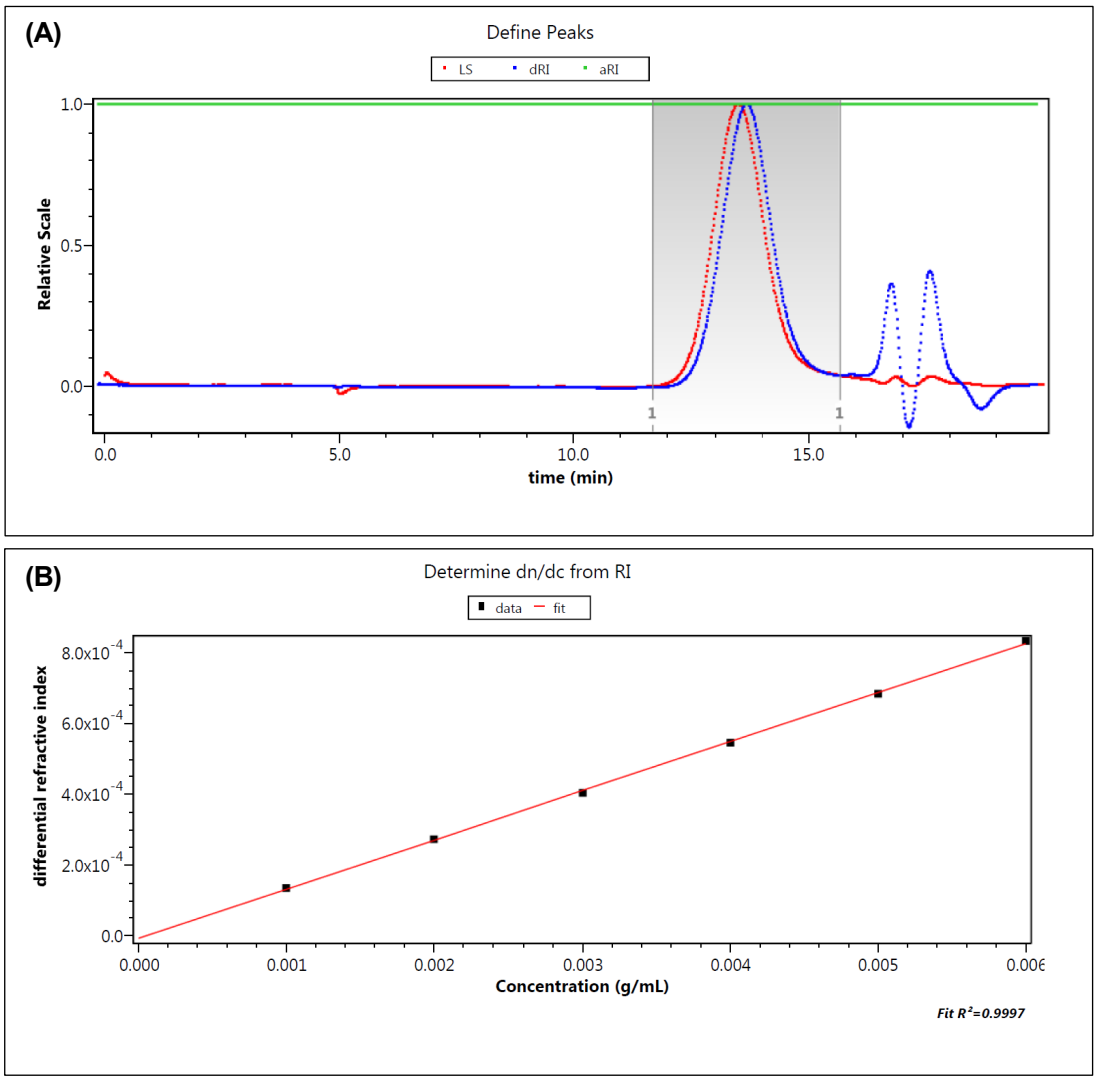

Figure 2-11: A typical GPC-MALLS chromatogram of analysed GCPQ.

(A); GCPQ, Red-line; Light scattering, Blue-line; Refractive index, Grey area; measured area. **(B)**; dn/dc.

2.5. Conclusion

The amphiphilic polymer GCPQ was synthesised and characterised. GCPQ polymers with different molecular weights and a similar degree of DP% and varying degree of DQ% were synthesised, as previously mentioned, by altering the reaction parameters. As we are aiming to manufacture aqueous-based eye drops formulations, these polymers will be used for further studies in drug formulation and mammalian cells assays.

3. Drug encapsulation studies

3.1. Introduction

Emerging drugs candidates are generally hydrophobic, as these hydrophobic molecules show superior binding to receptor targets [135]. Their low aqueous solubility represents a significant obstacle in achieving adequate ocular bioavailability [154]. Different approaches have been exploited to overcome the low aqueous solubility of drugs including chemical modifications to form a more soluble salt, particle size reduction of the formulation through high-pressure homogenisation [155], complexation with cyclodextrins, the use of surfactants, and more recently the exploitation of the amphiphilic properties of polymers [135].

Amphiphilic polymers bearing an alkyl chain can form highly stable self-assemblies in aqueous media, with critical micellar concentrations in the μM range [135]. GCPQ is an amphiphilic polymer that has been utilised to facilitate the dissolution of hydrophobic drugs by forming polymeric micelles [156]. A previous study demonstrated that GCPQ micelles could improve the ability to encapsulate hydrophobic drugs and that GCPQ micelles adhere to and penetrate the mucus layer [135]. Also, GCPQ has been shown to increase the transport of hydrophobic drugs across the cornea [135].

Thus, this chapter will focus on using GCPQ to encapsulate rapamycin and tacrolimus as model drugs to investigate the topical ocular delivery to the posterior and anterior segment of the eye, respectively (Figure 3-1).

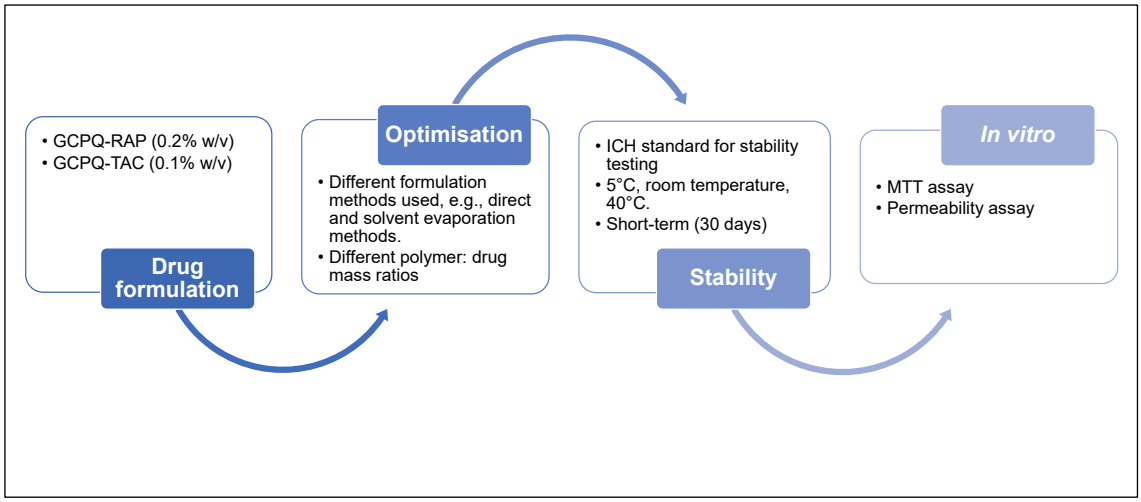

Figure 3-1: Illustration of the experimental plan for the drug formulations studies.

3.2. Model drugs:

3.2.1. Rapamycin

Rapamycin (RAP), also known as sirolimus, is a macrocyclic lactone (Figure 3-2) produced by *Streptomyces hygroscopicus* [157]. Rapamycin, (Rapamune®), developed by Wyeth Pharmaceuticals (New Jersey, USA), is available as an oral solution (1 mg/mL) and tablets (0.5, 1 and 2 mg) [158]. RAP is an immunosuppressive agent that acts on the mammalian target of rapamycin (mTOR) [159]. mTOR is a serine/threonine-specific protein kinase, which displays a central role in regulating cell growth and metabolism [160]. RAP binds to the immunophilin, FK binding protein (FKBP12) to interact with mTOR and inhibit its function, leading to inhibition of cell growth from the G_1 to S phase [161] and cell proliferation [159]. RAP does not interact with calcineurin or its downstream effectors [161].

An effective topical administration of RAP requires the permeation of the drug to the ocular tissues. However, due to its physicochemical characteristics (Table 3-1), RAP is unlikely to produce high ocular permeation rates. RAP is practically insoluble in water (2.6 µg/mL), has a high molecular weight (MW 914 Da), and contains no functional groups that are ionisable in the pH range between 1 and 10 [162]. RAP is extremely hydrophobic with a reported log P = 5.77 [34].

3.2.2. Tacrolimus

Tacrolimus (TAC) (Figure 3-2) is an immunomodulatory and anti-inflammatory agent, produced by *Streptomyces tsukabaensis* [163]. In contrast to RAP,

TAC/FKBP12 complex binds to calcineurin and inhibits its serine-threonine phosphatase activity, which is important for activating nuclear factors of activated T-lymphocytes (NFATs) [163]. The NFAT group of transcription factors regulates the production of IL-2 and several T-cell-specific stimulators [163]. Tacrolimus suppresses T cell activation and IL-2 production by binding to an immunophilin and inhibiting the enzymatic activity of calcineurin [164]. TAC inhibits the progression from the G_0 to G_1 phase of the cell cycle [161].

TAC displays similar effects to cyclosporine but at 100 times lower concentrations [165]. TAC topical ointment (Protopic®, 0.03 and 0.1% w/w) from Fujisawa Healthcare, Inc., (Illinois, USA) has received the FDA approval in 2006 [166]. One gram of Protopic 0.1% ointment contains 1.0 mg of TAC as TAC monohydrate (0.1% w/w) [167]. This TAC skin ointment is licensed for the treatment of moderate to severe atopic eyelid diseases and may have secondary benefits for AKC [168]. Ointment dosage forms are oily semisolid and may associate with discomfort and irritation if applied topically to the eye [169]. Also, ophthalmic ointments are coupled with greasiness and transient blurring of vision. Thus, patients may prefer aqueous ocular formulations or reserve the use of ophthalmic ointments to night-time application [170].

The development of TAC ophthalmic formulations as a clear aqueous solution is challenging due to its hydrophobic characteristics (log P = 2.74) [171]. TAC is insoluble in water (4-12 μg/mL) [172,173], and therefore aqueous formulations of the drug at clinically useful concentrations are not easy to manufacture.

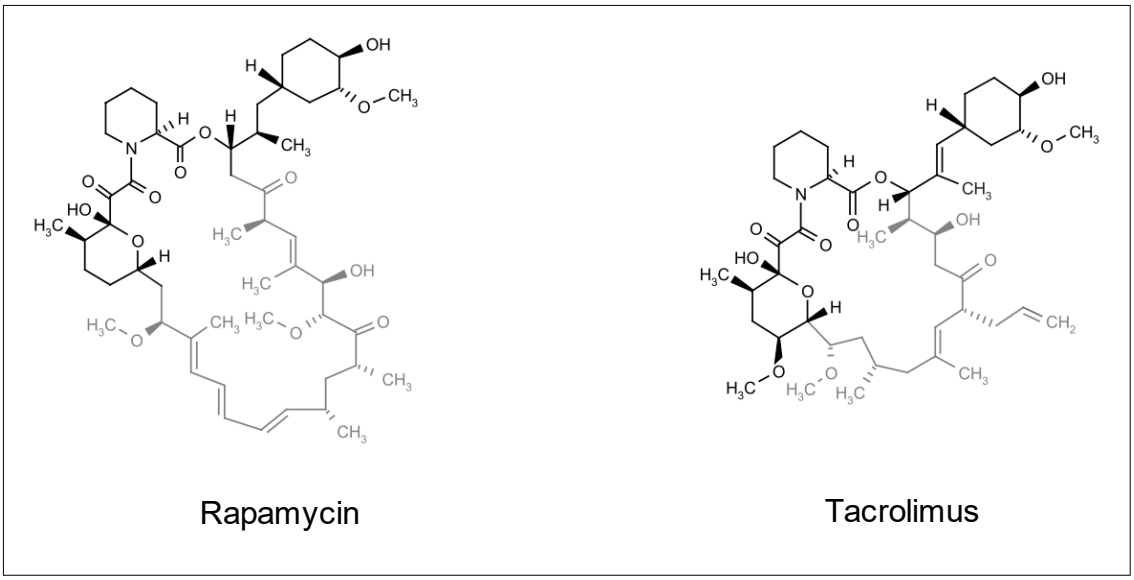

Figure 3-2: Chemical structure of rapamycin and tacrolimus.

The binding domain is highlighted in grey.

The physicochemical properties of model drugs are presented in (Table 3-1).

Table 3-1: Physicochemical properties of the model drugs

Property	**RAP**	**TAC**
Appearance	white to off-white powder [174]	white crystalline powder [175]
Molecular formula	$C_{51}H_{79}NO_{13}$ [176]	$C_{44}H_{69}NO_{12}$ [175]
Molecular weight	914.187 g/mol [176]	804.02 g/mol [177]
Water solubility	2.6 µg/mL [162]	4-12 µg/mL [172,173]
Log *P*	5.77 [34]	2.74 [171]

3.3. Encapsulation studies

3.3.1. Materials

Chemical	Supplier
Rapamycin	Cambridge Biosciences (Cambridge, UK)
Tacrolimus	Generon Ltd. (Slough, UK)
Ethanol (absolute)	UCL School of Pharmacy (London, UK)
Acetonitrile HPLC grade	Fisher Scientific (Loughborough, UK)
Sodium hydroxide	Sigma-Aldrich (Gillingham, UK)
Phosphoric acid (H_3PO_4) for HPLC	SLS LTD (Nottingham, UK)
Glycerol	Fisher Scientific (Loughborough, UK)
Osmometer reference standard (300 mOsmol/L)	Reagecon Diagnostics Ltd., (Clare, IE)
Polyethersulfone (PES) filters 0.22 µm	VWR (Leicestershire, UK)
Water double deionised	Merck Millipore (Hertfordshire, UK)

3.3.2. Methods

3.3.2.1. Encapsulation of RAP

Different approaches were used to encapsulate RAP with different GCPQ polymers. First, a direct approach was used to encapsulate RAP with GCPQ. This method was used to encapsulate GCPQ with propofol [178], and doxorubicin [179]. Briefly, an aqueous dispersion of GCPQ in 2.6% w/v glycerol (5 mg/mL) was added to the powdered RAP (1 mg) to produce RAP in the formulation with a nominal drug concentration (0.1% w/v). The mixture was vortex-mixed for 30 minutes at room temperature. The mixture was subsequently sonicated using MSE Soniprep 150 sonicator from MSE UK Ltd. (London, UK) at 50% of its maximum output (10 Amplitude microns) for 5 minutes in an ice bath. The mixture was subsequently adjusted for pH using a calibrated pH meter PHS-W Series Benchtop pH/mV meter from SciQuip Ltd. (Shropshire, UK) using 1.0 M NaOH, and a simulated sterile filtration step was carried out using a 0.22 µm sterile filter and the drug content, particle size distribution, and zeta potential were measured.

Secondly, a thin-film hydration method was used to encapsulate RAP with GCPQ. This method was previously reported to encapsulate hydrophobic compounds [180]. Briefly, RAP formulations (0.2% w/v) were prepared with (5:1, 7.5:1, and 10:1) polymer-to-drug mass ratios. RAP solution was produced from RAP powder (2 mg) dissolved in ethanol (1 mL). GCPQ dispersions were prepared from (10 mg, 15 mg, and 20 mg) of GCPQ dispersed in filtered deionised water (1 mL), respectively.

RAP solution (1 mL) was transferred into a glass vial, and the GCPQ dispersion (1 mL) was added to make a mixture of GCPQ: RAP (2 mL). The mixture was then vortex-mixed for 30 minutes at room temperature and evaporated to dryness within the speed vac using Savant Vacuum Evaporator from ThermoFisher Scientific (Waltham, USA) at 45°C and spun under vacuum for 2 hours until a thin, dry film was formed. The dry film was rehydrated by adding glycerol (2.6% w/v, 1 mL) as an osmotic agent [181], and mixed for 30 minutes to disperse the film in the solvent. The mixture was subsequently sonicated using MSE Soniprep 150 sonicator at 50% of its maximum output for 5 minutes in an ice bath. The probe sonication method was previously reported to encapsulate GCPQ with prednisolone for topical ocular delivery [136] and to encapsulate the hydrophobic drug cyclosporine A [135].

The mixture was subsequently adjusted for pH with 1.0 M NaOH using a calibrated pH meter, and a simulated sterile filtration step was carried out using a 0.22 µm sterile filter. The formulation was then analysed for drug content, particle size distribution, and zeta potential.

3.3.2.2. Characterisation of RAP formulation

3.3.2.2.1. High-performance liquid chromatography analysis of RAP

High-Performance Liquid Chromatography (HPLC) coupled with an ultra-violet (UV) detection is a commonly used analytical technique to quantify the concentration of a particular solute in sample [182]. There are two phases in HPLC; the stationary phase (column), and the mobile phase. The combination of a polar stationary phase

and a nonpolar mobile phase is a normal-phase chromatography. In reversed-phase chromatography (RP-HPLC), which is the more common form of HPLC, the stationary phase is nonpolar, and a gradient mixture of polar and organic solvents make up the mobile phase [183]. In RP-HPLC, the order of elution is the opposite of that in a normal-phase separation, with the more polar solute eluting first [183]. The intensity of the UV signal increases linearly with the concentration of the solute, which makes the quantification straightforward with the help of a standard curve.

A HPLC method was developed for RAP using the Agilent 1220 infinity chromatographic system fitted with a vacuum degasser, quaternary pump, auto-sampler, column compartment with a thermostat and a UV detector from Agilent technologies (Berkshire, UK).

A gradient method (Table 3-2) was developed using a mobile phase consisting of acetonitrile, phosphoric acid (0.1%), a reversed-phase Onyx monolithic C18 column from Phenomenex Inc. (Torrance, USA, 100 x 4.6 mm; particle size, 5µm). The column temperature was maintained at 50°C, and the UV detector was set at a wavelength of 298 nm. The flow rate was 1.0 mL/min, and the injection volume was 10.0 µL. The run time was 9 minutes.

For quantifying the RAP content in the formulation, an aliquot of the prepared filtered GCPQ: RAP formulations (100 µL) was diluted with acetonitrile (100 µL) and vortexed before sample injection. Ten µL of the sample was injected, and the RAP concentration was determined by HPLC from the standard curve.

The standard curve was prepared as follows. Briefly, RAP stock solution was prepared at a concentration of 2 mg/mL in acetonitrile. RAP working solutions were

prepared by serially diluting RAP stock solutions into acetonitrile to obtain RAP working solutions at a range of concentrations (0.0625 – 1.0 mg/mL).

Table 3-2: HPLC gradient conditions of RAP

Time (min)	**0.1% H_3PO_4 in H_2O**	**Acetonitrile**
	Solvent A (%)	**Solvent B (%)**
0.00	70	30
3.00	70	30
4.00	10	90
8.00	10	90
9.00	70	30

3.3.2.2.2. Particle size and zeta potential measurements

The particle size distribution and particle zeta potential of the formulations were determined by Dynamic light scattering (DLS) on a Malvern ZetaSizer Nano-ZS from Malvern Panalytical (Malvern, UK). The principle of DLS is that fine particles and molecules undergoing a Brownian motion to scatter light diffuse at speed related to their size; hence, smaller particles diffuse faster than larger particles [184]. The constant motion of these particles causes fluctuations in the light scattering intensity of the solution, which allows calculating the diffusion coefficient that is related to the particles' hydrodynamic size [185,186].

.An aliquot of the sample (100 µL) was added in a disposable cuvette and measured at 25°C. The light scattering was detected at 173º and collected in automatic mode, typically requiring a measurement duration of 150 seconds. The data were recorded as mean ± standard deviation (SD) from three independent measurements.

Transmission Electron Microscopy (TEM) was carried out using the Philips/FEI CM120 Bio Twin from Philips (Oregano, USA). The principle of TEM imaging relies on the ability of atoms to scatter a beam of electrons, which are focused on a photographic film or phosphorescent screen to form an image [187]. The resolving power of TEM is 1000 times higher than that of an optical microscope [188]. TEM provides a much higher spatial resolution than a scanning electron microscope. The sample for TEM is usually required to be pre-treated with heavy metals (staining) such as lead acetate, uranyl acetate and osmium tetroxide to allow the visualisation of small atoms or low electron-dense samples [187,189,190]. TEM can facilitate the study

of the inner structure and analysis of the features on an atomic scale and in the range of few nanometers [189]. Samples were submitted to a technician and prepared by drying a drop of the formulation on a copper TEM grid - a 300mesh-fomvar/carbon-coated grid and stained with a drop of uranyl acetate (1% w/v). The dried samples were then imaged under the microscope.

The charge acquired by a particle or molecule in a given medium is its zeta potential [184]. It arises from the surface charge and the concentration and types of ions in the solution [184]. Therefore, zeta potential is used as a measure of the electrical potential at the stern layer. The zeta potential of particles and molecules is determined by measuring their velocity while they are moving due to electrophoresis. Particles and molecules that have a zeta potential will migrate towards an electrode if a field is applied. The speed at which they move is proportional to the field strength and their zeta potential [184].

An aliquot of the samples (600 µL) was loaded into folded capillary cells (zeta cells, polycarbonate cell with gold-plated electrodes; Malvern Instruments, DTS1060C) and measured at 25°C and 40V. The results were presented as mean ± SD, and the resulting data were analysed using the DTS (Version 4.2) software, Malvern Instruments Ltd. (Malvern, UK).

3.3.2.2.3. Osmolarity measurements

The osmolarity of the formulation was determined by utilising Roebling Milliosmol Osmometer coupled with a digital display and a freezing needle, Geminibv (Apeldoorn, NL). The osmometer measures the freezing point of aqueous solutions.

The depression of freezing point compared to pure water is directly related to the osmotic concentration [191]. Compared with pure water, which freezes at 0°C, a solution with an osmolality of 1 Osmo/kg H_2O will freeze at (- 1.86°C) [191]. Due to the linear correlation between osmolality and freezing point, the measurement of the freezing point is a determination of osmolality [192].

The machine was calibrated before the measurement with distilled water for the zero points and 300 mOsmol/L reference standards solutions. An aliquot of the formulation (100 µL) was pipetted into a 1.5 mL polypropylene tube, and the measurements were done in triplicate.

3.3.2.2.4. Viscosity measurements

The viscosity of the formulation was measured using m-VROC viscometer Rheosense (San Ramon, USA). In M-VROC, the sample is injected at a constant flow rate through the flow channel where multiple pressure sensors mounted within the base, monitor the pressure drop from the inlet to the outlet. The pressure drop is correlated with the shear-stress at the boundary wall. The shear rate describes the velocity gradient. Hence, the shear rate is the speed of fluid inside the parallel plates generated when shear stress is applied [193]. The shear rate and shear stress are directly related to the geometry of the rectangular slit and the flow rate, which allow for viscosity measurements [194]

The samples (500 µL) is inserted into the measuring cell using a 0.5 mL syringe with extreme care to avoid air bubble formation. The viscosity was measured at different

shear rates (1000 s^{-1}, 2500 s^{-1}, 5000 s^{-1}, and 7500 s^{-1}) at 25°C, and the measurement was conducted in triplicate.

3.3.2.2.5. Solid-state measurements of GCPQ: RAP formulation

X-ray diffraction (XRD) confirmed the solid-state of the encapsulated RAP. XRD peaks are produced by constructive interference of a monochromatic beam of X-rays scattered at specific angles from each set of lattice planes in a sample. The peak intensities are determined by the distribution of atoms within the lattice. Consequently, the X-ray diffraction pattern is the fingerprint of periodic atomic arrangements in a given material [195].

The data were acquired on a Miniflex 600, Rigaku (Tokyo, Japan). The patterns of the powdered materials were collected over the 2θ range of 5 - 45° at a speed of 5° per minute. Briefly, a sample (5 mg) of freeze-dried GCPQ, RAP raw material, GCPQ: RAP physically mixed, and freeze-dried GCPQ: RAP formulation was added to an XRD plate and analysed. The data were analysed using Origin, OriginLab (Northampton, USA).

3.3.2.2.6. Stability study of GCPQ: RAP formulation

The stability of the GCPQ: RAP optimum formulation was determined by measuring the physicochemical properties over 28 days at different storage conditions and relative humidity (RH). Formulations were prepared using the solvent evaporation method and were stored at room temperature (25±2°C / 60±5% RH), under refrigeration (5±3°C) and at a critical condition (40±2°C / 75±5% RH). The storage stability conditions were chosen according to the International Conference on Harmonisation (ICH) guidelines [196,197], and the measurements were done in triplicate.

An aliquot of the formulation (750 µL) was withdrawn at each storage condition immediately after preparation day 0, day 7 and day 28 of storage. The samples were analysed to determine if the encapsulated drug concentration, size distribution, zeta potential, pH, osmolarity and viscosity were altered upon storage. The samples were also visually inspected for any macroscopic changes, including precipitation, turbidity and colour changes.

Statistical analysis was performed using two-way ANOVA with Tukeý́s post-test. All data were expressed as mean ± standard deviation (SD). ($p < 0.05$) was considered statistically significant.

3.3.2.3. Encapsulation of TAC

Different approaches were used to optimise the encapsulation of TAC with GCPQ amphiphile. We were aiming to manufacture a GCPQ - TAC formulation with a drug loading of 0.1% w/v, as this concentration was found to provide a clinical therapeutic response [198].

First, an application of a mechanical treatment approach utilising high-pressure homogenisation (HPH) to encapsulate TAC within GCPQ nanoparticles was used. This HPH method was previously reported to encapsulate tacrolimus into a nano-liposomal dry powder inhaler formulation [199]. The advantages of using HPH are that it may use to produce industrial-scale batches in a reproducible manner and at a comparatively low cost [200].

Briefly, TAC (0.1% w/v) formulations were prepared at 1:1, 2:1, 5:1 and 10:1 polymer, drug mass ratios. TAC solution was produced from TAC powder (2 mg) dissolved in ethanol (2 mL). GCPQ dispersions were prepared from (2 mg, 4 mg, 10 mg and 20 mg) of GCPQ dispersed in filtered deionised water (2 mL), respectively. TAC solution was then added to the polymer dispersion and thoroughly vortex-mixed for more than 10 minutes to produce a clear liquid. The resulting GCPQ: TAC mixture (4 mL) was loaded into a SpeedVac concentrator for 4 hours at 45°C to evaporate all the solvents. The residual thin-film was then reconstituted with glycerol (2.6% w/v, 2 mL) and mixed vigorously until a transparent liquid was obtained, thus producing a 1 mg/mL nominal drug concentration in the GCPQ: TAC formulation. Mixtures were subsequently adjusted for pH with 1.0 M NaOH using a calibrated pH

meter using 1.0 M NaOH. TAC formulations prepared from each polymer-to-drug mass ratio after evaporation of the solvents and reconstitution passed through a lab-scale high-pressure homogeniser, Emulsiflex C5 from Avestin (Ottawa, CA) for one cycle and ten cycles. The operating pressure of the homogeniser was kept between 10,000 and 15,000 psi. Finally, a simulated sterile filtration step was carried out using a 0.22 µm sterile filter, and the formulations were analysed.

Secondly, A thin-film hydration method was used to encapsulate TAC within GCPQ nanoparticles. This method was previously reported to encapsulate hydrophobic compounds [201] and was used to encapsulate RAP using GCPQ. The effect of GCPQ polymer, drug mass ratios on encapsulation efficiency of TAC was assessed by preparing formulations with 1:1, 2:1, 5:1 and 10:1 polymer, drug mass ratios without the application of any mechanical treatment. TAC powder was dissolved in absolute ethanol (0.1% w/v, 2 mL). GCPQ dispersions were prepared from (2 mg, 4 mg, 10 mg and 20 mg) of GCPQ dispersed in filtered deionised water (2 mL), respectively. TAC solution was then added to the polymer dispersion and thoroughly vortex-mixed for more than 10 minutes to produce a clear liquid. The resulting GCPQ: TAC mixture (4 mL) was loaded into a SpeedVac concentrator for 4 hours at 45°C to evaporate all the solvents. The residual thin-film was then rehydrated with glycerol (2.6% w/v, 2 mL) as a tonicity agent [181] and mixed vigorously for 30 minutes to disperse the film in the solvent, thus producing a nominal drug concentration of 1 mg/mL in the GCPQ: TAC formulation. Subsequently, 1.0 M NaOH was used to adjust the pH of the formulation to a value between 6.9 and 7.2 using a calibrated pH meter. Finally, prior to analysis, the formulation was filtered through a 0.22 µm

polyethersulfone membrane sterile filter to remove the unencapsulated drug and larger particles, as well as to simulate sterilisation of the formulation. The formulation was then analysed for drug content, particle size distribution, zeta potential distribution, viscosity and osmolarity.

3.3.2.4. Characterisation of TAC formulation

3.3.2.4.1. High-performance liquid chromatography analysis of TAC

The HPLC method was developed for TAC using an Agilent 1220 infinity chromatographic system fitted with a vacuum degasser, quaternary pump, auto-sampler, column compartment with a thermostat and an ultraviolet detector (Agilent Technologies, Berkshire, UK). A gradient method (Table 3-3) was developed using a mobile phase consisting of acetonitrile, phosphoric acid (0.1%), a reversed-phase Onyx monolithic C18 column from Phenomenex Inc. (Torrance, USA) (100 x 4.6 mm; particle size, 5µm). The column temperature was maintained at 50°C, and the UV detector was set at a wavelength of 215 nm. The flow rate was 1.0 mL/min, and the injection volume was 10.0 µL, the run time was 7 minutes.

For quantifying the TAC content in the formulation, an aliquot of the prepared filtered GCPQ: TAC formulation (100 µL) was diluted with acetonitrile (100 µL) and vortexed before sample injection. Ten µL of the sample was injected, and the TAC concentration was determined by HPLC from the standard curve.

The standard curve was prepared as follows. Briefly, TAC stock solution was prepared at a concentration of 2 mg/mL in acetonitrile. TAC working solutions were prepared by serially diluting TAC stock solutions into acetonitrile to obtain TAC working solutions at a range of concentrations (0.0625 – 1.0 mg/mL).

Table 3-3: HPLC gradient condition of tacrolimus.

Time (min)	0.1% H_3PO_4 in H_2O	Acetonitrile
	Solvent A (%)	Solvent B (%)
0.00	40	60
4.00	5	95
5.50	5	95
7.00	40	60

3.3.2.4.2. Particle size and zeta potential measurements

The particle size distribution and particle zeta potential of the formulation were determined by dynamic light scattering on a Malvern ZetaSizer Nano ZS (Malvern Panalytical, Malvern, UK).

The size distribution analysis was performed at a backscattering angle of 173º and a temperature of 25ºC. An aliquot of the sample (100 µL) was placed in a disposable plastic cuvette and was subsequently loaded into the instrument without any dilution. The particle size was reported as intensity distribution, which describes the relationship between light scattering intensity and the particle hydrodynamic diameter [202]. The mean size of the individual peaks and their corresponding percentages were determined and recorded as mean ± standard deviation from three independent measurements.

The zeta potential is the electrokinetic potential in a colloidal system and measures the surface particle charge in a given medium [203]. The zeta potential was obtained via the electrophoretic light scattering technique. An aliquot of the sample (500 µL) was loaded into the folded capillary cells (zeta cells, polycarbonate cell with gold-plated electrodes; Malvern Instruments, DTS1060C) and measured at 25°C, 40V. Measurements were performed in triplicate, and the results were presented as mean ± SD.

Transmission Electron Microscopy was carried out using the Philips/FEI CM120 Bio Twin from Philips (Oregano, USA). Samples were submitted to a technician and prepared by drying a drop of the formulation on a copper TEM grid - a 300mesh-

fomvar/carbon-coated and stained with a drop of uranyl acetate (1% w/v). The dried samples were then imaged under the microscope.

3.3.2.4.3. Osmolarity measurements

The osmolarity of the formulation (100 µL) was determined using Roebling Milliosmol Osmometer (Geminibv, Apeldoorn, NL) coupled with a digital display and a freezing needle. The machine was calibrated before each measurement with 300 mOsm/kg reference standards solution from Reagecon Diagnostics Ltd. (Clare, IE). The measurements were conducted in triplicate.

3.3.2.4.4. Viscosity measurements

The viscometer of the formulation was measured by utilising m-VROC viscometer (Rheosense Inc., San Ramon, USA). Samples (500 µL) were inserted into the measuring cell using a 0.5 mL syringe with extreme care to avoid air bubble formation. The viscosity was measured at three different shear rates (5,000 s^{-1}, 7,500 s^{-1} and 10,000 s^{-1}) at 25°C.

3.3.2.4.5. Stability study of GCPQ: TAC formulation

The stability of the GCPQ: TAC formulation was determined by measuring the physicochemical properties over 30 days at different storage conditions and relative humidity. Formulations were stored at room temperature (25±2°C / 60±5% RH), under refrigeration temperature (5±3°C), and at accelerated conditions (40±2°C / 75±5% RH). The storage stability conditions were chosen according to the ICH guidelines [196,197], and the measurements were done in triplicate.

Samples (750 µL) were withdrawn from the formulation at each storage condition immediately after preparation, at day 7, and day 30 of storage. The samples were analysed to determine if the encapsulated drug concentration, size distribution, zeta potential, pH, osmolarity and viscosity were altered upon storage. The samples were also visually inspected for any macroscopic changes, including precipitation, turbidity and colour changes.

Statistical analysis was performed using two-way ANOVA with Tukeý́s post-test. All data were expressed as mean ± SD. ($p < 0.05$) was considered statistically significant.

3.4. Results and discussion

3.4.1. Encapsulation of RAP

The HPLC chromatogram (Figure 3-3, A) shows a retention time of RAP at 6.5 minutes. The standard curve plotted from this chromatogram shows linearity over a concentration range of 62.5 – 1000 µg/mL with a correlation coefficient of 0.9964 (Table 3-4). The equation of the average standard curve from three independent experiments (y = 6.7149x + 270.34) was used to determine the concentration of the encapsulated RAP in the formulation.

The measured lower limit of quantification (LLOQ) for RAP was 62.5 µg/mL. The calculated limit of quantification (LOQ) and limit of detection (LOD) were presented in Table 3-4. The following equations were used to calculate LOQ and LOD according to ICH guidelines [204]:

$$\boldsymbol{LOD = \frac{3.3\,\sigma}{S}} \qquad \text{Equation 3-1}$$

$$\boldsymbol{LOQ = \frac{10\,\sigma}{S}} \qquad \text{Equation 3-2}$$

where σ is the standard deviation of the response, and S is the slope of the calibration curve.

Table 3-4: HPLC assay parameters of RAP.

Parameter	Quantification range (µg/mL)	Equation of the straight line	R^2	Limit of detection (µg/mL)	Limit of quantification (µg/mL)
Value	62.5 – 1000	y= 6.7149x + 270.34	0.9964	58.8	178.1

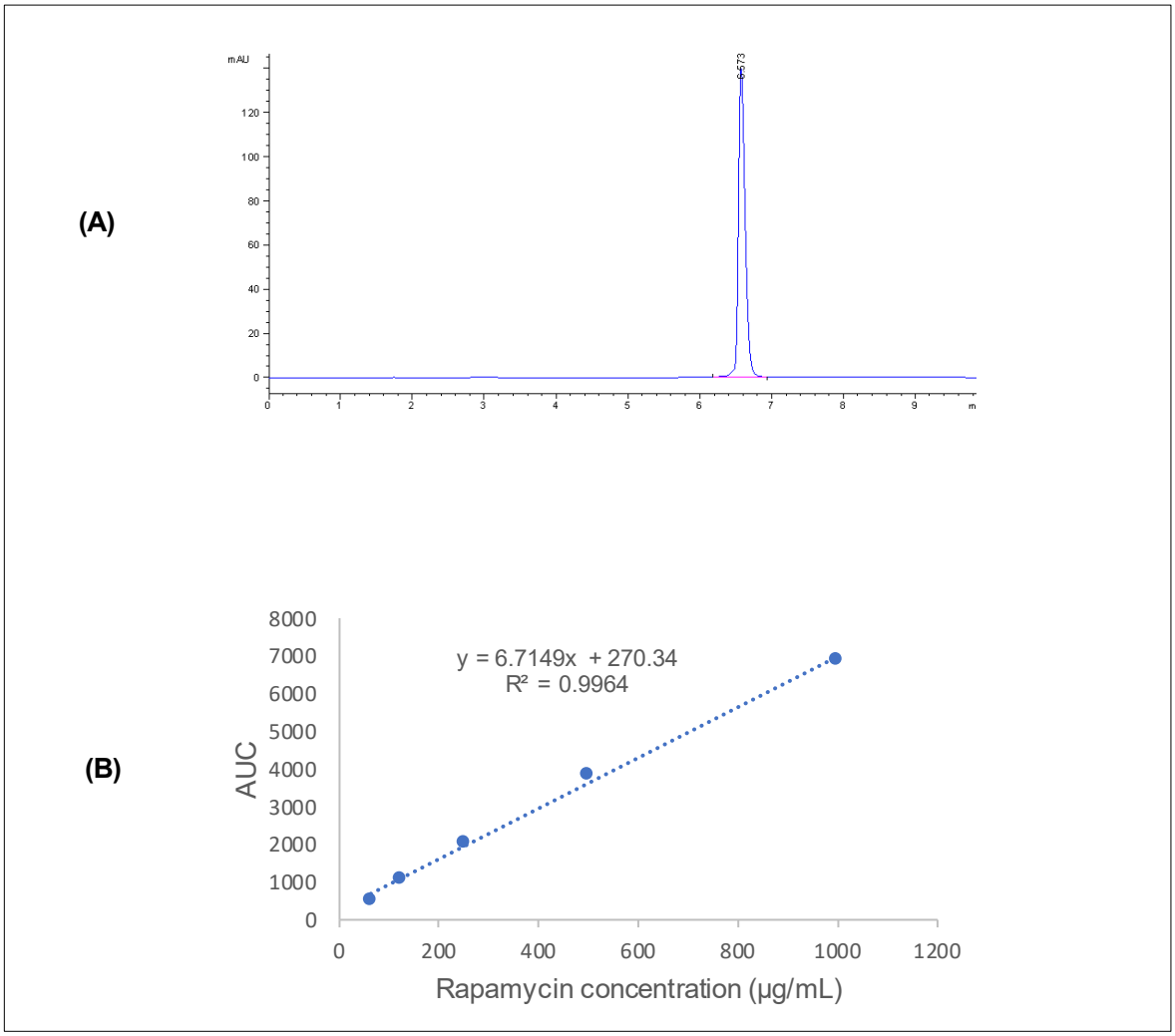

Figure 3-3: RP-HPLC chromatogram of RAP.

The optimum formulation was selected based on various methods studied to compare the drug content, particle size distribution, zeta potential, and pH. Table 3-5 shows the drug content of the initial formulations. First, a direct approach was used to incorporate the drug into the polymer aggregates. Two polymers GCPQ04 (MW; not determined, P20, Q09), and GCPQ10 (MW16, P18, Q19) were used with RAP at (5:1) polymer: drug weight ratio. We have selected these polymers initially with a nearly similar degree of palmitoylation and different degrees of quaternisation. GC16P18Q19 is a more hydrophilic polymer owing to the presence of a higher degree of quaternary ammonium group compared to GCP20Q09; QPR 1.020, and 0.463, respectively.

We were aiming to manufacture GCPQ: RAP with a drug content of more than 1 mg/mL as this concentration was sufficient to detect RAP in rabbit eyes posterior tissues [34]. Unfortunately, neither of these polymers achieved adequate drug content. The encapsulation efficiency was reported as 32% and 29% for the GC16P18Q19 and GCP20Q09, respectively. The low encapsulation efficiency in the direct approach could be attributed to the physicochemical property of RAP which favours being solubilised before encapsulation, and as a result, enhances its encapsulation [205]. This in line with a previous report that showed RAP enhanced solubility is detectable only if the drug is dissolved in methanol and evaporated to dryness before cyclodextrins and water is added [162]. This is probably due to the fact that RAP has different crystalline polymorphs with different water solubilities [162].

Table 3-5: Summary of different approaches used to encapsulate RAP within GCPQ.

Polymer		Encapsulation method	Polymer:drug mass ratio (w/w)	Measured Drug content (% w/v)	Theoretical Drug content (% w/v)	Z-average (nm)	PDI	Zeta potential (mV)	pH
GCPQ04	**GCP20Q09**	**Direct**	5:1	0.03±0.01	0.1	376 ± 4.6	0.41 ± 0.04	43 ± 0.32	7.0±0.1
GCPQ10	**GC16P18Q19**		5:1	0.03±0.01	0.1	190 ± 10.3	0.44 ± 0.4	29 ± 2.04	7.4±0.1
GCPQ04	**GCP20Q09**	**Solvent evaporation**	5:1	0.13±0.06	0.2	268 ± 0.4	0.23 ± 0.01	26 ± 0.7	7.4±0.1
GCPQ10	**GC16P18Q19**		5:1	0.14±0.01	0.2	332 ± 3.1	0.29 ± 0.04	52 ± 1.5	6.9±0.1
			7.5:1	0.14±0.01	0.2	150 ± 3.4	0.25 ± 0.01	31 ± 0.7	7.2±0.2
			10:1	0.15±0.01	0.2	160 ± 1.5	0.33 ± 0.02	27 ± 4.7	7.4±0.1
GCPQ12	**GC18P22Q16**		7.5:1	0.11±0.02	0.2	376 ± 4.6	0.41 ± 0.04	43 ± 0.32	7.0±0.1

Secondly, the solvent evaporation method approach was utilised to formulate RAP with GCPQ as described in the method section. The following polymers were used to encapsulate RAP; GCP20Q09 (MW; not determined, QPR 0.463), GC18P22Q16 (QPR 0.727), and GC16P18Q19 (QPR 1.020). These polymers were selected as they have low, moderate, and high quaternary ammonium to palmitoyl group ratios, respectively. Thus, GCP20Q09 is the most hydrophobic polymer followed by GC18P22Q16 and GC16P18Q19 (most hydrophilic). As shown in Table 3-5, from the drug content data, solubilising RAP with ethanol before mixing with the GCPQ dispersion, enhances the drug encapsulation, as the drug content was significantly higher than the direct approach for all polymers.

GCP20Q09 with a low QPR showed a good drug content of RAP in the formulation (0.13±0.06% w/v), with a narrow particle size distribution (diameter = 268 ± 0.4 nm, polydispersity index = 0.23 ± 0.01). GC18P22Q16 encapsulated a lower level of RAP in the formulation (0.11±0.02% w/v) and presented with a higher particle size distribution (376 ± 4.6 nm). GC16P18Q19 with high QPR produced the highest concentration of RAP in the formulation (~ 0.15% w/v). An increase in the polymer-drug ratio did not improve the drug content in the formulation, and as such, the polymer to drug ratio of 7.5:1, which shows a sufficient concentration of the drug (0.14±0.01 % w/v), was chosen for subsequent studies to formulate RAP with GCPQ and achieve a nominal drug concentration of 0.2% w/v.

Particle size distribution **Zeta potential**

Direct approach

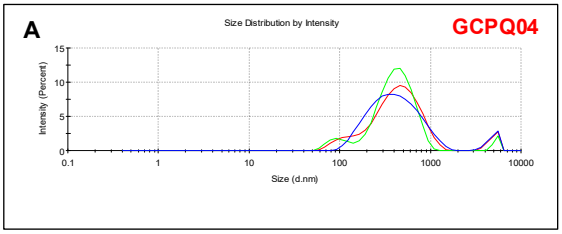

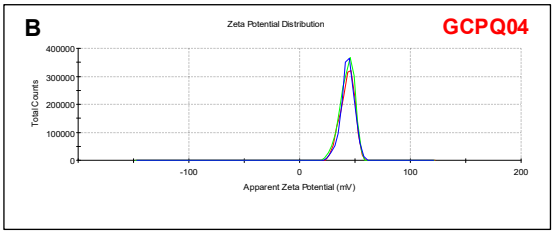

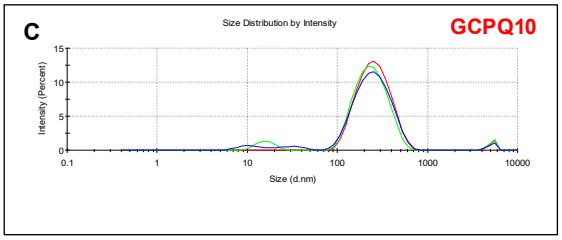

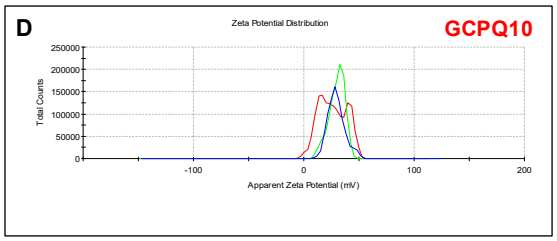

Solvent evaporation approach

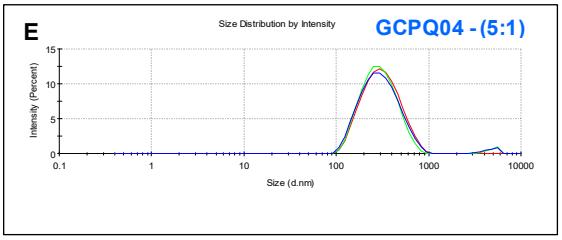

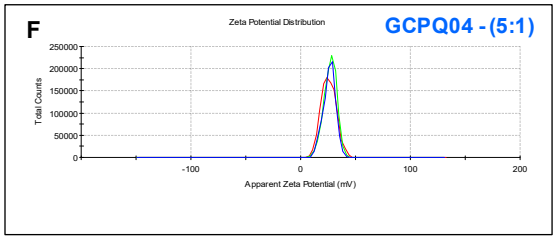

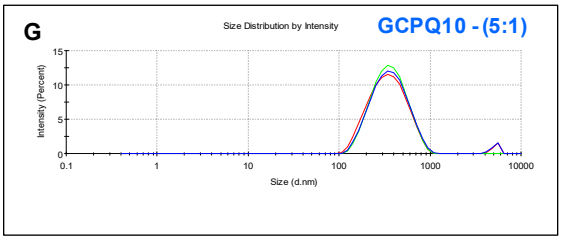

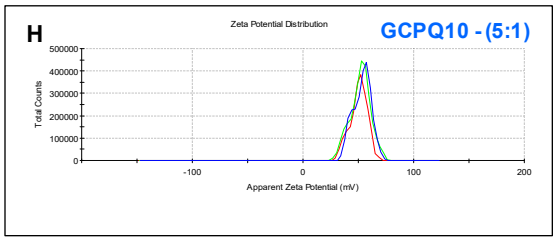

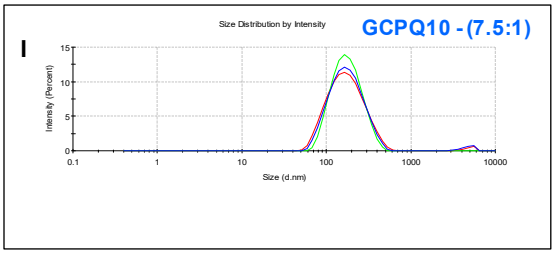

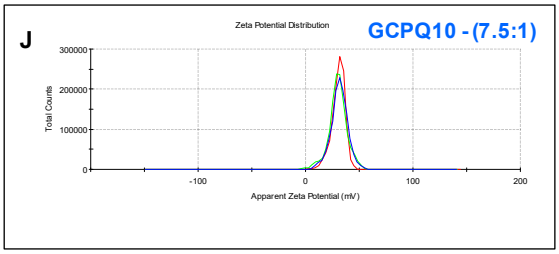

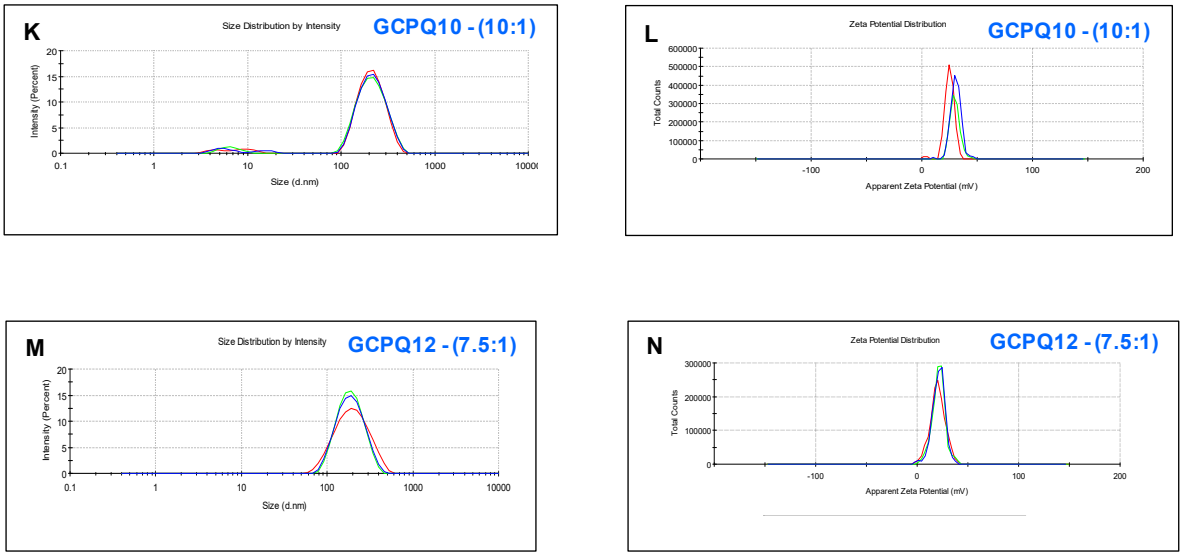

Figure 3-4: Dynamic light scattering experiments of the GCPQ: RAP formulations.

Direct approach: GCPQ04 - (5:1) (A) particle size distribution (376 ± 4.6 nm), (B) zeta potential (43 ± 0.32 mV); **GCPQ10 - (5:1)** (C) particle size distribution (190 ± 10.3 nm), (D) zeta potential (29 ± 2.04 mV).

Solvent evaporation approach: GCPQ04 - (5:1) (E) particle size distribution (268 ± 0.4 nm), (F) zeta potential (26 ± 0.7 mV); **GCPQ10 - (5:1)** (G) particle size distribution (332 ± 3.1 nm), (H) zeta potential (52 ± 1.5 mV); **GCPQ10 - (7.5:1)** (I) particle size distribution (150 ± 3.4 nm), (J) zeta potential (31 ± 0.7 mV); **GCPQ10 - (10:1)** (K) particle size distribution (160 ± 1.5 nm), (L) zeta potential (27 ± 4.7 mV); **GCPQ12 - (7.5:1)** (M) particle size distribution (376 ± 4.6 nm), (N) zeta potential (43 ± 0.32 mV).

Measurements were conducted in triplicate from three independent samples, n=3.

The particle size distribution and the zeta potential for all formulations were studied. With the direct method, both polymers showed a high polydispersity of 0.41 ± 0.04 and 0.44 ± 0.4 for GCP20Q09 and GC16P18Q19 (Figure 3-4, A, C), respectively.

The formulations had a positive zeta potential value due to the presence of GCPQ on the surface of the nanoparticles. The positive charge of the particles is desirable to prevent particle aggregation and promote the electrostatic interaction with the negatively charged sialic acid residues of mucin on the eye surface [105]. The overall positive value of the zeta potential of the formulation is an indication of that the formulation will be colloidally stable due to greater electrostatic repulsion between the particles [105], and this positive value may be essential to enhance the mucoadhesion on the corneal surface and thus might increase the drug residence time at ocular surface [105]. The zeta potential was reported as +43 ± 0.32 and +29 ± 2.04, for GCP20Q09 and GC16P18Q19, respectively. The difference in the zeta potential is attributed mainly to the slight differences in the pH values between both formulations.

For the solvent evaporation method, all tested formulations had a relatively lower polydispersity compared to the direct method; this indicates the uniformity of the formulations synthesised (Table 3-5).

The size distribution of the optimised formulation is shown in (Figure 3-4, I). GCPQ10: RAP formulations had a z-average mean size of 150 ± 3.4 nm with a narrow polydispersity index of 0.25 ± 0.01. The size distribution graph (Figure 3-4, I) shows that the formulations mainly were monomodal in their distribution, demonstrating the size uniformity of our formulations.

The pH of all formulations was adjusted to ~ 7.0 - 7.4 with 1.0 M NaOH. The optimum pH for eye drops equals that of tear fluid and is about 7.4 [206].

To further examine the characteristics of the optimum formulation, electron microscopy was used to observe the morphology of the nanoparticles formed using the GCPQ polymer. Figure 3-5 shows that the GCPQ10: RAP formulation formed spherical nanoparticles, which are presumed to contain the encapsulated RAP.

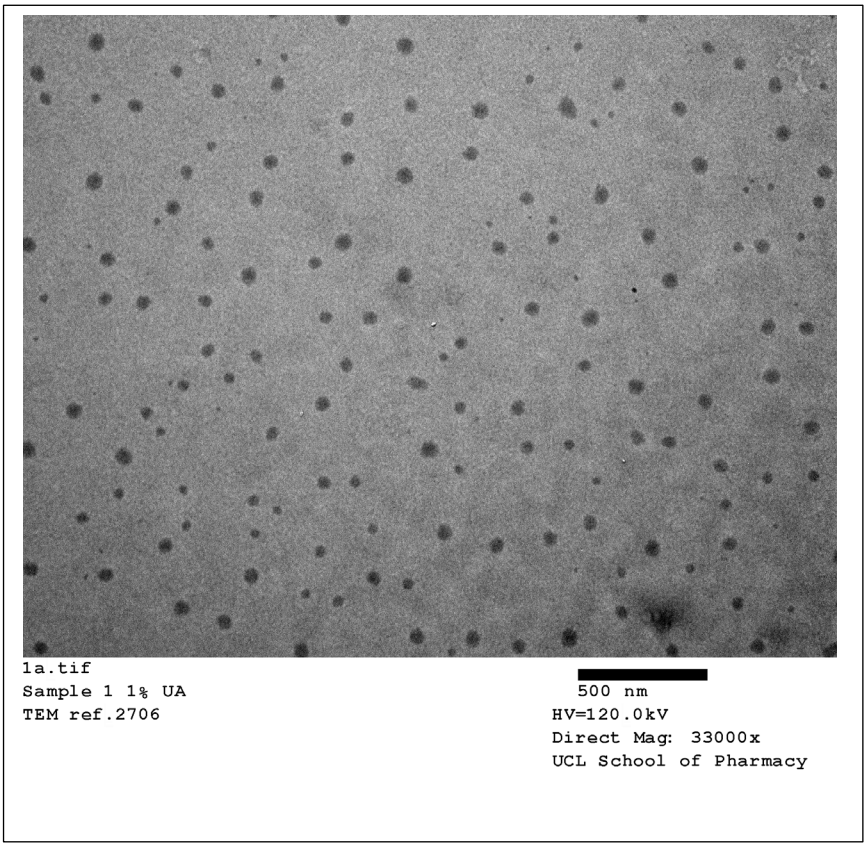

Figure 3-5: Transmission electron microscopy image of GCPQ10: RAP formulation.

3.4.1.1. Solid-state measurements of GCPQ: RAP formulation

XRD patterns of tested compounds are presented in Figure 3-6. GCPQ displays no distinct visible Bragg reflections (Figure 3-6, A); this demonstrates that GCPQ is an amorphous material. RAP raw material has sharp peaks (Figure 3-6, B); this confirms the raw drug to be a crystalline material, consistent with the literature [207]. The physical mixture of the freeze-dried GCPQ and RAP raw material still shows some crystalline peaks (Figure 3-6, D). In the case of the GCPQ: RAP freeze-dried formulation, the reflections of RAP crystals have disappeared, and therefore the formulation comprises an amorphous solid dispersion (Figure 3-6, C). This represents an advantage, as the amorphous form of the drug often has rapid dissolution and greater absorption compared to their crystalline forms. This is important for eye drops formulations that could enjoy an enhanced solubility advantage for amorphous pharmaceutical materials compared to their crystalline counterparts [208].

The two peaks at about 40° in all the spectra are due to the plates' background reflections. Elsaid et al. reported RAP crystallography loaded with amphiphilic chitosan derivative, O-octanoyl-chitosan-polyethylene glycol (OChiPEG) graft copolymer [23]. They showed that upon the addition of RAP to the OChiPEG micelles, the characteristic crystal peaks for the drug disappeared [23]. This data indicates that the drug is no longer crystalline and could mean the formation of intermolecular interactions between the drug and the hydrophobic core of the micelles before drying [23].

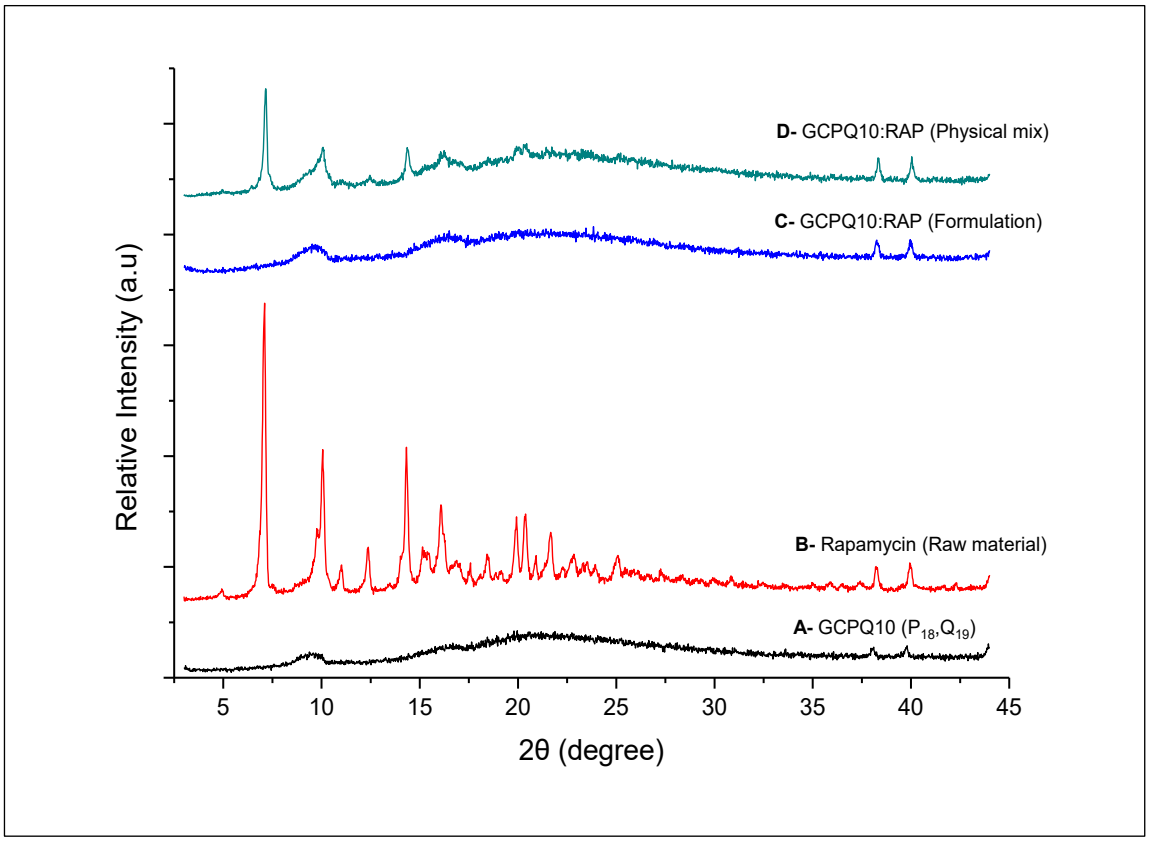

Figure 3-6: X-Ray Diffraction analysis.

(A) GCPQ, **(B)** RAP raw material, **(C)** freeze-dried formulation, and **(D)** GCPQ: RAP powder physical mix.

3.4.1.2. Stability studies of GCPQ: RAP formulation

The stability of the GCPQ: RAP formulations was determined by measuring the physicochemical properties over 28 days. GCPQ10 amphiphilic polymer with characteristics (GC16P18Q19, QPR = 1.0) was selected as it results in the highest encapsulation of RAP with reproducible results over three independent experiments. Due to the unavailability of the polymer quantity for the stability study, another polymer with similar characteristics GCPQ15 (GC15P18Q20, QPR = 1.1) was synthesised and used for further studies.

Table 3-6 shows the properties of all formulations upon storage at different conditions for one month. The formulation stored in the fridge (28 days, 2.5 mg/mL) displayed a similar drug content compared to formulations stored in the fridge at day 0 (2.3 mg/mL), and day 7 (2.6 mg/mL). Formulations stored at room temperature (25±2°C / 60±5% RH) showed no significant differences in drug content at day 28 compared to day 0 ($p > 0.05$). GCPQ: RAP stored at accelerated conditions (40±2°C / 75±5%) showed no significant change in drug content at day 7 as compared to day 0, while the change in drug content was significant at day 28 as compared to day 0 ($p < 0.05$).

The pH of all the prepared formulations was examined. The pH of the formulation was adjusted to 7.2 ± 0.1 with 1.0 M NaOH. The optimum pH for eye drops equals that of tear fluid and is 7.4 [206]. If the pH value gets outside the acceptable range that is tolerated by eye (i.e. 6.6 – 7.8 [209]), the patient may feel discomfort, there may be irritation, and the drug bioavailability may decrease

because of increased tearing [210]. Our results showed that the pH was at the acceptable range at all conditions and time points for all formulations (pH = 6.7 – 7.2).

The particle size and zeta potential were determined for the formulations. The formulation prepared for the stability study possessed two nanoparticle populations after filtration. The main peak population with larger particle sizes (~ 174 nm) was presumed to be the encapsulated RAP in the formulation. In contrast, the second peak population with smaller particle sizes (~ 14 nm) was assumed to be empty GCPQ micelles as has been reported previously [178]. It has been reported that in aqueous environments, GCPQ self-assembles to form polymeric micelles with a particle size of between 5 and 30 nm [211]. Our size distribution results in the stability studies showed a bimodal distribution and this bimodal size is thought to be due to an equilibrium being established between drug-filled nanoparticles and empty micelles [211]. There were no significant differences in the formulation particle size at day 0 to day 7 of storage at all conditions and time points. The formulation particle size that had been stored in the fridge at Day 28 was not significantly different from the particle size of the formulation on Day 0. However, there was a significant difference in the formulation particle size when stored at room temperature and at accelerated conditions; when Day 28 day was compared to Day 0.

The zeta potential is very sensitive to dilution, as this could cause variations in pH and ionic strength, both of which affect the particle zeta potential [212]. GCPQ possesses an overall positive charge due to the presence of quaternary ammonium

groups [137]. As such, we obtained a positive zeta potential with the GCPQ: RAP formulation (+26 ± 4.7 mV) on Day 0 over three independent experiments. There were significant changes in the measured zeta potential on Day 28 when compared to Day 0, irrespective of the storage conditions ($p < 0.05$).

The tears have a tonicity equivalent to 0.9% w/v NaCl solution [34] (300 mOsm/L) [209,213]. Topical ophthalmic drops require to be at optimal osmolarity ~ 300 mOsm/L to avoid adverse effects on the eye, with a mean osmolarity for healthy eyes ranging from 270 (confidence interval (CI) ± 261–309 mOsm/L) to 328 mOsm/L (CI ± 279–365 mOsm/L) [214]. The eye can accommodate tonicity values between 0.6% and 1.3% w/v of sodium chloride solution [2], which is equivalent to 200-450 mOsm/kg. Our formulation has an osmolarity value of 322 – 332 mOsm/kg, within the range tolerable by the eye, and the change in osmolarity was not significant, irrespective of the storage conditions.

The viscosity of the formulation was measured. There were no significant changes in the viscosity at day 28 compared to day 0, irrespective of the storage conditions. The viscosity of the formulation is higher than that of plain water (1.4 mPa and 0.89 mPa.s [35], respectively at 25°C), due to the presence of the GCPQ polymer in the formulation [136]. Clearance from the eye is reduced with the more viscous eye drop formulations, and increasing viscosity of an instilled dose can extend the residence time of solution in the conjunctival sac [37]. As this formulation is intended for topical ocular administration in the eye, the slightly increased viscosity and GCPQ bioadhesive properties are important when it comes to promoting drug residence time at the ocular surface.

Different approaches have been utilised to aqueous incorporation of RAP including; complexes with cyclodextrins, liposomal formulations, microemulsion, and solid dispersion [157]. The solubility of RAP in cyclodextrin complexes increased to 60-70 µg/mL compared to RAP alone, which has an aqueous solubility of 2.6 µg/mL with the aim of the authors to achieve (1 mg/mL) solubility [162]. This low increase in solubility is presumed to be due to the size of RAP molecules being too large for complete inclusion in cyclodextrin complexes, and only an inclusion of the side chain of the RAP molecule into the cyclodextrins complexes occurred [162]. Also, RAP formulated with phospholipid liposomes, with the aim to achieve (1 mg/mL), did not result in enhanced RAP solubility, and the drug could not be detected in these liposomes by HPLC [162]. Probably, the hydration of the lipid films in the aqueous medium or the extrusion procedure (Liposofast® extruder, 21 cycles) is not suitable for the preparation of formulations containing RAP [162]. Linares-Alba et al. reported that the inclusion of a lyophilization step is necessary to the manufacturing process of a liposomal formulation containing RAP [215]. However, this approach could have a limitation in the large-scale production of RAP [215]. Another study showed enhanced aqueous incorporation of (196.7 µg/mL) was achieved when spray-dried with polymethacrylate-based copolymers (Eudragit®) due to the formation of micelle-like structures [157]. The incorporation of 1 mg/mL of RAP in an aqueous-based formulation was achieved with a microemulsion containing triacetin and propylene glycol [162]. Formulation modifications resulted in improving the RAP aqueous levels to 1 mg/mL when amphiphilic block copolymer micelles of polyethylene glycol-b-poly(e-caprolactone) were used [216]. Another report showed a RAP-loaded mixed

nanomicellar formulation, i.e., vitamin E tocopherol polyethylene glycol succinate and octoxynol-40 had led to high RAP aqueous concentrations (2 mg/mL) [34]. All these approaches used high levels of excipients, e.g., a viscosity enhancer povidone K 90 was used, triacetin (20%), and propylene glycol (40%) to enhance RAP aqueous levels. Our work showed that GCPQ alone as a vehicle at a concentration of 7.5 mg/ mL was able to achieve a high concentration of RAP (2.3 mg/ mL). GCPQ increased the RAP solubility in the formulation by 1000-fold (from 2.6 µg/mL for RAP alone to 2300 µg/mL for the GCPQ: RAP formulation).

Table 3-6: Parameters of GCPQ: RAP optimum formulation stored at the fridge (5 ± 3°C), room temperature (25 ± 2°C), and at accelerated conditions of (40 ± 2°C) for 28 days.

Storage conditions	Parameters	Day 0	Day 7	Day 28
5±3°C	Drug concentration (mg/mL)	2.3 ± 0.01	2.6 ± 0.02 #	2.5 ± 0.01 #
	pH	7.2 ± 0.10	6.9 ± 0.04 #	6.9 ± 0.04 #
	Main peak size (nm) Peak intensity(%)	174 ± 2.2 (66 ± 0.4%)	217 ± 23.1 ns (36 ± 4.3%)	411 ± 18.7 ns (35 ± 1.1%)
	Second peak size (nm) Peak intensity (%)	14 ± 1.2 (33 ± 0.8%)	18 ± 3.01 ns (64 ± 4.3%)	14 ± 7.7 ns (45 ± 18.02%)
	Zeta potential (mV)	+26 ± 4.7	+14 ± 2.4 #	+5 ± 0.6 #
	Osmolarity (mOsm/kg)	322 ± 5.5	331 ± 10.02 ns	326 ± 7.6 ns
	Viscosity (mPa.s)	1.4 ± 0.01	1.6 ± 0.03 #	1.4 ± 0.001 ns
25±2°C 60 ± 5% RH	Drug concentration (mg/mL)	2.3 ± 0.01	2.5 ± 0.02 #	2.4 ± 0.04 ns
	pH	7.2 ± 0.10	6.7 ± 0.03 #	6.7 ± 0.10 #
	Main peak size (nm) Peak intensity(%)	174 ± 2.2 (66 ± 0.4%)	276 ± 30.9 ns (28 ± 3.9%)	665 ± 169.2 # (40 ± 5.3%)
	Second peak size (nm) Peak intensity (%)	14 ± 1.2 (33 ± 0.8%)	24 ± 6.6 ns (61 ± 15.2%)	29 ± 7.3 * (39 ± 12.6%)
	Zeta potential (mV)	+26 ± 4.7	+15 ± 1.4 #	+5 ± 0.4 #
	Osmolarity (mOsm/kg)	322 ± 5.5	332 ± 6.1 ns	329 ± 3.6 ns
	Viscosity (mPa.s)	1.4 ± 0.01	1.6 ± 0.1 #	1.4 ± 0.01 ns
40±2°C 75 ± 5% RH	Drug concentration (mg/mL)	2.3 ± 0.01	2.3 ± 0.01 ns	1.9 ± 0.02 #
	pH	7.2 ± 0.10	6.8 ± 0.10 #	6.5 ± 0.04 #
	Main peak size (nm) Peak intensity (%)	174 ± 2.2 (66 ± 0.4%)	395 ± 85.5 ns (15 ± 1.6%)	766 ± 244.2 # (11 ± 2.5%)
	Second peak size (nm) Peak intensity (%)	14 ± 1.2 (33 ± 0.8%)	25 ± 1.9 ns (86 ± 1.6%)	31 ± 4.7 # (77 ± 20.01%)
	Zeta potential (mV)	+26 ± 4.7	+18 ± 2.5 ns	+16 ± 1.4 *
	Osmolarity (mOsm/kg)	322 ± 5.5	324 ± 9.3 ns	322 ± 5.5 ns
	Viscosity (mPa.s)	1.4 ± 0.01	1.7 ± 0.03 #	1.4 ± 0.01 ns

ns = not significant; * = $p < 0.05$; # = $p < 0.005$.

Figure 3-7 shows the results of the drug content and visual appearance of all formulations upon storage at three different conditions. As shown in (Figure 3-7, A) there is a slight loss of the drug content (~17%) for the formulation stored at (40 ± 2°C / 75 ± 5%), and this drug loss can be observed with slight precipitation of the formulation after 28 days (Figure 3-7, B).

RAP is very unstable in phosphate-buffered saline and HEPES buffer under all conditions; their degradation effect on the drug is slower at 4° - 8°C and fastest at 37°C, at which temperature almost all of the drug is destroyed within 24 hours [207]. RAP is unstable in electrolyte solutions, and it can be degraded in an acidic environment via ring-opening and fragmentation [157]. Previous studies reported a rapid degradation of RAP in simulated gastric fluid (pH 1.2) compared to intestinal fluid (pH 6.8), acetate buffer (pH 4.0), and distilled water [207].

Sun et al. reported on the stability of RAP formulated in self-microemulsifying drug delivery systems stored in at 4°C, 25°C, and 40°C [205]. They found that the storage stability of RAP was improved significantly with decreasing temperature, suggesting that formulations of RAP should be stored at a lower temperature. Another study reported the stability of RAP (1 mg/mL) at room temperature [162]. RAP microemulsion containing 20% triacetin and 40% propylene glycol was stable over a storage period of 12 months at 15 - 35°C [162].

We have shown that RAP, when encapsulated with the amphiphilic GCPQ, exhibits excellent stability over 28 days of storage at 5°C, and room temperature and this stability was due to the formation of a micelle-like structure. Siew et al. reported that the GCPQ CMC values to range from 21 to 26 μM [135]. Qu et al. showed that the

GCPQ CMC values are between 6 – 100 μM [136]. This low CMC value makes the GCPQ a prime candidate for use in drug delivery. Highly stable nanosystems will be less likely to prematurely disaggregate on dilution within biological fluids *in vivo*, and as a result, will be able to transport their payload as intended [135].

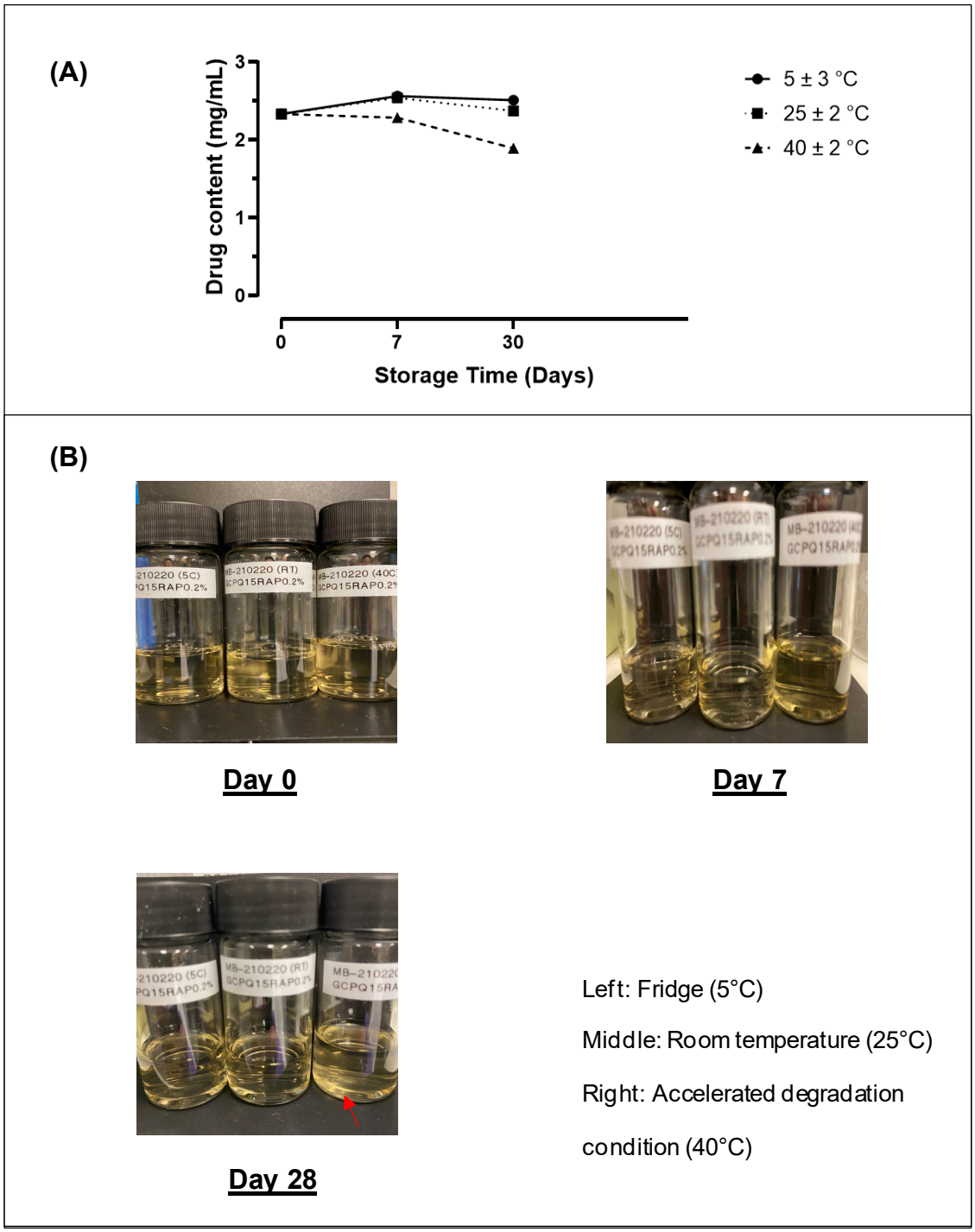

Figure 3-7: GCPQ:RAP physical stability over 28 days of storage.

(A) Drug content; **(B)** visual appearance. The 40°C sample shows drug sedimentation after 28 days.

3.4.2. Encapsulation of TAC

A reverse-phase HPLC was developed and used to quantify tacrolimus drug content in the formulation. A calibration curve was constructed (Figure 3-8) by plotting the average peaks areas of TAC against concentration. The method developed showed linearity of TAC in a concentration range (0.0625 – 1.0 mg/mL). The straight-line equation ($y= 5667.3x + 11.85$) with $r^2 = 0.9996$ was used to quantify the concentration of the encapsulated TAC in the formulation (Table 3-7).

The measured lower limit of quantification for tacrolimus was 62.5 µg/mL. The calculated limit of quantification and limit of detection were presented in Table 3-7. Equations (Equation 3-1, Equation 3-2), as previously described, were used to calculate LOQ and LOD according to ICH guidelines [204].

Table 3-7:Tacrolimus HPLC Assay Parameters

Parameter	Quantification range (µg/mL)	Equation of the straight line	R^2	Limit of detection (µg/mL)	Limit of quantification (µg/mL)
Value	62.5 - 1000	y= 5667.3x + 11.85	0.9996	13.46	40.80

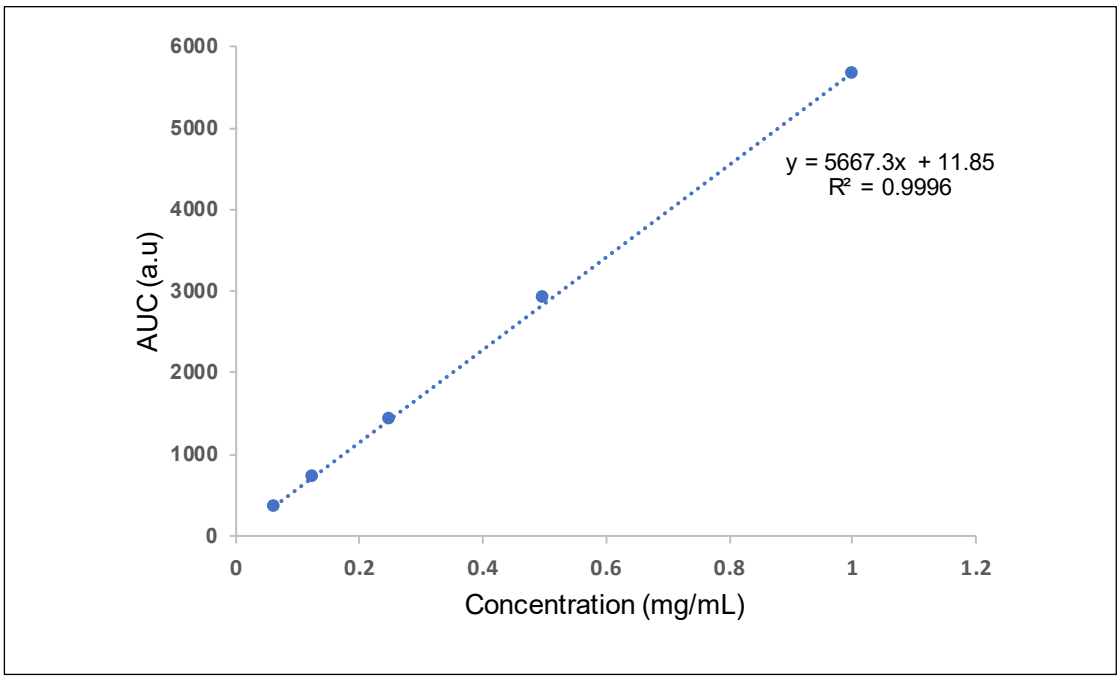

Figure 3-8: Average standard curve of tacrolimus in RP-HPLC.

The level of palmitoylation and quaternisation of GCPQ can be altered to meet the specific requirements of the formulation [138]. In this study, we chose GCPQ with similar levels of palmitoylation and quaternisation, (GCPQ16: GC10P18Q18, QPR 1.0), to balance the lipophilicity and hydrophilicity of the polymer. We adopted this strategy in order to overcome the corneal barrier functions, precisely the opposite characteristics of the tight junction epithelium and stroma of the cornea [217,218]. The corneal epithelium is lipophilic, which will restrict the movement of hydrophilic compounds, whereas the stroma is hydrophilic and will limit the movement of lipophilic compounds. This dual nature of the cornea acted as a strong barrier for drug entry into the ocular globe. Therefore, compounds must possess both hydrophilic and lipophilic properties to overcome the corneal barrier.

The results of the encapsulation of tacrolimus within GCPQ using high-pressure homogenisation method are presented in (Table 3-8). We passed the formulation through the machine for one cycle and ten cycles. For the one cycle method, the polymer-to-drug mass ratios (5:1, and 10:1) did not show a high encapsulation of tacrolimus in the GCPQ (0.25, and 0.3 mg/mL), respectively. Also, after ten cycles, the polymer-to-drug mass ratios (5:1, and 10:1) did not produce a sufficient encapsulation of tacrolimus in the GCPQ (0.32, and 0.46 mg/mL), respectively. These results demonstrated that mechanical treatment significantly alters the concentration of the encapsulated tacrolimus, possibly due to the drug being adhered to the inner part of the homogeniser. Zhang et al. reported the cationic nanoemulsion formulation of tacrolimus for ophthalmic delivery [219]. They passed the tacrolimus formulated in a blend of the two non-ionic surfactants, Tween 80 and

poloxamer 188, the cationic agent, Cetalkonium chloride, osmotic pressure regulator, glycerine, the oily component, medium-chain triglyceride as well as castor oil, and water for (8 cycles, 600 bar) in high-pressure homogeniser with a cooling jacket at the exit of the valve to reduce the risk of high temperature [219]. They have achieved high tacrolimus encapsulation efficiency (99 ± 1%) [219]. As reported, they have used a blend of materials and excipients that could provide stable media to formulate tacrolimus. The cooling jacket at the exit of the HPH valve offers a cooling process to avoid tacrolimus degradation at elevated temperature. In contrast, we used GCPQ to formulate tacrolimus without cooling process at HPH. This process could give rise to an elevated temperature of the formulation, and as a result, low tacrolimus encapsulation efficiency using HPH was observed. Another report showed that tacrolimus formulated in self-micro emulsifying drug delivery system was not stable under high temperature and high humidity [220]. It is clear that formulation strategies involving tacrolimus should not encounter high temperature and as such, high encapsulation of tacrolimus could be achieved.

The effect of GCPQ polymer-to-drug mass ratios on the encapsulation efficiency of tacrolimus was assessed by preparing formulations with 1:1, 2:1, 5:1 and 10:1 polymer-to-drug mass ratios without the application of any mechanical treatment (Table 3-8). Polymer to drug mass (F5, F6) have a low encapsulated tacrolimus concentration within GCPQ, encapsulation efficiency (EE) = (0.20 ± 0.02 mg/mL and 0.3 ± 0.03 mg/mL), respectively. We observed a cloudy appearance in both formulations upon reconstitution with (2.6% w/v) glycerol solutions. This observation may suggest that the polymer composition was insufficient to encapsulate tacrolimus and that most of the drug particles were suspended rather than dispersed in the aqueous phase. Hence, we increased the polymer to drug mass (F7, F8) to 5:1 and 10:1, respectively. With F7 and F8, we obtained clear liquids upon reconstitution with (2.6 % w/v) glycerol solution, suggesting that most of the drug was encapsulated in the formulations (F7; EE = 75 ± 7.6%, F8; EE = 87 ± 5.8%).

Generally, treatments with a high-pressure homogeniser generated high shear forces as a result of extreme pressure change, thus producing nanoparticle populations with smaller in size [221]. However, GCPQ: TAC formulation (5:1) treated with ten cycles of HPH showed the highest particle size distribution (346 ± 4 nm). This may have occurred due to a substantial increase in the surface area of the nanoparticles following the mechanical treatment, thus promoting aggregation.

As shown in Table 3-8, polymer-to-drug mass ratio (10:1) with the solvent evaporation method give the best encapsulation of tacrolimus with the GCPQ (~ 0.9 mg/mL), with a particle size (~ 200 nm). Thus, we decided to test this formulation further for stability studies and subsequent animal pharmacokinetic work.

Table 3-8: Summary of different approaches used to encapsulate tacrolimus within GCPQ.

Polymers	Encapsulation method	Formulation	Polymer: drug mass ratio (w/w)	Measured Drug content (% w/v)	Theoretical Drug content (% w/v)	EE (%)	Particle size (nm) Peak intensity (%)	
							Main peak	Second peak
GCPQ16 (GC10-P18 Q18)	HPH (1 cycle)	F1	5:1	0.025±0.001	0.1	25 ± 7	200 ± 29 (81 ± 2%)	10 ± 0.5 (12 ± 1%)
		F2	10:1	0.030±0.001	0.1	30 ± 10	247 ± 20 (61 ± 4%)	10 ± 0.3 (37 ± 4%)
	HPH (10 cycles)	F3	5:1	0.032±0.001	0.1	32 ± 12	346 ± 4 (81 ± 2%)	56 ± 7 (9 ± 1%)
		F4	10:1	0.046±0.001	0.1	46 ± 10	145 ± 2 (72 ± 1%)	10 ± 0.4 (28 ± 1%)
	Solvent evaporation	F5	1:1	0.02±0.002	0.1	20 ± 2	198 ± 11 (57 ± 2%)	9 ± 0.2 (43 ± 0.5%)
		F6	2:1	0.03±0.003	0.1	34 ± 3	133 ± 4 (46 ± 0.3%)	9 ± 0.04 (51 ± 1%)
		F7	5:1	0.07±0.001	0.1	75 ± 7.6	149 ± 2 (86 ± 0.1%)	11 ± 0.1 (14 ± 0.1%)
		F8	10:1	0.09±0.001	0.1	87 ± 5.8	195 ± 28 (52 ± 4%)	11 ± 0.4 (47 ± 3%)

Electron microscopy was used to observe the morphology of the nanoparticles formed using GCPQ polymer. Figure 3-9 shows that GCPQ: TAC formulation form spherical vesicles which expectedly contains the encapsulated tacrolimus. Images showed two distinct nanoparticle populations with larger particles are the encapsulated tacrolimus, and the smaller particles are the empty GCPQ micelles.

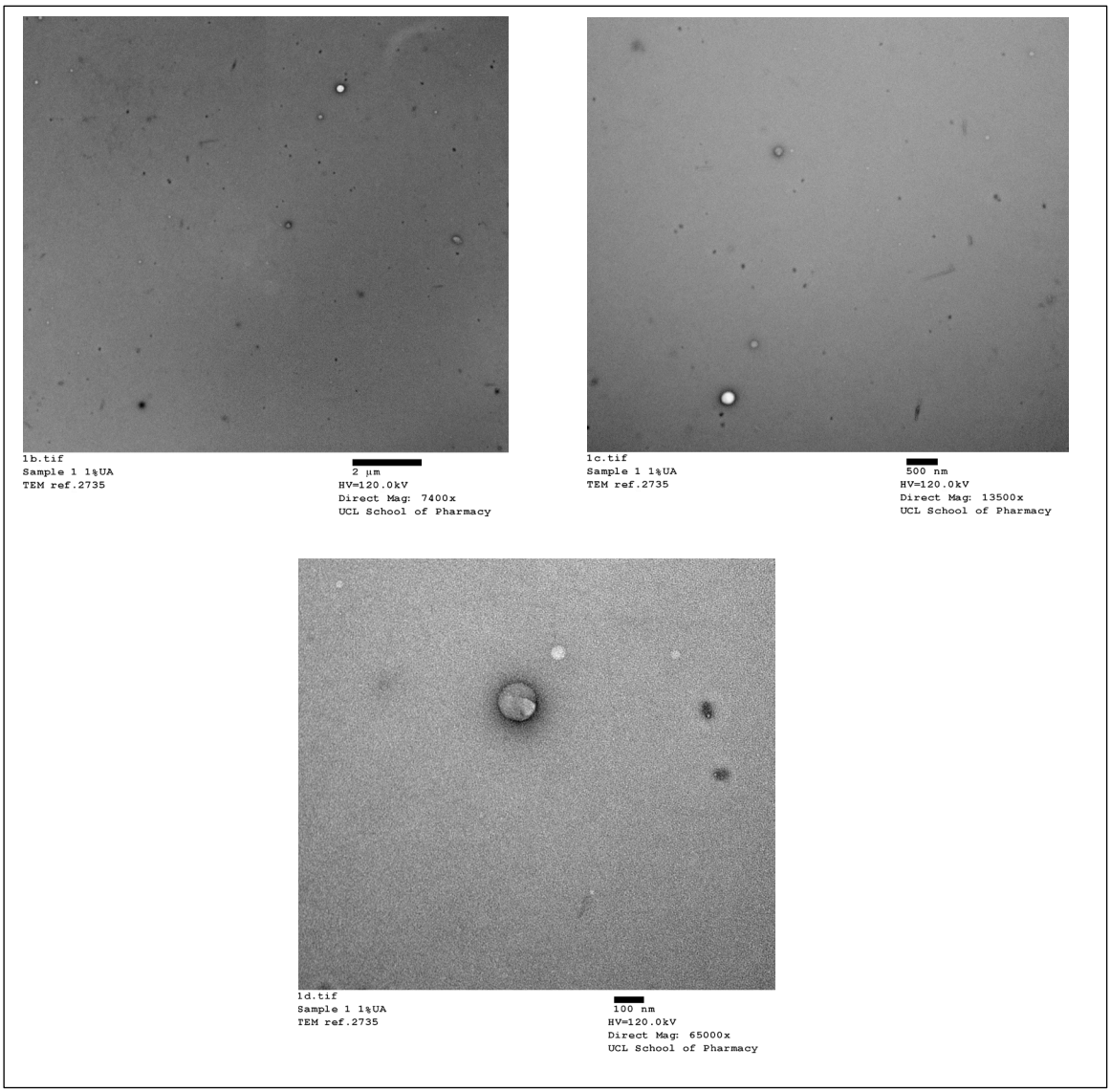

Figure 3-9: Transmission electron microscopy of GCPQ: tacrolimus formulation.

3.4.2.1. Stability studies of GCPQ: TAC formulation

The stability of the GCPQ16: TAC formulations were determined by measuring the physicochemical properties over 30 days. Table 3-9 shows the properties of all formulations upon storage at different conditions for 30 days. After 30 days of storage, the formulation stored in the fridge displayed excellent drug content stability compared to formulations stored at room temperature and 40°C at all time points ($p < 0.05$). The tacrolimus in the formulation stored at (5±3°C) displayed a similar drug content at Day 0 (0.99 ± 0.002 mg/mL) as compared to Day 30 (0.94 ± 0.049 mg/mL) ($p > 0.05$).

GCPQ: TAC Formulations stored at room temperature and under accelerated storage conditions showed significant changes in drug content at Day 7, and Day 30 compared to day 0. Analysis of most of the parameters had suggested that the formulation stored under accelerated storage conditions (40 ± 2°C / 75 ± 5% RH) had the lowest stability. The tacrolimus concentration fell substantially from (0.99 ± 0.002 mg/mL) to (0.04 ± 0.001 mg/mL) after 30 days, indicating that almost 95% of the drug was lost from its original content.

All prepared formulations were examined for pH. The pH of the formulation was adjusted to 7.1 ± 0.1 with 1.0 M NaOH. The pH of the GCPQ: TAC formulation stored at 40 ± 2°C showed a reduction in the pH after 30 days of storage; with the pH falling to 6.3 ± 0.01. As described, the optimum pH for eye drops equals that of tear fluid and is 7.4 [206]. If the pH value gets outside the acceptable range that is tolerated by eye 6.6 – 7.8 [209], the patient may feel discomfort, there may

be irritation, and the drug bioavailability can decrease because of increased tearing [210]. The GCPQ: TAC formulation stored in the fridge showed a pH value within the acceptable range (6.8 – 7.1). The pH of the GCPQ: TAC formulation stored at room temperature and accelerated degradation conditions showed a reduction in the pH after 30 days of storage (6.5 ± 0.05) and (6.3 ± 0.01), respectively. GCPQ is a weak base with a pKa of 6.0 but yet forms micellar dispersions over a range of pH values, up to a pH value of 9 [138]. The 6-O-glycol unit enables GCPQ to produce micelles at neutral pH, as chitosan is insoluble in neutral media and is only soluble at acidic pH, whereas GC is soluble at neutral pH [138]. Moreover, temperature plays a significant role in pH measurements. As the temperature rises, molecular vibrations increase, resulting in water's ability to ionise and form more hydrogen ions. As a result, the pH will drop [222]. This principle is observed when GCPQ: TAC formulations are stored at an elevated temperature, and as such, the pH value decreases. A similar outcome was observed with GCPQ: RAP formulation. The pH of the GCPQ: RAP formulation stored at 40 ± 2°C showed a reduction in the pH after 30 days of storage; with the pH falling from 7.2 ± 0.1 to 6.5 ± 0.04.

The size and surface potential were determined for the prepared formulations. The GCPQ: TAC formulation possessed two nanoparticle populations after filtration. The main peak population with larger particle sizes (~ 200 nm) was presumed to be the encapsulated tacrolimus in the formulation. In contrast, the second peak population with smaller particle sizes (~ 10 nm) was assumed to be empty GCPQ micelles as has been reported previously [105]. The average size

of the main peak population following filtration was 235 ± 64 nm, and the corresponding percentage intensity was 49 ± 4.6%. The size of the smaller population was 13 ± 0.5 nm, with a percentage intensity of 48 ± 2.0%.

There were no significant differences in the formulation particle size on Day 0, Day 7, and Day 30 day of storage at room temperature and at accelerated conditions ($p > 0.05$). The change in the formulation particle size stored in the fridge at Day 30 when compared to Day 0 was significant, but the sample remained clear of any visual precipitation (Figure 3-10, B).

GCPQ possess an overall positive charge due to the presence of quaternary ammonium groups on their surface [137]. As such, we obtained a positive zeta potential value with the GCPQ: TAC formulation (16 ± 4.6 mV) over three independent experiments. There were no significant differences in the formulation zeta potential when Day 0 was compared to Day 7 and Day 30 irrespective of the storage, indicating that the formulations remained colloidally stable as there should be electrostatic repulsions between the individual nanoparticles [223].

Our formulations are isotonic and have an osmolarity value range of 308 – 327 mOsm/kg, which is within the range tolerable by the eye. Hypertonic and hypotonic formulations can induce a burning sensation after instillation, leading to excessive lacrimation and consequently drug removal from the ocular surface [224]. Clinical evaluation of tacrolimus eye drops with high osmolality values of more than 1000 mOsm/kg has been shown to induce ocular irritation in patients following the formulation's instillation into the eyes [225].

The viscosity of the formulations ranged from 1.4 - 1.7 mPa.s at 25°C ($p > 0.05$, two-way ANOVA). The viscosity of the formulation is higher than that of plain water (0.89 mPa.s at 25°C) [35], due to the presence of the GCPQ polymer in the formulation [136]. GCPQ is known to be mucoadhesive in the gastrointestinal tract [226]. As this formulation is intended for topical ocular administration in the eye, the slightly increased viscosity and the GCPQ bioadhesive properties are essential when it comes to promoting drug residence time at the ocular surface.

Table 3-9: Parameters of GCPQ: TAC optimum formulation stored at the fridge (5±3°C), room temperature (25±2°C), and at a critical condition of (40±2°C) for 30 days.

Storage conditions	Parameters	Day 0	Day 7	Day 30
5±3°C	Drug concentration (mg/mL)	0.99 ± 0.002	1.00 ± 0.001 ^{ns}	0.94 ± 0.049 *
	pH	7.1 ± 0.1	6.8 ± 0.01 #	6.9 ± 0.1 #
	Main peak size (nm)	235 ± 64	234 ± 16 ^{ns}	373 ± 7 *
	Peak intensity (%)	(49 ± 5%)	(53 ± 2%)	(61 ± 2%)
	Second peak size(nm)	13 ± 1	11 ± 1 ^{ns}	13 ± 2 *
	Peak intensity (%)	(48 ± 2%)	(47 ± 2%)	(39 ± 2%)
	Zeta potential (mV)	+16 ± 4.6	+21 ± 4.2 ^{ns}	+19 ± 2.4 ^{ns}
	Osmolarity (mOsm/kg)	327 ± 3.1	319 ± 3.1 ^{ns}	326 ± 10.02 ^{ns}
	Viscosity (mPa.s)	1.7 ± 0.003	1.6 ± 0.04 #	1.5 ± 0.01 #
25±2°C 60 ± 5% RH	Drug concentration (mg/mL)	0.99 ± 0.002	0.87 ± 0.004 #	0.41 ± 0.006 #
	pH	7.1 ± 0.1	6.7 ± 0.02 #	6.5 ± 0.05 #
	Main peak size (nm)	235 ± 64	194 ± 17 ^{ns}	174 ± 11 ^{ns}
	Peak intensity (%)	(49 ± 5%)	(40 ± 2%)	(38 ± 1%)
	Second peak size(nm)	13 ± 1	12 ± 1 ^{ns}	12 ± 1 ^{ns}
	Peak intensity (%)	(48 ± 2%)	(60 ± 2%)	(62 ± 1%)
	Zeta potential (mV)	+16 ± 4.6	+21 ± 3.1 ^{ns}	+24 ± 2.3 ^{ns}
	Osmolarity (mOsm/kg)	327 ± 3.1	314 ± 4.5 *	314 ± 3.1 *
	Viscosity (mPa.s)	1.7 ± 0.003	1.5 ± 0.02 #	1.7 ± 0.01 ^{ns}
40±2°C 75 ± 5% RH	Drug concentration (mg/mL)	0.99 ± 0.002	0.27 ± 0.002 #	0.03 ± 0.001 #
	pH	7.1 ± 0.1	6.8 ± 0.01 #	6.3 ± 0.01 #
	Main peak size (nm)	235 ± 64	156 ± 12 ^{ns}	218 ± 52 ^{ns}
	Peak intensity (%)	(49 ± 5%)	(34.43±2.19)	(33.97±3.12%)
	Second peak size(nm)	13 ± 1	12 ± 1 ^{ns}	13 ± 1 ^{ns}
	Peak intensity (%)	(48 ± 2%)	(65.57±2.19%)	(65.33±3.10%)
	Zeta potential (mV)	+16 ± 4.6	+18 ± 3.1 ^{ns}	+23 ± 3.5 ^{ns}
	Osmolarity (mOsm/kg)	327 ± 3.1	308 ± 2.5 #	310 ± 4.5 #
	Viscosity (mPa.s)	1.7 ± 0.003	1.4 ± 0.03 #	1.6 ± 0.01 #

ns = not significant, * = $p < 0.05$, # = $p < 0.005$.

Figure 3-10 showed the results of the drug content and visual appearance of all formulations upon storage at three different conditions. As shown in Figure 3-10, A there is a loss of the drug content for the formulation stored at room temperature (25±2°C / 60±5% RH) and at accelerated conditions (40±2°C / 75±5% RH). This drug loss is observed as the precipitation of the formulation after 30 days (Figure 3-10, B). The GCPQ: TAC stored at the fridge for 30 days was a clear formulation at the end of the storage period. This finding was consistent with the findings of others. Rodriguez et al. demonstrated that tacrolimus formulated with Liquifilm eye drops containing polyvinyl alcohol (0.03% w/v), did not degrade when stored for 90 days at low temperature, either in the fridge (5±3°C) or the freezer (-17.5±2.5°C) [225]. They concluded that the tacrolimus formulation stored at room temperature showed a considerable decline by 50% in the drug content (0.015% w/v) [225]. We have found a similar observation where tacrolimus stored at room temperature showed a reduction in the drug content by ~ 50% after 30 days (0.99 mg/mL for day 0, and 0.41 mg/mL for day 30).

The temperature is an essential factor in the stability under the storage of tacrolimus ophthalmic formulations [225]. Peterka et al. reported the sensitivity of an amorphous form of tacrolimus at an elevated temperature and humidity (50°C / 75% RH) [227]. The proportion of TAC impurities in amorphous material increased with higher moisture content. Amorphous material has higher thermodynamic activity and tends to be chemically and physically less stable than the corresponding crystalline material [227]. This can be explained by the fact that amorphous material is more hygroscopic than crystalline material, and

water absorbed on the surface increases the chemical degradation of amorphous material by providing a reaction medium or acting as a reactant [227]. Based on these results, our formulation appeared to be stable against degradation when stored in the fridge. Thus, samples of tacrolimus should be analysed immediately and formulations stored at low temperatures (+4°C).

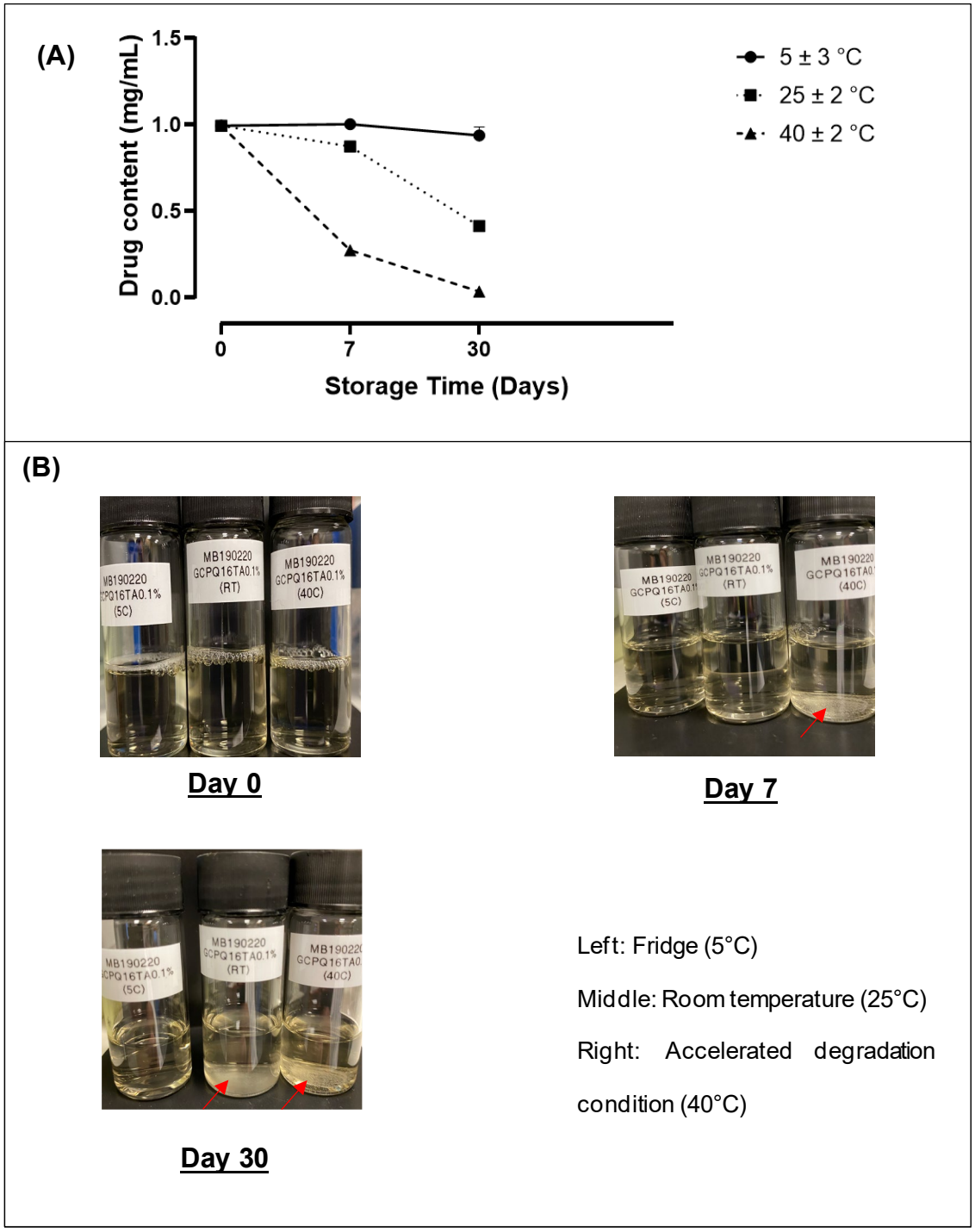

Figure 3-10: GCPQ: TAC physical stability over 30 days of storage.
Precipitation is clearly seen in the formulations stored at room temperature and accelerated degradation conditions.
(A) Drug content; **(B)** visual appearance.

3.5. Conclusion

The amphiphilic polymers GCPQ with different molecular weights and similar degrees of DP% and varying degrees of DQ% were synthesised and used for manufacturing an aqueous-based eye drop formulations of the model drugs, RAP and TAC. The solvent evaporation method approach utilising the GCPQ polymer was used to formulate the model drugs. When encapsulated within GCPQ nanoparticles, we have shown that RAP exhibits excellent aqueous incorporation levels with an increase of up to 1000-fold compared to RAP alone. The GCPQ: RAP formulation (~0.2% w/v) was stable over 30 days of storage at 5°C, and room temperature and this stability were due to the formation of micelle-like structures. This formulation will be used for a further pharmacodynamics experiment on a diseased animal model. Also, the biodistribution pharmacokinetic profile will be studied in a healthy New Zealand rabbits' model. We manufactured a clear aqueous TAC eye drops formulation (0.1% w/v). GCPQ as a novel delivery system for ocular delivery was able to enhance the TAC solubility up to 100-fold. A GCPQ: TAC formulation was stable against degradation when stored in the fridge for 30 days. This formulation will be used to study its pharmacokinetic profile in healthy New Zealand rabbits' model.

4. Biological *in vitro* Studies

4.1. Introduction

Upon topical ocular administration, precorneal factors and anatomical barriers negatively affect the bioavailability of topical formulations; leading to bioavailabilities of less than 5% [8]. The pre-corneal factors that inhibit drug absorption are: rapid drainage of eye drops, blinking, the tear film, tear turn over and induced lacrimation [228]. The cornea is the main ocular anatomical barrier. It is the anterior-most layer of the eye and is considered the primary barrier limiting the entry of exogenous substances into the eye and protects the intraocular tissues [8,20]. The existence of tight junctions on the conjunctival epithelium [229] and the possible systemic absorption through the conjunctiva [27] also limit the ocular drug absorption. The presence of the proteoglycan matrix in the sclera also plays a central role in ocular drug permeation [8].

Cellular barriers in the body act as a gateway between the external environment and internal compartments; therefore, drug molecules can traverse these barriers through two distinct pathways: the paracellular and transcellular pathways (Figure 4-1, A). The paracellular pathway involves the movement of drug molecules between the junctions of the cells, whilst with the transcellular pathway, drugs can penetrate these barriers through cell membranes [230].

The epithelial barrier consists of various intercellular junctions, such as the adherens junction, gap junction, desmosome and tight junctions [231]. Tight junctions are the most apically located intercellular junctions in epithelial cell sheets [232,233]. There are

four primary groups of transmembrane proteins that have been described at conventional epithelial tight junctions; occludin, members of the claudin family, tricellulin, and junction adhesion molecules [232,233]. These proteins form the paracellular seals by interacting with their extracellular domains to occlude the intercellular space [231]. Tight junctions act as a semipermeable barrier to the paracellular transport of ions, solutes and water, and are considered to function as a fence that divides apical and basolateral domains of membranes [233].

It has been reported that tight junctions' proteins were found in rat corneal epithelium including occludin, localised at the cell borders of the superficial layer, whereas claudin-1 was found mainly in the basal and wing cell layers [13]. Chen et al. reported the presence of zonula occludens-1 (ZO-1), zonula occludens-2 (ZO-2), occludin and claudin-1 in rabbit corneas and these were all localised contiguously at the superficial cell boundary [234].

As the cornea is considered the main barrier for topically applied drugs and we intend to use rabbits as an animal model for the *in vivo* studies, we decided to use the Statens Seruminstitut Rabbit Cornea (SIRC) cell line to study the cytotoxicity profile of GCPQ and the effect of GCPQ's structure on the transport of drugs across the cornea. Also, the Madin-Darby Canine Kidney (MDCK) cell line was employed as the MDCK cell line is a well-known model for the study of tight junctions, and it was thus used as a model to explore the effect of the GCPQ's structure on drug transport across the corneal epithelium.

Whereas intracellular trafficking is often studied in standard wells or coverslips, the absence of a basolateral compartment precludes cell polarisation and the ability to

study transport across cell layers. To overcome this obstacle, transport across cell monolayers has been long studied using transwell inserts (Figure 4-1, B), which consist of an upper (apical) chamber, a porous, permeable membrane where cells attach and form a tight monolayer, and a lower (basolateral) chamber [235]. In the transwell, transport can be measured in the apical-to-basolateral direction by administering a treatment into the upper chamber, followed by the transport through the cell monolayer and the underlying porous membrane, and finally collecting the medium in the lower chamber for quantification of transported material. Transport in the basolateral-to-apical direction can also be measured by initial administration to the lower chamber and subsequent collection from the upper chamber [235]. While many factors involved in the *in vivo* delivery are eliminated, the transwell *in vitro* model provides useful preliminary information regarding transport mechanisms [235]. This chapter is focused on the study of the cytotoxicity of GCPQ and the formulation, and the effect of different properties of GCPQ on the epithelial barriers. Two cell lines will be tested for the cytotoxicity and the permeability studies: the MDCK and the SIRC cell lines.

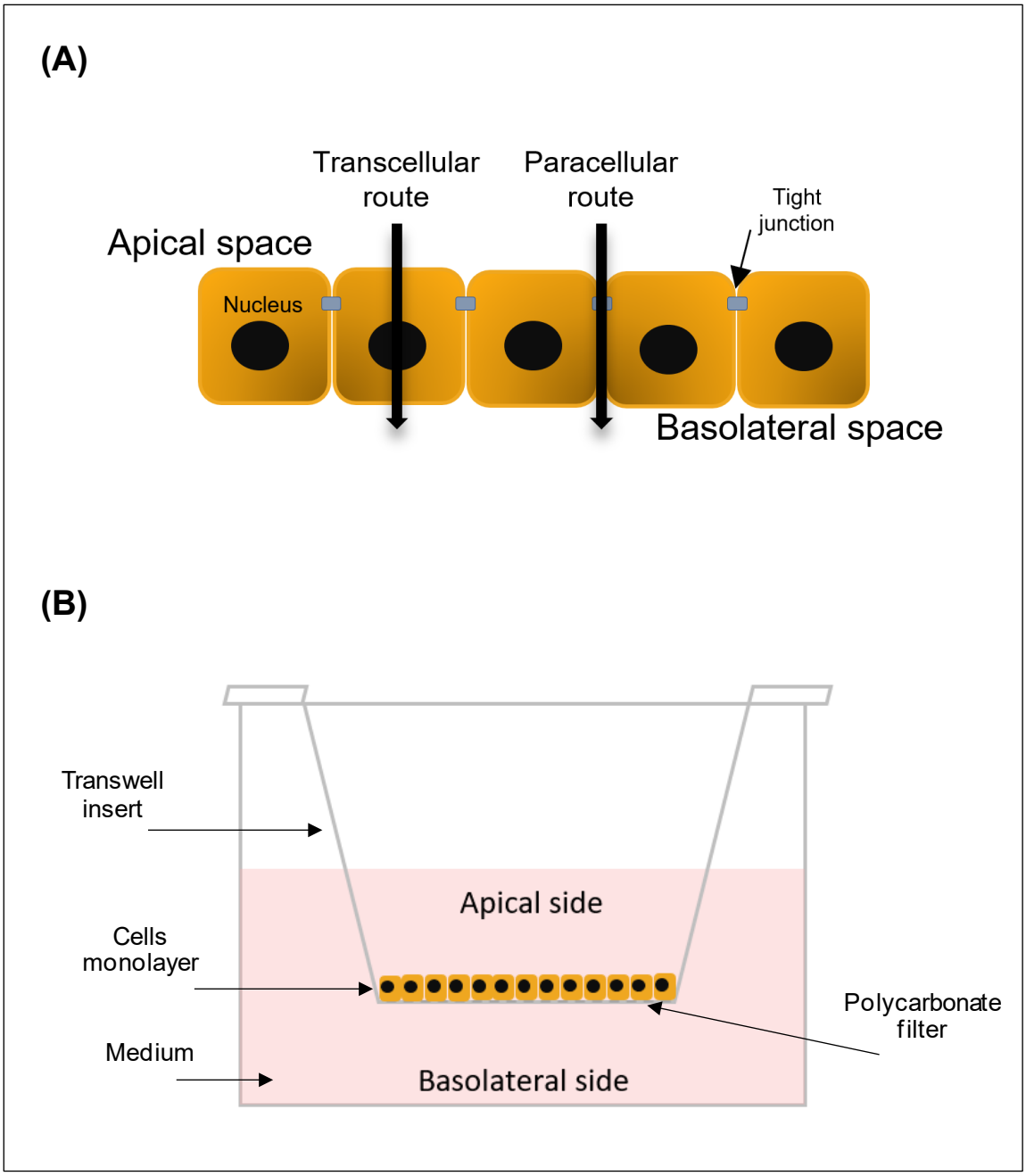

Figure 4-1: Schematic diagram of **(A)** mechanisms of drug transport through the cell membrane; **(B)** cells monolayer formed on the transwell membrane.

The experimental design for the *in vitro* cytotoxicity and permeability assays is shown in Figure 4-2.

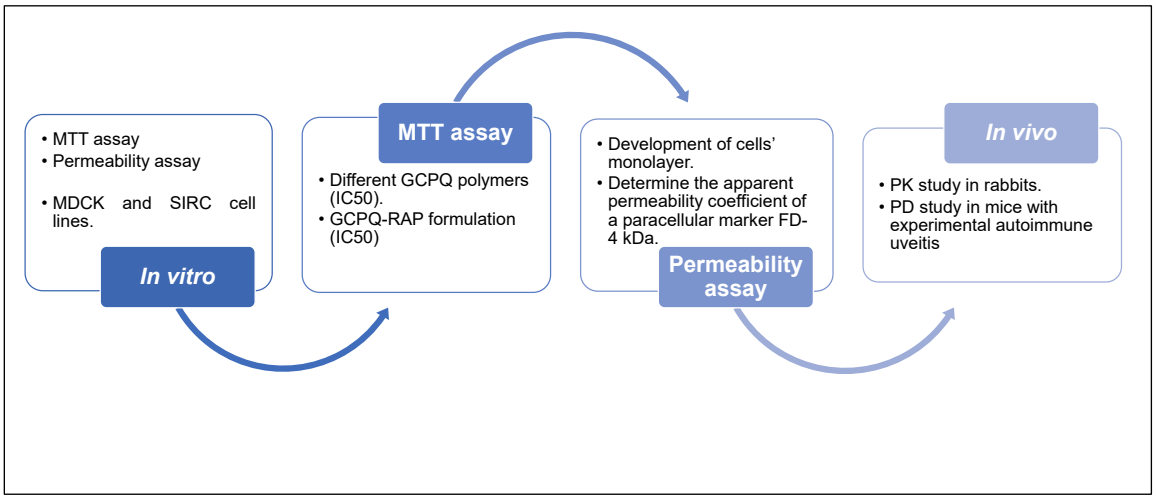

Figure 4-2: Illustration of the experimental plan for the *in vitro* studies.

4.2. Effect of GCPQ polymeric nanoparticles on cellular toxicity

4.2.1. Introduction

It is essential to determine the concentration or dose at which the therapeutic agent becomes unsafe for therapeutic purposes. Preclinical testing is vitally important to eliminate unsuitable candidates before the expense of clinical research is incurred. The use of cell culture for the initial preclinical screening of potential therapeutic compounds is common as cultured cells can be selected to represent the disease of interest or its associated biochemical anomalies. It is vital to obtain accurate, reliable results from the *in vitro* cytotoxicity assays employed in the initial stages of preclinical research as this data may influence the success of a drug candidate to proceed into the development process [236].

The 3-(4,5-dimethylthiazol-2-yl)-2,5-diphenyl-2H-tetrazolium bromide (MTT) assay has become the gold standard for the determination of cell viability and proliferation [236]. Several tetrazolium-based assays, such as the XTT, MTS, and WST assays, in which water-soluble formazan products are generated, eliminate the need for washing, and solvent solubilisation steps, have been developed but have not replaced the well-established MTT assay [236]. However, MTT assay is associated with certain limitations such as background interference and a necessary step to solubilise the crystal formazan [237]. Thus, this section focuses on determining the effect of GCPQ polymeric nanoparticles on the cells metabolic activity by measuring the IC50 values using the MTT assay.

4.2.2. Materials

Chemical	Supplier
MDCK cell line	LGC standards – ATCC (Teddington, UK)
SIRC cell line	LGC standards – ATCC (Teddington, UK)
Eagle's minimum essential medium	Sigma-Aldrich (Gillingham, UK)
Foetal bovine serum	Sigma-Aldrich (Gillingham, UK)
Non-essential amino acids	Sigma-Aldrich (Gillingham, UK)
MTT reagent	Sigma-Aldrich (Gillingham, UK)
Penicillin-streptomycin	Life technologies Ltd. (Paisley, UK)
Sodium pyruvate	Life technologies Ltd. (Paisley, UK)
glutaMAX	Life technologies Ltd. (Paisley, UK)
DMSO	Fisher Scientific (Loughborough, UK)

4.2.3. Methods

4.2.3.1. MTT assay

The MTT assay is a colourimetric assay that measures the reduction of water-soluble (yellow) MTT reagent to an insoluble coloured (dark purple) formazan product by mitochondrial succinate dehydrogenase [238]. The tetrazolium ring is cleaved in active mitochondria, and so the reaction occurs only in living cells [239]. The cytotoxicity of GCPQ was assessed by the measurement of the IC50 value in a standard MTT assay.

The SIRC and the MDCK cell lines were seeded at $1x10^4$ cells per well in 96-well plates and allowed to grow for one day in cell growth medium containing minimum essential medium supplemented with foetal bovine serum (10% v/v, 50 mL), glutaMAX (1% v/v, 5 mL), non-essential amino acids (1% v/v, 5 mL), penicillin-streptomycin (1% v/v, 5 mL), and sodium pyruvate (1% v/v, 5 mL).

The MDCK cell line was treated with GCPQ10, and the SIRC cell line was treated with GCPQ07, GCPQ09, and GCPQ10. Both cell lines were treated with increasing concentrations of polymers dispersed in filtered deionised water (10 mg/mL) and diluted with medium (9.7×10^{-3} – 5 mg/mL, 100 µL per well).

On the SIRC cell line, cells were treated with increasing concentrations of GCPQ13 and GCPQ14 dispersed in filtered deionised water (15 mg/mL) and diluted with medium (14.6×10^{-3} – 7.5 mg/mL, 100 µL per well). These concentrations were selected based on screening experiments conducted to determine the appropriate working ranges.

GCPQ10: RAP formulations were prepared (2 mg/mL rapamycin) at 5:1 and 7.5:1 polymer to drug mass ratio. SIRC cells were treated with increasing RAP concentrations. GCPQ10: RAP formulation diluted with medium (1.9×10^{-3} – 1 mg/mL, 100 µL per well).

The cell viability using RAP was also determined. Rapamycin was prepared by dissolving RAP in DMSO (1 mg/mL), followed by a further dilution of rapamycin to give a concentration of 20 µg/mL using DMSO in water (1% v/v). This stock solution of RAP was used to treat SIRC cells with increasing concentrations of RAP diluted with medium (1.9×10^{-2} – 10 µg/mL, 100 µL per well). Control groups received treatment with DMSO solution at the same volume and concentration used to prepare the RAP treatments.

Cells were treated and incubated for 4 hours at 37°C and in a 5% CO_2 environment. The four-hour treatment time was chosen to mimic the possible dose frequency. After the incubation time, the treatment was discarded, and the cells washed with Dulbecco's phosphate-buffered saline (DPBS). Then, supplemented cell growth medium (MEM, FBS 10%, glutaMAX 1%, non-essential amino acids 1%, penicillin-streptomycin 1%, sodium pyruvate 1%, 200 µL) was added, and the cells were incubated for 24 hours to allow for recovery. Subsequently, the medium was aspirated from five wells, and some cells were treated with 1% Triton X-100 prepared in DPBS (100 µL per well) as a positive control for 20 minutes. It is well-known that the Triton X-100 causes 100% of cells lysis [240,241]. The toxicity of Triton X-100 molecules arises because of the disrupting action of its polar head group on the hydrogen bonding present within the cell's lipid bilayer, leading to the disruption of

cellular structure of the cell membrane at concentrations above the Triton X-100 CMC (0.19 to 0.20 mM) [241].

MTT solution was prepared by adding MTT reagent to DPBS (5 mg/mL). This MTT solution was then diluted with medium to a final concentration of 0.5 mg/mL and filtered through a 0.22 µm filter protected from light. The medium in the plate was removed, and the MTT solution (0.5 mg/mL, 200 µL) was added to each well followed by incubating the cells with the MTT solution for two hours at 37°C and in a 5% CO_2 environment. Following this incubation period, the MTT solution was gently aspirated. Subsequently, DMSO (200 µL) was added to each well, followed by mixing to ensure complete solubilisation of the resulting formazan crystals. The plates were then read on a UV spectrophotometer, SpectraMax M2 from Molecular Devices (Wokingham, UK) at a wavelength of 570 nm.

For the analysis, the absorbance of the background values was subtracted. The background value for the RAP treatment group was DMSO solution at the same volume and concentration used to prepare the RAP treatments plus empty wells. The background for all other groups was the value obtained from empty wells. The cytotoxicity was determined as the ratio between the measured absorbance values of treated and untreated cells. The IC50 values (concentration of the treatment at which 50% of cells are viable) were determined by analysing the data using Prism software (GraphPad Software, USA).

4.2.4. Results and discussion

Table 4-1 shows the IC50 values for the GCPQ polymers, GCPQ: RAP formulations, and rapamycin on MDCK and SIRC cell lines. The IC50 values of treatment groups were obtained through the dose-response curves.

Table 4-1: Ranking of minimum inhibitory concentration (IC50) of the tested materials on MDCK and SIRC cell lines.

Compound	Properties	QPR	Cell line	IC50 (µg/mL) (mean ± SE)
GCPQ10	(GC16, P18, Q19)	1.05	MDCK	$4.54 \pm 0.36 \times 10^3$
GCPQ13	(GC27, P22, Q15)	0.68	SIRC	$3.31 \pm 0.19 \times 10^3$
GCPQ09	(GC60, P18, Q16)	0.89	SIRC	$2.78 \pm 1.43 \times 10^3$
GCPQ07	(GC16, P22, Q10)	0.45	SIRC	$2.05 \pm 0.22 \times 10^3$
GCPQ10	(GC16, P18, Q19)	1.05	SIRC	632.90 ± 48.90
GCPQ14	(GC30, P19, Q19)	1	SIRC	438.2 ± 0.1
GCPQ10: RAP	(5:1) polymer to drug mass ratio	-	SIRC	36.75 ± 4.41
GCPQ10: RAP	(7.5:1) polymer to drug mass ratio	-	SIRC	23.69 ± 2.76
Rapamycin	-	-	SIRC	3.77 ± 0.59

GCPQ polymers with high DQ% and a relatively high QPR value ~1, showed low IC50 values. GCPQ10 (P18%, Q19%, QPR 1.05) and GCPQ14 (P19%, Q19%, QPR 1) has an IC50 of 632.9 ± 48.9 µg/mL, and 438.2 ± 0.1 µg/mL, respectively, compared to GCPQ13 (P22%, Q15%, QPR 0.68) that has an IC50 of 3.31 ± 0.19 mg/mL on SIRC cell line (Table 4-1, Figure 4-3). Hence, irrespective of the molecular weight, as the DQ increases, the toxicity increases significantly ($p < 0.05$), as shown with GCPQ10 (P18%, Q19%, QPR 1.05) and GCPQ07 (P22%, Q10%, QPR 0.45). GCPQ10 was also tested for cytotoxicity on MDCK cell line. We observed a higher IC50 value on the MDCK compared to SIRC cell line 4.54 ± 0.36 mg/mL and 632.90 ± 48.90 µg/mL, respectively. The IC50 of GCPQ10 in the MDCK cell line is about seven-fold higher than in the SIRC cell line. It has been reported that there is a trend of decreasing cell viability with increasing DQ% or decreasing DP% in both MDCK and colon adenocarcinoma (Caco-2) cells by the MTT assay [242].

GCPQ is a polycation polymer that has a positive charge that might destabilise the cell membrane to a certain extent and cause cytotoxicity even in the absence of the drug [243]. MDCK is a canine kidney cell line while SIRC is a rabbit corneal cell line; the previous results indicate that the polymer's cytotoxicity is a cell type-dependent. The cytotoxicity of GCPQ was reported and assessed by measuring the IC50 value in a standard MTT assay seeded at 700 cells per well, and exposure time = 4 hours [134]. A prototype of GCPQ with a high molecular weight of 176 kDa, 6 mole % of palmitoylation and 4 mole % of quaternisation was reported to have an IC50 of 1.28 mg/mL in A431 cell line [134]. Compared with some other permeation enhancers, this value is much higher and represents a safer system for drug delivery. The cationic

polymer poly-L-lysine has an IC50 of 0.007 mg/mL while poly-L-ornithine has an IC50 of 0.004 mg/mL in the A431 cell line seeded at 700 cells per well, and exposure time = 4 hours [244]. The cytotoxicity of chitosan derivatives has also been reported. Trimethylated chitosan derivatives were shown to have IC50 values ranging from about 0.05 mg/mL to about 1.0 mg/mL in a breast cancer epithelial (MCF-7) cell line seeded at $1x10^4$ cells/well in a 96-well plate, exposure time = 6 and 24 hours. The IC50 value (0.05 mg/mL) was lower for trimethyl chitosan derivatives with higher trimethylation levels (76%) [245]. A general trend of increasing toxicity with increasing trimethylation degree was reportedly related to toxicity, with no effect on cell viability when molecular weight was increased [245].

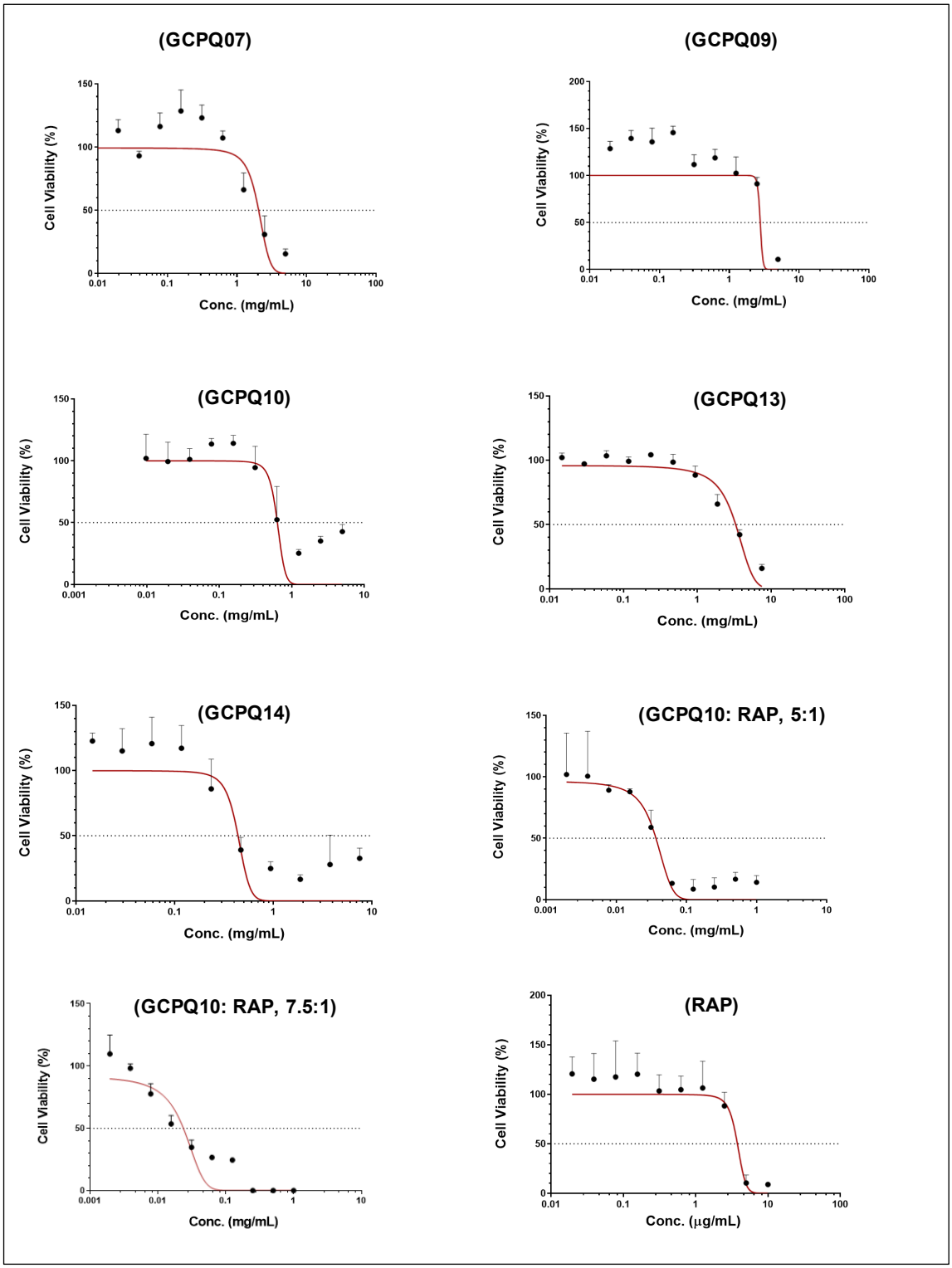

Figure 4-3: MTT assay on SIRC cell line.

n= 3 independent experiments.

The cytotoxicity of the formulations and the drug alone was evaluated on the SIRC cell line. The IC50 values of GCPQ10: RAP at a polymer-drug ratio of 5:1 and 7.5:1 are presented (Table 4-1, Figure 4-4). Formulations exhibited concentration-dependent IC50 values. GCPQ10: RAP (5:1) has an IC50 value of 36.75 ± 4.41 µg/mL, compared to GCPQ10: RAP (7.5:1) that has an IC50 value of 23.69 ± 2.76 µg/mL ($p < 0.05$). It is conceivable that the higher polymer concentration relative to the drug that presents in the formulation derived the lower IC50 value measured. Cells treated with GCPQ10: RAP (7.5:1) will be exposed to a slightly more mol % quaternary ammonium groups units as compared to (5:1) polymer to drug mass ratio, and with a presence of RAP in the formulation, a lower IC50 value was observed.

Rapamycin alone in the SIRC cell line shows an IC50 value of 3.77 ± 0.59 µg/mL that is significantly lower when compared to formulations ($p < 0.05$). Table 4-2 shows some literature data on the reported IC50 value of RAP. Wang et al. reported the IC50 of RAP on human retinoblastoma cell line (Y79) using Cell Counting Kit-8 assay [246]. Cells were treated with (0.1, 0.2, and 0.4 µmol/L) of RAP for 48 hours. The proliferation of Y79 cells was inhibited by RAP in a dose-dependent manner. The IC50 value of RAP was reported (0.122 ± 0.026 µM = 0.11 µg/mL) on Y79 cell line. Rapamycin was found to induce G1 cell cycle arrest in the human retinoblastoma cells [246]. Another study showed that the IC50 value of RAP against Y79 cells was (0.136 ± 0.032 µM = 0.12 µg/mL) using MTT assay [247]. The IC50 value of RAP using MTT assay on a human retinal pigment epithelial cells was reported as 0.18 µg/mL [248]. In cytotoxicity studies on an epithelial human breast cancer cell line (MDA-MB-231), the IC50 of RAP solution and RAP-PLGA nanoparticles were 20.3 µM (18.5

μg/mL) and 11.4 μM (10.4 μg/mL), respectively [249,250]. Another report showed that the IC50 value of RAP in MCF-7 cells was (0.4 μg/mL) [251].

Table 4-2: Literature data reported the IC50 of RAP in different cell lines.

Cell line	Assay	Seeding density	Plate	Exposure time	RAP (IC50)
Human retinoblastoma cell line (Y79)	Cell Counting Kit-8	3 x 10^3 cells/well	96-well plates	48 hours	0.122 ± 0.026 μM (0.11 μg/mL) [246]
Human retinoblastoma cell line (Y79)	MTT	3 x 10^3 cells/well	96-well plates	72 hours	0.136 ± 0.032 μM (0.12 μg/mL) [247]
Human retinal pigment epithelial cell line (RPE)	MTT	5 x 10^3 cells/well	96-well plates	12 hours	0.18 μg/mL [248]
Epithelial human breast cancer cell line (MDA-MB-231)	MTT	5 x 10^3 cells/well	96-well plates	24 hours	RAP solution = 20.3 μM (18.5 μg/mL) [249,250]
Epithelial human breast cancer cell line (MDA-MB-231)	MTT	5 x 10^3 cells/well	96-well plates	24 hours	RAP nanoparticles = 11.4 μM (20.4 μg/mL) [249,250]
Human breast cancer cell line (MCF-7)	Trypan blue exclusion	1 x 10^5 cells/well	6-well plates	8 days	0.4 μg/mL [251]

The IC50 value of RAP on the SIRC cell line in our work was 3.77 ± 0.59 μg/mL (4.13 μM). Milani et al. reported that RAP did not show toxicity at concentrations (0.1 – 10 μg/mL) using the MTT assay in a human corneal fibroblast culture [252]. To our knowledge, this is the first data reporting the IC50 value of RAP on the SIRC cell line, and these results demonstrate the variability of the IC50 values on different cell lines. There were statistically significant differences when comparing the IC50 values of the formulations to the IC50 of the RAP alone ($p < 0.05$) (Figure 4-4). Therefore, the formulation reduces the toxicity of the drug so that tissues on the surface are less likely to be affected. Our results demonstrated the good biocompatibility of the synthesised polymers and formulations against rabbit cornea cell line.

Rapamycin IC50 result indicates the sensitivity of the SIRC cell line to the mTOR inhibitor, rapamycin. mTOR is a serine/threonine-specific protein kinase, which displays a central role in regulating cell growth and metabolism [160]. Rapamycin binds to the immunophilin, FK binding protein to interact with mTOR and inhibit its function, leading to inhibition of cell growth and cell proliferation [159]. The exact effect on how RAP reduced the metabolic activity of the SIRC cell line has not been evaluated. Rapamycin has been approved for the prophylaxis of organ rejection in patients aged ≥13 years receiving renal transplants [253]. Further studies are needed to define precisely the role of RAP on inhibition of the cell growth in the SIRC cell line.

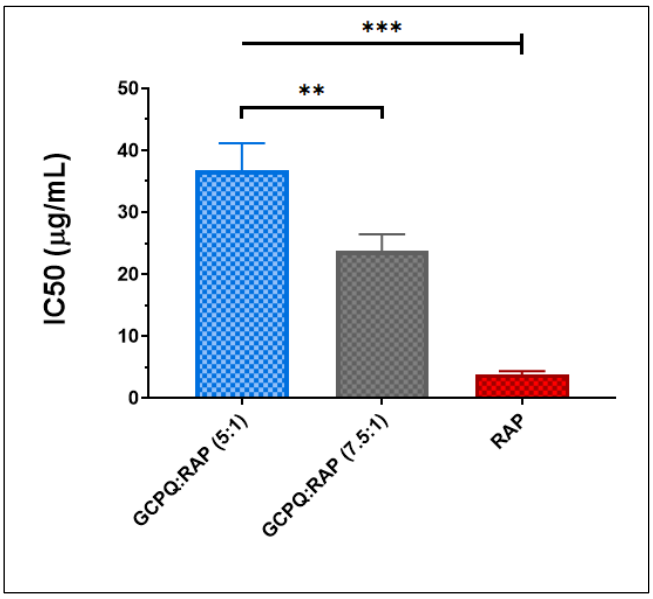

Figure 4-4: Minimum inhibitory concentration (IC50) of the formulations and rapamycin on SIRC cell line.
Statistical significance was determined by one-way ANOVA with Tukey' multiple comparison post-test, n=3; *= $p < 0.05$ was considered significant.

This *in vitro* screening study will enable the selection of molecules with acceptable toxicity profiles and inform the starting dose for the subsequent *in vivo* studies. The starting *in vivo* dose may be selected with reference to the cytotoxicity data. For example, an *in vivo* dose of the carrier in weight per kg body weight may not exceed 1000X the IC50 value in weight per mL and as such a particulate carrier with an IC50 value of 1 mg/mL will be administered at a starting dose of less than 1000 mg/kg. In fact, a fraction of this dose will be given, for example, 10% of this calculated dose. This threshold IC50-dose relationship has been reported in the animal project license number (70/7224) and has been obtained from previous work [254].

Therefore, the cytotoxicity data raises the question of what effect these modifications will have on other biological processes in cells, including permeation enhancement. It has been reported that the GCPQ promotes the absorption of both hydrophobic and hydrophilic drugs through enhancing the dissolution of the drug from the nanoparticles, bioadhesion of the nanoparticles to the functional aspects of the gastrointestinal tract, and the promotion of transcellular transport [135]. The effect of the GCPQ structural modifications on enhancing paracellular transport has not been fully elucidated.

Therefore, we designed a series of experiments to test the hypothesis that increasing the level of DQ% will increase the permeation enhancement across epithelial barriers. We used two barrier models, the MDCK and the SIRC cell lines. Therefore, we treated MDCK cell monolayer and SIRC cells with GCPQ polymers under similar conditions as the cytotoxicity assays and determined the effects on paracellular transport enhancement which will be discussed in the next section.

4.3. Effect of GCPQ structural modifications on transport across epithelial barriers

4.3.1. Introduction

There are two main pathways for particles to diffuse across the epithelium, namely: the transcellular (i.e., across the cell membrane) and the paracellular (i.e., between the aqueous pores of the cells) pathways. Due to the narrow diameter of the junctions between the epithelial cells (~ 0.8 nm), it is possible that only the transcellular route is effective for colloidal translocation [255]. The transcellular pathway can be further divided into; simple diffusion, carrier-mediated, and endocytosis [2]. This section focuses on studying the effect of different properties of GCPQ on the paracellular transport on epithelial barriers of MDCK and SIRC cell lines.

MDCK cells differentiate into a columnar epithelium when grown on a suitable membrane and form tight junctions [256]. They are considered a good model for the study of mammalian epithelia [257]. The MDCK cell line has been used extensively to study the transepithelial transport of drug candidates with some reports showing similar apparent permeability coefficient (Papp) values as Caco-2 cells [258]. The MDCK cell line has an advantage over the Caco-2 cell line as it may be used for higher throughput studies due to the cell's faster growth and rapid formation of tight junctions. This rapid growth makes the MDCK cell line a useful tool for rapid membrane permeability screening as monolayers form tight junctions in 3-5 days compared to 21-25 days for Caco-2 cells [259]. Also, the MDCK cell line has been used

to study the functional nature and P-glycoprotein (P-gp) role in lowering the bioavailability of ocular topical drugs [260].

The SIRC cell line has been used *in vitro* to assess the corneal physiology, immunology, toxicology, and permeability of compounds [261]. SIRC cells have characteristics similar to human corneal epithelial cells, and they have been used as a model for corneal epithelial cell research [262]. SIRC cells have been reported to form multiple elongated epithelial-like cell layers when grown for ten days on the surface of transwell inserts [263]. Therefore, the SIRC cell line was used in this study.

4.3.2. Materials

Chemical	Supplier
Fluorescein isothiocyanate dextran four kDa (FD-4)	Sigma-Aldrich (Gillingham, UK)
Hank's Balanced Salt Solution (HBSS)	Fisher Scientific (Loughborough, UK)
Sodium caprate (C10)	Santa Cruz biotechnology (Texas, USA)
Collagen Type I solution from rat tail	Life technologies Ltd. (Paisley, UK)
Transwells with a polycarbonate membrane (pore size = 0.4 µm, surface area = 1.12 cm^2)	Corning®, VWR International (Leicestershire, UK)
Transwells collagen-coated polytetrafluoroethylene (PTFE) membrane (pore size = 0.4 µm, surface area = 1.12 cm^2)	Corning®, VWR International (Leicestershire, UK)

4.3.3. Methods

Transport experiments were conducted to investigate the effect of the degree of quaternisation (DQ%) and the degree of palmitoylation (DP%) of GCPQ on the transepithelial electrical resistance (TEER). The TEER value was used as a measure of monolayer integrity [264]. The permeability of the paracellular marker FD-4 [265] was assessed, and the permeation enhancer sodium caprate (C10) [266] was employed as a positive control on MDCK and SIRC cell lines.

Since the MDCK cell line is primarily used to study the transport across the intestinal mucosa at pH 6.8 [267], further studies were carried out to determine the influence of changing the pH to the physiological range (pH = 7.4) on the permeability across the MDCK cell monolayer.

Transport studies using filtered HBSS, supplemented with (4-(2-hydroxyethyl)-1-piperazineethanesulfonic acid - HEPES, 10 M), and sodium bicarbonate (0.75% v/v), with the pH adjusted to 6.8 and 7.4 with NaOH (1 M) were carried out. pH values of 6.8 and 7.4 were chosen as this lies within the pH range in the small intestine and the eye, respectively. GCPQ (2 mg/mL) was prepared by dispersing the polymer in filtered deionised water and diluting with HBSS (1 mL) to provide a working solution at (1 mg/mL).

MDCK and SIRC cells (passage number 7-15), were grown on 12 transwells with permeable support using supplemented growth medium for five and ten days for MDCK and SIRC cell lines, respectively. Transwells with a polycarbonate membrane

(pore size = 0.4 μm, surface area = 1.12 cm^2) were employed for the transport experiments on MDCK cells.

The SIRC cells were grown on polycarbonate membranes coated with collagen Type I as recommended by Corning®, VWR International (Leicestershire, UK). The recommended coating volume is (0.25 mL), and the washing volume is (0.4 mL) on 12 transwell inserts. Briefly, transwells were coated with collagen at a coating density (10 μg/cm^2). Collagen stock solution (3 mg/mL, 0.45 mL) diluted with acetic acid (0.02 M, 2.55 mL) to make a working solution (3 mL) of collagen at a coating density (10 μg/cm^2) in transwells on the growth surface area (1.12 cm^2). The collagen working solution (0.25 mL) was added to the apical side of the transwells, and the inserts were allowed to dry in a biological safety cabinet, partially covered for one hour. The remaining collagen was aspirated from the inserts, and the inserts rinsed once with DPBS (0.4 mL) and once with the cell culture medium (0.4 mL). The collagen coating helps the cells to attach to the transwell support and stimulates their proliferation and differentiation [20,268]. To ensure the suitability of our results after coating, transwells readily coated from the company with collagen on polystyrene permeable support (pore size = 0.4 μm, surface area = 1.12 cm^2) were used as reference transwells for our own coated transwells.

Both cells lines were seeded on transwells at a density of $5x10^5$ cells per well and cultured according to standard protocols [256]. Briefly, cells with medium (0.5 mL) in the apical compartment and medium (1.5 mL) in the basolateral compartment were allowed to grow and differentiate on the transwells for five and ten days for MDCK and SIRC cells, respectively, before the experiment was conducted, at 37°C and 5%

CO_2. The cell culture medium in both chambers was changed every day for the MDCK cells, and on alternate days for SIRC cells. The TEER measurements (Figure 4-5) were taken regularly using a MILLIPORE Millicell®-ERS voltohmmeter (Merck Millipore, Watford, UK). All TEER and transport experiments were carried out in triplicate.

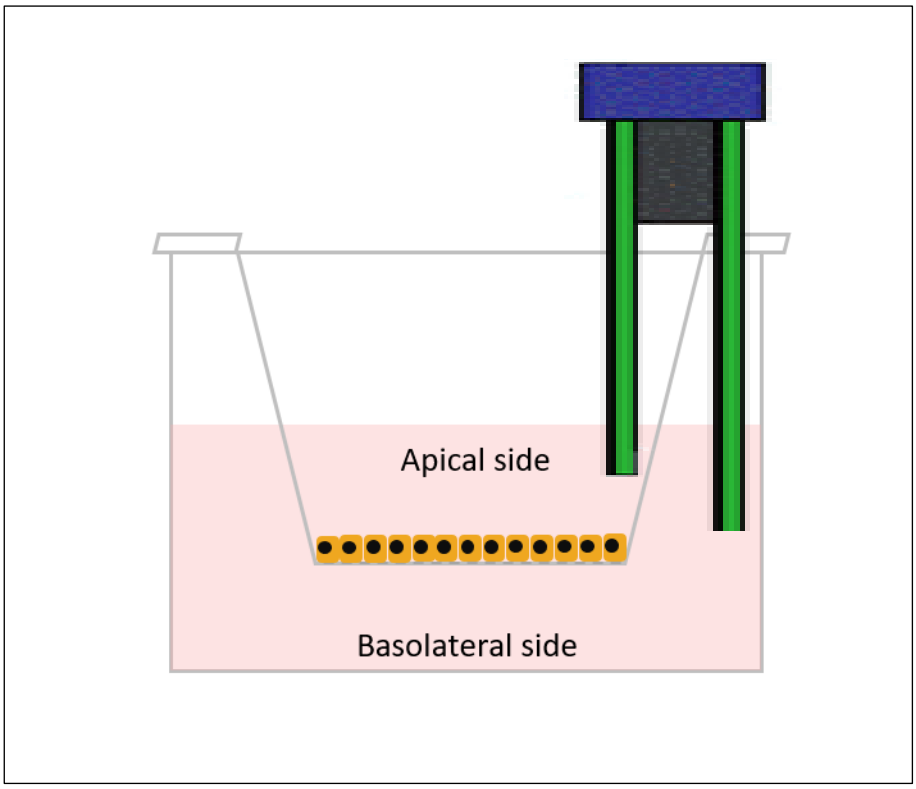

Figure 4-5: Schematic diagram of the measurement of the TEER on the transwell.

On the day of the experiment, the cell culture medium was removed, and monolayers were rinsed twice with HBSS, and then incubated for one hour with HBSS (0.5 mL) at 37°C before taking a baseline TEER measurement. Subsequently, HBSS on the apical chamber was removed, and different GCPQs, blank HBSS as a negative control, and sodium caprate (10 mM) [266] as a positive control were added to the apical chamber (0.5 mL) and incubated for two hours at 37°C and 5% CO_2, and the after-treatment TEER was taken.

Following treatment, both chambers were washed once with HBSS, and HBSS (1.5 mL) was added to the basolateral chamber, and filtered FD-4 in HBSS buffer (1 mg/mL, 0.58 mL) was added to the apical chamber. Samples (80 µL) were taken immediately at the beginning of the experiment from the apical chamber to calculate the initial donor concentration (C_0), and at the end of the experiment to facilitate mass balance calculations. The plates were then incubated for two hours at 37°C and 5% CO_2, and samples (250 µL) were taken from the basolateral chamber at 30-minute intervals. The samples taken were replenished with an equal volume of HBSS, and the TEER measurement was taken after FD-4 incubation.

Later, the FD-4 was removed, and the cells were washed once with HBSS and once with the cell culture medium. The medium was then added to both chambers, and the cells were incubated at 37°C and in 5% CO_2 to allow recovery.

Samples taken from the apical and basolateral chambers were placed in black 96 well-plates covered with foil and analysed using BioTek Synergy™ HT Multi detection microplate reader (SpectraMax M2, Molecular Devices, Wokingham, UK) at an excitation wavelength of 485 nm and an emission wavelength of 528 nm [269].

The apparent permeability coefficient (Papp) in cm/s of FD-4 was calculated using the following equation:

$$P_{app} = \frac{dQ}{dt} X \frac{1}{AC}$$ Equation 4-1

where, dQ/dt is the rate of change of concentration in the basolateral chamber over time, A is the surface area of the cell monolayer, C is the initial concentration in the apical chamber. The concentration of the collected samples was determined from a freshly prepared standard curve of FD-4. The Papp is defined as the flux or the flow rate of a compound normalised by the membrane surface area and the initial donor concentration [270].

4.3.4. Results and discussion

This section of the thesis will present data aimed at elucidating the possible mechanism by which different GCPQs interact with epithelial barriers. The MDCK cell line is a well-established cell line that has been extensively used as a model for studying the mechanisms underlining the transport of materials across the differentiated epithelial cells [271]. MDCK was also used to study the role of P-gp as a barrier to the ocular drug absorption of erythromycin [260].

Thus, the MDCK cell line was used initially as a well-known transport model that forms tight junctions and as a surrogate model to explore the effect of the GCPQ structure on the transport across epithelia. A previous report showed the use of the MDCK monolayer transport model to test the functionality of the P-gp efflux pump in rabbits corneas [260]. Dey et al. reported the existence of the P-gp efflux pump in rabbit cornea and suggested that the efflux pump may be responsible for the low ocular bioavailability [260]. Hence, the MDCK cell line may be used to predict the transport across the corneal epithelium, and we are using this cell line for this purpose in this work.

Different GCPQ polymers were tested to determine the best GCPQ candidate that can be used for the subsequent *in vivo* studies. Furthermore, a study was carried out to ascertain the influence of pH on the transport as the normal tear pH is reported to be at 7.4 [272].

Then, SIRC cell line was employed to study the effect of GCPQ on corneal epithelial cells. Therefore, a series of experiments were designed to investigate the effect of

DQ% and DP% on TEER and the permeability of the paracellular marker FD-4. Sodium caprate (C10), a well-reported paracellular permeation enhancer was used as a positive control [266].

4.3.4.1. Transport across MDCK cell line

Figure 4-6 shows the development of tight junctions in MDCK cells at pH 6.8 and 7.4, as measured using a voltohmmeter. TEER values showed an initial rapid exponential increase before a peak is reached at a value of about 1200 ohm.cm^2 (Ω.cm^2) (1 day) followed by a steep decline (2 days), and then a period where the TEER values of about 300 Ω.cm^2 are stable (3-4 days). The TEER values increased during the exponential phase [273], with the steep increase in TEER corresponding to growth and multiplication of cells before reaching confluence. This is followed by a subsequent drop in TEER due to tight junction formation. The TEER values were then stabilised in the stationary growth phase [273]. Reaching a stable value of TEER is regarded as an indication of full differentiation of the epithelial monolayer with the formation of tight junctions in MDCK cells [257].

Figure 4-6 shows that there were no statistically significant differences in the development of TEER values between pH 6.8 and 7.4 on day four. Thus, the subsequent transport assays were carried out during the periods of stable TEER values, i.e., Day 4-5 for the MDCK cell line at pH 6.8 and 7.4.

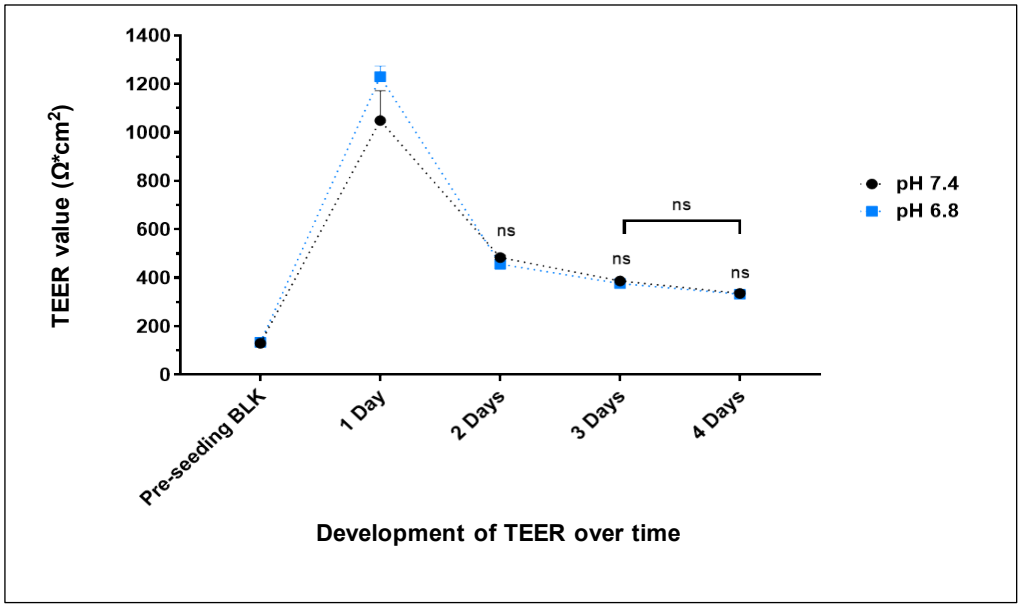

Figure 4-6: The development of TEER for MDCK cells monolayer on transwells. The MDCK cells were grown over five days. Statistical significance was determined by two-way ANOVA with Tukey post-test, n=3.

Table 4-3 shows the characteristics of the GCPQ polymers that have been used in the transport studies. We aimed to synthesise polymers with similar DP ~ 20% as described in chapter 2. A wide range of GCPQ polymers with different molecular weights and DQ% were used to establish the effect of structural modifications on cellular transport mechanisms. Polymers with a DQ of more than 10% were selected as these polymers are more hydrophilic and were required to encapsulate the cargo, as shown in Chapter 3.

Screening experiments were conducted to test the different properties of GCPQ and select the optimum polymers for subsequent studies. UO-GCPQ03 was obtained from a former lab member and is a known polymer that can open the tight junctions on MDCK cell monolayers.

Table 4-3: Characteristics of the different batches of GCPQ used in the transport studies.

Polymer	MW (kDa)	DP (%)	DQ (%)	QPR
GCPQ02	15	28	10	0.357
UO-GCPQ03*	09	19	12	0.632
GCPQ04	not determined	20	9	0.450
GCPQ06	53	18	13	0.722
GCPQ07	16	22	10	0.454
GCPQ09	60	18	16	0.889
GCPQ10	16	18	19	1.056

*UO-GCPQ03 polymer was obtained from Dr Uchechukwu Odunze as a control of a known polymer that opens the tight junctions on MDCK cells monolayer.

A standard curve of FD-4 was freshly prepared with each replicate of the experiment. Figure 4-7 shows the FD-4 standard curve that has been used to determine the unknown concentration of the collected samples on MDCK and SIRC cell lines. The standard curve plotted shows linearity over a concentration range of 0.977 – 125 µg/mL with a correlation coefficient of 0.999. The equation of the standard curve (y = 244.34x + 12.585) was used to determine the concentration of the transported paracellular marker FD-4.

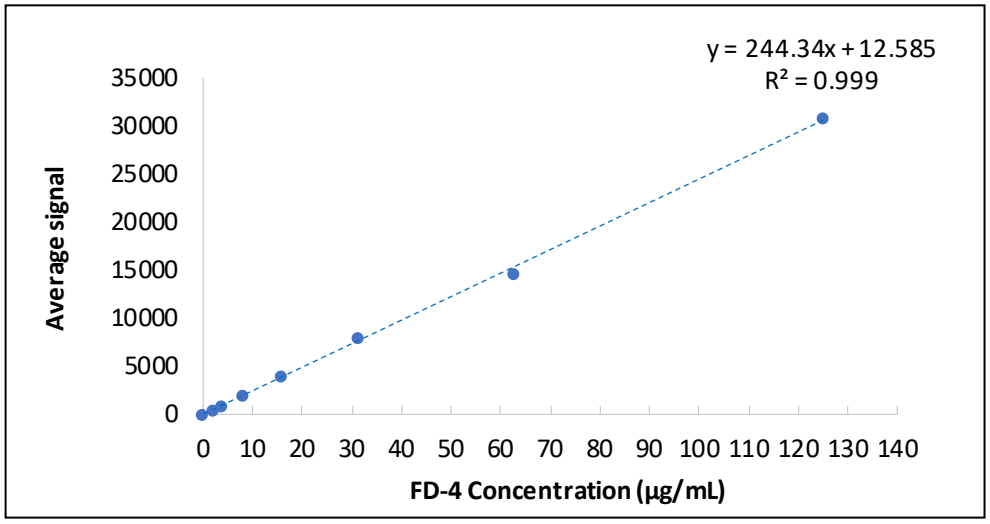

Figure 4-7: A standard curve of fluorescein isothiocyanate-dextran (MW = 4 kDa).

Figure 4-8 shows the apparent permeability coefficient and the cumulative transport of FD-4 across MDCK cell monolayer after exposure to GCPQ polymers. No increase in transport was seen with cells treated with HBSS, pH 6.8, which served as a negative control.

Sodium caprate is a sodium salt of the aliphatic saturated 10-carbon medium-chain fatty acid capric acid that is clinically employed as an absorption-enhancing agent in a rectal ampicillin suppository [274]. Sodium caprate, the positive control, significantly enhanced the transport of FD-4 across the monolayer. It has been reported that the presence of protein kinase C is required for the proper assembly of tight junctions [275], and the effect of sodium caprate on permeation enhancement is due to the increase in the intracellular calcium level through activation of protein kinase C to induce the contraction of calmodulin-dependent actin filaments, followed by dilation of the paracellular pathway [276]. Krug et al. reported that the effect of sodium caprate in enhancing the paracellular absorption is due to the reduction of tricellulin in tricellular tight junctions and of claudin-5 in bicellular tight junctions while no effect of C10 has been observed in the transcellular pathway [266].

Polymers with relatively high DP% and low DQ% were studied. GCPQ02 (DP28%, DQ10%), GCPQ04 (DP20%, DQ09%), and GCPQ07 (DP22%, DQ10%) did not show any significant differences in the transport of FD-4 compared to the negative control. Siew et al. reported that the GCPQ (MW = 12 kDa, DP16%, DQ08%, 5 mg/mL), and the palmitoylated glycol chitosan (pGC, DP49%, 5 mg/mL) did not open the tight junction on Caco-2 cell line [135]. There were no significant differences in the

transport of the paracellular marker Lucifer Yellow (0.4 µg/mL) as compared to the negative control [135]. This is in line with our observation in which GCPQ with low DQ% did not result in tight junctions opening.

High molecular weight polymers (GCPQ06; MW = 53 kDa, GCPQ09; MW = 60) showed no significant difference in the apparent permeability coefficient compared to the negative control. GCPQ06 and GCPQ09 shared the same DP of 18%, but slightly different in DQ, 13% and 16% for GCPQ06 and GCPQ09, respectively. This result showed that despite a high DQ%, the molecular weight of the polymer could play a role in opening the tight junctions on MDCK cells monolayer. Kowapradit et al. showed that trimethyl (64% degree of substitution) chitosan (parent MW = 276 kDa) did not enhance the transport of FD-4 in Caco-2 monolayers [277]. A recent report showed that the permeability of oligopeptides across Caco-2 cell monolayers decreases with increasing the molecular weight of oligopeptides [278].

Chitosan in solution has been shown to open tight junctions [279] and results in a reduction of TEER across Caco-2 cell monolayers. Thus, polymers in solution may behave differently from their aggregated amphiphilic analogues. Although the cationic polymer−poly(ethylenimine) in solution opens tight junctions, the amphiphile cetyl quaternary ammonium poly(ethylenimine) did not open tight junctions [280]. It is speculated that the self-assembly of the amphiphile prevents the interaction of the polymer monomers, presumably polymer monomer cationic groups with the appropriate tight junction proteins to a certain extent and in this way prevents the opening of tight junctions [135].

Interestingly, there is an increased rate of transport of FD-4 for the polymer with the highest DQ%, and low molecular weight (GCPQ10, DP18%, DQ19%, MW = 16 kDa). GCPQ10 shows a significantly different increase in the transport of FD-4 compared to the negative control. A positive linear slope was observed, suggesting a constant increase in the rate of FD-4 transport across the MDCK cells monolayer layer (Figure 4-8, B). This shows that DQ% plays a role in paracellular transport of FD-4 as shown in (GCPQ10, DP18%, DQ19%, MW = 16 kDa) as compared to (UO-GCPQ03, DP19%, DQ12%, MW = 9 kDa)

Thus, polymers with high DP% and low DQ% (GCPQ02, GCPQ04, GCPQ07) did not show a statistically significant difference in the apparent permeability coefficient compared to the negative control. In contrast, GCPQ10 with a high DQ% relative to DP% showed a significant difference in the transport of FD-4 across the monolayer compared to the negative control.

These results are in contrast to previous reports on the mechanism of permeation enhancement by GCPQ, which suggested that there is no involvement of the paracellular transport pathway [135,137]. Therefore, there appears to be a balance between the effect of DP and DQ's effect on the paracellular permeability enhancing effect of GCPQ. For polymers of similar DP, the effect on paracellular transport is graded upwards with increasing DQ as is evident for polymers with DP of about 20%, and different DQ 9%, 10%, and 19%. It has been reported that polymer with only high palmitoyl chain (DP49%) and no quaternary group does not affect the paracellular transport enhancement [135].

It should be stated that the effect on paracellular transport of the level of DQ in GCPQ may depend on the degree of palmitoylation. Previous research in our group showed that a steep increase in flux is observed at a QPR of around one, after which the flux increases at a slower rate over a wide QPR range [281]. A maximum flux appears to be reached at a QPR just under two, so increasing the QPR further does not cause significant increase flux [281]. It has been reported that GCPQ with a high DP of about 37%, even with a very high DQ of 23% (MW = 10 kDa, QPR 0.62) did not result in a statistically significant increase in paracellular transport [281].

The molecular weight could also play a role in determining the enhancement of the paracellular transport of GCPQ. We have shown that GCPQ10 (MW = 16 kDa) was able to open the tight junctions on MDCK monolayers compared to high molecular weight polymers (GCPQ06; MW = 53 kDa, GCPQ09; MW = 60), and low molecular weight polymers (MW = 10 - 12 kDa) [135,281]. Kaiser et al. reported that chitosan nanocapsule loaded capsaicin (MW = 17 kDa) lowered the TEER and enhanced the permeability of FD-4 in MDCK cell monolayers [282].

Apparently, positive charges contribute to the effects of chitosan and its derivatives on paracellular transport [283]. However, our results also suggest that an increase in the hydrophobic palmitic acid chains or the decrease in QPR and increase in the molecular weight reduce the ability of positive charges on the polymer to modulate the tight junctions. The exact reason for this is not clear, but one plausible explanation might be steric hindrances to electrostatic interactions between the positive charges of more soluble polymer with relatively high DQ%, low DP%, low molecular weight and the negatively charged membrane components. These results

suggest that the MW, DP, and DQ are important parameters for achieving an enhanced effect on paracellular transport in MDCK cells. Thus, GCPQ10 will be further explored in the transport across the epithelium and will be compared at different pH values with an extensively studied polymer (UO-GCPQ03, MW = 09 kDa, DP19%, DQ12%) obtained from a former lab member.

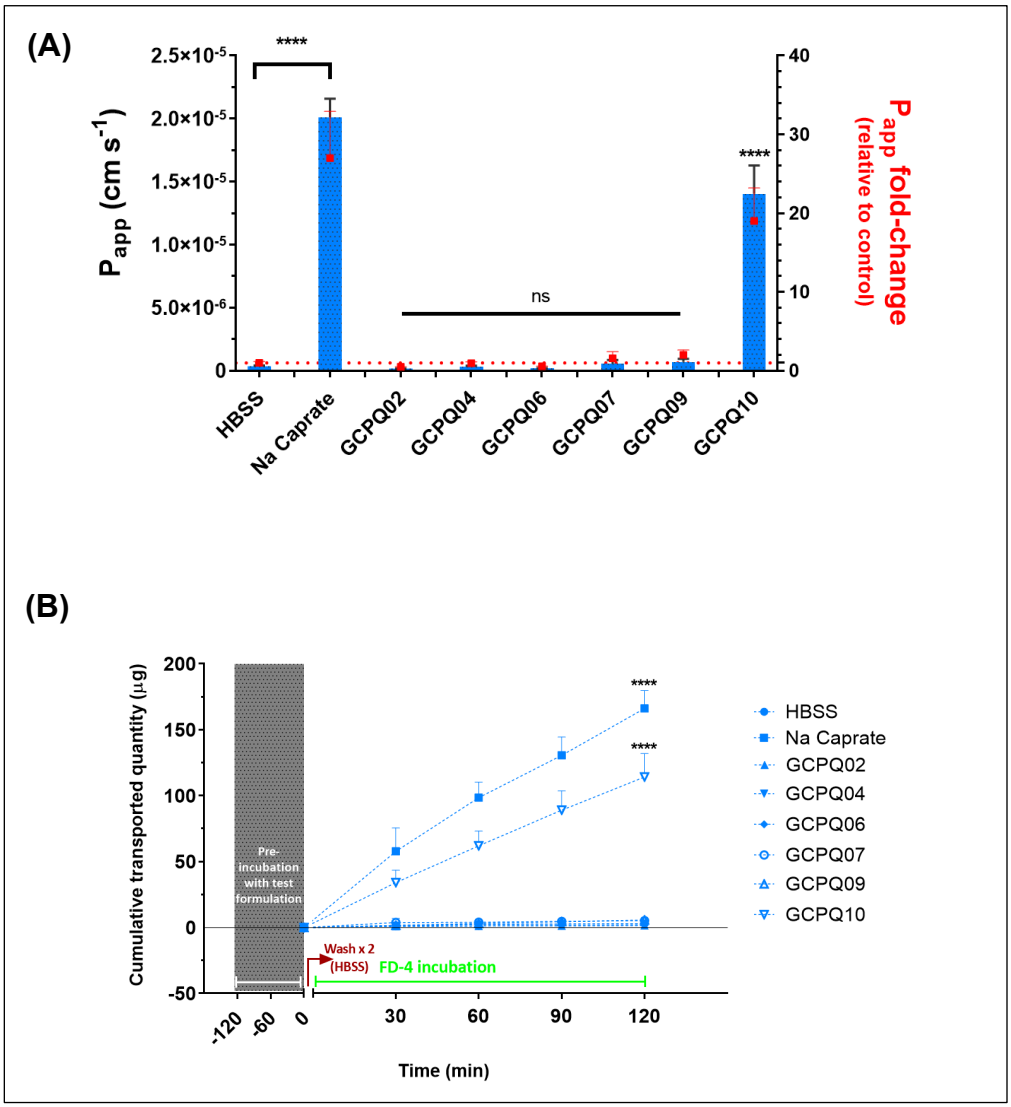

Figure 4-8: Screening experiments on the effect of different properties of GCPQ (1 mg/mL) on the paracellular transport of FD-4 across MDCK cell monolayer.

(A) Apparent permeability coefficient Papp – left axes -, and the Papp folds change relative to negative control – right axes -; **(B)** The cumulative transported quantity of FD-4 from the apical to basolateral chambers over-time points.
Statistical significance was determined by **(A)** one-way ANOVA with Tukey' multiple comparison post-test, **(B)** two-way ANOVA with Tukey post-test, n=3; *= $p < 0.05$ was considered as a significant difference.

Figure 4-9 shows the effect of the GCPQ structure on transport across epithelial barriers in MDCK cell monolayers at pH 6.8, and 7.4. Two polymers were compared for this experiment, with similar DP but different DQs, GCPQ03 (DP19%, DQ12%), and GCPQ10 (DP18%, DQ19%).

At pH = 6.8, both polymers showed a gradual response compared to their response at pH = 7.4 (Figure 4-9, A). Moreover, the polymer with the highest DQ retained its potency as a transport facilitator at both pH values with no significant differences due to pH observed ($p = 0.1642$). GCPQ03 (DP19%, DQ12%) showed a significantly different permeability value at pH = 6.8, compared to pH = 7.4 ($p < 0.05$). GCPQ is a weak base with a pKa reportedly about 6.0 [138]; this means that GCPQ is less protonated at pH 7.4 compared to pH 6.8. At a pH of 6.8, we can expect a different response depending on the DQ. Therefore, at acidic pH, GCPQ03 and GCPQ10 are likely to enhance the paracellular transport. Only the polymer with very high QPR will enhance tight junction opening and thus the paracellular transport at the tear's pH. This is in line with our findings in which GCPQ10 (QPR = 1.056) at pH = 7.4, showed a significantly different transport of the paracellular marker FD-4 compared to GCPQ10 at pH = 6.8 ($p < 0.05$). It has been reported that GCPQ polymers with high QPR are more hydrophilic and will have more surface charge density compared to polymers with low QPR at neutral pH [281]. These results could suggest that GCPQ with high DQ could have an impact on increasing the ocular transport at pH 7.4.

Moreover, GCPQ10 showed significantly different transport kinetics of FD-4 at both pH values, when compared to the negative control at 120 minutes ($p < 0.05$). A positive linear slope was observed, suggesting a constant increase in the rate of FD-

4 transported across the MDCK cell monolayers (Figure 4-9, B). In line with this work, the effect of GCPQ on the TEER value was assessed for all the tested compounds and at both pH values. The TEER value dropped two hours after treatment, suggesting an opening of the tight junctions [264]. The TEER value returned to its pre-treatment value 72 to 96 hours after treatment with GCPQ03.

For GCPQ10, cells did not fully recover at 96 hours post-treatment, as the TEER value was significantly lower than the control at both pH values. A recent report showed that the chitosan-based nanoparticles could be internalised inside the cells up to two weeks [284]. GCPQ is a polycation polymer that forms nanoparticles with a positive surface charge. The degree of the cytotoxicity has been shown to depend on the extent of the positive charge on the surface of the nanoparticles [243]. The IC50 value of GCPQ10 on MDCK was (4.54 ± 0.36 mg/mL), which was 4-folds higher than the concentration used in the transport study (1 mg/mL); this means that GCPQ10 is not toxic and cells might need a temporal exposure to the growth medium for a full recovery.

GCPQ is an amphiphilic polymer that has a quaternary ammonium group. Quaternary amine polymers have been reported to open tight junctions at intestinal pH [156]. The tight junction opening depends on the degree of quaternisation, meaning with a high degree of quaternisation, the polymer will be more likely to have a higher charge density and be more likely to open tight junctions with the net result that such polymers with high levels of quaternary ammonium groups have a high solute transport capability [156]. For example, trimethyl chitosan (TMC) was studied as a tight junction opening polymer at pH 6.2 and 7.2. The TMC with 60% quaternisation was

more potent than TMC that had 40% quaternisation in enhancing the transport of a paracellular marker at both pH values [285].

The underlying mechanism for chitosan opening the tight junctions is presumed to be mediated by the electrostatic interaction between the positively charged chitosan and the negatively charged integrin [286]. This electrostatic interaction leads to a conformational change of integrin and its clustering along the cell border, F-actin reorganisation, and Claudin-4 down-regulation, eventually disrupting the tight junctions, and increase in the paracellular permeability [286]. Thus, GCPQ can be structurally modified by increasing or decreasing its DQ to maintain its charge density at various pH values and therefore retain its paracellular permeability enhancement effect. These results indicate the potential utility of GCPQ polymers in different physiological pH environments, such as the eye.

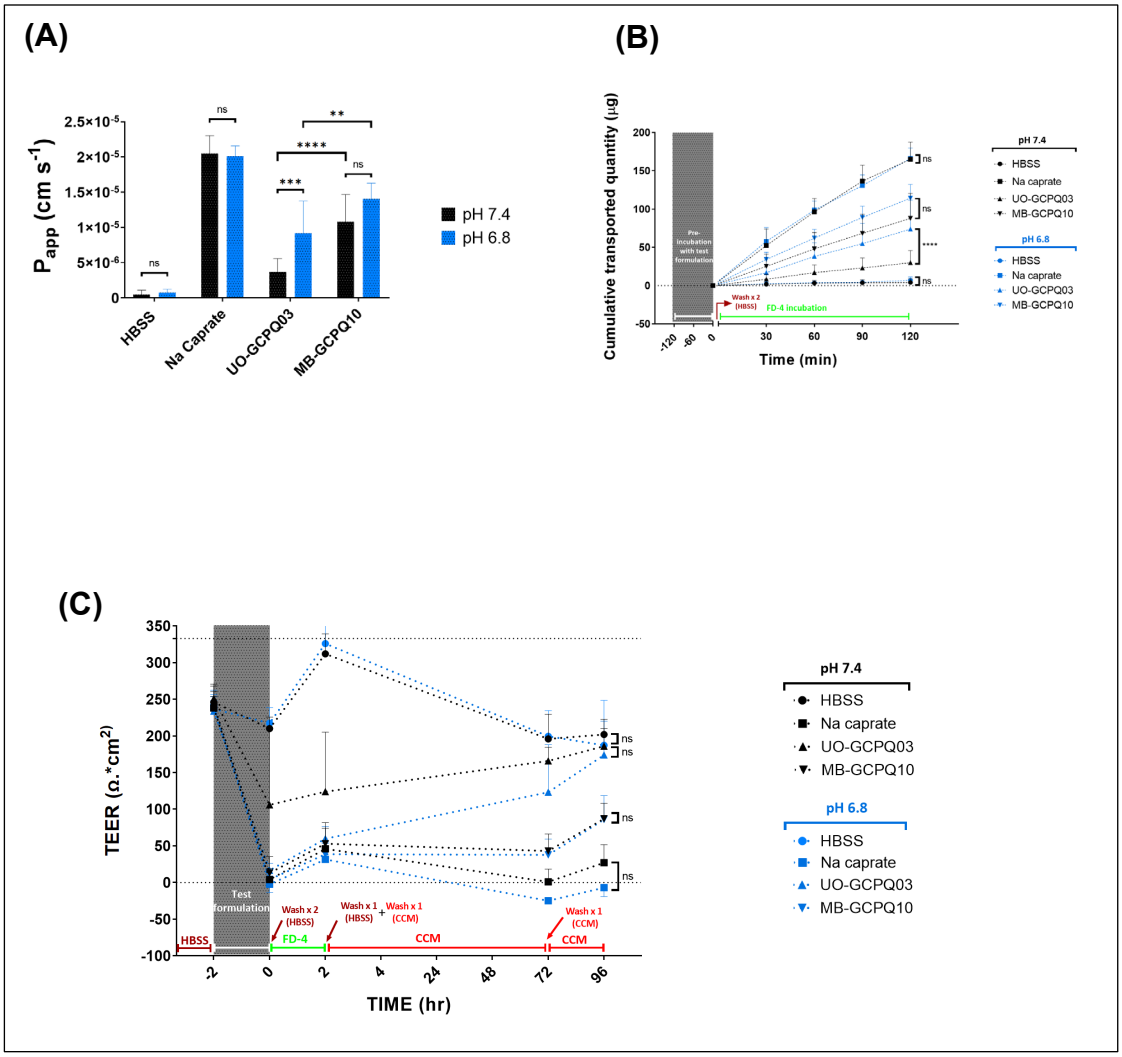

Figure 4-9: Comparison of the effect of GCPQ (1 mg/mL) on the paracellular transport of FD-4 across MDCK cell monolayer (pH: 6.8, 7.4).

(A) Apparent permeability coefficient Papp combined graph for pH 6.8 and 7.4; **(B)** Transport of FD-4 at pH 6.8, and 7.4; **(C)** TEER value at pH 6.8 and 7.4.
Statistical significance was determined two-way ANOVA with Tukey post-test, n=3; *= $p < 0.05$ was considered as a significant difference.

The QPR, which is the ratio of DQ% to DP%, serves as a measure of hydrophilicity and can be plotted against the Papp and molecular weight, as shown in (Figure 4-10). The figure shows that while the Papp increases with QPR (DQ13%, DQ16%), the effect is still dependent on the level of DP% and molecular weight as no effect can be seen with GCPQ06 (DP18%, MW 53 kDa), and GCPQ09 (DP18%, MW 60 kDa), respectively.

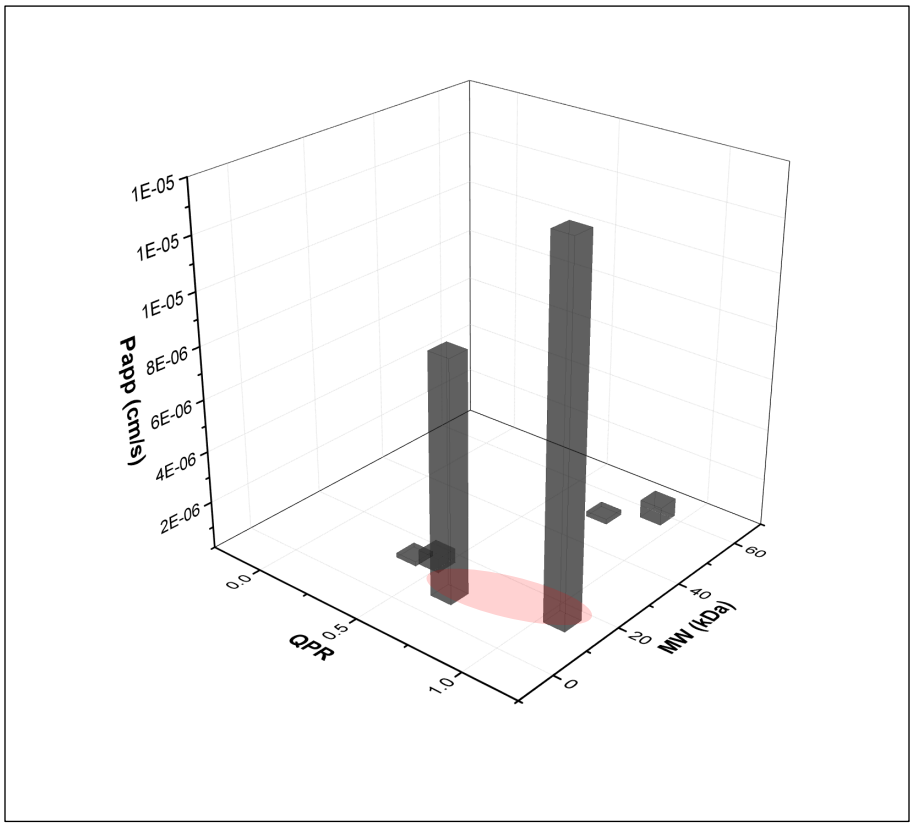

Figure 4-10: Correlation of Papp permeability of GCPQ polymers relative to its structural modifications across MDCK cell monolayer, pH = 6.8.

The highlighted area is assumed to be the suitable range of polymers that can enhance the transport across the epithelium and open the tight junctions on the MDCK cell line.

Table 4-4 shows the order of GCPQ polymers by Papp in MDCK cells compared with HBSS relative to the pH. There is a positive correlation between Papp and QPR suggesting that hydrophilicity (QPR = 0.5 – 1) increases permeation enhancement with molecular weight (10 – 16 kDa) while hydrophobicity (QPR < 0.5) decreases permeation enhancement even with a similar molecular weight (Figure 4-10). However, high molecular weight polymers (> 50 kDa) even with high hydrophilicity (QPR > 0.7) did not result in a significant permeation enhancement (Figure 4-10, Table 4-4).

Table 4-4: Ranking of GCPQ polymers by Papp in MDCK cells compared with HBSS relative to pH = 6.8, and 7.4.

ID	Properties (MW kDa, DP%, DQ%)	Mean Papp x 10^{-6} (cm/s)	Papp fold change	Cumulative transport of FD-4 at 2 h (µg)	QPR	pH
HBSS	-	0.77 ± 0.47	1	2.99 ± 0.41	-	6.8
GCPQ02	(15, 28, 10)	0.17 ± 0.01	0.49	1.56 ± 0.02	0.357	6.8
GCPQ06	(53, 18, 13)	0.20 ± 0.01	0.56	1.73 ± 0.1	0.722	6.8
GCPQ04	(nd, 20, 09)	0.34 ± 0.05	0.96	2.84 ± 0.25	0.450	6.8
GCPQ07	(16, 22, 10)	0.56 ± 0.29	1.59	5.24 ± 2.66	0.454	6.8
GCPQ09	(60, 18, 16)	0.71 ± 0.23	2.01	5.74 ± 1.52	0.889	6.8
GCPQ03*	(09, 19, 12)	9.20 ± 4.56	12.23	73.75 ± 37.68	0.632	6.8
GCPQ10	(16, 18, 19)	14.00 ± 2.25	19.02	114.17 ± 17.77	1.056	6.8
C10	-	20.10 ± 1.48	27.44	166.18 ± 13.58	-	6.8
HBSS	-	0.51 ± 0.62	1	4.15 ±4.65	-	7.4
GCPQ03*	(09, 19, 12)	3.70 ± 1.91	12.86	29.92 ± 15.79	0.632	7.4
GCPQ10	(16, 18, 19)	10.80 ± 3.83	35.73	87.90 ± 32.21	1.056	7.4
C10	-	20.50 ± 2.50	57.17	164.98 ± 22.48	-	7.4

*GCPQ03 polymer was obtained from Uchechukwu Odunze as a control of a known polymer that opens the tight junctions on MDCK cells monolayer.

4.3.4.2. Transport across SIRC cell line

It has been reported that SIRC cells grown on six-well transwell filters without collagen did not develop enough trans electrical epithelial resistance (TEER value < 100 Ω.cm^2) [261]. In contrast, another report showed that SIRC cells grown on collagen-coated polycarbonate transwell for 8 - 14 days formed a monolayer (TEER value ~ 1800 Ω.cm^2) and were used for transport experiments [287].

Figure 4-11 shows the development of tight junctions in SIRC cells on the transwell filters coated with collagen at pH 7.4, as measured using voltohmmeter. TEER values showed an initial period of rapid exponential increase before a peak was reached at a value of about 1100 Ω.cm^2 (2 days), followed by a slight decline at a value of about 1000 Ω.cm^2 (5 days), and then a period where the TEER values of about 1350 Ω.cm^2 are stable (7-10 days). The TEER values increased during the exponential phase [273]. The TEER value was then stabilised in the stationary growth phase [273]. Reaching a stable value of TEER is regarded as an indication of full differentiation of the cells with the formation of tight junctions in SIRC cells [287].

Figure 4-11 showed that there was no statistically significant difference in the development of TEER between Days 7, 9, and 10. This is in line with a previous report that showed that SIRC cells grown on collagen-coated polycarbonate transwell for 8 - 14 days were used for transport experiments [287]. The collagen coating helps the cells to attach to the transwell support and stimulates their proliferation and differentiation [20,268]. It has been reported that different receptors, such as integrins, receptor tyrosine kinases and immunoglobulin-like superfamilies,

can mediate cell adhesion to collagen [288]. In our initial work, Growing of SIRC cell monolayers for ten days using the same conditions as with the MDCK cell monolayers on transwells with a polycarbonate membrane (pore size = 0.4 μm, surface area = 1.12 cm^2) and without collagen did not result in the formation of tight junctions as TEER values were at the baseline level. Becker et al. reported that when SIRC cells were cultured on permeable polyester transwell filters, the TEER values remained at the level of those obtained with the blank filter inserts, suggesting that the cells did not develop tight junctions [289]. These results demonstrated the importance of using collagen as an attachment factor when working with the SIRC cell line in transport studies. Thus, the subsequent transport assays were carried out during the periods of stable TEER values, i.e., on Day 10 for the SIRC cell line and at pH = 7.4.

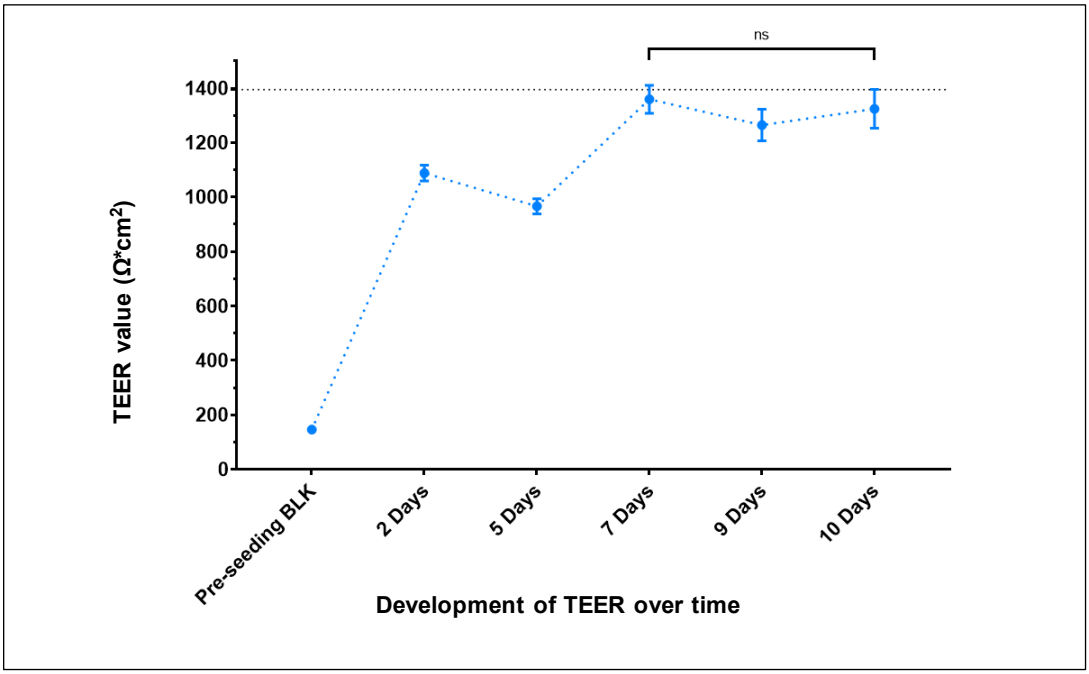

Figure 4-11: The development of TEER for SIRC cells on transwells coated with collagen.
SIRC cells were grown over ten days. Statistical significance was determined by one-way ANOVA with Tukey post-test, n=3; *= $p < 0.05$.

The effect of GCPQ on the FD-4 transport across the SIRC cell monolayer, grown on collagen, was studied. Transwells coated with collagen at 10 μg/cm^2 were prepared in the lab according to the protocol from the company. To confirm the utility of this coating, readily coated transwells with collagen on polystyrene with 0.4 μm pore PTFE membrane were used for comparison.

Figure 4-12 showed the apparent permeability coefficient and the cumulative transported quantity of FD-4 due to the effect of GCPQ on both transwells. Neither of the polymers used GCPQ03 (DP19%, DQ12%, QPR 0.632), and GCPQ10 (DP18%, DQ19%, QPR 1.050) showed any significant transport enhancement of the paracellular marker FD-4 on the SIRC cell line compared to the negative control. The positive control (C10) showed a significant enhancement in the transport of FD-4 compared to the negative control ($p < 0.05$). TEER values showed no significant difference between pre-and post-treatment of GCPQ03 and GCPQ10 when compared to the negative control ($p = 0.501$).

The comparative results showed there were no significant differences between the transwells coated from the company to the transwells coated in the lab. This indicates the efficiency of our coating for any subsequent work.

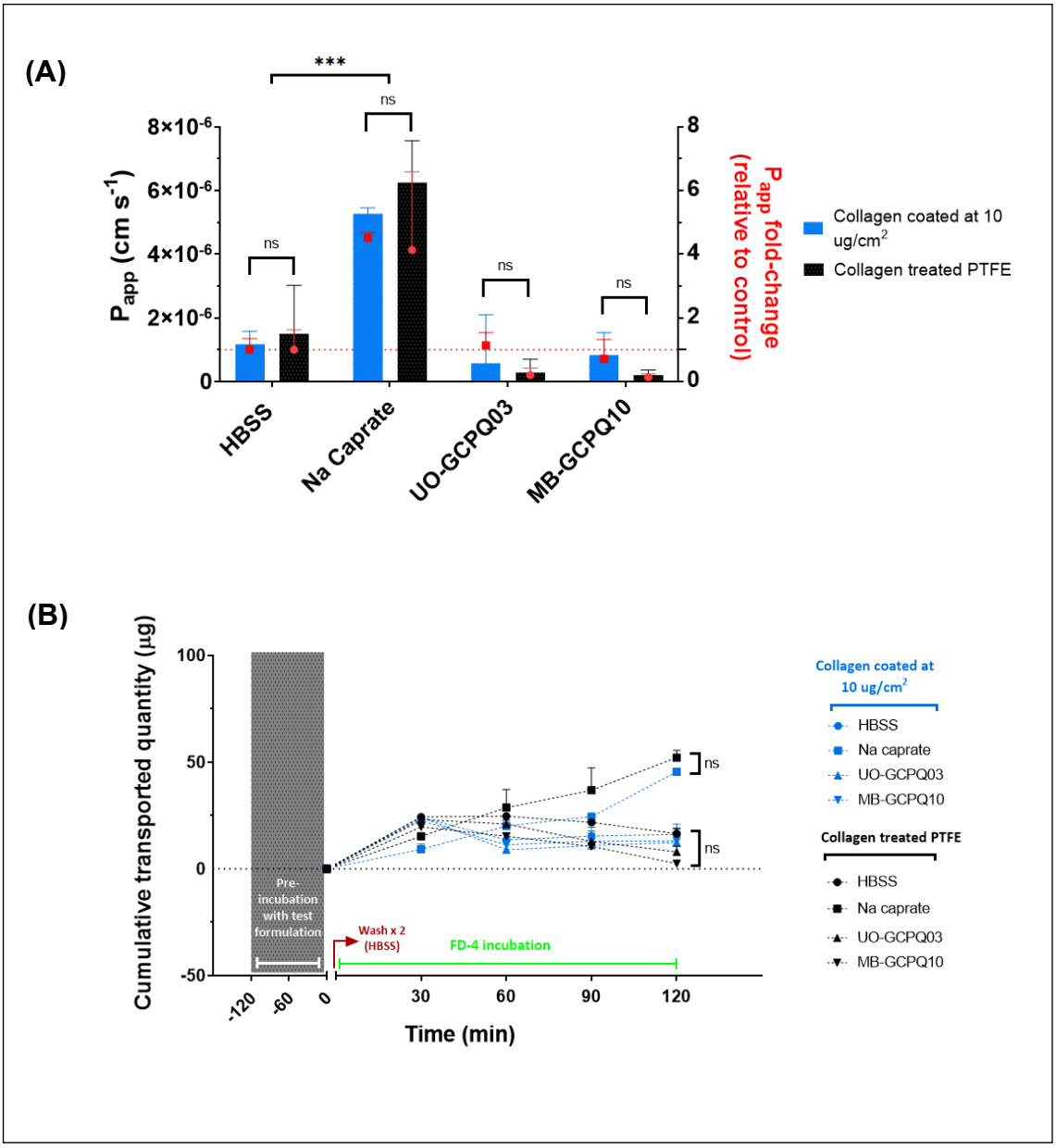

Figure 4-12: Effect of GCPQ (1mg/mL) on the paracellular transport of FD-4 across SIRC cell line coated with collagen.

(A) the apparent permeability coefficient of GCPQ03 and GCPQ10 coated with (collagen at 10 µg/cm^2 in the lab, collagen treated PTFE from the company); **(B)** Transport of FD-4.
Statistical significance was determined two-way ANOVA with Tukey post-test, n=3; *= $p < 0.05$.

Tight junction proteins are the primary determinant of the paracellular permeability [233]. They primarily include tetraspan proteins, occludin, the claudin family, and tricellulin which are associated with the cytoskeleton via scaffolding proteins, such as zonula occludens [266].

The cornea is a tissue that has tighter junctions than the intestine, lung and nasal mucosa; making drug absorption via the paracellular route more difficult compared to other organs [2]. The cornea is divided into three distinct layers (Figure 4-13): epithelium, stroma, and endothelium. The epithelium is a tight junction tissue with five to seven layers of cells (0.1 mm thick) that are relatively impervious to hydrophilic compounds [290]. The superficial corneal epithelial cells are joined to one another by desmosomes and are surrounded by ribbon-like tight junctional complexes zonula occludens. The presence of these tight junctional complexes retards paracellular drug permeation from the tear film into intercellular spaces of the epithelium as well as inner layers of the cornea [8].

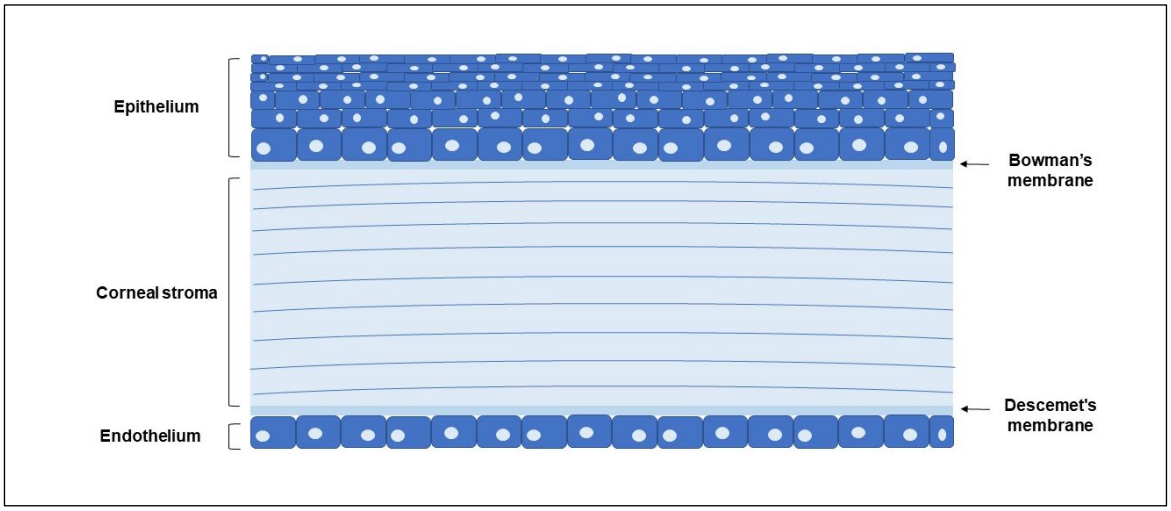

Figure 4-13: Schematic diagram of distinct layers of the cornea.

Goskonda et al. showed that the mannitol as a hydrophilic marker, which is transported predominantly via the paracellular pathway, has low permeability on the SIRC cell line (Papp = 0.58 × 10^{-6} cm/s) [287]. It has been shown that SIRC cells grown on the membrane support for ten days developed four to six layers of cells as compared to the standard corneal epithelial monolayer [261], while the MDCK showed a monolayer on the polycarbonate membrane transwell without any matrix treatment [256]. Although the MDCK cell line developed a polarised epithelial cell monolayer on transwells [257], a recent study showed that SIRC cell line, when grown on collagen-coated transwells, were a mixture of epithelial and fibroblast cells [291]. Tight junctions proteins are specific for epithelial/endothelial cells and should be absent in fibroblast cells [291]. Olivieri et al. investigated the expression of epithelial and fibroblast markers in SIRC cell lines when compared to the level of expressions of the markers in the human retinal pigmented epithelial (ARPE-19) cell line, and the human keratocyte (HK) cell line [291]. The SIRC cells were shown to express the tight junctions protein markers occludin, claudin-1, and claudin-5 but to a lower extent than ARPE-19 ($p \leq 0.05$) [291]. SIRC and ARPE-19 expressed the fibroblast markers lumican and vimentin but to a lesser extent than HK cell line ($p \leq 0.05$) [291]. Thus, the presence of the fibroblast character in the SIRC cell line could explain the different permeability profile of GCPQ in SIRC as compared to MDCK cell lines.

Sodium caprate, the sodium salt of capric acid is an amphiphilic substance, with a hydrophilic “head” (carboxylate ion) and a hydrophobic “tail” (aliphatic C10 chain) and has a critical micelle concentration of about 50 mM [292]. It has been approved as an absorption enhancer in a rectal suppository [292]. The mode of action of C10 has

been reported, in MDCK cells: claudins-4, -5 and occludin were displaced from lipid rafts to more liquid membrane domains, whereas claudins-1, -2 and -3 were unchanged after C10 treatment [293]. A recent report showed that C10 selectively influences the solubility of membrane microdomains primarily associated with claudin-5 and tricellulin, and this effect is mediated by reversible removal of tricellulin from the tricellular tight junction [266].

The exact mechanism by how GCPQ would act in the cornea is still unclear. In the current work, we speculate that GCPQ, like C10, could increase paracellular transport through an occludin, and ZO-1 dependent mechanism [281,294], and MDCK cells are more susceptible to GCPQ tight junction modulations than SIRC cells.

4.4. Conclusions

The biocompatibility of GCPQ and GCPQ drug formulations was assessed by measuring the IC50 value in a standard MTT assay. GCPQ has shown to demonstrate good biocompatibility against MDCK and SIRC cell lines.

We have shown that GCPQ can be engineered to have various paracellular transport enhancements in MDCK cells. This degree of enhancement in paracellular transport is dependent on the ratio of DQ% to DP% with polymers having higher QPR and moderate MW between 10 – 20 kDa, resulting in higher apparent permeability coefficient values for the paracellular marker, FD-4. This effect is also pH-dependent. Polymers with high QPR values are likely to retain their permeation enhancement properties at physiological pH. However, GCPQ was not able to modulate tight junctions opening on SIRC cell line. The hybrid nature between epithelial and fibroblastic cells in the SIRC cell line may be attributed to the absence of the transport of FD-4. It is plausible to design a transport experiment on the SIRC cell line using a transcellular marker to study the effect of different modifications of GCPQ on SIRC cell line transcellular transport. Also, GCPQ could be studied on human epithelial corneal models such as transformed human corneal epithelial cell lines for future permeation experiments.

5. Biological *in vivo* Studies

5.1. Introduction

Intravitreal injection is a common route of drug administration to treat posterior ocular diseases [295]. The need for repeated eye puncture with intravitreal injections is associated with several side effects such as endophthalmitis, haemorrhage, and retinal detachment [296]. An alternative to intravitreal injections is the transscleral drug delivery route. Although transscleral delivery is comparatively easy and less invasive than the intravitreal injection, the drug permeation to posterior eye tissues is compromised by ocular static and dynamic barriers [297]. Ocular barriers to transscleral drug delivery include static barriers: sclera, choroid and retinal pigment epithelium. Dynamic barriers include: lymphatic flow in the conjunctival and episcleral tissues and blood flow in the conjunctiva and choroid [298]. However, these approaches only treat one eye and still carry the risks associated with injectables. For these reasons, a delivery system that avoids intraocular injections and facilitates drug entry to the posterior segment is of paramount importance.

The topical eye drop is the most widely preferred and non-invasive route of drug administration to treat diseases affecting the anterior segment [297]. Conventional eye drops account for 90% of the marketed ophthalmic formulations [10]. The reasons why eye drops are a popular dosage form include: the ease of administration and patient compliance [299]. The ease of application of eye drops in both eyes without the need for a surgical procedure makes them superior to the intravitreal injection. Although this route is a viable method of drug delivery for the treatment of anterior segment

diseases, it remains a significant challenge to deliver drugs topically to treat posterior segment diseases efficiently [300].

Thus, this chapter will focus on utilising rabbits as an animal model to test the possible delivery of our formulation GCPQ: RAP to the back of the eyes Figure 5-1. We hypothesised that by utilising an amphiphilic chitosan-based polymer, the residence time of a lipophilic drug in the corneal epithelium would be enhanced, leading to possible delivery of the drug particles to the posterior segment of the eye via a non-corneal (conjunctival-scleral) pathway. Healthy New Zealand White rabbits were used in this experiment. The main advantages of using rabbits as experimental models in eye research are the large size of the rabbit eye relative to its body and its similarity to the human eye [301]. Rabbits share ocular features with humans as shown in (Table 5-1) [300], including a comparable vitreous volume and internal structure, and thus a similar diffusional path for topically administered compounds to reach the posterior segment [300]. Also, the ease of handling and the economy of a large breed model compared to others makes rabbits ideal for ophthalmic research [301].

In a collaborative project, a well-studied experimental autoimmune uveitis is being used as a mouse model of retinal disease, to determine whether topically administered GCPQ: RAP may have clinical benefit. We aim to test the ability of GCPQ to deliver therapeutic quantities of RAP to the retina effectively. We hypothesise that by utilising GCPQ: RAP, this formulation should be able to suppress the inflammatory disease.

Furthermore, a novel formulation GCPQ: TAC was developed to study the feasibility of this formulation to deliver sufficient therapeutic quantities of TAC to the eyes' anterior tissues in healthy New Zeeland White rabbits. This last formulation may find use in the treatment of allergic ocular disorders.

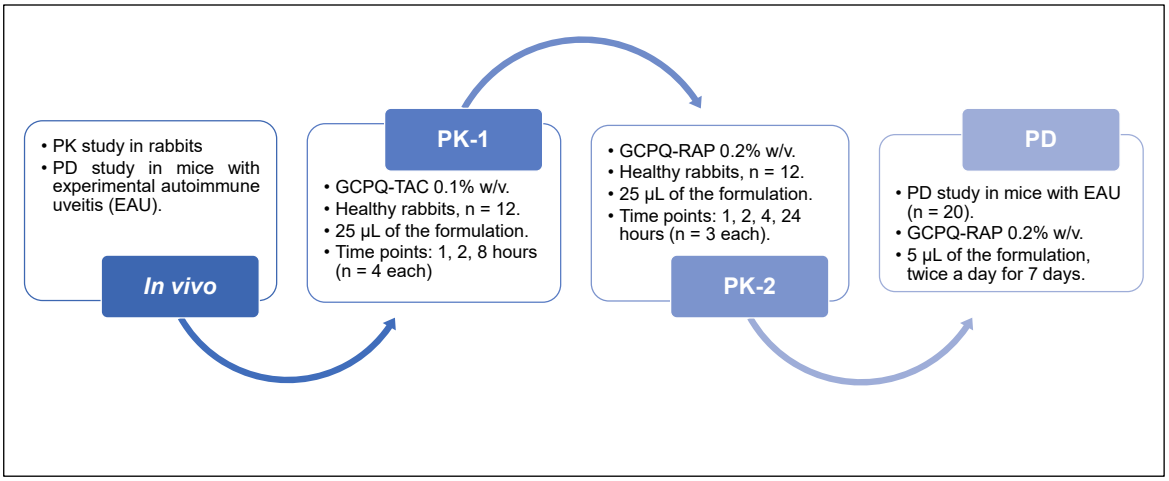

Figure 5-1: Illustration of the experimental plan for the *in vivo* studies.

Table 5-1: Comparison of human and rabbit eyes.

Factor		Rabbit	Human
Tear	Tear volume (μL)	5-10	7-30
	Tear turnover rate (μL/min)	0.5-0.8	0.5-2.2
	Osmolarity of tear (mOsm/L)	305	305
Lacrimal fluids	pH of lacrimal fluids	7.3-7.7	7.3-7.7
	Lacrimal volume (μL)	7.5	7
	Punctum/Puncta	1	2
Cornea	Thickness (mm)	0.35-0.45	0.52-0.54
	Diameter (mm)	15	11-12
	Surface area (cm^2)	1.5-2.0	1.04
Conjunctiva	The ratio of conjunctival surface area to the corneal surface area	9	17
Aqueous Humour	Aqueous humour volume (mL)	0.25-0.3	0.1-0.25
	Turnover rate (μL/min)	3-4.7	2-3
	pH	8.2	7.1-7.3
Other	Spontaneous blink rate	4-5 blinks/hr	6-15 blinks/min
	Nictitating membrane	Present	Absent

5.2. GCPQ: RAP *in vivo* pharmacokinetic study in New Zealand healthy rabbits

5.2.1. Introduction

Treatment of diseases affecting the posterior segment of the eye with topically applied eye drops has not been effective because of inefficient delivery of the active agent to the target site [302]. Up to date, there are no eye drop medications that target the posterior ocular tissues, i.e., the retina. A drug candidate that could provide proof-of-concept data in humans to deliver topical eye drops to the retina includes PAN-90806 from PanOptica, Inc. (New Jersey, USA). The phase I clinical trial of PAN-90806 eye drops was completed in 2016 with an advance to Phase II clinical trial. The preclinical data of PAN-90806 showed comparable performance to intravitreal vascular endothelial growth factor injections [302]. These data could suggest the feasibility of delivering an appropriate eye drop formulation to the back of the eye tissues in humans. However, there is no news on the progress of this formulation.

Various researches have shown the capability of nanoformulations to reach back of the eye tissues following topical application. Cholkar et al. reported a drug-loaded nanomicellar formulation utilising vitamin E tocopherol polyethylene glycol succinate and octoxynol-40 had been shown to reach the posterior tissues in rabbits [34]. Another study showed that a small unilamellar vesicle liposomal formulation was able to deliver transforming growth factor-β1 to the vitreous humour of New Zealand

White rabbits [303]. Despite this preclinical progress, successful translation to human studies has yet to be demonstrated [300].

Rapamycin (sirolimus), a natural product produced from the soil bacteria *Streptomyces hygrosopius*, was approved in 1999, by the Food and Drug Administration as a mammalian target of rapamycin (mTOR) inhibitor [159,304]. The approved drug, Rapamune, oral solution and tablets from Wyeth Pharmaceuticals Inc. (Philadelphia, USA) is an immunosuppressive agent indicated for the prophylaxis of organ rejection in patients aged ≥13 years receiving renal transplants [253].

Rapamycin binds to the immunophilin, FK binding protein to interact with mTOR and inhibit its function, leading to inhibition of cell growth and cell proliferation [159]. RAP also inhibits vascular endothelial growth factor production [304]. Recently, RAP was explored in eye research to prevent allograft rejections following corneal transplantation [305], as well as for chronic inflammatory disorders such as posterior uveitis [306], retinal and choroidal neovascularisation [307], diabetic macular oedema [308], and in autoimmune Sjogren's syndrome [309].

Oral or intravenous administration of RAP for the back of the eye delivery is not medically acceptable, due to its low solubility (water solubility = 2.6 μg/mL) [34], and high lipophilicity (log *P* = 5.77) [34]. Various formulation and route of administration methods have been used to deliver RAP to the eye. Strategies such as periocular, subconjunctival [310], and intravitreal implants/injections [310] of RAP are invasive and associated with side effects such as retinal detachment, and endophthalmitis [34]. Pharmaceutical approaches based on nanotechnologies and the development of

eye drops composed of the mucoadhesive chitosan derivative is an emerging strategy for the efficient treatment of ocular diseases [136].

The purpose of this section is to determine the feasibility of delivering the novel eye drop formulation (GCPQ: RAP, 0.2 % w/v) to the posterior segment of the eye, and to evaluate the pharmacokinetic profile of RAP in various ocular tissues upon single instillation to healthy rabbits.

5.2.2. Materials

Chemical	Supplier
Rapamycin (MW 914.187 g/mol)	Cambridge Biosciences (Cambridge, UK)
Ascomycin (MW 792.02 g/mol)	Generon Ltd. (Slough, UK)
Acetonitrile LCMS grade	VWR (Leicestershire, UK)
Methanol LCMS grade	Fisher Scientific (Loughborough, UK)
Water LCMS grade	VWR (Leicestershire, UK)
Formic acid LCMS grade	Fisher Scientific (Loughborough, UK)

5.2.3. Animals

New Zealand White male rabbits weighing between 2.0 – 3.0 kg were obtained from Envigo (Huntingdon, UK) and were acclimatised for at least seven days before the experiment. The rabbits had free access to water and food throughout the study. Treatment of animals conformed to the Association for Research in Vision and Ophthalmology statement for the use of animals in ophthalmic and vision research. All animal studies were ethically reviewed and performed in accordance with the Animals (Scientific Procedures) Act 1986.

5.2.4. Methods

5.2.4.1. Bioanalytical LC-MS/MS Assay

5.2.4.1.1. Preparation of working standard solutions:

The development of RAP working standard solutions is shown in Table 5-2 and Table 5-3. RAP stock solution (STK) was prepared at a concentration of 100 µg/mL in methanol. RAP dissolves in methanol at (25 mg/mL) [176]. RAP working stocks solutions (Stks) were prepared by serially diluting RAP STK into MeOH to obtain the Stks in Table 5-2, ranging from a concentration of (0.0167–33.4 µg/mL).

RAP working standards (WS) were prepared by serially diluting RAP working Stks in MeOH to obtain the RAP working standards in Table 5-3, ranging from a concentration of (0.5 – 1000 ng/mL). Ascomycin was used as an internal standard. A stock solution of the internal standard was freshly prepared at a concentration of 100 ng/mL in methanol.

Table 5-2: Preparation of RAP stocks solutions.

Stock (STK) is 100 µg/mL (RAP in MeOH)						
Prepare	**Take from**	**µL**	**Add MeOH (µL)**	**Final volume (µL)**	**Conc. (µg/mL)**	**ng/mL**
Stks 10	**STK**	668	1332	2000	33.4	33,400
Stks 9	**Stks 10**	1125	375	1500	25.05	25,050
Stks 8	**Stks 9**	1000	500	1500	16.7	16,700
Stks 7	**Stks 8**	750	750	1500	8.35	8,350
Stks 6	**Stks 7**	600	900	1500	3.34	3,340
Stks 5	**Stks 6**	750	750	1500	1.67	1,670
Stks 4	**Stks 5**	750	750	1500	0.835	835
Stks 3	**Stks 4**	600	900	1500	0.334	334
Stks 2	**Stks 3**	150	1350	1500	0.0334	33
Stks 1	**Stks 2**	750	750	1500	0.0167	17

Table 5-3: Preparation of RAP working standards solutions.

Prepare	RAP stock conc. (µg/mL)	RAP/MeOH (µL)	ASC/MeOH (µL) *	In final volume MeOH (µL)	Final conc. (ng/mL)
WS10	33.4	50	60	1670	1,000
WS9	25.05	50	60	1670	750
WS8	16.7	50	60	1670	500
WS7	8.35	50	60	1670	250
WS6	3.34	50	60	1670	100
WS5	1.67	50	60	1670	50
WS4	0.835	50	60	1670	25
WS3	0.334	50	60	1670	10
WS2	0.0334	50	60	1670	1
WS1	0.0167	50	60	1670	0.5

* Ascomycin concentration (100 ng/mL) in methanol.

5.2.4.1.2. Preparation of standard and quality control curves:

Working standard solutions were prepared to obtain an individual standard curve in each of the rabbits' eyes blank tissues, and in the cornea, conjunctiva, sclera, choroid-retina, aqueous humour, and vitreous humour.

Tissues were homogenised according to the following protocol. Briefly, the solid frozen tissue was cut into small pieces with scissors and ground to a fine powder with a mortar and pestle placed in dry ice (Figure 5-2, A), and the absolute tissue mass was weighed (30 mg). Aqueous samples (aqueous humour, and vitreous humour, 30 µL) were transferred into a sterile polypropylene tube, and the absolute mass was weighed. Normal saline was added to make a final volume (500 µL), and samples were vortex-mixed for 5 minutes. The mixtures were then homogenised using probe sonication (MSE Soniprep 150 sonicator) from MSE UK Ltd. (London, UK) at 50% of its maximum output for 25-50 seconds in an ice bath (Figure 5-2, B). The homogenised samples were spiked with RAP working standards (50 µL) in order to generate the standard curves (Table 5-4). In addition, samples were spiked with the internal standard ascomycin in MeOH (100 ng/mL, 60 µL). Methanol (1060 µL) was added to precipitate the protein.

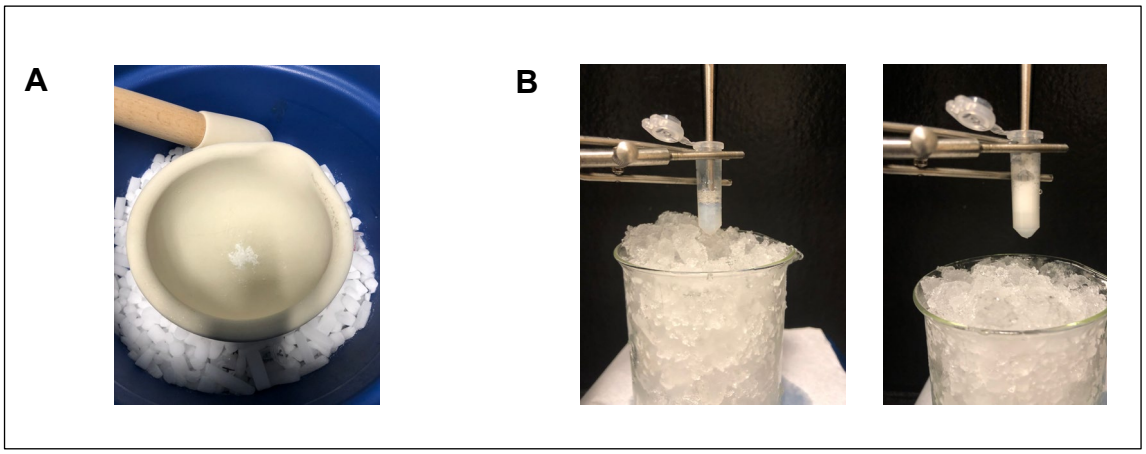

Figure 5-2: The homogenisation of solid tissue samples.
(A) the grinding of solid frozen tissue under dry ice; **(B)** homogenisation of ground tissue with probe sonication.

Table 5-4: Preparation of standard curves solutions of RAP in ocular tissue homogenates.

Prepare	Normal saline (µL) – in tissues	Spike with RAP/MeOH (50 µL) (µg/mL)	Spike with ASC/MeOH (µL) *	In final volume MeOH (µL)	Final conc. (ng/mL)
WS10	500	33.4	60	1670	1,000
WS9	500	25.05	60	1670	750
WS8	500	16.7	60	1670	500
WS7	500	8.35	60	1670	250
WS6	500	3.34	60	1670	100
WS5	500	1.67	60	1670	50
WS4	500	0.835	60	1670	25
WS3	500	0.334	60	1670	10
WS2	500	0.0334	60	1670	1
WS1	500	0.0167	60	1670	0.5

* Ascomycin concentration (100 ng/mL) in methanol.

The quality control standard curves were generated to evaluate the recovery rate and the matrix effect on drug extraction. Blank samples were prepared similar to tissue's standard curve (Table 5-5). Briefly, RAP working standards samples (50 µL) were added to normal saline (500 µL) to generate the standard curves. Samples were spiked with ascomycin in MeOH (100 ng/mL, 60 µL). Methanol (1060 µL) was added to mimic the extraction protocol.

The mixtures were then vortexed for 5 minutes and centrifuged at (5000 g x 10 min at 4°C) with Hettich Mikro 200R (Tuttlingen, DE). An aliquot (1 mL) of the centrifuged homogenate supernatant was evaporated to dryness within the speed vac at 45°C and spun under vacuum in the evaporator for at least 2 hours. The residues were reconstituted in the LC-MS/MS mobile phase (100 µL) and vortex-mixed for 5 minutes. The samples were centrifuged at (2000 g x 2 min at 4°C) to precipitate any tissues. Following this, samples (80 µL) were transferred to HPLC vials. Ten µL of the reconstituted sample was injected into the LC-MS/MS system.

Table 5-5: Preparation of quality control (blank) standard curves.

Prepare	Normal saline (µL) - blank	RAP stock conc. (µg/mL)	Spike with RAP/MeOH (µL)	Spike with ASC/MeOH (µL) *	In final volume MeOH (µL)	Final conc. (ng/mL)
WS10	500	33.4	50	60	1670	1,000
WS9	500	25.05	50	60	1670	750
WS8	500	16.7	50	60	1670	500
WS7	500	8.35	50	60	1670	250
WS6	500	3.34	50	60	1670	100
WS5	500	1.67	50	60	1670	50
WS4	500	0.835	50	60	1670	25
WS3	500	0.334	50	60	1670	10
WS2	500	0.0334	50	60	1670	1
WS1	500	0.0167	50	60	1670	0.5

* Ascomycin concentration (100 ng/mL) in methanol.

5.2.4.1.3. Chromatography:

Samples were analysed using an Agilent 6400 Series Triple Quadrupole LC/MS system from Agilent technologies (Berkshire, UK) comprising a degasser (HiP Degasser 1260/G4225A), a binary pump (HiP 1260 binary pump/G1312B), an autosampler (HiP sampler 1260/ G1367E), a column oven (G1316A) and a triple-quadrupole mass spectrometer (G6460A). An Agilent MassHunter workstation software was used for data acquisition and data processing.

A sensitive LC-MS/MS method was applied to determine RAP concentration in the eye tissue homogenates and blank tissue samples. Samples (10 µL) were chromatographed over an XBridge BEH C8 XP column (2.5 µm, 2.1 mm X 50 mm) equipped with a Vanguard Cartridge Holder guard column from Waters Limited (Herts, UK) and at a temperature of 50°C, with the mobile flow rate of 0.5 mL/min. The runtime was 6 minutes, followed by a 1-minute post run time. The mobile phase was formic acid (0.1% v/v) in water and acetonitrile containing (LC-MS grade solvents) in the following gradient conditions (Table 5-6):

Table 5-6: LC-MS/MS mobile phase composition of RAP and internal standard.

Time (min)	0.1% FA in H_2O Solvent A (%)	0.1% FA in ACN Solvent B (%)
0.00	60	40
1.00	60	40
3.00	5	95
5.00	5	95
6.00	60	40

Rapamycin and ascomycin were monitored by positive electrospray ionisation on an Agilent jet stream ion source with ionisation source parameters as shown in Table 5-7, and samples were scanned using multiple reaction monitoring transitions of RAP and ascomycin.

Table 5-7: LC-MS/MS source parameters for RAP and ascomycin.

Parameter	RAP (Analyte)	Ascomycin (Internal standard)
Capillary voltage (V)	3500	3500
Gas temperature (°C)	300	300
Gas flow (L/min)	5	5
Sheath gas heater (°C)	250	250
Sheath gas flow (L/min)	11	11
Nebuliser (psi)	45	45
Fragmentor (V)	200	300
Collision energy (V)	65	45
Precursor ion (m/z)	936.4	814.2
Product ion (m/z)	409.1	604.1

5.2.4.2. GCPQ: RAP pharmacokinetics animal study:

New Zealand White albino male rabbits weighing between 2.0 and 3.0 kg, were acclimatised for not less than seven days before the experiments. The rabbits had free access to water and food throughout the study. Twenty-five µL of the GCPQ: RAP 0.2 % w/v (Figure 5-3) formulation was administered to both eyes. Briefly, the lower eyelid was gently pulled away from the eye globe and using a calibrated micropipette, 25 µL of the formulation was applied in the lower conjunctival cul-de-sac. After dosing, the upper and lower eyelids were hand-held together for approximately 5 seconds to permit the formulation to come into contact with the cornea. The number of blinks in the next 60 seconds was recorded. Subsequently, after predetermined time points (1, 2, 4, 24 hours, n=3 each), the rabbit was culled with an IV over-dose injection of 20% w/v phenobarbital (5 mL) through the marginal ear vein using a 25-gauge butterfly needle.

The eye globe was enucleated using sterilised scissors, washed twice with 0.9% w/v normal saline and dried on a filter paper. Subsequently, the various tissues were dissected, rinsed twice with 0.9% w/v normal saline and dried on a filter paper. The eye tissues were harvested in the following order to minimise cross-contamination: conjunctiva, aqueous humour, vitreous humour, lens, iris/ciliary body, cornea, choroid-retina, sclera. The harvested dried tissues were immediately stored in ice for (2-5 hours after dissection), and eventually stored at -80°C until further analysis could be performed. The aqueous humour was withdrawn using a 26-gauge needle attached to 2 mL syringe, while vitreous

humour was aspirated using a 23-gauge needle attached to 2 mL syringe. All tissue dissections were performed using sterilised tools. Disposable scalpels, tweezers and scissors were used as necessary. Any other sharp tools were disinfected with 70% ethanol and washed with 0.9% w/v normal saline before moving to the following tissue. All tissues were rinsed twice with 0.9% w/v normal saline before being added to a pre-weighed tube.

For RAP extraction, the protein precipitation method was used. Briefly, the solid frozen tissue was cut into small pieces with scissors and ground to a fine powder with a mortar and pestle placed in dry ice, and the absolute tissue mass was weighed. Aqueous samples (aqueous humour and vitreous humour) were transferred into a sterile polypropylene tube, and the absolute mass was weighed. Normal saline was added to a final volume (500 µL), and samples were vortex-mixed for 5 minutes. The mixtures were then homogenised using probe sonication (MSE Soniprep 150 sonicator) from MSE UK Ltd. (London, UK) at 50% of its maximum output for 25-50 seconds in an ice bath.

To all the tissue homogenates, an aliquot of the internal standard (100 ng/mL, 60 µL) was added and vortexed for 5 min. Methanol (1110 µL) was added to precipitate the protein and extract the RAP. Mixtures were then vortexed for 5 minutes and centrifuged (5000 g x 10 min at 4°C). An aliquot (1 mL) of the centrifuged homogenate supernatant was evaporated to dryness within the speed vac at 45°C and spun under the vacuum evaporator for at least 2 hours. The residues were reconstituted in the LC-MS/MS mobile phase (100 µL) and vortex-mixed for 5 minutes. Samples were centrifuged (2000 g x 2 min at 4°C)

to precipitate any tissues. An aliquot of the resulting supernatant (80 µL) was transferred to HPLC vials. Ten µL of the reconstituted sample was injected into the LC-MS/MS system.

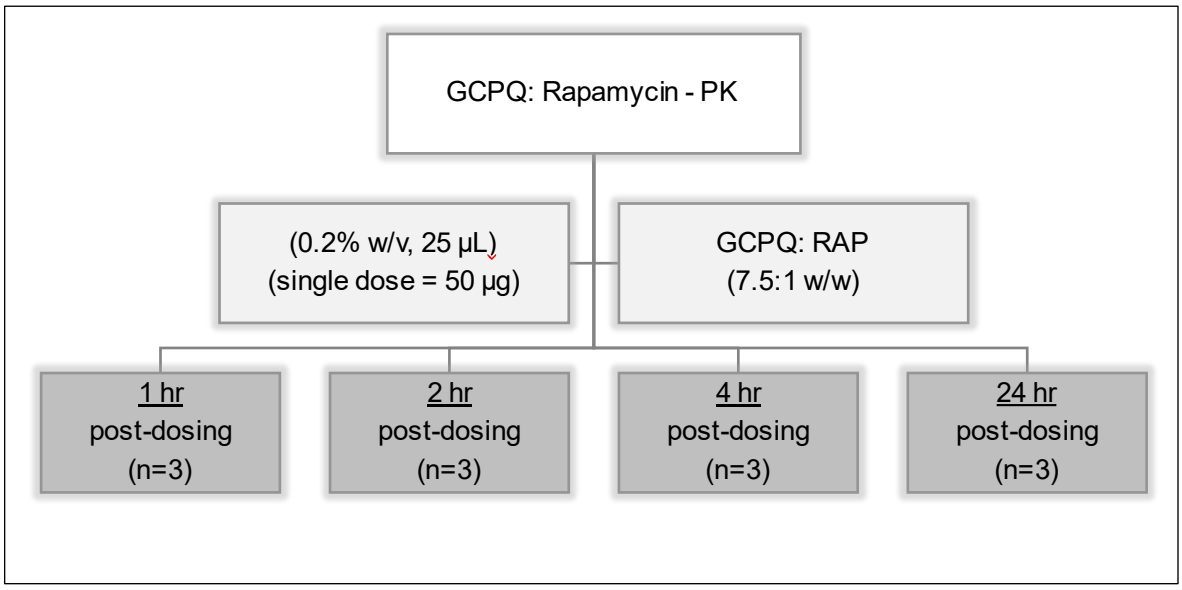

Figure 5-3: Pharmacokinetics *in vivo* study design of GCPQ: RAP (25 µL, 0.2% w/v) formulation.

5.2.5. Results and discussion

5.2.5.1. Preparation of standard and quality control curves:

Working standards solutions were prepared to obtain a standard curve of RAP in the mobile phase and each of the tissues: cornea, conjunctiva, sclera, choroid-retina, aqueous humour, and vitreous humour. Table 5-8 shows the assay parameters used to analyse the tissues. Individual calibration curves for the blank and each tissue was obtained by plotting the peak area ratios (RAP / internal standard) versus the analyte concentration. The calibration curves were linear for RAP in a concentration range of 0.5 - 500 ng/mL for the blank, with an r^2 greater than 0.99.

The measured lower limit of quantification (LLOQ) for RAP was (0.5 ng/mL) for the blank and the choroid-retina. The measured LLOQ for the cornea, aqueous humour and vitreous humour was (1 ng/mL), while for the conjunctiva and the sclera was (10 ng/mL).

The signal to noise ratio (SNR) explains the extraction efficiency of the assay and quantifies the capability to remove all endogenous interfering components, which are usually present in the biological matrix [304]. Generally, the SNR threshold of 10 is used for LC-MS analysis [311]. The SNRs calculated by MassHunter workstation software were ≥ ten for the blank and all tissues at the lower limit of quantification. Accuracy was examined by analysing ocular tissues and the blank sample, in which the drug was dissolved in the mobile phase (Table 5-8). Accuracy was calculated by dividing the ratio of the peak area in the presence of the matrix to the peak area in the absence of a matrix multiplied by 100 [312]. Accuracy of the method must be

between 85% and 115% of the nominal value in all the standards, except at the LLOQ level, which is 80 – 120% according to bioanalytical method validation in Food and Drug Administration guidelines [304,313]. The average percentage of the accuracy of all the standards is 90.97%; this is in line with the guideline on bioanalytical method validation in which a range ±15% of the nominal value is acceptable for the non-zero calibrators, and between ±20% at the LLOQ [312,313].

Precision was calculated using the coefficient of variation (CV) (standard deviation/mean) multiplied by 100 (Table 5-8). The precision of the analytical method describes the closeness of repeated individual measures of analyte [312]. The precision of the method should be within 15% of the nominal concentration except at the LLOQ, which is within 20% [13]. The average CV of all the standards is 21.40%.

Table 5-8: Assay parameters to analyse RAP in ocular tissues.

Parameters	Equation of the straight line	Linearity (ng/mL)	r^2	Accuracy (%)	Precision (%)
Blank	y = 0.0607x + 0.3745	0.5 – 500	0.9972	-	-
Conjunctiva	y = 0.04x + 0.5204	10 – 500	0.9973	70.94	16.79
Aqueous humour	y = 0.0612x + 0.8589	1 – 500	0.9965	101.73	26.68
Vitreous humour	y = 0.0551x + 1.2327	1 – 500	0.9933	107.47	28.00
Cornea	y = 0.0619x + 0.7489	1 – 250	0.9920	105.97	27.61
Choroid-Retina	y = 0.0689x + 0.1223	0.5 – 500	0.9984	107.30	18.20
Sclera	y = 0.0345x + 0.1643	10 – 500	0.9988	52.42	11.10
Average				90.97	21.40
SD				23.52	7.03

5.2.5.2. Bioanalytical LC-MS/MS assay

The LC-MS/MS chromatograms for RAP and ascomycin are presented in Figure 5-5. Both RAP and ascomycin were ionised under the positive electrospray ionisation for analyte quantification. The sodium adduct is employed as it was stable in the non-ammoniated mobile phase. The formation of the adduct is a standard ionisation method in electrospray ionisation mass spectrometry [314]. It has been reported that sodium adduct formation tends to dominate in weakly acidic mobile phases containing 0.1% formic acid [314]. Guan et al. observed the formation of [M + Na]+ in a mobile phase containing 0.1% formic acid [315]. The utilisation of formic acid-containing mobile phase has the advantage in that these mobile phases never clog the peak tubes and the seals [304]. Also, the sodium adduct could have originated from glassware, stainless steel, or as an impurity in chemicals or solvents [314,316]. The formation of sodium adducts in the analysis could be due to the addition of normal saline in the extraction process. Jurchen et al. reported the formation of sodium adduct when sodium chloride was employed in the extraction analysis [317].

Multiple reaction monitoring mode was used to detect RAP and ascomycin. The precursor ion to product ion transitions of *m/z* [M + Na]+ (936.4 → 409.1) and [M + Na]+ *m/z (*814.2 → 604.1) were chosen for RAP and ascomycin, respectively, based on the most abundant product ion. The MRM transition of RAP is in line with a recently reported study [34]. Ascomycin was used as the internal standard because of its structural similarity to RAP, and it has a similar fragmentation pattern. Figure 5-4 showing structure of RAP and ASC and the fragmentation pattern of RAP.

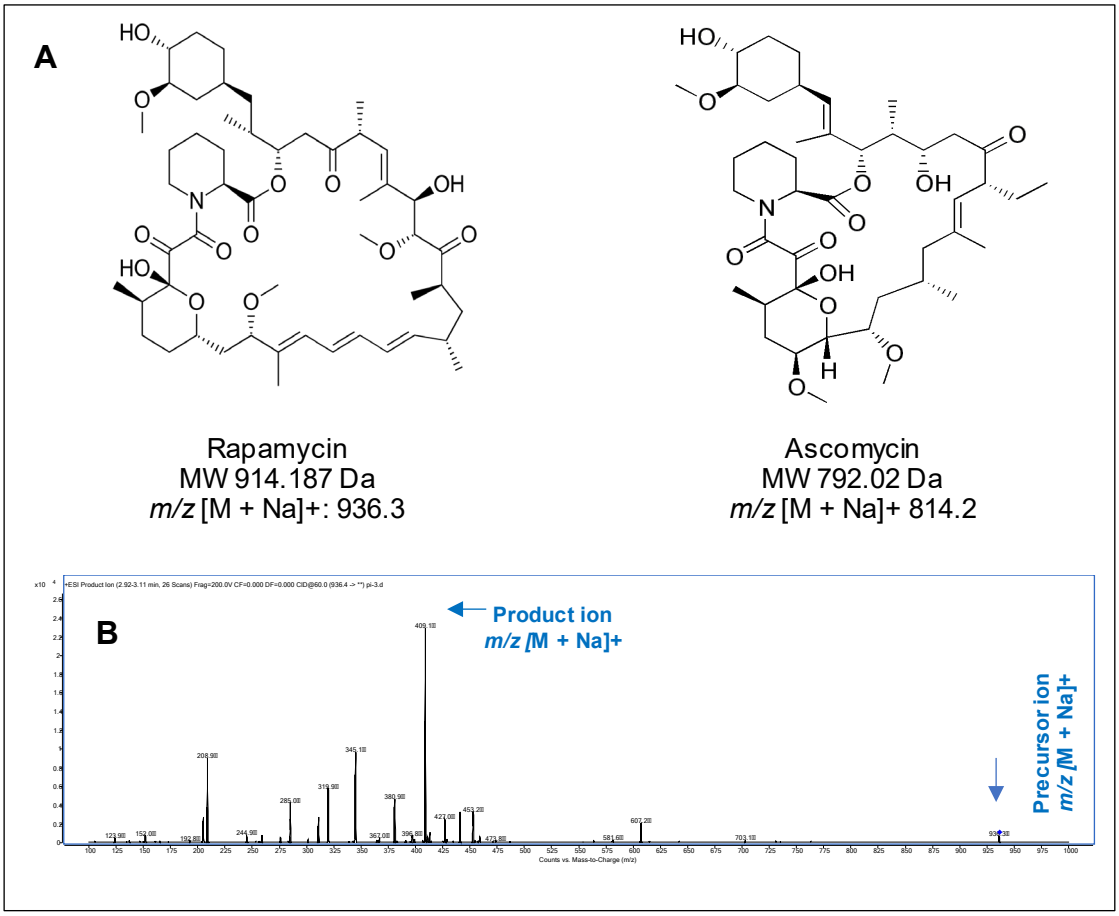

Figure 5-4: Structure of RAP and ascomycin **(A)**; fragmentation pattern of RAP **(B)**.

Rapamycin and ascomycin were extracted and separated from the blank matrices. The assay condition had an adequate specificity for RAP, while no interfering peaks were observed at its retention time. The retention time was 3.44 and 3.30 minutes for RAP and ascomycin, respectively Figure 5-5.

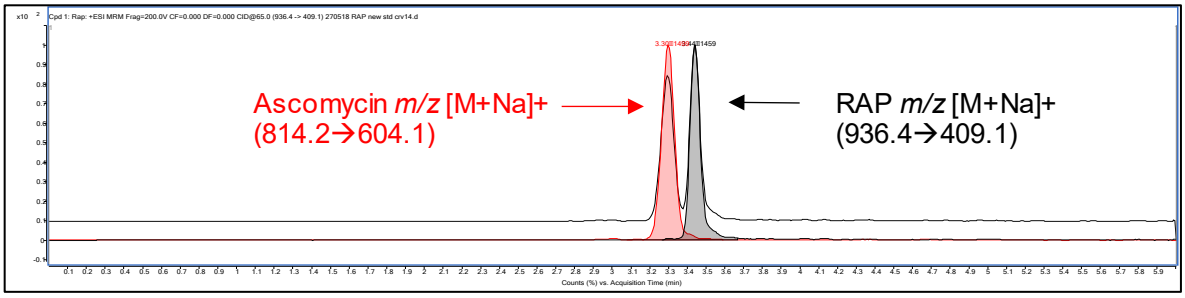

Figure 5-5: LC chromatogram for RAP at 100 ng/mL with retention time at 3.44 minutes (Right) and ascomycin 100 ng/mL with retention time at 3.30 minutes (Left).

5.2.5.3. GCPQ: RAP pharmacokinetics animal study:

We examined the possible delivery to the back of the eye using GCPQ: RAP (25 µL, 0.2% w/v). The ocular tissue distribution study was conducted in healthy New Zealand White rabbits following single topical instillation of the formulation into the conjunctival cul-de-sac.

Figure 5-6 shows the ocular drug distribution of RAP in a healthy rabbit model. Topical single dose instillation of GCPQ: RAP 0.2% w/v resulted in detectable and quantifiable RAP levels in the back of the eye tissues, i.e. sclera and choroid-retina (Figure 5-6). RAP concentrations were also quantified in the anterior chamber eye tissues; cornea, and conjunctiva (Figure 5-6). No RAP was detected in the aqueous humour and vitreous humour (LLOQ = 1 ng/mL) at all time points.

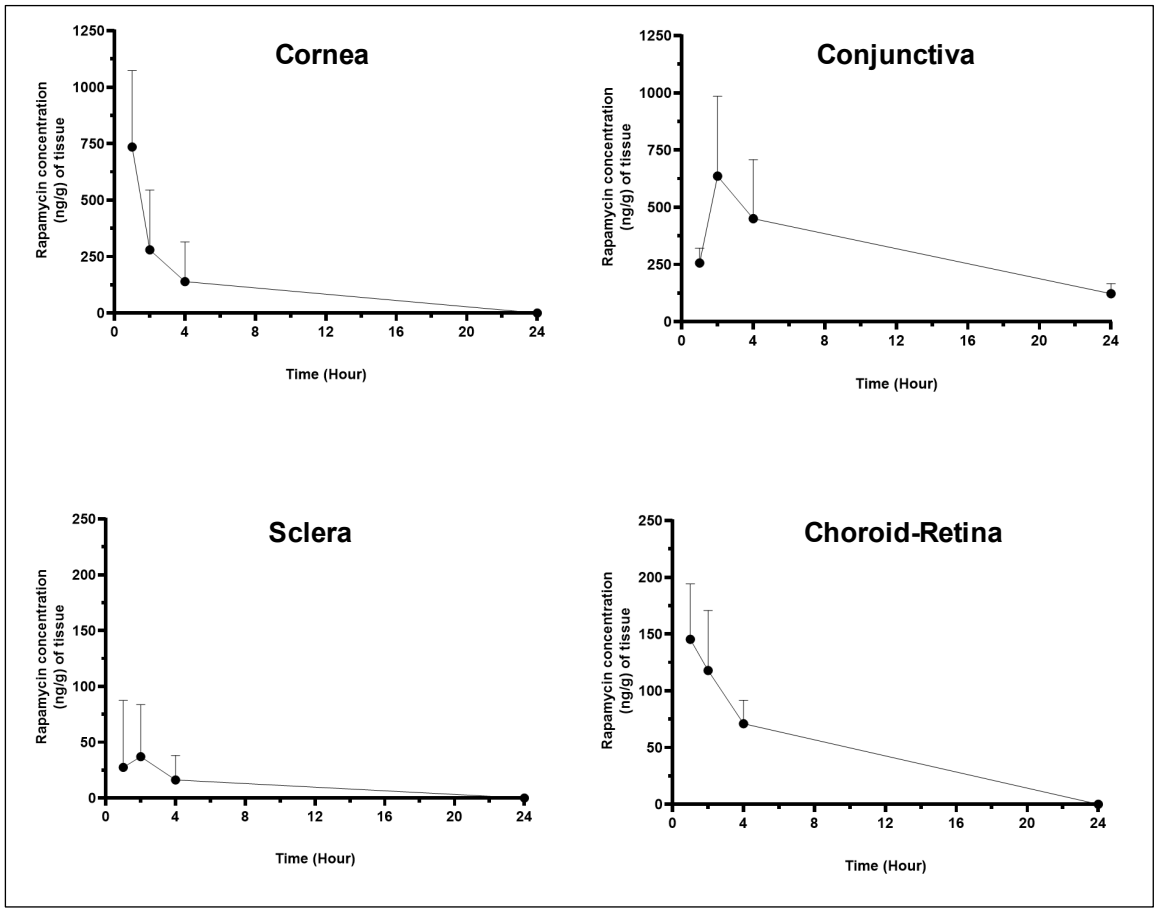

Figure 5-6: Pharmacokinetics *in vivo* RAP drug distribution study to rabbit's ocular tissues.

The Cmax of RAP in the sclera and the choroid-retina was 37 ± 47 ng/g (tmax = 2 hours) and 145 ± 49 ng/g (tmax = 1 hour), respectively (Table 5-9). The Cmax of RAP in the cornea and the conjunctiva was 735 ± 339 ng/g (tmax = 1 hour) and 636 ± 349 ng/g of tissue (tmax = 2 hours), respectively (Table 5-9).

These tissue levels were achieved following a single ocular dose of 50 µg RAP in the GCPQ: RAP formulation. A recent study reported RAP levels in the sclera and choroid-retina following the single-dose topical application of a nanomicellar eye drop formulation in a healthy rabbit (50 µL, 0.2% w/v, 100 µg RAP) [34]. Cholkar et al. used a polymeric matrix composed of vitamin E tocopherol polyethylene glycol succinate and octoxynol-40. RAP concentration in the sclera and choroid-retina was 486 ± 90, and 362 ± 56 ng/g of tissue, respectively [34]. No RAP was detected in the vitreous humour [34]. The level of RAP in the choroid-retina in the study was 2-fold the concentration that has been identified in our study. The volume used by Cholkar et al. [34] was higher than the current work, 50 µL vs 25 µL, which doubled the dose applied 100 µg in the Cholkar study vs 50 µg of RAP in the current study. When relating the level detected in the sclera to the total dose applied, only 0.1% RAP was detected in the sclera compared to 0.5% RAP in the sclera in Cholkar et al. work. The charge of the drug may affect its permeability across the sclera. Positively charged particles may exhibit reduced permeability, presumably due to their binding to the negatively charged proteoglycan matrix [8]. Our formulation has a net positive charge, while the formulation used by Cholakr et al. had a negative charge; this probably explains the slightly lower level of the sclera that has been detected. Our results capitulate the absence of RAP in the vitreous humour.

High RAP drug concentrations were detected in the cornea, and conjunctiva 1-hour post-dosing. The level of RAP in the cornea was 735 ± 339 ng/g of tissue and in the conjunctiva was 256 ± 65 ng/g of tissue. Earla et al. have reported the level of RAP in the cornea (2261 ± 507 ng/g tissue) after 1 hour following 50 µL administration of vitamin E tocopherol polyethylene glycol succinate: octoxynol-40: RAP formulation 0.2% w/v [304]. The level of RAP in the aqueous humour was below their reported limit of quantification [304]. The level of RAP in the cornea in Earla et al. (2.3% of the total dose applied) study was nearly 2-fold the concentration that has been detected in the current work (1.5% of the total dose applied); this can be explained as the volume they used was higher than the present work, 50 µL vs 25 µL, which subsequently doubled the used dose to 100 µg in the Earla report vs 50 µg of RAP in the current study. In addition, all animals in the previous two studies [34,304] were anaesthetised before the dosing, and the anaesthesia was maintained throughout the experiment. Also, there is growing evidence that gravity markedly influences vertical eye position and movement [318]. Arguably, when the eyelids are closed there will be an absence of gravity associated with preventing rapid drainage of applied eyedrops. Our work was conducted on vigilant rabbits, and so the blink rate was recorded. The average tear fluid volume is approximately 7 µL in both rabbits and humans [319]. It has been reported that tear turnover rate in non-anaesthetised rabbits is about 0.53 µL/min, with a range of 0.47-0.66 µL/min. At the same time, in anaesthetised animals, it is negligibly small or absent [320]. This process could impact the residence of the formulation in the corneal pocket and could lead to a lesser extent of the formulation being in contact with the cornea.

The pharmacokinetics parameters of RAP after single ocular instillation of GCPQ: RAP (25 µL, 0.2% w/v) ophthalmic solution in rabbits are shown in Table 5-9. The pharmacokinetic parameters calculated were Cmax, tmax, and area under the concentration-time curve (AUC). The AUC for each time point was calculated based on the trapezoidal rule (Equation 5-1) [321];

$$\boldsymbol{AUC_1 = \frac{c_0 + c_1}{2} \times Time_{1-0}} \qquad \text{Equation 5-1}$$

which c_0 is the concentration at the initial time point, c_1 is the concentration at the second time point, $time_{1\text{-}0}$ is the difference in the duration of time. Then, the sum of all AUC's was calculated to obtain the total $AUC_{0\text{-}24}$ for each tissue in the function of time. The AUC describe the drug concentration as a function of time and reflects in this context the actual eye exposure to the drug after administration with respect to time [322]. The choroid-retina AUC/cornea AUC ratio is (0.41); this represents almost half of the absorbed dose in the cornea find its way to arrive at the choroid-retina, while no RAP was detected in the aqueous humour at all time points.

For a topical drug to reach back of the eye tissue, it may follow the corneal and/or conjunctival-scleral pathway [323]. RAP is practically insoluble in water (water solubility = 2.6 µg/mL) [304], and due to its high lipophilicity (log *P* = 5.77) [34,324] and a relatively high molecular weight (MW = 914 Da) [304], the drug was not able to translocate across the cornea to the aqueous humour and vitreous humour. Since the drug must cross the blood-ocular barriers to reach the aqueous humour and retina before diffusing

passively into the vitreous humour [325], this indicates that RAP may follow the conjunctival/scleral pathway to arrive at the retina.

One of the significant drawbacks of topically applied drug formulations is subtherapeutic drug levels reaching the posterior tissues [34]. Rapamycin possesses this challenge as it cannot permeate easily into the cell. This is because RAP is lipophilic and may encounter the aqueous barrier in the tear fluid. Therefore, it is less effective to maintain sufficient therapeutic concentration at the site of action. However, we have shown that GCPQ with its mucoadhesive properties acts as a permeation enhancer, enabling RAP to come in close proximity to the cells and permeate the tissues, and to deliver the drug to the choroid-retina in a concentration higher than its therapeutic levels (7–12 ng/mL) [162]. A compound with a large molecular weight is generally considered to have reduced transcorneal permeability, and much of its intraocular access is by the non-corneal route [326]. This suggests that RAP would instead distribute mainly by the non-corneal route rather than the transcorneal route [171]. These results indicate that GCPQ may be used as a novel carrier for RAP, and the formulation could be an alternative to the current invasive injections/implants approaches used to access the retina.

Table 5-9: Pharmacokinetics parameters of RAP after single ocular instillation of GCPQ: RAP (25 µL, 0.2% w/v) ophthalmic formulation solution in rabbits.

Pharmacokinetic parameters	**Cornea**	**Conjunctiva**	**Sclera**	**Choroid-Retina**
C_{max} (ng/g tissue)	735 ± 339	636 ± 349	37 ± 47	145 ± 49
T_{max} (hr)	1	2	2	1
AUC_{0-24} (ng.hr/g)*	2691	7387	262	1103

* AUC value is an approximation from four-time points.

5.2.5.4. Ocular tolerability

The blink rate following dosing is an acceptable method of assessing acute ocular irritation, although other parameters such as erythema and swelling are also used to assess ocular irritation. In the first 60 seconds post-dosing after a single instillation of GCPQ: RAP (25 µL, 0.2% w/v), the blink rate was assessed

After topical drop instillation, the upper and lower eyelids were hand-held together for approximately 5 seconds to permit the formulation to come into contact with the cornea, and the blink rate in the next 60 seconds was recorded. Normal saline was used as a control (n = 3). Normal saline is frequently utilised as a control in ocular formulations [327] to assesses the blinks rate in rodents [328] and evaluates the lacrimation characteristics in rabbits [329]. The average blink rate in both eyes in the normal saline group was recorded as 1.0 ± 0.41 blinks/min. The average blink rate in both eyes in all treatment groups was reported as (5.10 ± 0.52 blinks/min, $p > 0.05$) (Figure 5-7).

The assessment of irritation of the GCPQ: RAP formulation to rabbits' eyes was visually evaluated using the criteria of erythema and swelling (Figure 5-7). There were no visible signs of erythema, tearing or swelling, following the ocular administration of GCPQ: RAP. These data suggested that GCPQ: RAP as a formulation does not cause dose-limiting ocular irritation to rabbits' eyes, and it is a capable system for topical treatment of diseased animal models such as autoimmune uveitis.

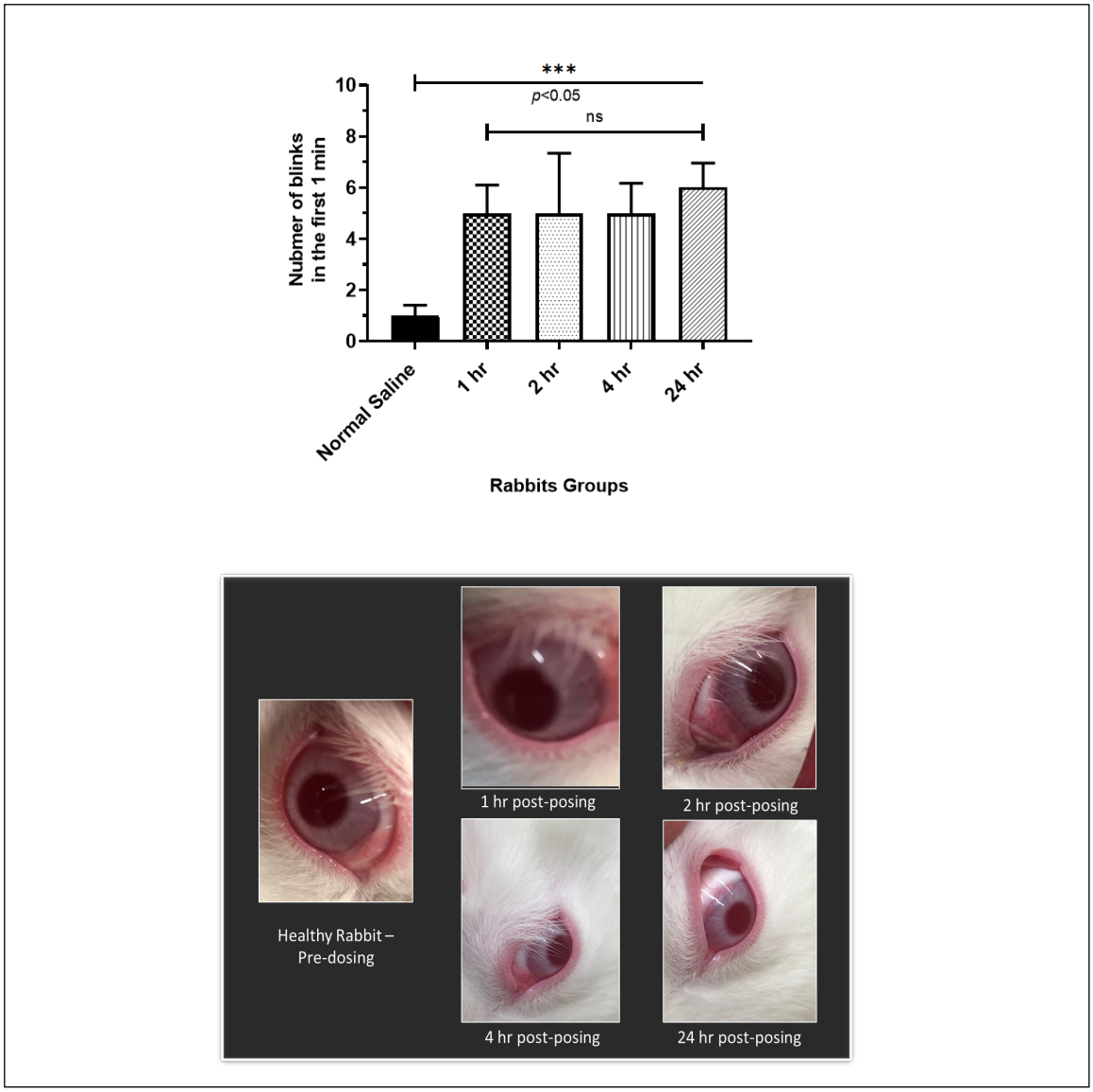

Figure 5-7: Assessment of ocular tolerability of the GCPQ: RAP formulation to rabbits' eyes.

(Top) Number of blinks in rabbits following single instillation of GCPQ: RAP (25 µL, 0.2% w/v); (Bottom) visual assessment of irritation of the GCPQ: RAP formulation to rabbits' eyes.
Time points: 1, 2, 4, 24 hours post-dosing (n=3 rabbits, each group). Statistical analysis was performed with One-way ANOVA with Tukey's multiple comparison analysis. The values $p < 0.05$ were considered significant.

5.3. GCPQ: RAP *In vivo* pharmacodynamic study in C57BL/6J mice

5.3.1. Disclaimer

The following work was conducted in collaboration with a research group at UCL Institute of Ophthalmology. A sincere appreciation is attributed to Dr Virginia L. Calder and Dr Malihe Eskandarpour.

5.3.2. Introduction

The major retinal diseases associated with vision loss - age-related macular degeneration, diabetic retinopathy, non-infectious posterior uveitis - all involve impaired retinal function due to cell loss or damage [224]. These diseases are difficult to treat, as they are poorly understood. Despite some drugs known to be clinically useful, they do not work in all cases and carry substantial risks [56,118,330,331]. The use of bevacizumab (anti-VEGF mAb) in the wet form of AMD is well established, but only 40-50% of patients respond [330]. This treatment is only successful if the drug is administered as an intravitreal injection to access the back of the eye [331]. While there is an increased risk from this route of administration such as infection and elevated intraocular pressure [56,118], it has also required considerable investment to deliver specialist training to ophthalmic nurses.

Uveitis is a condition that involves inflammation of the uveal tract, i.e., iris, ciliary body, and choroid, or adjacent ocular structures, e.g., retina, optic nerve, vitreous humour, and sclera [67]. Uveitis can be broadly classified as infectious when a prominent infectious agent is recognised, or non-infectious, when it is believed to be

immune-mediated [332]. Uveitis is mainly categorised based on the site of the inflammation. Figure 5-8 shows the anatomical classifications of uveitis that is commonly distinguished as anterior, intermediate, posterior, and panuveitis.

Anterior uveitis is the most common form of intraocular inflammation that mainly affects the anterior chamber of the eye. Intermediate uveitis is the least common form of the disease, and the primary site of inflammation is in the vitreous. Posterior uveitis is the second most common form of uveitis that primarily involves the choroid and the retina of the eye. Panuveitis is a form of uveitis in which the inflammation affects the anterior chamber, vitreous, choroid, and retina [73] (Figure 5-8).

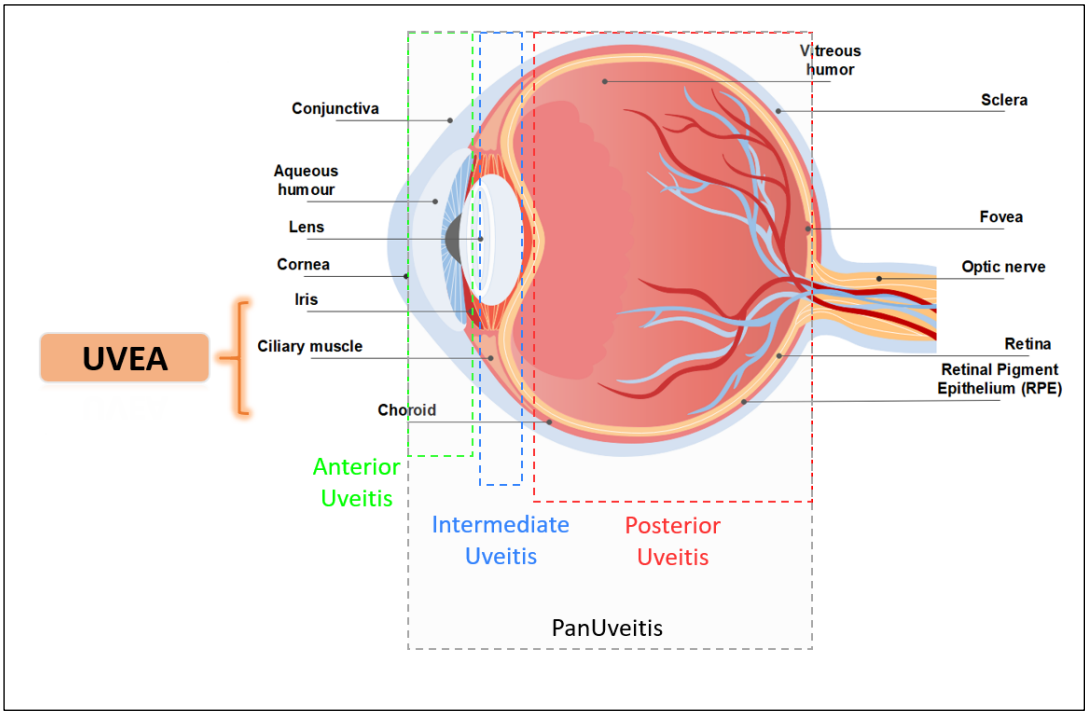

Figure 5-8: Classification of uveitis based on anatomical sites.

Posterior uveitis is an intraocular inflammatory disease that affects the retina and choroid. It is classified as an autoimmune disease because of the involvement of effector $CD4^+$T cells [68]. Some uveitis conditions are associated with specific Human Leukocyte Antigen (HLA) associations and common responses to retinal antigens [69–71].

Further evidence for the role of $CD4^+$T cells has been demonstrated using the experimental autoimmune uveitis (EAU) model in which a localised retinal inflammation is induced by immunisation with retinal peptides [333,334]. $CD4^+$T cells are essential to the immuno-pathogenesis of EAU. There are two subsets of $CD4^+$T cells, Th1 and Th17 cells which are involved in EAU development, and uveitogenic Th1 and Th17 can adoptively induce EAU in naïve mice [335,336]. This well-characterised model, which reproduces particular aspects of the human disease, is used to study disease mechanisms and validate the efficacy of treatments in preclinical studies [335,337]. The hallmarks of EAU are the onset of ocular inflammation, disruption of the retinal architecture, and partial to complete destruction of the photoreceptor cell layer, which leads to visual loss [338]. The retinal disease can be clinically scored throughout the study using advanced retinal imaging as a non-invasive approach.

The first-line treatments for patients with posterior uveitis are mainly limited to systemic immunosuppressive drugs (steroids, CsA) that can have serious side effects when given long-term [339]. Also, it is unclear what levels of these drugs reach the posterior chamber of the eye. Several studies reporting intraocular injectable devices involve the use of slow-release of implanted steroids (Ozurdex, 700 µg) from

Allergan plc. (Dublin, IE) [340], thus minimising the frequency of treatment. Recently, dexamethasone sodium phosphate salt-PLGA nanoparticles-incorporated divalent zinc ion using a solvent diffusion nanoprecipitation method was injected subconjunctivally to a rat model of EAU and was found to reduce the inflammation significantly [340].

Moreover, based on ongoing research, intravitreal sirolimus (Opsiria) from Santen Pharmaceutical Co., Ltd. (Osaka, JP) was accepted by the FDA for review to treat non-infectious posterior uveitis [341]. However, these approaches arguably only treat one eye per injection and still carry the risks associated with injectables, such as endophthalmitis, retinal and vitreous haemorrhage, and retinal detachment [340]. Thus, the ease of application of eye drops in both eyes without the need for a surgical procedure makes them superior to the intravitreal injection.

As described earlier, RAP is a specific inhibitor of mTOR that has been shown to have potent immunosuppressive activity [342,343]. Recently, RAP has shown a great promise in eye research. In particular, RAP was explored for the prevention of chronic inflammatory diseases such as uveitis [306]. Oral RAP has been reported to be effective in non-infectious posterior uveitis. However, gastrointestinal and dermatological side effects have been observed, which limit its long term use [344]. Uveitis is a predominantly T cell-mediated autoimmune disease [345]. RAP suppresses the cytokine driven T-cell proliferation and inhibits the production, signalling, and activity of many growth factors relevant to uveitis [346].

As shown in the previous section, GCPQ: RAP has been applied topically to rabbits' eyes, and we demonstrated the ability of the formulation to deliver the drug to the

choroid-retina compartments. We detected a high RAP concentration in the choroid-retina tissue of healthy rabbits, and this concentration was above the RAP therapeutic level (7–12 ng/mL).

In this section, EAU is being used as a model of retinal disease. This animal model is used to explore the impact of an aqueous-based lipophilic drug-loaded polymeric nanoparticle GCPQ: RAP intended for a topical ocular delivery to treat inflammatory/autoimmune ocular mouse disease and to investigate the mechanism by which RAP would exert its pharmacological benefits on the EAU model.

5.3.3. Materials

Chemical	Supplier
Interphotoreceptor retinoid-binding protein $(IRBP)_{1-20}$ peptide (GPTHLFQPSLVLDMAKVLLD)	Cambridge Peptides, (Cambridge, UK)
Complete Freund's Adjuvant (CFA)	Sigma-Aldrich (Gillingham, UK)
Pertussis toxin (PTX)	Sigma-Aldrich (Gillingham, UK)
Mycobacterium tuberculosis	Difco Voigt Global Distribution (Kansas, USA).
RORγt- R-phycoerythrin (PE)	BD Biosciences (Oxford, UK)
Fluorescein isothiocyanate (FITC)	BD Biosciences (Oxford, UK)
CD4-Brilliant Ultraviolet 395 nm	BD Biosciences (Oxford, UK)
Interleukin-17 (IL-17) -Brilliant Violet 421 nm and -PE	BioLegend (London, UK)
Forkhead box protein P3 (FOXP3)-FITC	BioLegend (London, UK)
T-box gene expressed in T cells (T-bet) -allophycocyanin and -Alexa Fluor 642 nm	BioLegend (London, UK)
CD25-Brilliant Violet 421 nm	BioLegend (London, UK)
IL-10-PE and FITC	BioLegend (London, UK)

5.3.4. Animals

Female, 6-8-week-old C57BL/6J mice (n=20) weighing between 18.0 - 20.0 g were used for the pharmacodynamics study. Animals were obtained from Charles River (Harlow, UK) and were acclimatised for at least seven days before the experiment. All animals had free access to water and food for the duration of the experiment. Treatment of animals conformed to the Association for Research in Vision and Ophthalmology statement for the use of animals in ophthalmic and vision research [347]. All animal studies were ethically reviewed, and experiments performed in accordance with the Animals (Scientific Procedures) Act 1986 and under a Home Office project licence.

5.3.5. Methods

5.3.5.1. Experimental autoimmune uveitis

Experimental autoimmune uveitis was induced as previously described [335]. Briefly, six- to eight-week-old female C57BL/6J mice (n = 20) were immunised with a subcutaneous injection (200 µL) of $IRBP_{1-20}$ peptide in PBS (300 µg/100 µL) emulsified with CFA and supplemented with *Mycobacterium tuberculosis* (1.5 mg/mL,100 µL). Mice also received an intraperitoneal injection of pertussis toxin (0.4 µg/100 µL). Mice were left to develop the EAU for 13 days (Figure 5-9).

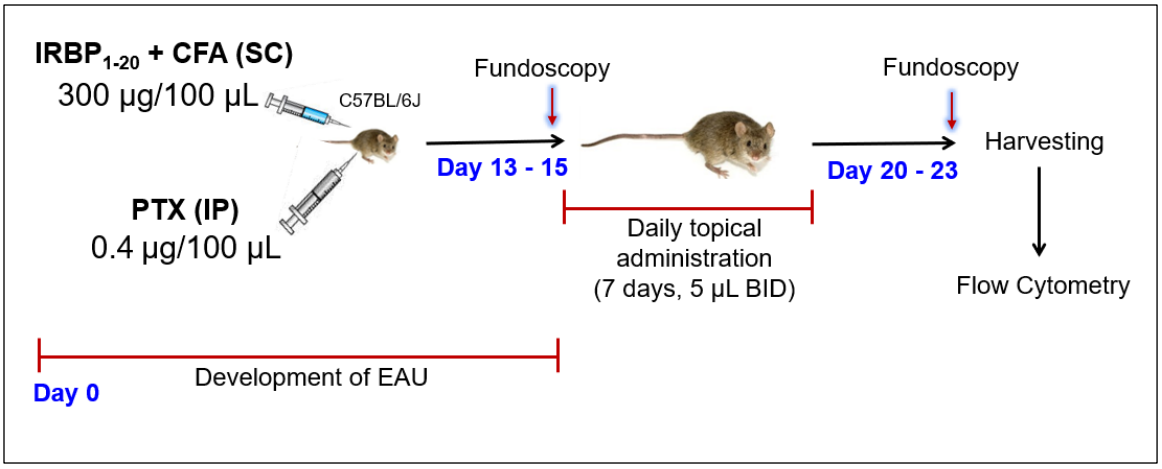

Figure 5-9: Design of the induction of Experimental Autoimmune Uveitis and treatments.

5.3.5.2. Distribution of animals

Animals were housed under specific pathogen-free conditions. Upon arrival, all mice (n = 20) were housed in individually vented cages in a group of five animals in four separate cages (Table 5-10). The untreated control group received topical normal saline (pH = 7.4) as a negative control. Normal saline has been shown not to affect the progression of EAU [335]. The GCPQ polymer (0.75% w/v dispersed in 2.6% w/v glycerol in water, pH = 7.4) was topically applied as vehicle control. The clear solution formulation GCPQ: RAP (0.2% w/v, pH ~ 7.0-7.4) was topically applied as the treatment group. A commercial preparation of dexamethasone suspension Maxidex 0.1% w/v from Alcon (Camberley, UK) was applied topically as a positive control. Maxidex has been shown to reduce the retinal inflammation in EAU [335]. All animals received treatment twice a day (5 µL) for seven days after signs of EAU was observed using fundoscopy on day 13 post immunisation.

Table 5-10: Distribution of animals and treatments groups in EAU experiment.

Mice groups	Number of animals per group	Group name	Treatment	Dose
Group 1	5	Negative control	Normal Saline	(5 uL), twice a day for seven days
Group 2	5	Vehicle control	GCPQ polymer (0.75% w/v) dispersed in (2.6% w/v) glycerol in water	
Group 3	5	Treatment group	GCPQ: RAP (0.2% w/v)	
Group 4	5	Positive control	Maxidex (0.1% w/v)	

5.3.5.3. EAU clinical scoring

Mice were assessed for early signs of EAU by fundoscopic observation using a Micron III fundus camera, Phoenix Research Labs (Pleasanton, USA). Micron III can produce precision *in vivo* imaging of mice retinae with excellent quality bright-field images. It has video-rate frame image acquisition capabilities and relatively high signal to noise ratio. Its unique contact objective lens affords a large field of view and excellent lateral resolution with easy operation [348].

Images were assessed by two blinded (unaware of which animals belonged to which groups) experienced independent observers and scored according to the criteria in Table 5-11 before and after treatment at days 13, and 20 post immunisation, respectively.

Table 5-11: The scoring system of Experimental Autoimmune Uveitis.

Criteria / Score	Optic Disc	Retinal Vessels	Retinal Tissue Infiltrate	Structural Damage
1	Minimal inflammation	1-4 mild cuffings	1-4 small lesions or 1 linear lesion	Retinal lesions or retinal atrophy involving ¼ to ¾ retina area
2	Mild inflammation	>4 mild cuffings or 1-3 moderate cuffings	5-10 small lesions or 2-3 linear lesions	Pan retinal atrophy with multiple small lesions (scars) or <3 linear lesions (scars)
3	Moderate inflammation	> 3 moderate cuffings	>10 small lesions or >3 linear lesions	Pan retinal atrophy with >3 linear lesions or confluent lesions (scars)
4	Severe inflammation	> 1 severe cuffings	Linear lesion confluent	Retinal detachment with folding
5	Not visible (white out or extreme detachment	Not visible (white out or extreme detachment	Not visible (white out or extreme detachment	Not visible

5.3.5.4. Retinal immunophenotyping by flow cytometry

Immunophenotyping describes a process used to identify cells based on the types of antigens or markers on the surface of cells [349]. These markers are usually functional membrane and intracellular proteins and, by the use of specific antibodies, cells can be identified by detecting particular antigens expressed by these cells [350]. Flow cytometry technique allows for the analysis of multiple individual cell parameters from heterogeneous population [351]. In flow cytometry, cells are passed through a narrow channel one at a time. Then, light is used to illuminate the cells in the channel, and by utilising a serious of sensors, the types of light that are refracted or emitted from the cells are detected. The forward scattered light is detected by a sensor in the light path and is typically used to identify particle size. In contrast, side scattered light is usually used to determine the granularity and complexity of the cell in the light path [352]. Fluorescence-activated cell sorting (FACS) analysis provides additional flow cytometer functionality that allows for sorting a heterogeneous mixture of cells into different populations by using specific antibodies tagged with fluorescent dyes [352].

Anti-mouse antibodies were used for retinal cell flow cytometry. Briefly, retinal layers from enucleated eyes were collected at day 20 post immunisation, minced, and filtered to remove any debris and then resuspended in FACS buffer (eBioscience, Hatfield, UK) for cell surface marker staining. Retinal cells isolated for flow cytometry were collected to study the effect of treatments on disease progression and to determine the level of the expression of $CD4^+$, $CD25^+$, and FOXP3. The level of intracellular expression of RORγt/IL-17 was determined to detect the percentage of T-helper 17 (Th17) cells in the sample. The level of expression of T-bet was determined to detect the percentage of T-helper 1 (Th1), and the level of expression IL-10 as a regulatory cytokine in $foxp3^+$ Treg cells was also detected.

Flow cytometry data were acquired using an LSRFortessa, BD Biosciences (San Jose, USA) and BD FACSDiva version 6.1.3 software. Statistical data analysis was performed with GraphPad Prism v.8.0.1, GraphPad Software (San Diego, USA). Differences between groups were determined by one-way ANOVA with a Kruskal-Wallis test. The values $p < 0.05$ were considered significant.

5.3.6. Results and discussion

5.3.6.1. EAU clinical scoring

The clinical scorings of EAU experiments are shown in (Figure 5-10). Fundoscopy images using Micron III were assessed by two independent observers and scored according to the criteria in (Table 5-11) before and after treatment at days 13, and 20 post immunisation, respectively.

Figure 5-10, A shows the clinical scoring at day 13 before starting the treatment. All animals in all groups have shown early signs of the development of EAU. The average score of the negative control groups were (2.90 ± 0.88, and 3.80 ± 0.79), for the saline and GCPQ group before treatment, respectively. The average score of the positive control group DEX was (4.00 ± 0.94), while the treatment group GCPQ: RAP scored at (3.50 ± 0.94). There were no statistically significant differences ($p > 0.05$) among all groups at day 13 before starting the treatment.

The clinical scoring at the end of treatment (day 20, 7 days of treatment) are shown in (Figure 5-10, B). The average scores of the negative control groups were (10.70 ± 4.88, and 13.60 ± 3.81) for the saline and GCPQ group after treatment, respectively. There were no statistically significant differences ($p > 0.05$) among the negative control groups at day 20 at the end of the treatment; suggesting a severe progression of the EAU, and no effect of the negative control groups on suppressing EAU development. The treatment group GCPQ: RAP showed a statistically significant difference ($p < 0.05$) compared to negative control groups. The average score of all animals in the formulation GCPQ: RAP group at the end of the treatment

was (4.80 ± 2.30). Also, the positive control group DEX scored (6.50 ± 1.90) on day 20. Despite a lower scoring of the formulation GCPQ: RAP to DEX, there were no statistically significant differences ($p > 0.05$) between the formulation GCPQ: RAP group and the positive control groups at day 20 at the end of the treatment. These results suggest that GCPQ: RAP formulation was able to suppress EAU progression, and it was as effective as marketed eye drops Maxidex®.

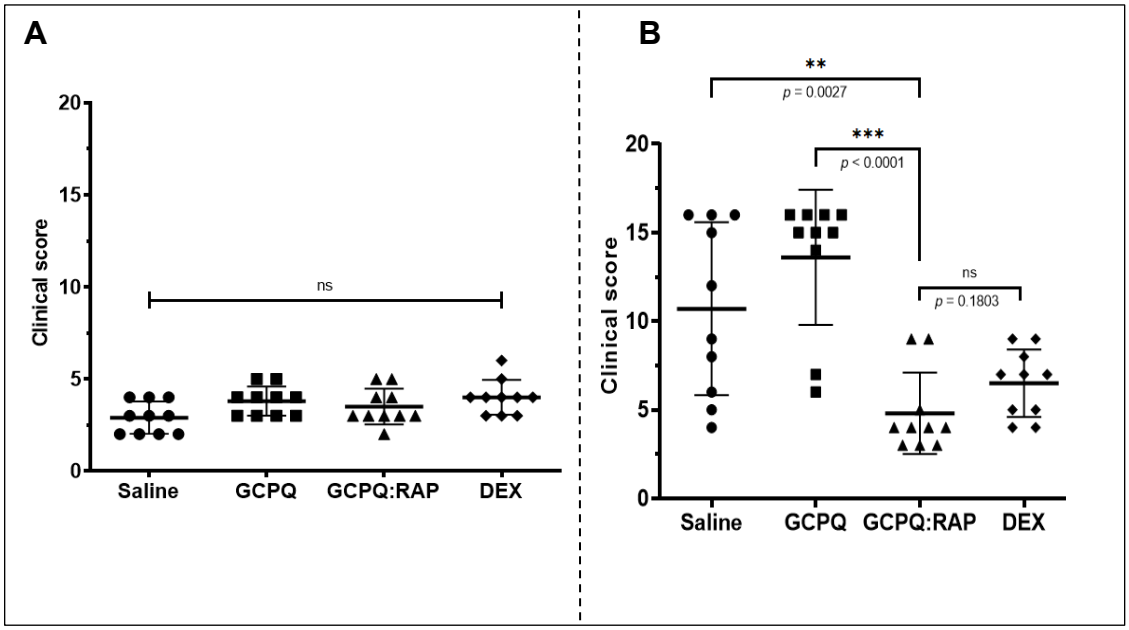

Figure 5-10: Clinical scoring of EAU experiment**.**

(A) at day 13, before-, **(B)** at day 20, after treatment.

Figure 5-11, A showed a direct comparison of clinical scoring within the groups' pre- and post-treatment, at day 13 and day 20, respectively. There were statistically significant differences ($p < 0.05$, two-way ANOVA) within the saline and the GCPQ groups before and after treatment. The treated mice with GCPQ: RAP group showed no statistically significant differences ($p > 0.05$, two-way ANOVA) before and after treatment. Similarly, the positive control group DEX showed no statistically significant differences ($p > 0.05$, two-way ANOVA).

Figure 5-11, B showed the specific criteria in which the clinical scoring has been evaluated at the end of the experiment. In particular, the negative control groups scored highly in all four criteria mentioned in (Table 5-11). As clearly shown, there was a lower score for structural damage in the GCPQ: RAP and DEX groups compared to the negative control groups. Moreover, the GCPQ: RAP group showed a marginal reduction in retinal vessel cuffing, suggested by the lower clinical scoring compared to all groups.

Nevertheless, the percentage differences in clinical scoring before and after treatment are shown in (Figure 5-11, C). The saline group showed an overall percentage increases in clinical scoring by (72.09%). Similarly, the GCPQ group showed a percentage increase (72.06%). In contrast, the formulation GCPQ: RAP group showed a slight percentage difference increase by (27.08%), while the positive control group clinical scoring increased by (38.46%). We can notice a lower percentage difference increase in clinical scoring in the treatment groups than negative control groups. These results demonstrated the efficiency of the GCPQ: RAP as a formulation in controlling the EAU progression.

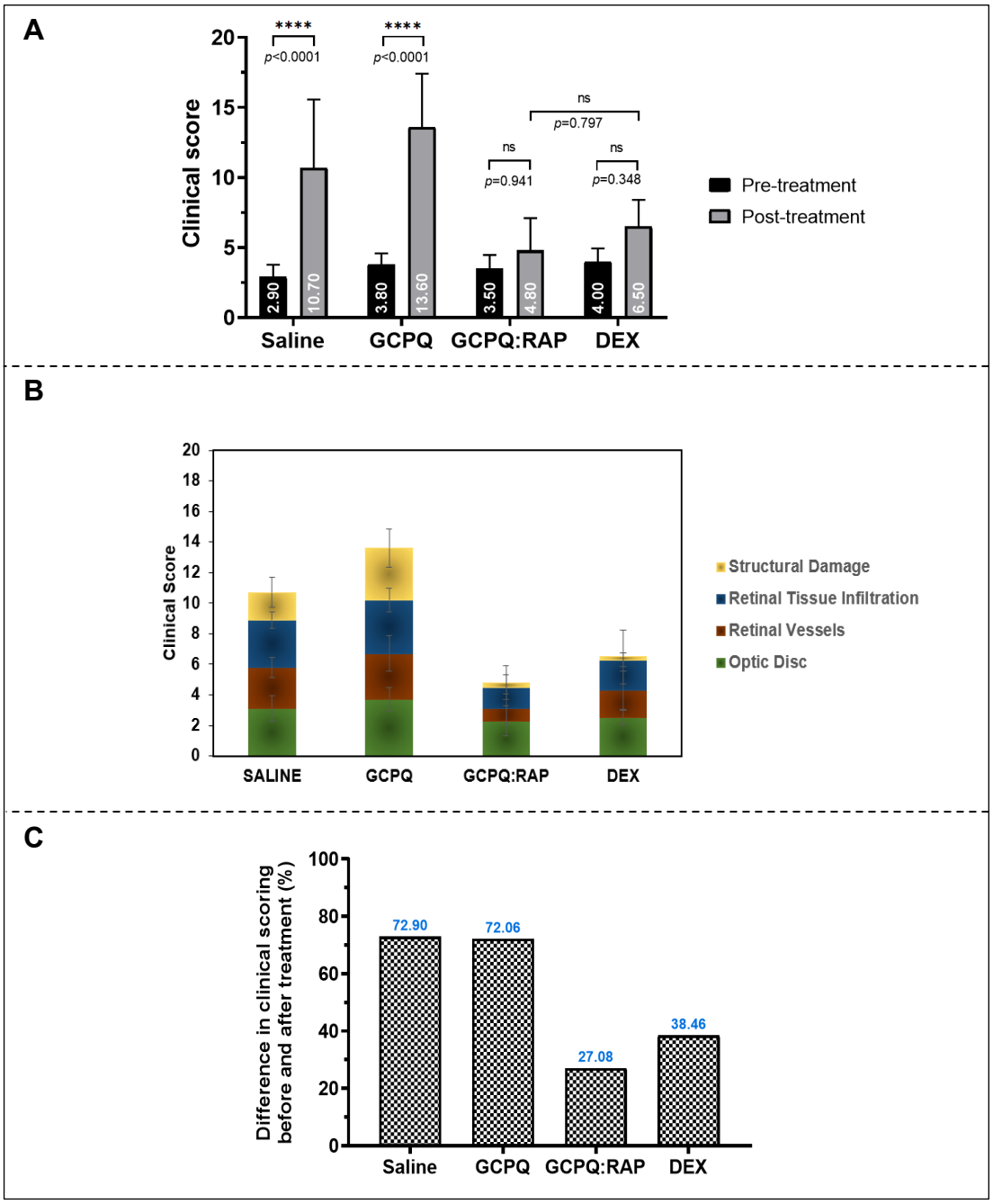

Figure 5-11: Comparison of clinical scoring of EAU experiment**.**

(A) numeric value before and after treatment, **(B)** specific criteria at the endpoint, **(C)** percentage differences before and after treatment,
A: Two-way ANOVA with Tukey's multiple comparison analysis. The values $p < 0.05$ were considered significant.

Figure 5-12 gives the individual animal data in all groups in both eyes before and after treatment. These are essential data as they allow us to document the variability in each treatment group and further understand the pharmacological effects observed in the EAU model.

Animals treated with saline showed a wide distribution of clinical scoring after treatment. In the saline group, three out of five animals (6 eyes), showed a high clinical scoring (>10). While, in the GCPQ group, four out of five animals (8 eyes), showed a high clinical scoring (>15). Only one animal (2 eyes) in the GCPQ group did not develop severe EAU. This is maybe due to technical error in dosing the animal to establish EAU. Generally, clinical scoring of more than ten was reported as severe EAU [335].

However, in the formulation group GCPQ: RAP, four out of five animals (8 eyes), showed a low clinical scoring (< 5). Also, only one animal showed a moderate increase in clinical scoring. Despite this increase, the clinical scoring remains below the level defined as severe EAU (< 10). Figure 5-12, A showed statistically significant differences ($p < 0.05$, two-way ANOVA) between the formulation GCPQ: RAP group to negative control groups at the end of the treatment.

In the positive control group DEX, we can notice a slight increase in clinical scoring. However, these values remain lower than the negative control groups (<10). Figure 5-12, A showed no statistically significant difference ($p > 0.05$, two-way ANOVA) between the formulation GCPQ: RAP group to the positive control group at the end of the treatment.

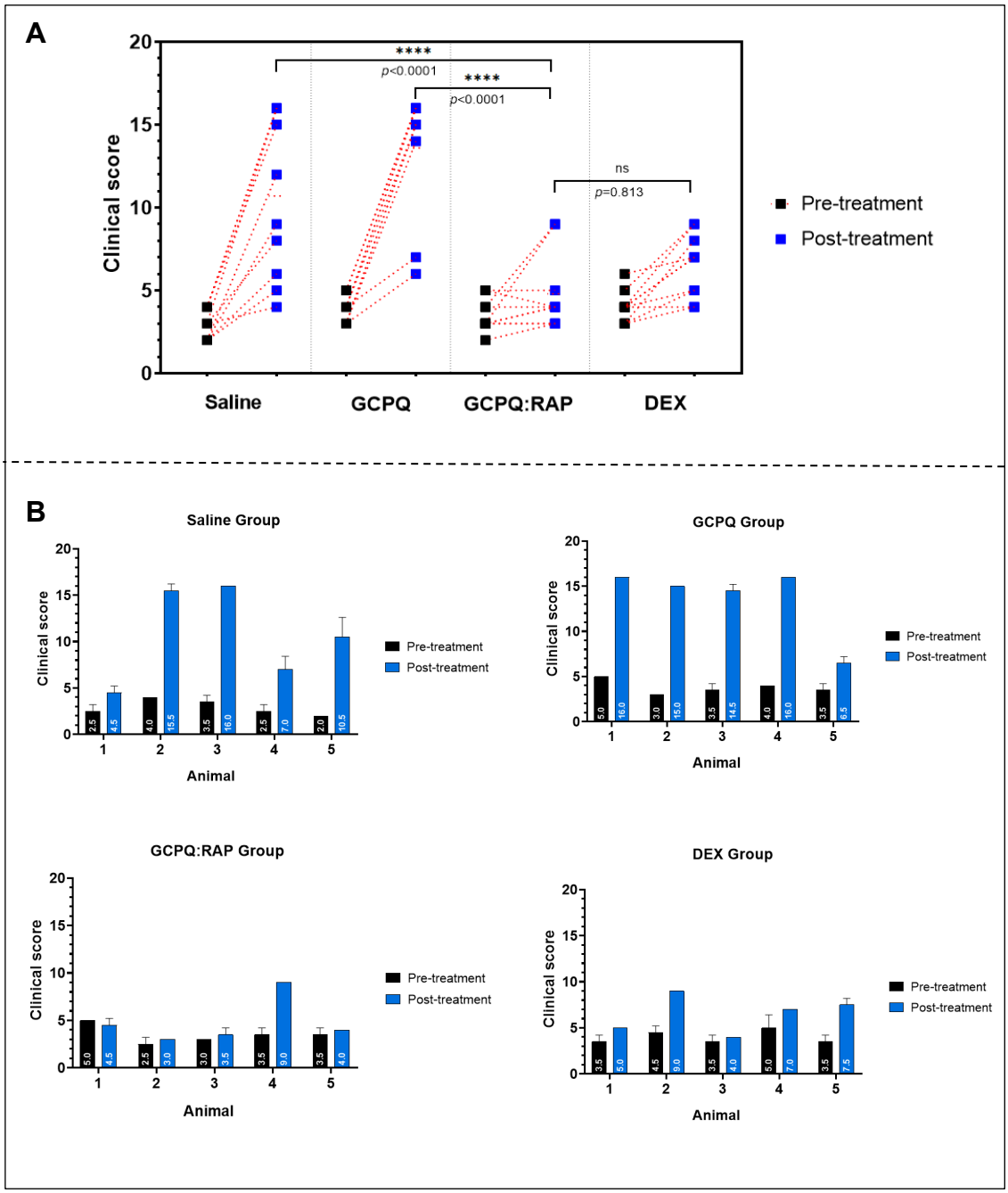

Figure 5-12: Individual animal data of EAU.

(A) right and left eye before and after treatment. **(B)** Individual groups average animal data before and after treatment; data were expressed as mean (two eyes) ± SD.

A: Two-way ANOVA with Tukey's multiple comparison analysis. The values $p < 0.05$ were considered significant.

Figure 5-13 shows the fundoscopy data from the EAU experiment, as imaged with Micron III. Before the treatment, both groups (GCPQ, and GCPQ: RAP) showing clear evidence of disease with inflammation around the optic nerve (Figure 5-13, A-B), respectively. The representative fundus images from an IRBP-immunised mouse treated with GCPQ control showing a severe EAU on day 20 (Figure 5-13, C), while a substantial attenuation of clinical disease following topical treatment of GCPQ: RAP formulation was observed at the end of the experiment, on day 20 (Figure 5-13, D).

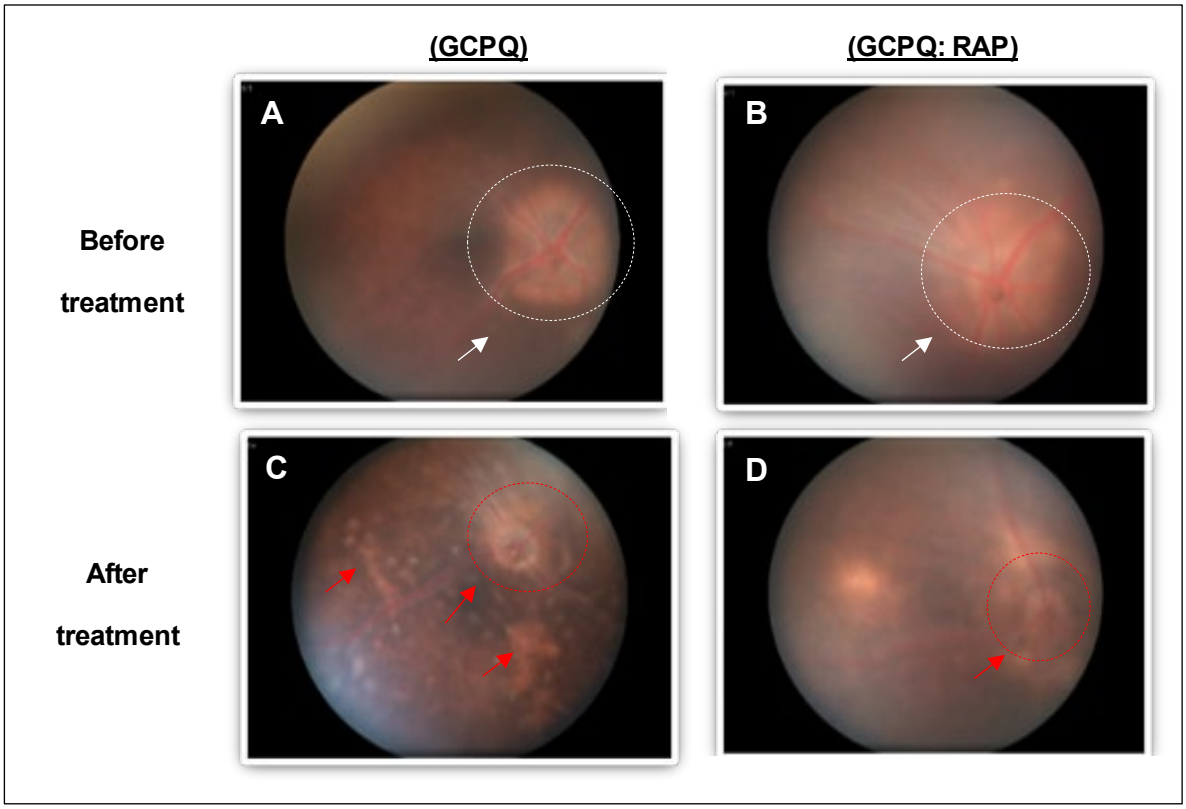

Figure 5-13: Fundoscopy images of EAU.

Fundus images from an IRBP-immunised mouse show EAU development before treatment in **(A)** GCPQ control groups, **(B)** GCPQ: RAP formulation group. Fundus images after treatment showing severe EAU in **(C)** GCPQ control groups. **(D)** GCPQ: RAP formulation after treatment group showing no signs for progression of EAU.

5.3.6.2. Retinal immunophenotyping by flow cytometry

Immunophenotyping of retinal cells isolated from enucleated eyes after treatments using flow cytometry are presented in this section.

Flow cytometry performed on the dissected retina from EAU eyes identified the presence of CD4-expressing cells (Figure 5-14). Both subsets of $CD4^+$ T cells, Th1 and Th17, have been detected in human uveitis and mediate the disease in EAU [335]. Treating EAU with topical administration of DEX showed a reduction in the level of the expression of $CD4^+$ compared to the control samples ($p < 0.05$). Despite a marginal decrease in $CD4^+$ level in the GCPQ: RAP treatment group, flow cytometric analysis found this reduction was not significant as compared to the saline control sample.

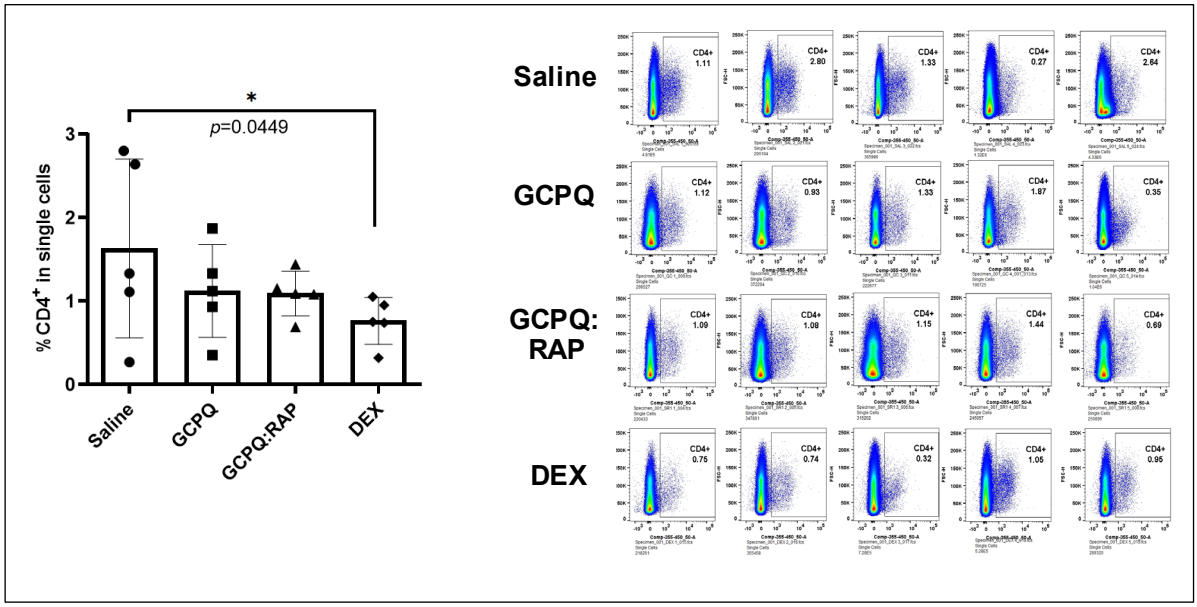

Figure 5-14: Flow cytometer plot of $CD4^+$ T cell.

The level of expression of CD25 is presented in (Figure 5-15). CD25 is the α-chain of the interleukin 2 (IL-2) receptor, and when expressed with α-, β-, γ-chain, the receptor acquires a high affinity for IL-2 [353]. The expression of the IL-2α chain is tightly restricted to peripherally activated T and B cells [353]. Activation of CD25-IL-2 signalling is a sign of T cell activation and proliferation. Our results showed that there were no significant differences in the expression of CD25 between all the groups.

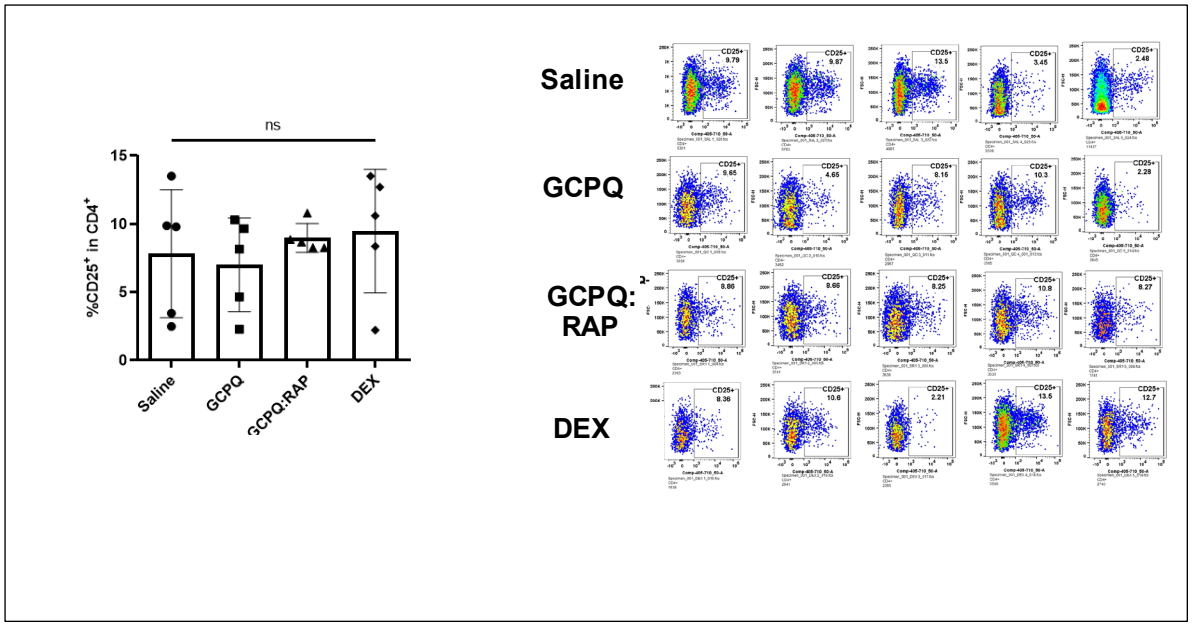

Figure 5-15: Flow cytometer plot of CD25+ T cell.

Flow cytometric analysis showed a statistically significant decrease in total RORγt expression within $CD4^+$ T cells treated with GCPQ: RAP, compared to the negative control ($p = 0.037$) and the positive control ($p = 0.022$, Figure 5-16, A). RORγt is a specifying transcription factor of Th17, which belongs to the RAR-related orphan nuclear receptor family and regulates Th17-associated genes such as IL-17 and Th17 differentiation [354].

The level of the expression of IL-17 is presented in (Figure 5-16, B). There was no statistically significant difference between all groups ($p > 0.05$). Th17 cells play an essential role in the development of autoimmune diseases. The cytokines productions involved in Th17-mediated autoimmune diseases are important contributors to the pathogenic changes observed in EAU [355].

The level of the expression of RORγt in $CD4^+$ T cells of individual animals and its clinical scoring association is illustrated in (Figure 5-16, C). As shown, the GCPQ: RAP treatment group presented with the lowest level of RORγt expression relative to the lowest assessed clinical scoring compared to all groups. The level of RORγt expression in GCPQ: RAP ranged from 13.9 to 26.1%, with a clinical scoring before treatment (2.5 - 5) and after treatment (3 - 9). In contrast, in the saline group, RORγt expression ranged from 22.4 to 42.4%, with a clinical scoring before the treatment (2 - 4) and after treatment (4.5 - 16). These results suggest the specificity of our novel formulation on attenuating the EAU progression by lowering the RORγt expression. It has been reported that RAP has been shown to have an inhibitory potential against acute Th17-polarized airway inflammation [356].

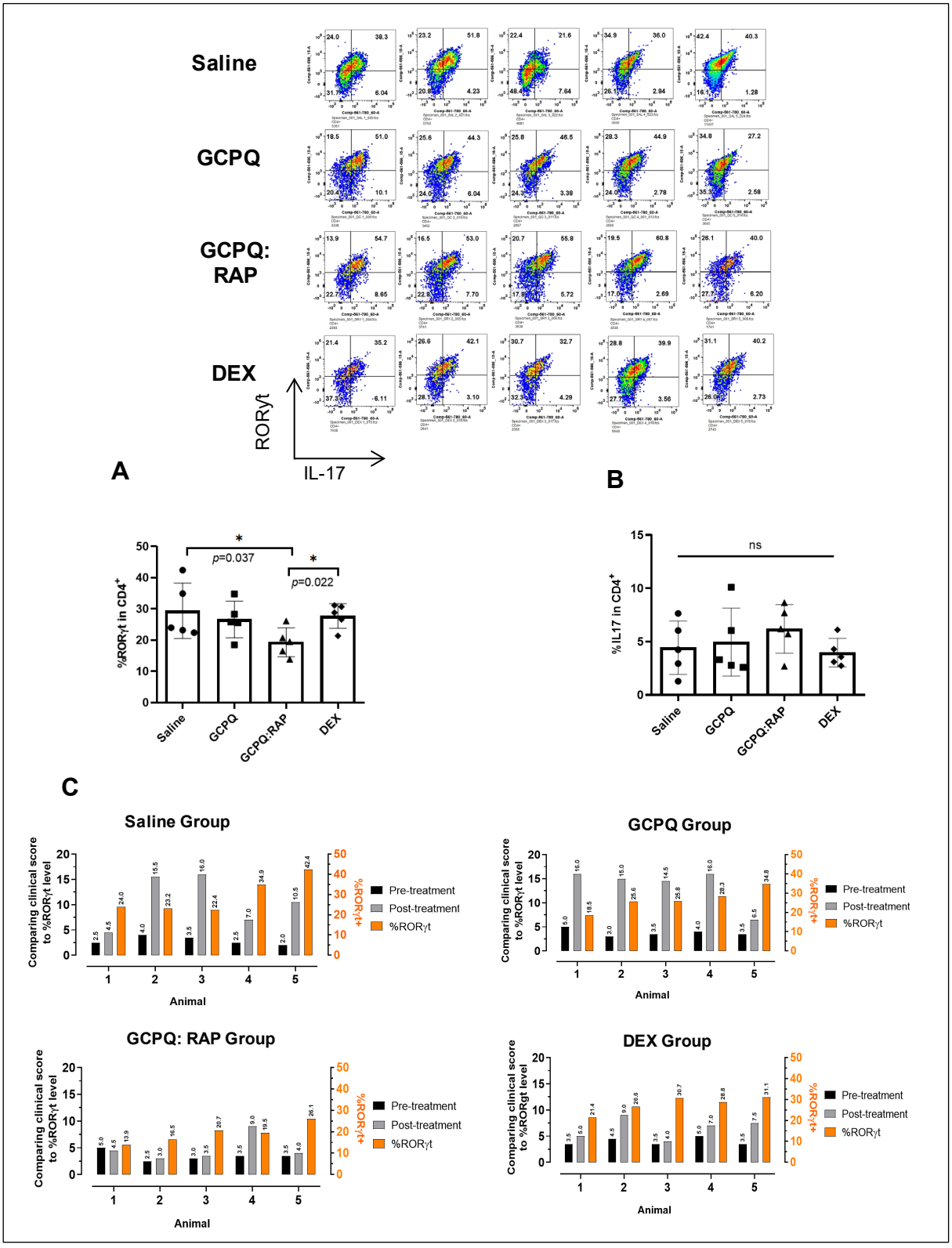

Figure 5-16: Flow cytometer plot of RORγt/IL-17.

Figure 5-17 shows the expression of RORγt and T-bet. The T-box transcription factor is expressed in $CD4^+$ T lymphocytes committed to Th1 T-cell development [357]. We found no significant differences in the level of the expression of RORγt and T-bet for the GCPQ: RAP formulation as compared to other groups. Double positive $ROR\gamma t^+/T\text{-}bet^+$ cells have been reported in EAU [358], but their uveitogenicity remains to be investigated. This could suggest that GCPQ: RAP does not affect Th1/17 or Th1 cells in EAU progression when compared to controls. Unfortunately, we did not obtain reliable data on the IFNγ expression as a cytokine marker for Th1 cells to conclude the impact of GCPQ: RAP on Th1 cells.

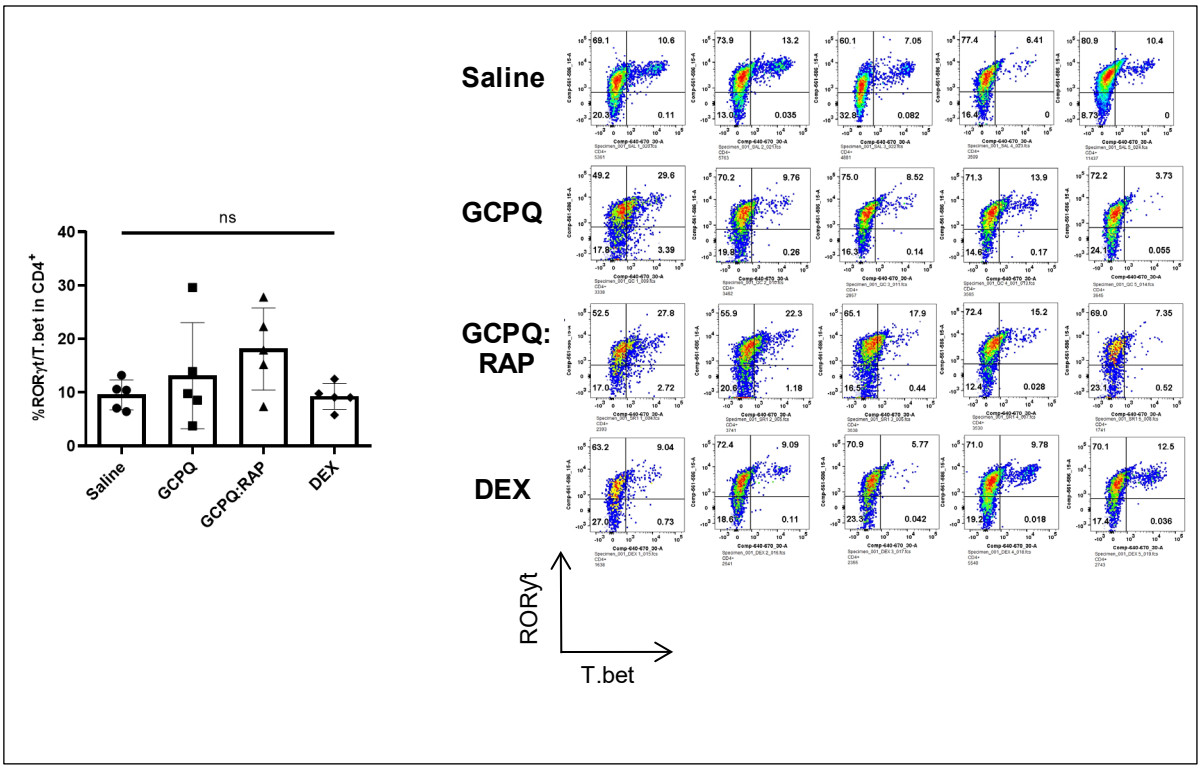

Figure 5-17: Flow cytometer plot of RORγt/T.bet.

The transcription factor forkhead box P3 (FoxP3) is an important marker and functional molecule for Treg cells. FoxP3 is considered the most specific marker for Treg within the $CD4^+CD25^+$ T cell population [359], and responsible for the differentiation and function of Treg cells [360].

Figure 5-18, A showed the increased expression of FoxP3 and IL-10 in the GCPQ: RAP group compared to the vehicle control group ($p < 0.05$). The level of expression of FoxP3/IL-10 in individual animals and its clinical scoring association is illustrated in Figure 5-18, B. As shown, the GCPQ: RAP treatment group had the highest level of Foxp3 and IL-10 expression relative to the lowest clinical scoring compared to all groups, suggesting the specificity of our novel formulation on attenuating EAU progression by upregulating Treg cells. Rapamycin has been shown to significantly increase the expression of FoxP3 in induced Treg cells *in vivo* and *in vitro* [360].

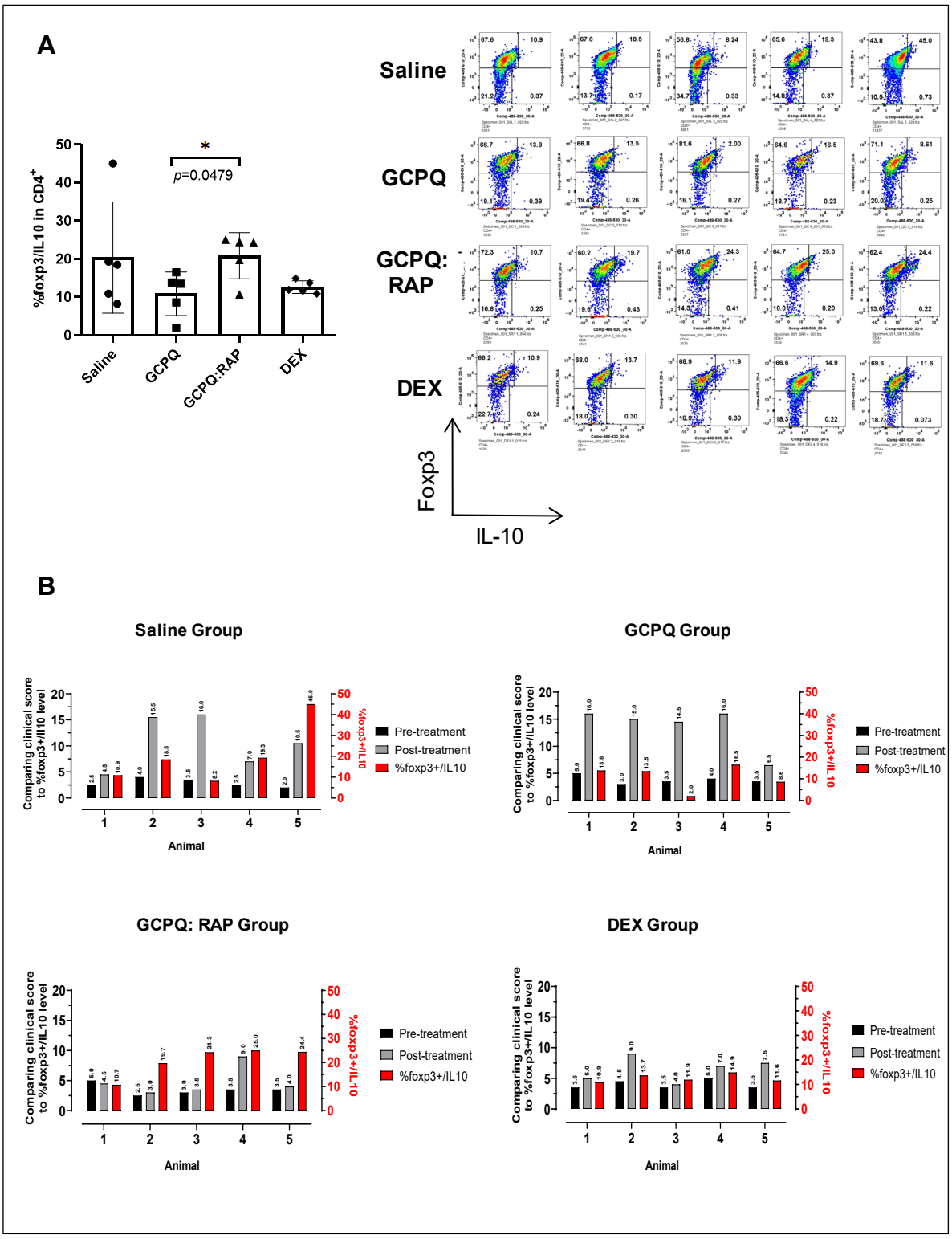

Figure 5-18: Flow cytometer plot FoxP3/IL-10.

Posterior uveitis is a non-infectious, intraocular inflammatory disease affecting the uvea and retina that can impair vision. Most of our understanding of the T cell mechanisms involved have come from studies with experimental autoimmune uveitis. Both subsets of $CD4^+$ T cells, Th1 and Th17, have been detected in human uveitis, and they mediate disease in EAU.

There are two distinct populations of T regulatory cells; natural Treg (nTreg) and induced Treg (iTreg) cells [361]. nTreg cells develop in the thymus and can express FoxP3 cells, which serves as a marker to identify these cells [361]. In contrast, iTreg cells are derived from a population of conventional CD4+ T cells secrete both IL-10-producing Tr1 (type 1 regulatory T) cells and TGF-β-producing $CD4^+$ Th3 (T helper 3) cells [361,362]. While effector T cells promote inflammation, regulatory T cells serve to control it. Therefore, Treg cells play a vital role in autoimmune pathogenesis by maintaining self-tolerance and by controlling expansion and activation of autoreactive $CD4^+$ T effector cells [363]. $CD4^+CD25^+Foxp3^+$ regulatory T cells are the most physiologically relevant due to their broad and indispensable roles [362]. Loss of FoxP3 expression impairs the suppressive activity of Treg cells [362]. Thus, Treg cell dysfunction is considered to be a significant factor in conferring the risk of human autoimmune diseases [364].

In the present study, we explored the impact of GCPQ: RAP novel formulation on delivering the formulation to the back of the eye upon topical eye drops and contains the EAU progression. We have shown that GCPQ: RAP suppressed the expression of RORγt, upregulated Foxp3 expression and IL-10 secretion, and downregulated the disease progression. Battaglia et al. reported that RAP selectively expands the

murine $CD4^+CD25^+FoxP3^+$ Treg cells and suppresses the proliferation of the effector T cells *in vitro* [365,366]. Human $CD4^+CD25^+$ Treg cells are similar to the murine counterpart, are generated in the thymus and are characterised by the ability to suppress proliferation of responder T cells [365]. Therefore, RAP as an mTOR inhibitor can both expand naturally occurring Treg and induced Treg cells from conventional $CD4^+$ T cells [367]. These results suggest that GCPQ: RAP may switch $CD4^+$ T cell polarity from a Th17 to Treg phenotype (Figure 5-19) and thus represents a possible therapeutic point for a wide range of inflammatory and autoimmune disorders, including posterior uveitis.

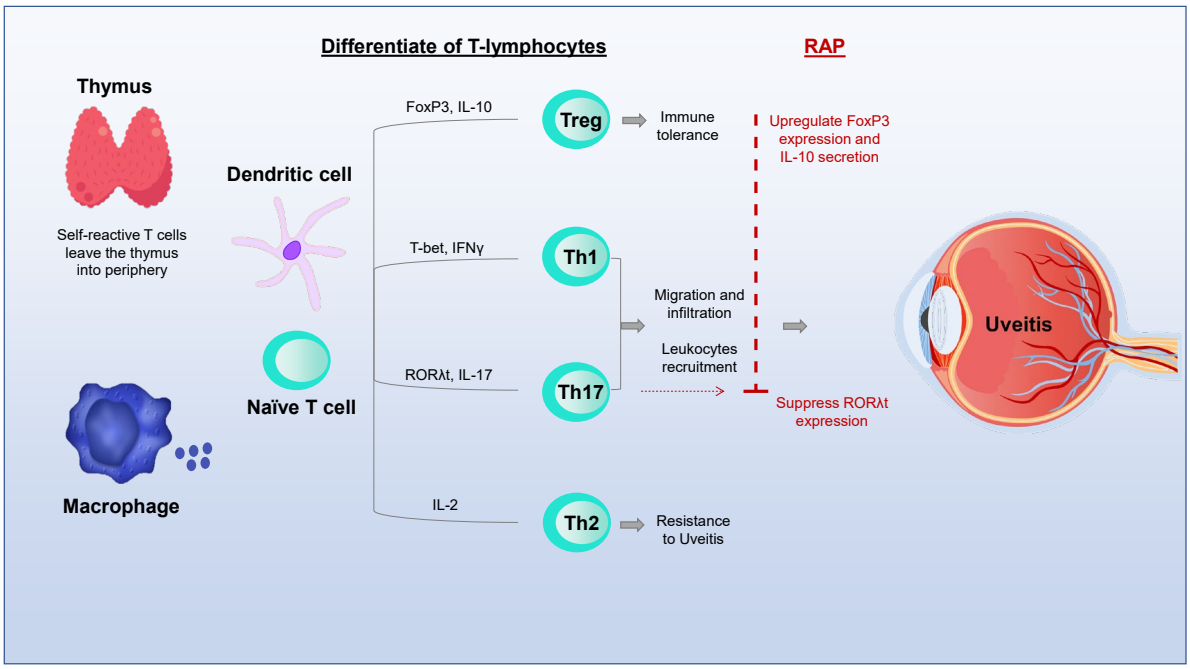

Figure 5-19: Schematic diagram of the development of uveitis and the role of RAP.

Uveitis acute inflammation is initiated by cells previously present in affected tissues, mainly resident macrophages and dendritic cells [368]. In autoimmune uveitis, self-reactive T cells leave the thymus, and when they reach the eye, they come in contact with retinal antigens. Myeloid dendritic cells present a solid ability to capture antigens, which enables them to stimulate T cells. Therefore, T-lymphocytes may differentiate into Tregs, Th1, Th17 or Th2 for precise immune response in function of the antigen encountered and cytokine presence. Th1 and Th17 cells participate in inflammatory and autoimmune uveitis. Th1 cells are crucial for the development of uveitis, whereas Th17 cells play a relevant role in the chronic phase of uveitis. Furthermore, the migration of Th1 and Th 17 to the eye results in the breaking down of the blood-retinal barrier and, consequently, different leukocytes from the circulation are recruited [368]. However, induced Treg cells defeat both Th1 and Th17 cell responses [368].

In the figure, we can also see the role of RAP in uveitis. RAP suppresses the expression of RORγt, upregulates Foxp3 expression and IL-10 secretion, and significantly reduces the disease progression.

Nguyen et al. developed intravitreal RAP (Santen Pharmaceutical Co., Ltd., Osaka, JP) for treating non-infectious uveitis [369]. In the Nguyen study, the 440 µg dose every two months to humans gave the best outcome: 22% of patients reaching the primary endpoint and 52% (includes primary endpoint patients) achieving a secondary endpoint. This is similar to the 220 µg dose to rabbits where RAP choroid-retina levels were maintained at 30 - 2000 ng/ g over the two-months period (remaining over 500 ng/ g for the first 30 days). With the 44 µg dose: 10% of patients achieved the primary endpoint, and 35% (includes primary endpoint patients) achieved the secondary endpoint. This is similar to the 22 µg dose in rabbits where RAP choroid-retina levels were maintained at 0.5 - 600 ng/g over the two-months period (remaining over 30 ng/ g for the first seven days) [306,369]. Our GCPQ: RAP formulation was given at 20 µg/day for seven days to mice of EAU. We have observed a strong attenuation of EAU progression with this dose. In a recent study, RAP has been shown to attenuate the ocular inflammation of EAU after 7.5 µg/day intraperitoneal injections [370]. On the pharmacokinetics study on a larger species, i.e. rabbits, RAP was given at 50 µg/dose (single instillation). The level of RAP on the choroid-retina after one-hour post-dosing was 145 ± 49 ng/g of tissue. This may suggest that a repeated dose of the 0.4% w/v formulation is likely to yield an effect in humans (assuming this gives us a tissue level of at least 300 ng/g). GCPQ: RAP given to C57BL/6J mice with an already established EAU model was found to have no hypersensitivity reaction or toxicity to the corneal tissues and to delay disease progression as shown by fundoscopy imaging. Also, we have observed no effect of GCPQ alone on the suppression of EAU.

5.4. GCPQ: TAC *In vivo* pharmacokinetic study in New Zealand healthy rabbits

5.4.1. Introduction

Allergic conjunctivitis affects 6 – 30% of the general population in Europe, with 25% of cases involving severe and persistent disease [89]. Allergic ocular symptoms affect 40% of the US population at least once in their lifetime, with a prevalence rate of 29.7% [371]. The majority of allergic conjunctivitis patients (55 - 81%) suffer from seasonal allergic conjunctivitis, while the more severe forms of the disease: atopic keratoconjunctivitis (AKC) and vernal keratoconjunctivitis (VKC) affect 4 – 39% of allergic conjunctivitis patients, depending on geographical location; with particularly high numbers of VKC (39% of allergic conjunctivitis patients) and AKC (39% of allergic conjunctivitis patients) in Brazil [89]. VKC affects children, resolves around puberty and is more prevalent in boys with a prevalence of 1.16 – 10.55 per 10,000 of the general population in Western Europe [91] and 18% in Nigerian primary school children [372]. VKC is a sight-threatening disease with no overall gold standard form of therapy [92]. AKC is also a sight-threatening condition which affects adults mostly and is usually present as a co-morbidity with atopic dermatitis [93], with 67.5% of atopic dermatitis patients diagnosed with AKC in one Japanese study [373]. Notwithstanding the rare diseases of AKC and VKC, an estimated 25% of ocular allergy patients have frequent episodes (more than four times a week) for more than four weeks and are classed as having a severe disease which impacts negatively on their quality of life [89]. Patients with severe disease are treated with anti-allergy drugs, and

corticosteroids and treatments are frequently inappropriate [89]. Prolonged steroid use is associated with glaucoma [83] and hence is not ideal, especially with the younger patients.

Tacrolimus acts by binding to FK506 binding protein forming a complex which inhibits calcineurin [374]. This inhibition of calcineurin suppresses dephosphorylation of nuclear factor activated T-cells (NFAT), resulting in suppression of the interleukin 2 gene, interferon gamma and interleukin 4 and interleukin 5; ultimately inhibiting the proliferation of T-cells [375]. Tacrolimus also inhibits the release of histamine from mast cells [376]. These mechanisms contribute to the effectiveness of TAC in allergic conjunctivitis. In a 56 patient randomised controlled trial involving severe allergic conjunctivitis (patients who were not responding to anti-allergy drugs and corticosteroids, n = 28 patients per arm), there was a significant drop in the objective sign score in the treatment arm (Talymus 0.1% twice daily) when compared to the placebo arm after 1 month of treatment, with a significant decrease in the objective signs score observed one week into the treatment course [377]. There were significant changes in the giant papillae and corneal involvement scores with Talymus 0.1% [377]. A visual analogue scale was used to assess seven subjective symptoms, and five of these symptoms (itching, discharge, hyperaemia, lacrimation and foreign body sensation) were also significantly reduced in the treatment arm after 4 weeks of treatment [377]. A subsequent 1436 patient prospective observational study revealed that the total signs and symptoms score reduced significantly from baseline one month after dosing with Talymus 0.1% twice daily and that giant papillae and corneal lesions were also significantly reduced [378]. Both studies reported ocular irritation as

the main side effect with mild ocular irritation affecting 46.2% of patients in the 56 patient study and a transient burning sensation affecting 3.2% of patients in the 1436 patient study [378], although general ocular adverse events affected 6.2% of patients in the 1436 patient study [378]. Other studies have shown that a hospital compounded TAC (TAC injection - Prograf - formulated in a balanced salt solution) containing 0.005% TAC was found to alleviate the signs and symptoms of VKC in a 10-patient study [379]. Additionally, a hospital compounded TAC formulation (TAC capsules – Prograf – formulated in a balanced salt solution) containing 0.01% TAC was found to be effective in reducing the signs and symptoms of VKC in a 62-patient study [380]. There is thus substantial evidence of the efficacy of TAC eye drops in severe allergic conjunctivitis.

Talymus is approved in Japan [381,382]. A cationic emulsion of CsA (Vekacia®, 0.1% w/v), has been granted orphan drug status by the European Commission for the treatment of VKC [83,374]. However, Talymus is reported to provide a therapeutic response in allergic conjunctivitis patients not responding to CsA [378].

In order to overcome the limitations associated with the use of TAC, such as ocular irritation and pain [378] transient blurring of vision due to the opacity of the formulation [92] and plasma exposure [383], we used a known non-irritant, mucoadhesive ocular penetration enhancer (GCPQ) [135,136] to formulate the hydrophobic drug TAC within positively charged nanoparticles, presenting as a clear liquid. This formulation may be useful in the treatment of AKC and VKC. The development of aqueous and clear TAC ophthalmic formulations is challenging due to its hydrophobic characteristics (log *P* = 2.74) [381] and poor water solubility (water solubility = 4 - 12 μg mL^{-1}) [382,383].

Here, we demonstrated the utility of delivering a novel eye drop formulation (GCPQ: TAC, 0.1 % w/v) to the anterior segment of the eye and determine the ocular pharmacokinetic profile of TAC in healthy rabbits.

5.4.2. Materials

Chemical	Supplier
Tacolimus (MW 804.02 g/mol))	Generon Ltd. (Slough, UK)
Ascomycin (MW 792.02 g/mol)	Generon Ltd. (Slough, UK)
Acetonitrile LCMS grade	VWR (Leicestershire, UK)
Water LCMS grade	VWR (Leicestershire, UK)
Formic acid LCMS grade	Fisher Scientific (Loughborough, UK)

5.4.3. Animals

New Zealand white male rabbits weighing between 2.0 – 3.0 kg were obtained from Envigo (Huntingdon, UK) and were acclimatised for at least seven days before the experiment. The rabbits had free access to water and food throughout the study. Treatment of animals conformed to the Association for Research in Vision and Ophthalmology statement for the use of animals in ophthalmic and vision research. All animal studies were ethically reviewed, and experiments performed in accordance with the Animals (Scientific Procedures) Act 1986.

5.4.4. Methods

5.4.4.1. Bioanalytical LC-MS/MS Assay

5.4.4.1.1. Preparation of working standards solutions

Tacrolimus stock solution (STK) was prepared at a concentration of 100 µg/mL in MeOH. Tacrolimus is reported to dissolve in organic solvents, such as DMSO, methanol, and ethanol (> 25 mg/mL) [384]. Tacrolimus working stocks solutions (Stks) were prepared by serially diluting TAC stock solutions into MeOH to obtain Stks in Table 5-12, ranging from a concentration of (0.0167 – 33.4 µg/mL).

Tacrolimus working standards (WS) were prepared by serially diluting TAC working stocks solutions into MeOH to obtain the working standards in Table 5-13 ranging from a concentration of (0.5 – 1000 ng/mL). A stock solution of the ascomycin internal standard was freshly prepared at a concentration of 100 ng/mL in methanol.

Table 5-12: Preparation of TAC stocks solutions.

Stock (STK) is 100 µg/mL (TAC in MeOH)						
Prepare	**Take from**	**µL**	**Add MeOH (µL)**	**Final volume (µL)**	**Conc. (µg/mL)**	**ng/mL**
Stks 10	**STK**	668	1332	2000	33.4	33,400
Stks 9	**Stks 10**	1125	375	1500	25.05	25,050
Stks 8	**Stks 9**	1000	500	1500	16.7	16,700
Stks 7	**Stks 8**	750	750	1500	8.35	8,350
Stks 6	**Stks 7**	600	900	1500	3.34	3,340
Stks 5	**Stks 6**	750	750	1500	1.67	1,670
Stks 4	**Stks 5**	750	750	1500	0.835	835
Stks 3	**Stks 4**	600	900	1500	0.334	334
Stks 2	**Stks 3**	150	1350	1500	0.0334	33
Stks 1	**Stks 2**	750	750	1500	0.0167	17

Table 5-13: Preparation of TAC working standards solutions.

Prepare	TAC stock conc. (µg/mL)	TAC/MeOH (µL)	ASC/MeOH (µL) *	In final volume MeOH (µL)	Final Conc. (ng/mL)
WS10	33.4	50	60	1670	1,000
WS9	25.05	50	60	1670	750
WS8	16.7	50	60	1670	500
WS7	8.35	50	60	1670	250
WS6	3.34	50	60	1670	100
WS5	1.67	50	60	1670	50
WS4	0.835	50	60	1670	25
WS3	0.334	50	60	1670	10
WS2	0.0334	50	60	1670	1
WS1	0.0167	50	60	1670	0.5

* Ascomycin concentration (100 ng/mL) in methanol.

5.4.4.1.2. Preparation of standard and quality control curves:

Working standard solutions were prepared to obtain an individual standard curve for each of the rabbit eye blank tissues: the cornea, conjunctiva, sclera, choroid-retina, aqueous humour, vitreous humour, and whole blood. Tissues were homogenized according to the following protocol. Briefly, the solid frozen tissue was cut into small pieces with scissors and ground to a fine powder with a mortar and pestle placed in dry ice, and the absolute tissue mass was weighed (30 mg). Aqueous samples (aqueous humour, vitreous humour, and whole blood, 30 µL) were transferred into a sterile polypropylene tube, and the absolute mass was weighed. Normal saline was added to a total volume (500 µL), and samples were vortex-mixed for 5 minutes. The mixtures were then homogenized using probe sonication (MSE Soniprep 150 sonicator, MSE UK Ltd., London, UK) at 50% of its maximum output for 25 - 50 seconds in an ice bath. The homogenized samples were spiked with TAC working standards (50 µL) in order to generate the standard curves. Samples were then spiked with the internal standard ascomycin in MeOH (60 µL). MeOH (1060 µL) was added to precipitate the protein, as shown in (Table 5-14).

Table 5-14: Preparation of standard curves solutions of TAC in ocular tissue homogenates.

Prepare	Normal saline (µL) – in tissues	Spike with TAC/MeOH (50 µL) (µg/mL)	Spike with ASC/MeOH (µL) *	In final volume MeOH (µL)	Final Conc. (ng/mL)
WS10	500	33.4	60	1670	1,000
WS9	500	25.05	60	1670	750
WS8	500	16.7	60	1670	500
WS7	500	8.35	60	1670	250
WS6	500	3.34	60	1670	100
WS5	500	1.67	60	1670	50
WS4	500	0.835	60	1670	25
WS3	500	0.334	60	1670	10
WS2	500	0.0334	60	1670	1
WS1	500	0.0167	60	1670	0.5

* Ascomycin concentration (100 ng/mL) in methanol.

The quality control standard curves were generated to evaluate the recovery rate and the matrix effect on drug extraction (Table 5-15). Blank samples were prepared similar to tissue's standard curve. Briefly, TAC working standards samples (50 µL) were added to normal saline (500 µL) to generate the standard curves. Samples were spiked with ascomycin in MeOH (60 µL). Methanol (1060 µL) was added to mimic the extraction protocol.

The mixtures were then vortexed for 5 minutes and centrifuged at (5000 g x 10 min at 4°C) with Hettich Mikro 200R (Tuttlingen, DE). An aliquot (1 mL) of the centrifuged homogenate supernatant was evaporated to dryness within the speed vac at 45°C and spun under vacuum in the evaporator for at least 2 hours. The residues were reconstituted in the LC-MS/MS mobile phase (100 µL) and vortex-mixed for 5 minutes. The samples were centrifuged at (2000 g x 2 min at 4°C) to precipitate any tissues. Following this, samples (80 µL) were transferred to HPLC vials. Ten µL of the reconstituted sample was injected into the LC-MS/MS system.

Table 5-15: Preparation of quality control (blank) standard curves.

Prepare	Normal saline (µL) - blank	TAC stock conc. (µg/mL)	Spike with TAC/MeOH (µL)	Spike with ASC/MeOH (µL) *	In final volume MeOH (µL)	Final conc. (ng/mL)
WS10	500	33.4	50	60	1670	1,000
WS9	500	25.05	50	60	1670	750
WS8	500	16.7	50	60	1670	500
WS7	500	8.35	50	60	1670	250
WS6	500	3.34	50	60	1670	100
WS5	500	1.67	50	60	1670	50
WS4	500	0.835	50	60	1670	25
WS3	500	0.334	50	60	1670	10
WS2	500	0.0334	50	60	1670	1
WS1	500	0.0167	50	60	1670	0.5

* Ascomycin concentration (100 ng/mL) in methanol.

5.4.4.1.3. Chromatography:

Samples were analyzed using an Agilent 6400 Series Triple Quadrupole LC/MS system from Agilent technologies (Berkshire, UK) comprising a degasser (HiP Degasser 1260/G4225A), a binary pump (HiP 1260 binary pump/G1312B), an autosampler (HiP sampler 1260/ G1367E), a column oven (G1316A) and a triple-quadrupole mass spectrometer (G6460A). Agilent MassHunter Workstation Software was used for system control, data acquisition and data processing.

A sensitive LC-MS/MS method was applied to determine the concentration of TAC in the eye tissue homogenates and blank tissue samples. Extraction samples (10 µL) were chromatographed over an XBridge BEH C8 XP column (2.5 µm, 2.1 mm X 50 mm) equipped with a Vanguard Cartridge Holder guard column from Waters Limited (Herts, UK) and at a temperature of 50°C, with the mobile flow rate of 0.5 mL/min. The runtime was 4 minutes, followed by a 1-minute post run time. The mobile phase was formic acid (0.1% v/v) in water and acetonitrile containing (LC-MS grade solvents) in the following gradient conditions (Table 5-16):

Table 5-16: LC condition of TAC and internal standard in LC-MS/MS analysis.

Time (min)	0.1% FA in H_2O	0.1% FA in ACN
	Solvent A (%)	Solvent B (%)
0.00	60	40
0.50	60	40
1.00	0	100
3.00	0	100
4.00	60	40

Tacrolimus and Ascomycin were monitored by positive electrospray ionization on an Agilent jet stream ion source with the LC-MS parameters, as shown in (Table 5-17). Samples were scanned using multiple reaction monitoring mode for transitions of TAC *m/z* [M + Na]+ (826.3 → 415.2), and for ascomycin *m/z* [M + Na]+ (814.2 → 604.1), respectively.

Table 5-17: LC-MS/MS source parameters for TAC and ascomycin.

Parameter	**TAC (Analyte)**	**Ascomycin (Internal standard)**
Capillary voltage (V)	4000	4000
Gas temperature (°C)	300	300
Gas flow (L/min)	9	9
Sheath gas heater (°C)	325	325
Sheath gas flow (L/min)	12	12
Nebuliser (psi)	45	45
Fragmentor (V)	300	300
Collision energy (V)	50	45
Precursor ion (m/z)	826.3	814.2
Product ion (m/z)	415.2	604.1

5.4.4.2. GCPQ: TAC pharmacokinetics animal study:

New Zealand White male rabbits weighing between 2.0 and 3.0 kg, were acclimatized for not less than seven days before the experiments. The rabbits had free access to water and food throughout the study. Twenty-five µL of the GCPQ: TAC 0.1 % w/v formulation was administered to both eyes (Figure 5-20). Briefly, the lower eyelid was gently pulled away from the eye globe and using a calibrated micropipette, 25 µL of the formulation was applied in the lower conjunctival cul-de-sac. After dosing, the upper and lower eyelids were hand-held together for approximately 5 seconds to permit the formulation to come into contact with the cornea. The number of blinks in the next 60 seconds was recorded. Subsequently, after predetermined time points (1, 2, 8 hours, n=4 each), the blood sample was withdrawn (1-3 mL) through the marginal ear vein using a 23-gauge butterfly needle. After blood collection, the rabbit was culled with an IV over-dose injection of 20% w/v phenobarbital (5 mL) through the marginal ear vein using a 25-gauge butterfly needle. The eye globe was enucleated using sterilized scissors, washed twice with 0.9% w/v normal saline and dried on a filter paper. Subsequently, the various tissues were dissected, rinsed twice with 0.9% w/v normal saline and dried on a filter paper. The eye tissues were harvested in the following order to minimize cross-contamination: conjunctiva, aqueous humour, vitreous humour, lens, iris/ciliary body, cornea, choroid-retina, sclera. The harvested dried tissues were immediately stored in ice for (2-5 hours after dissection), and eventually stored at -80°C until further

analysis could be performed. The aqueous humour was withdrawn using a 26-gauge needle attached to 2 mL syringe, while vitreous humour was aspirated using a 23-gauge needle attached to 2 mL syringe. All tissue dissections were performed using sterilized tools. Disposable scalpels, tweezers and scissors were used as necessary. Any other sharp tools were disinfected with 70% ethanol and washed with 0.9% w/v normal saline before moving to the following tissue. All tissues rinsed twice with 0.9% w/v normal saline before they were added to a pre-weighed tube.

For TAC extraction, a volume of the tissue homogenates (500 µL) and aqueous samples were used. Briefly, to extract TAC, the protein precipitation method was used. To all the tissue homogenates, an aliquot of IS (100 ng/mL, 60 µL) was added and vortexed for 5 min. Methanol (1110 µL) was added to precipitate the protein and extract the TAC. The mixture was then vortexed for 5 minutes and centrifuged at (5000 g x 10 min at 4 °C). For each sample, an aliquot (1 mL) of the centrifuged homogenate supernatant was evaporated to dryness within the speed vac at 45 °C and spun under the vacuum evaporator for at least 2 hours. The residue was reconstituted in the LC-MS/MS mobile phase (100 µL) and vortex-mixed for 5 minutes. The reconstituted residue was centrifuged (2000 g x 2 min at 4 °C) to precipitate any tissues. An aliquot of the resulting supernatant (80 µL) was transferred to HPLC vial. Ten µL of the reconstituted sample was injected into the LC-MS/MS system.

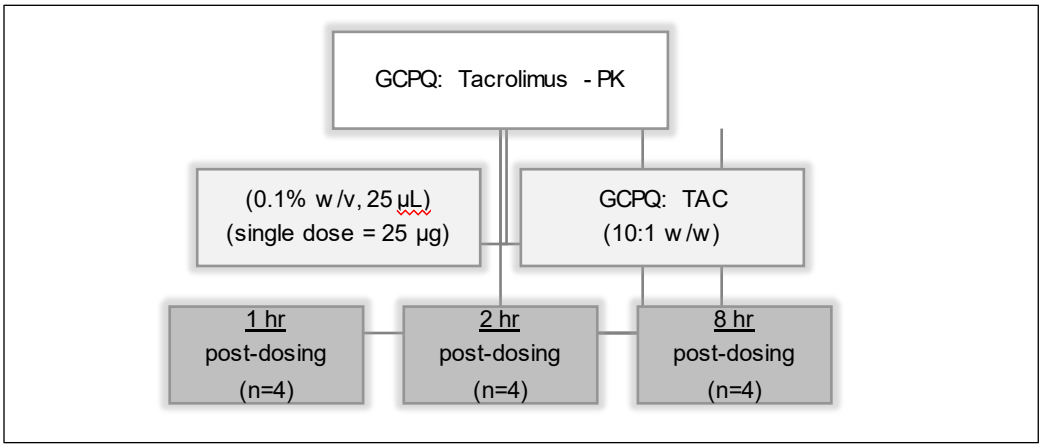

Figure 5-20: Pharmacokinetics *in vivo* study design of GCPQ:TAC (25 µL, 0.1% w/v) formulation.

5.4.5. Results and discussion

5.4.5.1. Preparation of standard and quality control curves:

Working standards solutions were prepared to obtain a standard curve of TAC in the mobile phase and in each of the tissues: cornea, conjunctiva, sclera, choroid-retina, aqueous humour, vitreous humour, and whole blood.

Table 5-18 shows the assay parameters used to analyse the tissues. Individual calibration curves for the blank and each tissue obtained by plotting the peak area ratios (TAC / internal standard) versus the analyte concentration. The calibration curves were linear for TAC in a concentration range (0.5 - 250 ng/mL) when extracted from all tissues, with an r^2 greater than 0.99.

Tacrolimus and ascomycin were efficiently extracted and separated from the blank matrices. The measured LLOQ for TAC was 0.5 ng/mL for the blank and all the tissues with SNR ≥ 10 at the lower limit of quantification.

Accuracy and precisions were calculated as previously described (section 5.2.5.1). The average percentage of the accuracy of all the standards is 101.87%; this is in line with the guideline on bioanalytical method validation in which a range of between 85 and 115% of the nominal value are acceptable [312]. The average CV of all the standards is 13.52%. Our results demonstrate a CV within the acceptable value.

Table 5-18: Assay parameters of TAC in blank and ocular tissues.

Parameters	Equation of the straight line	r2	Linearity (ng/mL)	Accuracy (%)	Precision (%)
Blank	y = 0.4936x + 2.5483	0.9939	0.5 – 250	-	-
Conjunctiva	y = 0.5766x + 0.9188	0.9980	0.5 – 250	114.25	10.65
Aqueous humour	y = 0.4865x + 1.5001	0.9973	0.5 – 250	98.92%	11.88
Vitreous humour	y = 0.4937x + 1.2581	0.9987	0.5 – 250	110.32	26.65
Cornea	y = 0.5369x + 1.528	0.9964	0.5 – 250	105.53	11.86
Choroid-retina	y = 0.4892x + 0.6221	0.9998	0.5 – 250	96.30	14.14
Sclera	y = 0.5126x + 2.1769	0.9942	0.5 – 250	99.33	4.92
Whole blood	y = 0.4389x + 0.8	0.9994	0.5 – 250	88.41	14.52
Average				101.87	13.52
SD				8.81	6.60

5.4.5.2. Bioanalytical LC-MS/MS assay

The LC-MS/MS chromatograms for TAC and ascomycin are presented in (Figure 5-21). Both TAC and ascomycin were ionised under the positive electrospray ionization for analyte quantification.

Multiple reactions monitoring mode was utilized to detect TAC and ascomycin. The precursor ions to product ions transitions of *m/z* [M + Na]+ (826.3 → 415.2) and *m/z* [M + Na]+ (814.2 → 604.1) were chosen for TAC and ascomycin, respectively, based on the most abundant product ions. The assay conditions had an adequate specificity for TAC, while no interfering peaks were observed at its retention time. The retention time was 2.11 and 2.10 minutes for TAC and ascomycin, respectively (Figure 5-21). The MRM transition of TAC is in line with a recently reported study [385]. Ascomycin was used as the internal standard because of its structural similarity to TAC, and it has a similar fragmentation pattern.

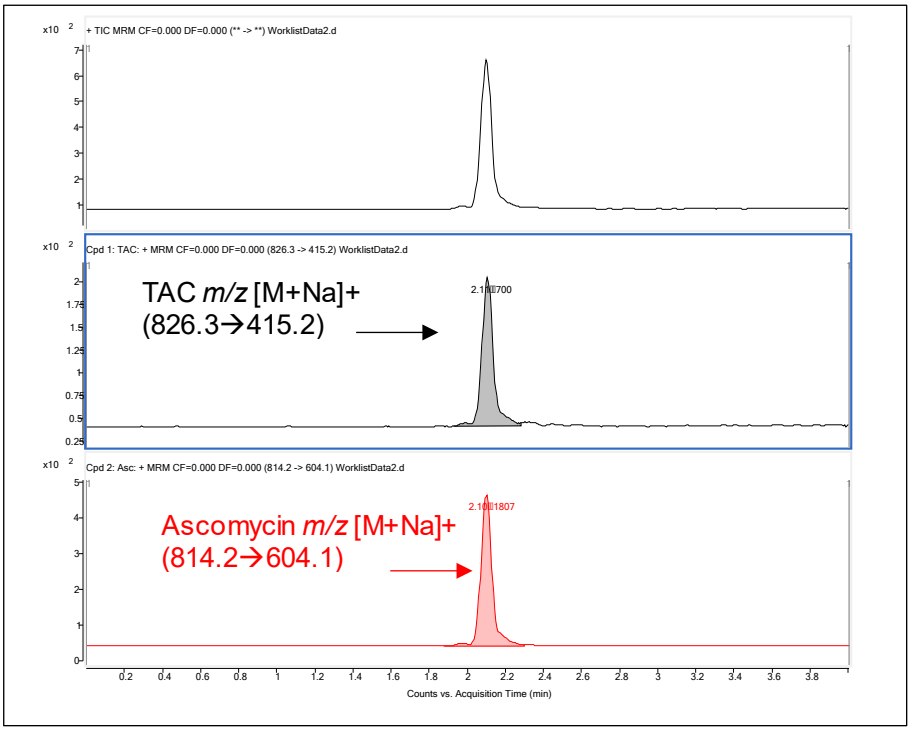

Figure 5-21: LC chromatogram for TAC at 0.5 ng/mL with retention time at 2.11 minutes (top) and ascomycin at 100 ng/mL with retention time at 2.10 minutes (bottom).

5.4.5.3. GCPQ: TAC pharmacokinetics animal study:

We examined the delivery to the front of the eye using GCPQ: TAC (25 µL, 0.1% w/v). The ocular tissue distribution study was conducted in New Zealand White healthy rabbits following topical instillation of the formulation into the conjunctival cul-de-sac.

Topical single instillation of 0.1% w/v GCPQ: TAC resulted in detectable and quantifiable TAC levels in the front of the eye tissues, i.e. cornea (LLOQ = 0.5 ng/mL) and conjunctiva (LLOQ = 0.5 ng/mL) (Figure 5-22). Tacrolimus concentrations were also quantified in the aqueous humour (LLOQ = 0.5 ng/mL). Moreover, TAC was detected in posterior chamber eye tissues; choroid-retina (LLOQ = 0.5 ng/mL) (Figure 5-22). No TAC was discovered in the vitreous humour (LLOQ = 0.5 ng/mL) and the whole blood (LLOQ = 0.5 ng/mL) at all time points.

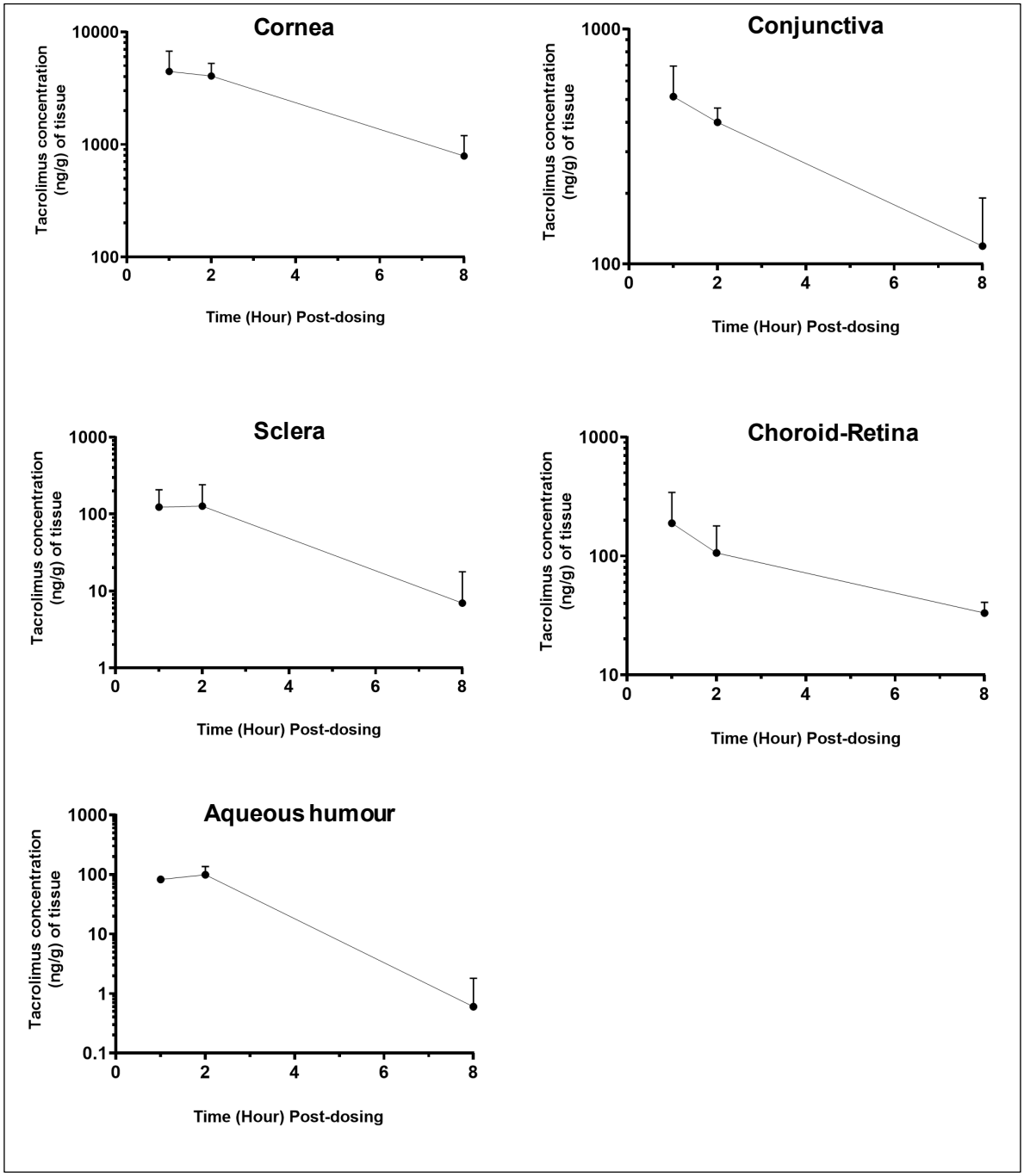

Figure 5-22: *In vivo* TAC drug distribution in rabbit ocular tissues following the instillation of 25 µL of GCPQ: TAC 0.1% w/v.

Figure 5-22 shows the ocular drug distribution of TAC in a healthy rabbit model. The Cmax of TAC in the cornea, conjunctiva and sclera after 1 hour was 4452 ± 2289 ng/g, 516 ± 180 ng/g and 123 ± 84 ng/g of tissue, respectively with a tmax of 1 hour in all tissues except the sclera where the tmax was 2 hours (Table 5-19). These tissue levels were achieved following a single ocular dose of 25 µg TAC in the GCPQ: TAC formulation. A recent study reported TAC levels in pig corneas following multiple instillations of an aqueous formulation (50 µL, 0.07%) [385]. This formulation is based on Marinosolv technology containing glycyrrhizin (2% w/v), escin (0.03% w/v), dexpanthenol (5% w/v), EDTA (0.1% w/v), mannitol (2.7% w/v), iota-carrageenan (0.24% w/v), and propylene glycol (3% w/v) in a buffered solution with TAC added after being dissolved in propylene glycol. The dissolved TAC was then added to the aqueous solution [385]. With two doses per day (70 µg TAC/day), and four doses per day (140 µg TAC/day), samples were collected one hour after the last dose, and the TAC Cmax was reported as ~ 4.0 µg/g of the cornea, irrespective of the dose (tmax = 1 hour) [385]. For comparison, the ocular corneal Cmax of TAC in eyes instilled four times with Talymus, an ophthalmic TAC suspension (50 µL, 0.1% w/v, 200 µg TAC/day), was < 0.5 µg/g (tmax = 1 hour) [385]. In the current work, the GCPQ: TAC (25 µL, 0.1% w/v, 25 µg TAC) formulation resulted in a higher corneal TAC level than that achieved with the higher Talymus dose (25 µg TAC in GCPQ: TAC versus 200 µg TAC in Talymus). Another study reported the Cmax of TAC following a single ocular instillation in rabbits (30 µL, 0.1% w/v, 30 µg TAC/day) of TAC ophthalmic suspension [171] with TAC levels in the cornea of ~ 300 ng/g, TAC levels in the conjunctiva of ~ 100 ng/g,

and TAC levels in the sclera ~ 100 ng/g of tissue after 1 hour, respectively [171]. Once again, the current GCPQ: TAC formulation delivered higher levels to the cornea and conjunctiva even though the TAC doses were similar (25 µg versus 30 µg). The nanoparticle GCPQ: TAC formulation is clearly superior in delivering the drug to the cornea and conjunctiva when compared to suspensions. In a study comparing the drug delivery efficiency in steroid solutions, gels, and suspensions [386], Nourry et al. found that eye drop suspensions delivered less drug when compared to solutions and gels [386]. The suspensions delivered variable levels of drug (23-99%) into each drop of the formulation, compared to solutions and gels, which released about 100% of the content of the drug in each drop [386]. This could explain the higher tissue levels found with solutions and gels when compared to the use of a suspension [171,385]. It must be stated that a straightforward comparison between both formulations was not carried out in these reported studies. These TAC tissue levels from the GCPQ: TAC 0.1% w/v formulation would be sufficient to modify the local immune responses to suppress the inflammatory and dry-eye conditions, to treat other ocular autoimmune diseases and may be used to prevent the corneal transplant rejection [327].

Following the ocular administration of GCPQ: TAC (25 µg), the Cmax of TAC in the aqueous humour was 99 ± 37 ng/mL (tmax = 2 hours), while no drug was detected in the vitreous humour (Figure 5-22, Table 5-19). In a recent study, Abul Kalam et al. reported the level of TAC in the aqueous humour of rabbits eyes after a single instillation of TAC loaded ploy-lactide-co-glycolide (PLGA) nanoparticles in comparison to TAC aqueous suspension (50 µL, 0.03% w/v, 15 µg TAC) [327]. The concentration of TAC in the aqueous humour was 20 ng/mL and 30 ng/mL, form the

TAC-PLGA and TAC aqueous suspension, respectively [327]. When adjusting for dose and assuming linearity, GCPQ: TAC delivers a 2-fold greater level of TAC in the aqueous humour when compared to the use of PLGA nanoparticles or a suspension. The PLGA nanoparticles described by Abul Kalam et al. had a net negative charge [327]. In contrast, our GCPQ: TAC formulation nanoparticles have a permeant positive charge, and this may explain the higher levels of TAC in the aqueous humour obtained with GCPQ: TAC when compared to the PLGA nanoparticle formulation.

TAC from GCPQ: TAC (25 µL, 0.1% w/v, 25 µg TAC) was also delivered to the back of the eye on topical ocular administration with a Cmax of TAC in the choroid-retina of 189 ± 154 ng/g (tmax = 1 hour). On administration of the TAC suspension, the levels of TAC in the choroid-retina were <10 ng/g of tissue after a single instillation of 30 µg TAC from the TAC ophthalmic suspension [171]. Siegl et al. have reported the Cmax level of TAC in the pig choroid was 100 ng/g, or 50 ng/g of tissue (tmax = 1 hour), after two doses per day (70 µg TAC/day) or four doses per day (140 µg TAC/day), respectively of the TAC formulation based on Marinosolv technology [385]. In the same studies, TAC Cmax in the pig retina was 60 ng/g and 90 ng/g of tissue (tmax = 1 hour) after dosing 70 µg TAC/ day or 140 µg TAC/ day, respectively [385]. 25 µg TAC dosed from GCPQ: TAC delivered higher levels of TAC to the choroid-retina when compared to these two formulations. We have shown (section 5.2) that GCPQ delivered RAP to the back of the eye's tissues (choroid-retina) effectively.

We examined the plasma exposure to TAC following ocular dosing. We reasoned that the conjunctival blood capillaries might lead to TAC being detected in the blood. A certain fraction of the drug may reach the systemic circulation via conjunctival

vessels and nasolacrimal duct [108]. Thus, we examined the distribution of TAC in the whole blood of the treated rabbits at all time points. The distribution of TAC between whole blood to plasma is > 20:1; therefore, measurements of TAC are generally undertaken in the blood rather than plasma [387]. TAC was not detected in whole blood (LLOQ 0.5 ng/mL) at all time points. Fujita et al. reported the level of TAC in whole blood following 0.1% TAC suspension eye drops (~1 ng/g of tissue after 1-hour post-dosing) [171]. Although the therapeutic level of TAC is (5 – 10 ng/mL) [388], such a formulation tends to work locally in the eye, and it is not desirable for TAC to be in the systemic circulation, due to the possibility of adverse drug events. The FDA has issued a black box warning about the potential toxicity associated with prolonged use Protopic (TAC 0.1% or 0.03% ointment) for children aged 2 – 15 years [389,390]. These concerns were based on rare cases of skin malignancy and lymphoma, and a theoretical risk from the systemic use of TAC [389]. Our results demonstrated an absence of TAC in the blood, which is preferable in managing allergic ocular diseases.

TAC has a molecular weight of 804.02 daltons [177], and (log *P* = 2.74) [171]. We hypothesise that such a lipophilic drug, when presented to the cornea in molecular form (e.g. when released from GCPQ nanoparticles) may partition into the cornea through the epithelium and be gradually released into the aqueous humour through the stroma and endothelium [171]. It is conceivable that the positively charged nanoparticles would allow an electrostatic interaction with the negatively charged mucin from the ocular surface [108]. Due to the presence of the sialic acid residues from the terminal ends of the mucopolysaccharide chain, the mucin could interact

electrostatically with the cationic GCPQ particles [108]. GCPQ nanoparticles have a permanent positive charge, due to the presence of quaternary ammonium groups on the surface of the nanoparticles [211,391,392]. Thus, we postulated that GCPQ would be electrostatically attached to the negatively charged membrane in particulate form and prolong the corneal and conjunctival retention of TAC, and may lead to slow diffusion of the drug from the cornea to the aqueous humour [37].

The transcorneal absorption route has been considered the main pathway for ophthalmic drugs to gain access to intraocular tissues; however, the noncorneal absorption route across the conjunctiva and sclera also contribute significantly to drug penetration [171,327]. We have shown that GCPQ was able to act as a permeation enhancer for the water-insoluble TAC into ocular tissues and to deliver the drug to the cornea and conjunctiva (target tissues) in a concentration higher than its therapeutic levels (5–10 ng/mL) [388]. These results indicate that GCPQ may be used as a novel carrier for TAC and overcome both the static and dynamic barriers to reach to target ocular tissues. The exact mechanism by which GCPQ delivered TAC to the back of the eye tissues is not clear and further studies to confirm the mechanistic pathway are required.

Table 5-19: Pharmacokinetics parameters of TAC after single ocular instillation of GCPQ: TAC ophthalmic formulation solution in rabbits.

Pharmacokinetic parameters	**Cornea**	**Conjunctiva**	**Sclera**	**Choroid-Retina**	**Aqueous humour**
C_{max} (ng/g tissue)	4452 ± 2289	516 ± 180	123 ± 84	189 ± 154	99 ± 37
T_{max} (hr)	1	1	2	1	2
AUC_{0-8} (ng.hr/g)*	21026	2277	587	660	430

* AUC value is an approximation from three-time points.

5.4.5.4. Ocular tolerability

The blink rate following dosing is an acceptable method of assessing acute ocular irritation, although other parameters such as erythema and swelling are also used to assess ocular irritation [393]. In the first 60 seconds post-dosing after a single instillation of GCPQ: TAC (25 µL, 0.1% w/v), the blink rate was assessed. After topical drop instillation, the upper and lower eyelids were hand-held together for approximately 5 seconds to permit the formulation to come into contact with the cornea, and the blink rate in the next 60 seconds was recorded. Normal saline was used as a control, n = 4. The average blink rate in both eyes in the normal saline group was recorded as 1.0 ± 0.41 blinks/min. Normal saline is frequently utilized as a control solution [327] in assessing the blinks rate in rodents [328] and evaluating the lacrimation characteristics in rabbits [329]. The average blink rate in both eyes in all treatment groups was reported as (7.33 ± 1.32 blinks/min, $p > 0.05$, One way ANOVA) (Figure 5-23).

Toshida et al. reported the blink rate in 3 minutes post-dosing in healthy rabbits receiving a single instillation of 40 µL, 0.1% w/v CsA eye drops [394]. The blink rate of CsA-treated eyes (4.86 ± 0.86 blinks per 3 minutes) was significantly higher than that of vehicle-treated eyes (1.71 ± 0.42 blinks per 3 minutes, $p < 0.05$) [394]. The average spontaneous blink rate of healthy human subjects has been reported to be (17.6 ± 2.4 blinks/min during rest) [328,395], while the average blink rate of healthy rabbits to be three blinks/hr [396]. It is not clear how the presence of the nictitating membrane in rabbits can negligibly or can readily alter drug kinetics since it would

appear to be little more than a moderate extension of the conjunctival surface [396]. In rabbits, the tear flow rate and the total volume of tears are both similar to that in the human [396]. The blink rate data in rabbit treatment groups for the RAP and TAC formulations as compared to human blink rate may suggest that there may be a more considerable contact time for drugs topically applied in the animal [396].

The irritation of the GCPQ: TAC formulation to rabbits' eyes was visually evaluated using the criteria of erythema and swelling (Figure 5-23). There were no visible signs of erythema, tearing or swelling following the ocular administration of GCPQ: TAC (Figure 5-23). These data suggest that GCPQ: TAC as a formulation does not cause dose-limiting ocular irritation to rabbits' eyes, and its use as a patient treatment for AKC and VKC warrants further study.

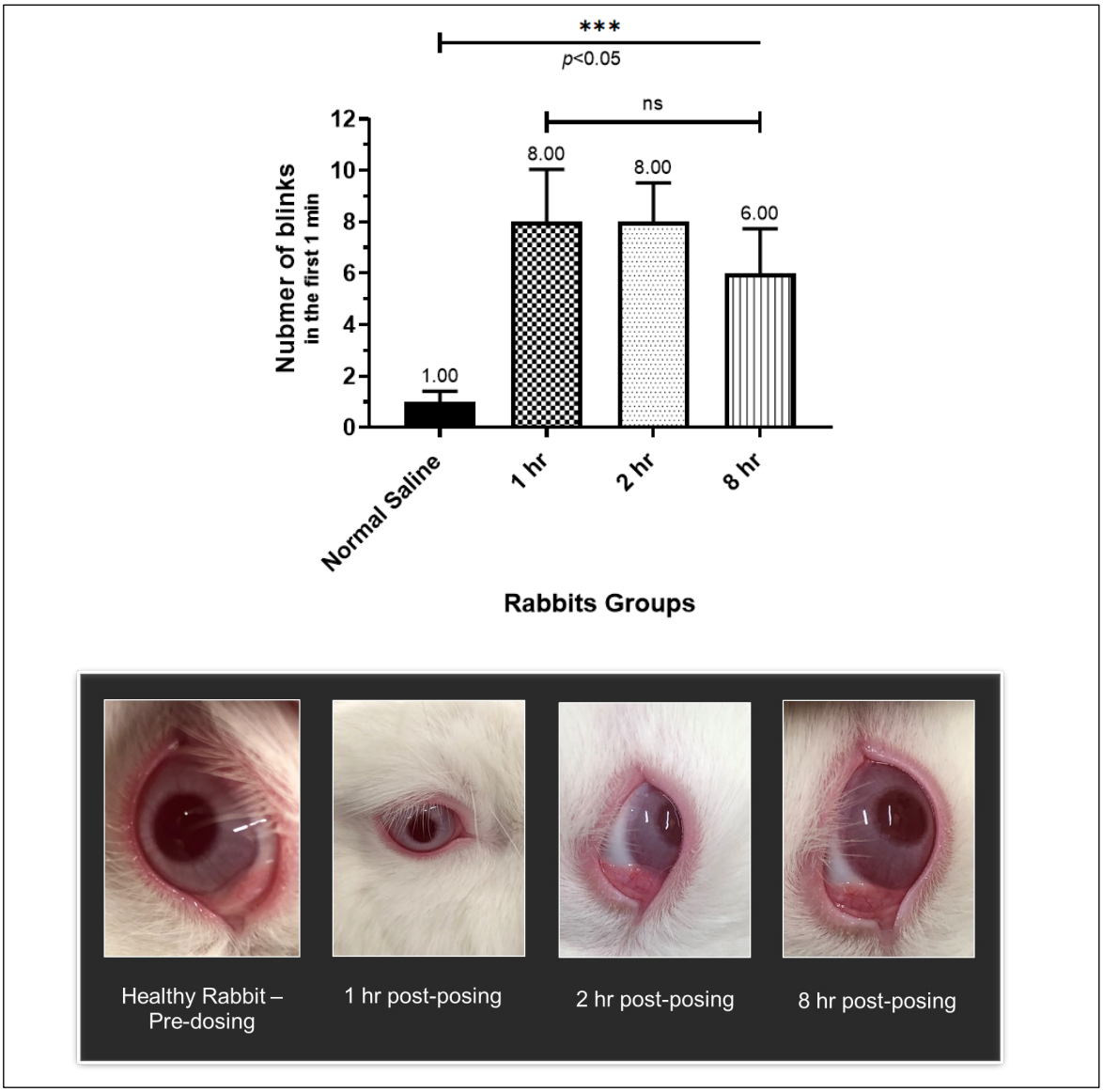

Figure 5-23: Assessment of ocular tolerability of the GCPQ: TAC formulation to rabbits' eyes.

(Top) Number of blinks in rabbits following single instillation of GCPQ: TAC (25 µL, 0.1% w/v); (Bottom) visual assessment of perceptible irritation of the GCPQ: TAC formulation to rabbits' eyes.
Time points: 1, 2, 8 hours post-dosing (n=4 rabbits, each group). The statistical analysis was performed with One-way ANOVA with Tukey's multiple comparison analysis. The values $p < 0.05$ were considered significant.

5.5. Conclusion

The corneal epithelial mucosa possesses an overall negative charge. Thus, the permeability of positively charged nanoparticles such as GCPQ is favoured at physiological pH. In essence, GCPQ is a permeation enhancer supported by detecting a sufficient drug in the ocular tissues and the resultant pharmacodynamics response. From the *in vivo* pharmacokinetic study, GCPQ: RAP showed promise as a formulation to reach the posterior eye tissues following a single topical application. We have shown that GCPQ was able to deliver RAP into the rabbits' ocular tissues, and to deliver the drug to the choroid-retina in a concentration higher than RAP therapeutic levels (7 – 12 ng/mL). Also, GCPQ: RAP 0.2% w/v was successfully utilised to control the progression of the mice model of EAU. We have shown that GCPQ: RAP suppresses the expression of RORγt, upregulates Foxp3 expression and IL-10 secretion, and reduces the disease progression. These results suggest that GCPQ: RAP may switch $CD4^+$ T cell polarity from a Th17 to Treg phenotype and thus represents a possible therapeutic point for a wide range of inflammatory and autoimmune disorders, including posterior uveitis.

With the difficulties of applying topical ointment and suspension forms of TAC, here, we demonstrated the utility of using a 0.1% w/v aqueous-based GCPQ: TAC formulation intended to treat VKC and AKC. From the *in vivo* pharmacokinetic study in healthy New Zealand White rabbits, GCPQ sufficiently delivered TAC to the cornea and conjunctiva (the target tissues) with a TAC concentration higher than the therapeutic level following a single topical application.

6. Conclusion and future work

6.1. Conclusion

GCPQ is a glycol chitosan-based polymer that has a permanent positive charge in the form of a quaternary ammonium group. GCPQ may provide mucoadhesive characteristics with negatively charged sialic acid residues of mucin in the eye surface, thus, promoting the ocular drug absorption possibly through intimate contact with the corneal surface and slowly diffuse the cargo into ocular tissues. We have further confirmed that GCPQ is an ocular penetration enhancer that significantly increases the ocular tissue levels of hydrophobic drugs. The natural anatomical and physiological ocular barriers represent significant challenges to ophthalmic drug delivery. Major problems in topical ocular drug delivery include rapid precorneal drug loss and low corneal permeability. For topical ocular formulations, highly hydrophobic compounds are challenging to formulate due to their low aqueous solubility. The use of intravitreal injections is problematic and associated with systemic adverse events, devastating ocular complications, and poor patient compliance. Such limitations may be overcome by utilising a novel drug delivery system such as polymeric amphiphiles to formulate hydrophobic compounds for anterior and posterior segments diseases. Glycol chitosan is a water-soluble chitosan derivative with hydrophilic ethylene glycol branches and reactive functional groups for facile chemical modifications. Thus, alterations with groups having amphiphilic properties allow for the encapsulation of hydrophobic substances, thus expanding the utility of chitosan in drug formulations. Glycol chitosan-based

polymeric amphiphiles (GCPQ) with different molecular weights and a similar degree of mole% palmitoylation (DP%) and varying degrees of mole% quaternary ammonium groups (DQ%) were synthesised and characterised successfully. These amphiphilic polymers were used to manufacture aqueous-based (RAP and TAC) eye drops formulations.

We have shown that RAP, when encapsulated within GCPQ nanoparticles, exhibits excellent aqueous incorporation levels with an increase of up to 1000-fold when compared to RAP alone. The GCPQ: RAP formulation (~ 0.2% w/v) was stable over 30 days of storage at 5°C, and room temperature. Also, we manufactured a clear aqueous TAC eye drops formulation (0.1% w/v) that was stable against degradation when stored in the fridge for 30 days. GCPQ, as a novel delivery system for ocular delivery, was able to enhance the TAC aqueous incorporation by up to 100-fold.

The biocompatibility of GCPQ and GCPQ drug formulations was assessed by measuring the IC50 value in a standard MTT assay. GCPQ has been shown to demonstrate good biocompatibility against MDCK and SIRC cell lines with IC50 values ranging from 0.44 – 4.5 mg/mL. *In vitro* assays on the transport of a paracellular marker, FITC dextran, suggests that GCPQ does enhance paracellular permeability on the MDCK cell line. This effect is dependant on the degree of functionalisation with the palmitoyl and the quaternary ammonium groups, with a high level of quaternisation (19 mole%) enabling paracellular transport.

From the *in vivo* pharmacokinetic study, GCPQ: RAP showed promise as a formulation to reach the posterior eye tissues following a single topical application. We have demonstrated that GCPQ was able to deliver RAP into the rabbits' ocular tissues and to deliver the drug to the choroid-retina in a concentration higher than RAP therapeutic levels. Also, GCPQ: RAP 0.2% w/v was successfully utilised to control disease progression in a mouse EAU model. We have shown that GCPQ: RAP suppresses the expression of RORγt, upregulates Foxp3 expression and IL-10 secretion, and significantly reduces the disease progression. Also, GCPQ sufficiently delivered TAC to the cornea and conjunctiva (the target tissues) following a single topical application.

We demonstrated in this project the delivery of rapamycin as eye drops formulated in an amphiphilic polymer to the posterior segment of the eye upon single instillation to healthy rabbits. In addition, this rapamycin aqueous-based formulation suppresses the retinal inflammatory disease in the pre-clinical mice model. These findings have shown that eye drops can reach the impervious back of the eye tissues and modulate the immune response. This formulation may be used in the future for patients with posterior eye diseases and could be used as an alternative to the current invasive intravitreal injection. The finding from this study could offer older patients the ability o

f self-administering their medications without the necessity of a surgical procedure. Also, the physician preference to describe an easily administered treatment over the risk of intravitreal injections could open the gate for a new route of administration to the back of the eye being developed by the pharmaceutical industry.

6.2. Future work

We have shown that GCPQ is efficient at encapsulating hydrophobic drugs. It will be interesting to determine if GCPQ can be structurally modulated to encapsulate hydrophilic drugs and determine how this hydrophilic drug encapsulation affects ocular bioavailability.

We know from this project that GCPQ does enhance paracellular transport across epithelial barriers of the MDCK cell line by disrupting the monolayer tight junctions' integrity. However, GCPQ was not able to modulate tight junctions opening on SIRC cell line. Possibly the hybrid nature between an epithelial and fibroblastic cell in the SIRC cell line may be the reason why there was no transport of the paracellular marker (FD-4) across the SIRC monolayer. It would be interesting to design a transport experiment on the SIRC cell line using a transcellular marker to study the effect of different modifications of GCPQ on SIRC cell line transcellular transport. Also, GCPQ could be studied on human epithelial corneal models such as transformed human corneal epithelial cell lines for future permeation experiments.

We hypothesised that an amphiphilic chitosan-based polymer would increase the transport of hydrophobic drugs into ocular tissues. We tested this hypothesis, and it was proven; however, the exact mechanism by how GCPQ would act as a penetration enhancer is still unclear. It would be interesting to construct an experiment including a fluorescently labelled GCPQ and study the mechanistic pathway for the ocular distribution of GCPQ. We know that GCPQ was able to deliver RAP and TAC to the rabbits' ocular tissues following single topical instillation. It is

interesting to study the pharmacokinetic profile of both model drugs upon repeated dosing to healthy rabbits' model. It is also interesting to study the pharmacodynamic effect of GCPQ: TAC eye drops formulation on allergic ocular diseases.

7. References

1. Zhang K, Zhang L, Weinreb RN. Ophthalmic drug discovery: novel targets and mechanisms for retinal diseases and glaucoma. *Nat Rev Drug Discov*. 2012;11(7):541-559. doi:10.1038/nrd3745
2. Aulton ME, Taylor K. *Aulton's Pharmaceutics : The Design and Manufacture of Medicines*. Churchill Livingstone/Elsevier; 2013.
3. Cholkar K, Dasari SR, Pal D, Mitra AK. *Eye: Anatomy, Physiology and Barriers to Drug Delivery*.; 2013. doi:10.1533/9781908818317.1
4. Wilson C, Washington N, Washington C. *Physiological Pharmaceutics*.; 2000. doi:10.1201/9780203483701
5. Sánchez-López E, Espina M, Doktorovova S, Souto EB, García ML. Lipid nanoparticles (SLN, NLC): Overcoming the anatomical and physiological barriers of the eye – Part I – Barriers and determining factors in ocular delivery. *Eur J Pharm Biopharm*. 2017;110:70-75. doi:10.1016/j.ejpb.2016.10.009
6. Havener WH (William H. *Ocular Pharmacology*. Mosby; 1983.
7. Lee VHL, Robinson JR. *Review: Topical Ocular Drug Delivery: Recent Developments and Future Challenges*. Vol 2. Mary Ann Liebert, Inc., Publishers; 1986. www.liebertpub.com. Accessed July 26, 2018.
8. Gaudana R, Ananthula HK, Parenky A, Mitra AK. Ocular Drug Delivery. *AAPS J*. 2010;12(3):348-360. doi:10.1208/s12248-010-9183-3
9. Janoria KG, Gunda S, Boddu SH, Mitra AK. Novel approaches to retinal drug delivery. *Expert Opin Drug Deliv*. 2007;4(4):371-388.

doi:10.1517/17425247.4.4.371

10. Edelhauser HF, Rowe-Rendleman CL, Robinson MR, et al. Ophthalmic Drug Delivery Systems for the Treatment of Retinal Diseases: Basic Research to Clinical Applications. *Investig Opthalmology Vis Sci*. 2010;51(11):5403. doi:10.1167/iovs.10-5392

11. Singh V, Ahmad R, Heming T. The Challenges of Ophthalmic Drug Delivery: A Review. *Int J Drug Discov*. 2011;3(1):56-51. http://www.bioinfo.in/contents.php?id=24. Accessed July 26, 2018.

12. Mun EA, Morrison PWJ, Williams AC, Khutoryanskiy V V. On the barrier properties of the cornea: A microscopy study of the penetration of fluorescently labeled nanoparticles, polymers, and sodium fluorescein. *Mol Pharm*. 2014;11(10):3556-3564. doi:10.1021/mp500332m

13. Yi XJ, Wang Y, Yu FSX. Corneal epithelial tight junctions and their response to lipopolysaccharide challenge. *Investig Ophthalmol Vis Sci*. 2000;41(13):4093-4100. http://www.ncbi.nlm.nih.gov/pubmed/11095601. Accessed July 28, 2018.

14. Hertsenberg AJ, Funderburgh JL. Stem Cells in the Cornea. *Prog Mol Biol Transl Sci*. 2015;134:25-41. doi:10.1016/BS.PMBTS.2015.04.002

15. Boddu SH, Gupta H, Patel S. Drug Delivery to the Back of the Eye Following Topical Administration: An Update on Research and Patenting Activity. *Recent Pat Drug Deliv Formul*. 2014;8:27-36. doi:10.2174/1872211308666140130093301

16. Zhang W, Prausnitz MR, Edwards A. Model of transient drug diffusion across

cornea. 2004. doi:10.1016/j.jconrel.2004.07.001

17. Watsky MA, Jablonski MM, Edelhauser HF. Comparison of conjunctival and corneal surface areas in rabbit and human. *Curr Eye Res*. 1988;7(5):483-486. doi:10.3109/02713688809031801

18. Barar J, Javadzadeh AR, Omidi Y. Ocular novel drug delivery: impacts of membranes and barriers Ocular novel drug delivery: impacts of membranes and barriers. *Expert Opin Drug Deliv Expert Opin Drug Deliv*. 2008;5(55):567-581. doi:10.1517/17425240802095061

19. Mitra A K. *Opthalmic Drug Delivery Systems 2nd Ed.*; 2003. http://www.dekker.com. Accessed July 26, 2018.

20. Hornof M, Toropainen E, Urtti A. Cell culture models of the ocular barriers *. 2005. doi:10.1016/j.ejpb.2005.01.009

21. Olsen TW, Edelhauser HF, Jennifer I, Geroski DH. Human Scleral Permeability Effects of Age, Cryotherapy, Transscleral Diode Laser, and Surgical Thinning. *Investig Ophthalmol Vis Sci*. 1995;36(9):1893-1903.

22. Fujiwara T, Imamura Y, Margolis R, Slakter JS, Spaide RF. Enhanced Depth Imaging Optical Coherence Tomography of the Choroid in Highly Myopic Eyes. *Am J Ophthalmol*. 2009;148(3):445-450. doi:10.1016/j.ajo.2009.04.029

23. Elsaid N, Jackson TL, Gunic M, Somavarapu S. Positively charged amphiphilic chitosan derivative for the transscleral delivery of rapamycin. *Investig Ophthalmol Vis Sci*. 2012;53(13):8105-8111. doi:10.1167/iovs.12-10717

24. Booij JC, Baas DC, Beisekeeva J, Gorgels TGMF, Bergen AAB. The dynamic nature of Bruch's membrane. *Prog Retin Eye Res*. 2010;29(1):1-18.

doi:10.1016/j.preteyeres.2009.08.003

25. Chakravarthy U, Evans J, Rosenfeld PJ. Age related macular degeneration. *BMJ*. 2010;340:c981. doi:10.1136/BMJ.C981

26. Cunha-Vaz J, Bernardes R, Lobo C. Blood-Retinal Barrier. *Eur J Ophthalmol*. 2011;21(6_suppl):3-9. doi:10.5301/EJO.2010.6049

27. del Amo EM, Rimpelä AK, Heikkinen E, et al. Pharmacokinetic aspects of retinal drug delivery. *Prog Retin Eye Res*. 2017;57:134-185. doi:10.1016/j.preteyeres.2016.12.001

28. Kennedy BG, Mangini NJ. P-glycoprotein expression in human retinal pigment epithelium. *Mol Vis*. 2002;8:422-430. http://www.ncbi.nlm.nih.gov/pubmed/12432340. Accessed July 28, 2018.

29. Chillistone S, Hardman J. Factors affecting drug absorption and distribution. *Anaesth Intensive Care Med*. 2008;9(4):167-171. doi:10.1016/j.mpaic.2008.02.005

30. Topical drug dosage forms for eye conditions. *Pharm J*. 2017:1. 20202915. Accessed October 28, 2020.

31. Allen L V, Ansel HC. Ansel ' s Pharmaceutical Dosage Forms and Drug Delivery Systems. *Ansel ' s Pharm Dos Forms Drug Deliv Syst*. 2011. doi:978-0-7817-7934-0

32. Zatz JL, Teixeira MG. *Pharmaceutical Calculations*. Wiley Interscience; 2005. https://books.google.co.uk/books?id=Ma_GAqsLgiEC&printsec=frontcover&dq=zats+pharmaceuticals+calculation+4th+edition&hl=en&sa=X&ved=0ahUKEwigrNjgt8LcAhUNfMAKHReABIIQ6AEIKTAA#v=onepage&q=zats

pharmaceuticals calculation 4th edition&f=false. Accessed July 28, 2018.

33. Zhu H, Chauhan A. Effect of viscosity on tear drainage and ocular residence time. *Optom Vis Sci*. 2008;85(8):E715-E725. doi:10.1097/OPX.0b013e3181824dc4

34. Cholkar K, Gunda S, Earla R, Pal D, Mitra AK. Nanomicellar Topical Aqueous Drop Formulation of Rapamycin for Back-of-the-Eye Delivery. *AAPS PharmSciTech*. 2015;16(3):610-622. doi:10.1208/s12249-014-0244-2

35. Korson L, Drost-Hansen W, Millero FJ. Viscosity of water at various temperatures. *J Phys Chem*. 1969;73(1):34-39. doi:10.1021/j100721a006

36. Hughes PM, Olejnik O, Chang-Lin JE, Wilson CG. Topical and systemic drug delivery to the posterior segments. *Adv Drug Deliv Rev*. 2005;57(14 SPEC. ISS.):2010-2032. doi:10.1016/j.addr.2005.09.004

37. Agrahari V, Mandal A, Agrahari V, et al. A comprehensive insight on ocular pharmacokinetics. *Drug Deliv Transl Res*. 2016;6(6):735-754. doi:10.1007/s13346-016-0339-2

38. Delplace V, Payne S, Shoichet M. Delivery strategies for treatment of age-related ocular diseases: From a biological understanding to biomaterial solutions. *J Control Release*. 2015;219:652-668. doi:10.1016/j.jconrel.2015.09.065

39. Kompella UB, Amrite AC, Pacha Ravi R, Durazo SA. Nanomedicines for back of the eye drug delivery, gene delivery, and imaging. *Prog Retin Eye Res*. 2013;36:172-198. doi:10.1016/j.preteyeres.2013.04.001

40. Veritti D, Lanzetta P, Perissin L, Bandello F. Posterior juxtascleral infusion of

modified triamcinolone acetonide formulation for refractory diabetic macular edema: One-year follow-up. *Investig Ophthalmol Vis Sci*. 2009;50(5):2391-2397. doi:10.1167/iovs.08-2518

41. Goldstein DA, Do D, Noronha G, Kissner JM, Srivastava SK, Nguyen QD. Suprachoroidal corticosteroid administration: A novel route for local treatment of noninfectious uveitis. *Transl Vis Sci Technol*. 2016;5(6). doi:10.1167/tvst.5.6.14

42. Joussen AM, Wolf S, Kaiser PK, et al. The Developing Regorafenib Eye drops for neovascular Age-related Macular degeneration (DREAM) study: an open-label phase II trial. *Br J Clin Pharmacol*. 2019;85(2):347-355. doi:10.1111/bcp.13794

43. Csaky KG, Dugel PU, Pierce AJ, et al. Clinical Evaluation of Pazopanib Eye Drops versus Ranibizumab Intravitreal Injections in Subjects with Neovascular Age-Related Macular Degeneration. *Ophthalmology*. 2015;122:579-588. doi:10.1016/j.ophtha.2014.09.036

44. Safety and Efficacy of ATG003 in Patients With AMD Receiving Anti-VEGF - Full Text View - ClinicalTrials.gov. https://clinicaltrials.gov/ct2/show/NCT00607750. Accessed July 28, 2018.

45. Pohl J. PanOptica Reports Progress with PAN-90806, a Topical Anti-VEGF Eyedrop for the Treatment of Neovascular (Wet) AMD | Business Wire. https://www.businesswire.com/news/home/20151112005385/en/PanOptica-Reports-Progress-PAN-90806-Topical-Anti-VEGF-Eyedrop. Published 2015. Accessed July 28, 2018.

46. Squalamine :: Ohr Pharmaceutical, Inc. (OHRP). https://www.ohrpharmaceutical.com/product-portfolio/squalamine. Accessed December 20, 2018.

47. Rosenfeld PJ, Feuer WJ. Lessons from Recent Phase III Trial Failures: Don't Design Phase III Trials Based on Retrospective Subgroup Analyses from Phase II Trials. *Ophthalmology*. 2018;125(10):1488-1491. doi:10.1016/j.ophtha.2018.06.002

48. Hunyor AP, Merani R, Darbar A, Korobelnik J-F, Lanzetta P, Okada AA. Topical antibiotics and intravitreal injections. *Acta Ophthalmol*. April 2017. doi:10.1111/aos.13417

49. Tian J, Liu J, Liu X, Xiao Y, Tang L. Intravitreal infusion: A novel approach for intraocular drug delivery OPEN. *Nat Publ Gr*. 2016. doi:10.1038/srep37676

50. Vinores SA. Pegaptanib in the treatment of wet, age-related macular degeneration. *Int J Nanomedicine*. 2006;1(3):263-268. https://www.ncbi.nlm.nih.gov/pmc/articles/PMC2426796/pdf/nano-0103-263.pdf. Accessed July 28, 2018.

51. Zou L, Lai H, Zhou Q, Xiao F. Lasting Controversy on Ranibizumab and Bevacizumab. *Theranostics*. 2011;1:395-402. doi:10.7150/thno/v01p0395

52. Chong V. Ranibizumab for the treatment of wet AMD: A summary of real-world studies. *Eye*. 2016;30(2):270-286. doi:10.1038/eye.2015.217

53. Food and Drug Administration. CENTER FOR DRUG EVALUATION AND RESEARCH. APPLICATION NUMBER22-512. Food and Drug Administration. www.fda.gov/medwatch. Published 2010. Accessed July 28, 2018.

54. Sharma A, Kumar N, Bandello F, Kuppermann BD, Loewenstein A, Regillo CD. Brolucizumab: The road ahead. *Br J Ophthalmol*. 2020;104(12):1631-1632. doi:10.1136/bjophthalmol-2020-317528

55. Al-Halafi AM. Vascular endothelial growth factor trap-eye and trap technology: Aflibercept from bench to bedside. *Oman J Ophthalmol*. 2014;7(3):112-115. doi:10.4103/0974-620X.142591

56. Ghasemi Falavarjani K, Nguyen QD. Adverse events and complications associated with intravitreal injection of anti-VEGF agents: a review of literature. *Eye*. 2013;27(7):787-794. doi:10.1038/eye.2013.107

57. O'Rourke M. DEVELOPMENT OF SUSTAINED-RELEASE OCULAR DELIVERY TECHNOLOGIES. *drug Deliv*. 2016:4-5. www.ondrugdelivery.com. Accessed July 28, 2018.

58. Boyle J, Vukicevic M, Koklanis K, Itsiopoulos C, Rees G. Experiences of patients undergoing repeated intravitreal anti-vascular endothelial growth factor injections for neovascular age-related macular degeneration. *Psychol Health Med*. 2017:1-14. doi:10.1080/13548506.2016.1274040

59. GLOBAL DATA ON VISUAL IMPAIRMENTS 2010. https://www.who.int/blindness/GLOBALDATAFINALforweb.pdf. Accessed November 6, 2020.

60. Tan HY, Agarwal A, Lee CS, et al. Management of noninfectious posterior uveitis with intravitreal drug therapy. *Clin Ophthalmol*. 2016;10:1983-2020. doi:10.2147/OPTH.S89341

61. Wong WL, Su X, Li X, et al. Global prevalence of age-related macular

degeneration and disease burden projection for 2020 and 2040: A systematic review and meta-analysis. *Lancet Glob Heal*. 2014;2(2):e106-e116. doi:10.1016/S2214-109X(13)70145-1

62. Owen CG, Jarrar Z, Wormald R, Cook DG, Fletcher AE, Rudnicka AR. The estimated prevalence and incidence of late stage age related macular degeneration in the UK. *Lab Sci*. 2011:1-5. doi:10.1136/bjophthalmol-2011-301109

63. Bhutto I, Lutty G. Understanding age-related macular degeneration (AMD): Relationships between the photoreceptor/retinal pigment epithelium/Bruch's membrane/choriocapillaris complex. *Mol Aspects Med*. 2012;33(4):295-317. doi:10.1016/j.mam.2012.04.005

64. Duh EJ, Sun JK, Stitt AW. Diabetic retinopathy: current understanding, mechanisms, and treatment strategies. *JCI insight*. 2017;2(14). doi:10.1172/jci.insight.93751

65. Leasher JL, Bourne RRA, Flaxman SR, et al. Global Estimates on the Number of People Blind or Visually Impaired by Diabetic Retinopathy: A Meta. *Diabetes Care*. 2016;39:1643-1649. doi:10.2337/dc15-2171

66. Yau JWY, Rogers SL, Kawasaki R, et al. *Global Prevalence and Major Risk Factors of Diabetic Retinopathy*.; 2012. http://care.diabetesjournals.org/lookup/suppl/. Accessed July 29, 2018.

67. Squires H, Poku E, Bermejo I, et al. A systematic review and economic evaluation of adalimumab and dexamethasone for treating non-infectious intermediate uveitis, posterior uveitis or panuveitis in adults. *Health Technol*

Assess (Rockv). 2017;21(68):1-170. doi:10.3310/hta21680

68. Calder VL, Shaer B, Muhaya M, et al. Increased CD4+ expression and decreased IL-10 in the anterior chamber in idiopathic uveitis. *Invest Ophthalmol Vis Sci*. 1999;40(9):2019-2024. http://www.ncbi.nlm.nih.gov/pubmed/10440256. Accessed April 17, 2020.
69. Mattapallil MJ, Silver PB, Mattapallil JJ, et al. Uveitis-Associated Epitopes of Retinal Antigens Are Pathogenic in the Humanized Mouse Model of Uveitis and Identify Autoaggressive T Cells. *J Immunol*. 2011;187(4):1977-1985. doi:10.4049/jimmunol.1101247
70. Tang WM, Pulido JS, Eckels DD, Han DP, Mieler WF, Pierce K. The association of HLA-DR15 and intermediate uveitis. *Am J Ophthalmol*. 1997;123(1):70-75. doi:10.1016/S0002-9394(14)70994-8
71. Caspi RR. A look at autoimmunity and inflammation in the eye. *J Clin Invest*. 2010;120(9):3073-3083. doi:10.1172/JCI42440
72. Durrani OM, Tehrani NN, Marr JE, Moradi P, Stavrou P, Murray PI. Degree, duration, and causes of visual loss in uveitis. *Br J Ophthalmol*. 2004;88(9):1159-1162. doi:10.1136/bjo.2003.037226
73. Tsirouki T, Dastiridou A, Symeonidis C, et al. A Focus on the Epidemiology of Uveitis. *Ocul Immunol Inflamm*. 2018;26(1):2-16. doi:10.1080/09273948.2016.1196713
74. Hayashi R. *Handbook of Nutrition, Diet, and the Eye*. Elsevier; 2019. doi:10.1016/c2017-0-01652-x
75. Gupta V, Rajagopala M, Ravishankar B. Etiopathogenesis of cataract: An

appraisal. *Indian J Ophthalmol*. 2014;62(2):103-110. doi:10.4103/0301-4738.121141

76. Nartey A. The Pathophysiology of Cataract and Major Interventions to Retarding Its Progression: A Mini Review. *Adv Ophthalmol Vis Syst*. 2017;6(3). doi:10.15406/aovs.2017.06.00178

77. Allen D, Vasavada A. Cataract and surgery for cataract. *Br Med J*. 2006;333(7559):128-132. doi:10.1136/bmj.333.7559.128

78. Could eye drops be an alternative treatment to cataract surgery? | AOA. https://www.aoa.org/news/clinical-eye-care/diseases-and-conditions/could-eye-drops-be-an-alternative-treatment-to-cataract-surgery?sso=y. Accessed November 6, 2020.

79. Craig JP, Nichols KK, Akpek EK, et al. TFOS DEWS II Definition and Classification Report. *Ocul Surf*. 2017;15(3):276-283. doi:10.1016/j.jtos.2017.05.008

80. Phadatare SP, Momin M, Nighojkar P, Askarkar S, Singh KK. A Comprehensive Review on Dry Eye Disease: Diagnosis, Medical Management, Recent Developments, and Future Challenges. *Adv Pharm*. 2015;2015:1-12. doi:10.1155/2015/704946

81. Stapleton F, Alves M, Bunya VY, et al. TFOS DEWS II Epidemiology Report. *Ocul Surf*. 2017;15(3):334-365. doi:10.1016/j.jtos.2017.05.003

82. Dry eyes - Diagnosis and treatment - Mayo Clinic. https://www.mayoclinic.org/diseases-conditions/dry-eyes/diagnosis-treatment/drc-20371869. Accessed November 6, 2020.

83. Kersey JP, Broadway DC. Corticosteroid-induced glaucoma: A review of the literature. *Eye*. 2006;20(4):407-416. doi:10.1038/sj.eye.6701895

84. Glaucoma - NHS. https://www.nhs.uk/conditions/glaucoma/. Accessed November 7, 2020.

85. Weinreb RN, Aung T, Medeiros FA. The pathophysiology and treatment of glaucoma: A review. *JAMA - J Am Med Assoc*. 2014;311(18):1901-1911. doi:10.1001/jama.2014.3192

86. Harasymowycz P, Birt C, Gooi P, et al. Medical Management of Glaucoma in the 21st Century from a Canadian Perspective. *J Ophthalmol*. 2016;2016. doi:10.1155/2016/6509809

87. Tham YC, Li X, Wong TY, Quigley HA, Aung T, Cheng CY. Global prevalence of glaucoma and projections of glaucoma burden through 2040: A systematic review and meta-analysis. *Ophthalmology*. 2014;121(11):2081-2090. doi:10.1016/j.ophtha.2014.05.013

88. La Rosa M, Lionetti E, Reibaldi M, et al. Allergic conjunctivitis: A comprehensive review of the literature. *Ital J Pediatr*. 2013;39(1). doi:10.1186/1824-7288-39-18

89. Leonardi A, Castegnaro A, Valerio ALG, Lazzarini D. Epidemiology of allergic conjunctivitis: Clinical appearance and treatment patterns in a population-based study. *Curr Opin Allergy Clin Immunol*. 2015;15(5):482-488. doi:10.1097/ACI.0000000000000204

90. Bremond-Gignac D. Atopic and vernal keratoconjunctivitis: differences and similarities. *Acta Ophthalmol*. 2016;94. doi:10.1111/j.1755-3768.2016.0005

91. Bremond-Gignac D, Donadieu J, Leonardi A, et al. Prevalence of vernal keratoconjunctivitis: A rare disease? *Br J Ophthalmol*. 2008;92(8):1097-1102. doi:10.1136/bjo.2007.117812

92. Addis H, Jeng BH. Vernal keratoconjunctivitis. *Clin Ophthalmol*. 2018;12:119-123. doi:10.2147/OPTH.S129552

93. Guglielmetti S, Dart JK, Calder V. Atopic keratoconjunctivitis and atopic dermatitis. *Curr Opin Allergy Clin Immunol*. 2010;10(5):478-485. doi:10.1097/ACI.0b013e32833e16e4

94. Chen H. Recent developments in ocular drug delivery. *J Drug Target*. 2015;23(7-8):597-604. doi:10.3109/1061186X.2015.1052073

95. Singh RB, Ichhpujani P, Thakur S, Jindal S. Promising therapeutic drug delivery systems for glaucoma: a comprehensive review. *Ther Adv Ophthalmol*. 2020;12:251584142090574. doi:10.1177/2515841420905740

96. Christoforidis JB, Chang S, Jiang A, Wang J, Cebulla CM. Intravitreal devices for the treatment of vitreous inflammation. *Mediators Inflamm*. 2012;2012. doi:10.1155/2012/126463

97. (No Title). https://www.accessdata.fda.gov/drugsatfda_docs/label/2014/022315s009lbl.pdf. Accessed November 5, 2020.

98. Sharma A, Kumar N, Kuppermann BD, Francesco B. Re: Campochiaro et al.: The Port Delivery System with ranibizumab for neovascular age-related macular degeneration: results from the randomized phase 2 Ladder clinical trial (Ophthalmology. 2019;126:1141-1154). *Ophthalmology*.

2019;126(11):e87-e88. doi:10.1016/j.ophtha.2019.06.019

99. Inherited Retinal Disease | LUXTURNA™ (voretigene neparvovec-rzyl). Spark Therapeutics. https://luxturna.com/. Published 2019. Accessed November 5, 2020.

100. About LUXTURNA® | LUXTURNA® (voretigene neparvovec-rzyl). *Spark Ther*. 2019. https://luxturna.com/about-luxturna/#how-does-luxturna-work. Accessed November 5, 2020.

101. Perez VL, Wirostko B, Korenfeld M, From S, Raizman M. Ophthalmic drug delivery using iontophoresis: Recent clinical applications. *J Ocul Pharmacol Ther*. 2020;36(2):75-87. doi:10.1089/jop.2019.0034

102. Annamalai B, Parsons N, Belhaj M, Brandon C, Potts J, Rohrer B. Encapsulated cell technology-based delivery of a complement inhibitor reduces choroidal neovascularization in a mouse model. *Transl Vis Sci Technol*. 2018;7(2). doi:10.1167/tvst.7.2.3

103. Loftsson T, Stefánssonb E. Cyclodextrins and topical drug delivery to the anterior and posterior segments of the eye. *Int J Pharm*. 2017;531:413-423. doi:http://dx.doi.org/10.1016/j.ijpharm.2017.04.010

104. Oculis. SNP Technology. https://www.oculis.com/science/snp-technology. Accessed January 22, 2019.

105. Silva MM, Calado R, Marto J, Bettencourt A, Almeida AJ, Gonçalves LMD. Chitosan Nanoparticles as a Mucoadhesive Drug Delivery System for Ocular Administration. *Mar Drugs*. 2017;15(12). doi:10.3390/md15120370

106. News | Nanomerics. http://www.nanomerics.com/news. Accessed November

6, 2020.

107. Technology | EyeGate Pharma. https://www.eyegatepharma.com/technology/. Accessed November 5, 2020.
108. Irimia T, Ghica MV, Popa L, Anuţa V, Arsene AL, Dinu-Pîrvu CE. Strategies for improving ocular drug bioavailability and cornealwound healing with chitosan-based delivery systems. *Polymers (Basel)*. 2018;10(11). doi:10.3390/polym10111221
109. Kompella UB, Amrite AC, Pacha Ravi R, Durazo SA. Nanomedicines for Back of the Eye Drug Delivery, Gene Delivery, and Imaging. *Prog Retin Eye Res*. 2013;36:172-198. doi:10.1016/j.preteyeres.2013.04.001
110. Omerović N, Vranić E. Application of nanoparticles in ocular drug delivery systems. *Health Technol (Berl)*. 2020;10(1):61-78. doi:10.1007/s12553-019-00381-w
111. *Oculis Announces Positive OCS-01 Phase 2 Data in Patients with Diabetic Macular Edema (DME)*. www.oculis.com. Accessed November 1, 2020.
112. Mizrahy S, Peer D. Polysaccharides as building blocks for nanotherapeutics. *Chem Soc Rev*. 2012;41(7):2623-2640. doi:10.1039/c1cs15239d
113. Das S, Suresh PK. Drug delivery to eye: Special reference to nanoparticle. *Int J Drug Deliv*. 2010;2(1):12-21. doi:10.5138/ijdd.2010.0975.0215.02007
114. Cadinoiu AN, Peptu CA, Fache B, Chailan JF, Popa M. Microparticulated systems based on chitosan and poly(vinyl alcohol) with potential ophthalmic applications. *J Microencapsul*. 2015;32(4):381-389. doi:10.3109/02652048.2015.1035682

115. Irimia T, Dinu-Pîrvu CE, Ghica MV, et al. Chitosan-based in situ gels for ocular delivery of therapeutics: A state-of-the-art review. *Mar Drugs*. 2018;16(10). doi:10.3390/md16100373

116. Szymańska E, Winnicka K. Stability of chitosan - A challenge for pharmaceutical and biomedical applications. *Mar Drugs*. 2015;13(4):1819-1846. doi:10.3390/md13041819

117. Jiang S, Franco YL, Zhou Y, Chen J. Nanotechnology in retinal drug delivery. *Int J Ophthalmol*. 2018:1038-1044. doi:10.18240/ijo.2018.06.23

118. Shima C, Sakaguchi H, Gomi F, et al. Complications in patients after intravitreal injection of bevacizumab. *Acta Ophthalmol*. 2008;86(4):372-376. doi:10.1111/j.1600-0420.2007.01067.x

119. Tiwari R, Pandey V, Asati S, Soni V, Jain D. Therapeutic challenges in ocular delivery of lipid based emulsion. *Egypt J Basic Appl Sci*. 2018;5(2):121-129. doi:10.1016/j.ejbas.2018.04.001

120. Mandal A, Bisht R, Rupenthal ID, Mitra AK. Polymeric micelles for ocular drug delivery: From structural frameworks to recent preclinical studies. *J Control Release*. 2017;248:96-116. doi:10.1016/j.jconrel.2017.01.012

121. Lombardo D, Kiselev MA, Magazù S, Calandra P. Amphiphiles self-assembly: Basic concepts and future perspectives of supramolecular approaches. *Adv Condens Matter Phys*. 2015;2015. doi:10.1155/2015/151683

122. Uchegbu IF. Low Molecular Weight Micelles. In: *Fundamentals of Pharmaceutical Nanoscience*. New York, NY: Springer New York; 2013:9-25. doi:10.1007/978-1-4614-9164-4_2

123. Durgun ME, Güngör S, Özsoy Y. Micelles: Promising Ocular Drug Carriers for Anterior and Posterior Segment Diseases. *J Ocul Pharmacol Ther*. 2020;36(6):323-341. doi:10.1089/jop.2019.0109

124. Georgieva V, Zvezdova D, Vlaev L. Non-isothermal kinetics of thermal degradation of chitosan. *Chem Cent J*. 2012;6(1). doi:10.1186/1752-153X-6-81

125. Thanou M, Verhoef JC, Junginger HE. Oral drug absorption enhancement by chitosan and its derivatives. *Adv Drug Deliv Rev*. 2001;52(2):117-126. doi:10.1016/S0169-409X(01)00231-9

126. Mourya VK, Inamdar NN. Chitosan-modifications and applications: Opportunities galore. *React Funct Polym*. 2008;68(6):1013-1051. doi:10.1016/j.reactfunctpolym.2008.03.002

127. Franca JR, Fuscaldi LL, Ribeiro TG, et al. Use of chitosan as pharmaceutical excipient in ocular drug delivery systems: Sterilization and pharmacokinetics. *J Biomed Mater Res Part B Appl Biomater*. 2020;108(5):2227-2237. doi:10.1002/jbm.b.34560

128. Zamboulis A, Nanaki S, Michailidou G, et al. Chitosan and its derivatives for ocular delivery formulations: Recent advances and developments. *Polymers (Basel)*. 2020;12(7):9-11. doi:10.3390/polym12071519

129. Szymańska E, Winnicka K. Stability of chitosan - A challenge for pharmaceutical and biomedical applications. *Mar Drugs*. 2015;13(4):1819-1846. doi:10.3390/md13041819

130. Lin F, Jia HR, Wu FG. Glycol chitosan: A water-soluble polymer for cell

imaging and drug delivery. *Molecules*. 2019;24(23). doi:10.3390/molecules24234371

131. Ritthidej GC. Nasal Delivery of Peptides and Proteins with Chitosan and Related Mucoadhesive Polymers. *Pept Protein Deliv*. January 2011:47-68. doi:10.1016/B978-0-12-384935-9.10003-3

132. Lim C, Lee DW, Israelachvili JN, Jho Y, Hwang DS. Contact time- and pH-dependent adhesion and cohesion of low molecular weight chitosan coated surfaces. *Carbohydr Polym*. 2015;117:887-894. doi:10.1016/J.CARBPOL.2014.10.033

133. Rodríguez I, Antonio Vázquez J, Pastrana L, Khutoryanskiy V V. Enhancement and inhibition effects on the corneal permeability of timolol maleate: Polymers, cyclodextrins and chelating agents. *Int J Pharm*. 2017;529:168-177. doi:10.1016/j.ijpharm.2017.06.075

134. Uchegbu IF, Sadiq L, Arastoo M, et al. Quaternary ammonium palmitoyl glycol chitosan--a new polysoap for drug delivery. *Int J Pharm*. 2001;224(1-2):185-199. http://www.ncbi.nlm.nih.gov/pubmed/11472828. Accessed July 21, 2018.

135. Siew A, Le H, Thiovolet M, Gellert P, Schatzlein A, Uchegbu I. Enhanced oral absorption of hydrophobic and hydrophilic drugs using quaternary ammonium palmitoyl glycol chitosan nanoparticles. *Mol Pharm*. 2012;9(1):14-28. doi:10.1021/mp200469a

136. Qu X, Khutoryanskiy V V, Stewart A, et al. Carbohydrate-based micelle clusters which enhance hydrophobic drug bioavailability by up to 1 order of magnitute. *Biomacromolecules*. 2006;7(12):3452-3459.

doi:10.1021/bm0604000

137. Lalatsa A, Garrett NL, Ferrarelli T, Moger J, Schätzlein AG, Uchegbu IF. Delivery of peptides to the blood and brain after oral uptake of quaternary ammonium palmitoyl glycol chitosan nanoparticles. *Mol Pharm*. 2012;9(6):1764-1774. doi:10.1021/mp300068j

138. Chooi KW, Simão Carlos MI, Soundararajan R, et al. Physical characterisation and long-term stability studies on quaternary ammonium palmitoyl glycol chitosan (GCPQ) - A new drug delivery polymer. *J Pharm Sci*. 2014;103(8):2296-2306. doi:10.1002/jps.24026

139. Holzgrabe U (Ulrike), Wawer I (Iwona), Diehl B (Bernd). *NMR Spectroscopy in Pharmaceutical Analysis*. Elsevier; 2008.

140. James TL. Chapter 1 Fundamentals of NMR. 1998:1-31.

141. NMR Spectroscopy - Theory. https://teaching.shu.ac.uk/hwb/chemistry/tutorials/molspec/nmr1.htm. Accessed January 24, 2019.

142. Claridge TDW. *High-Resolution NMR Techniques in Organic Chemistry*. Elsevier; 2009.

143. Williams Dudley, Ian Fleming. *Spectroscopic Methods in Organic Chemistry*. 3rd ed.; 1980. https://trove.nla.gov.au/work/9856036?q&sort=holdings+desc&_=1532169135470&versionId=49173047. Accessed July 21, 2018.

144. Bax A. *TWO-DIMENSIONAL NMR AND PROTEIN STRUCTURE*. www.annualreviews.org. Accessed January 24, 2019.

145. Podzimek S. The use of GPC coupled with a multiangle laser light scattering photometer for the characterization of polymers. On the determination of molecular weight, size and branching. *J Appl Polym Sci*. 1994;54(1):91-103. doi:10.1002/app.1994.070540110

146. Mori S, Barth HG. *Size Exclusion Chromatography*. Springer Berlin Heidelberg; 2013. https://books.google.co.uk/books/about/Size_Exclusion_Chromatography.html?id=wKbvCAAAQBAJ&redir_esc=y. Accessed July 21, 2018.

147. Grcev S, Schoenmakers P, Iedema P. Determination of molecular weight and size distribution and branching characteristics of PVAc by means of size exclusion chromatography/multi-angle laser light scattering (SEC/MALLS). *Polymer (Guildf)*. 2004;45(1):39-48. doi:10.1016/j.polymer.2003.10.077

148. Dufour G, Evrard B, de Tullio P. 2D-Cosy NMR Spectroscopy as a Quantitative Tool in Biological Matrix: Application to Cyclodextrins. *AAPS J*. 2015;17(6):1501-1510. doi:10.1208/s12248-015-9806-9

149. Martin L, Wilson CG, Koosha F, et al. The release of model macromolecules may be controlled by the hydrophobicity of palmitoyl glycol chitosan hydrogels. *J Control Release*. 2002;80(1-3):87-100. doi:10.1016/S0168-3659(02)00005-6

150. Thi Bich Le H, G. Schatzlein A, F. Uchegbu I. Polymer Hydrophobicity Has a Positive Effect on the Oral Absorption of Cyclosporine A from Poly(ethylenimine) Based Nanomedicines. *Pharm Nanotechnol*. 2012;1(1):15-25. doi:10.2174/22117385130106

151. Ahmed TA, Aljaeid BM. Preparation, characterization, and potential application of chitosan, chitosan derivatives, and chitosan metal nanoparticles in pharmaceutical drug delivery. *Drug Des Devel Ther*. 2016;10:483-507. doi:10.2147/DDDT.S99651

152. Verheul RJ, Amidi M, van der Wal S, van Riet E, Jiskoot W, Hennink WE. Synthesis, characterization and in vitro biological properties of O-methyl free N,N,N-trimethylated chitosan. *Biomaterials*. 2008;29(27):3642-3649. doi:10.1016/j.biomaterials.2008.05.026

153. Tumolo T, Angnes L, Baptista MS. Determination of the refractive index increment (dn/dc) of molecule and macromolecule solutions by surface plasmon resonance. *Anal Biochem*. 2004;333(2):273-279. doi:10.1016/j.ab.2004.06.010

154. Sahoo SK, Dilnawaz F, Krishnakumar S. Nanotechnology in ocular drug delivery. *Drug Discov Today*. 2008;13(3-4):144-151. doi:10.1016/j.drudis.2007.10.021

155. Kayser O, Olbrich C, Yardley V, Kiderlen AF, Croft SL. Formulation of amphotericin B as nanosuspension for oral administration. *Int J Pharm*. 2003;254(1):73-75. http://www.ncbi.nlm.nih.gov/pubmed/12615413. Accessed January 26, 2019.

156. Chen MC, Mi FL, Liao ZX, et al. Recent advances in chitosan-based nanoparticles for oral delivery of macromolecules. *Adv Drug Deliv Rev*. 2013;65(6):865-879. doi:10.1016/j.addr.2012.10.010

157. Cho Y, Ha ES, Baek IH, Kim MS, Cho CW, Hwang SJ. Enhanced

supersaturation and oral absorption of sirolimus using an amorphous solid dispersion based on Eudragit® E. *Molecules*. 2015;20(6):9496-9509. doi:10.3390/molecules20069496

158. Rapamune | European Medicines Agency. https://www.ema.europa.eu/en/medicines/human/EPAR/rapamune. Accessed September 13, 2020.
159. Dutcher JP, Motzer RJ, Atkins MB, et al. Mammalian target of rapamycin inhibition. In: *Clinical Cancer Research*. Vol 10. ; 2004. doi:10.1158/1078-0432.CCR-050008
160. Chi H. Regulation and function of mTOR signalling in T cell fate decisions. *Nat Rev Immunol*. 2012;12(5):325-338. doi:10.1038/nri3198
161. Cutler C, Antin JH. Sirolimus for GVHD prophylaxis in allogeneic stem cell transplantation. *Bone Marrow Transplant*. 2004;34(6):471-476. doi:10.1038/sj.bmt.1704604
162. Buech G, Bertelmann E, Pleyer U, Siebenbrodt I, Borchert HH. Formulation of sirolimus eye drops and corneal permeation studies. *J Ocul Pharmacol Ther*. 2007;23(3):292-303. doi:10.1089/jop.2006.130
163. Giordano A. Molecular basis of different outcomes for drug-eluting stents that release sirolimus or tacrolimus. *Curr Opin Drug Discov Dev*. 2010;13(2):159-168.
164. Abeysiri P, Johnston NR, Molteno ACB. The use of topical tacrolimus 0.1% skin ointment for anterior segment conditions: a case series. *Ophthalmol Eye Dis*. 2010;2:5-8. http://www.ncbi.nlm.nih.gov/pubmed/23861611. Accessed

February 20, 2019.

165. Barbarino JM, Staatz CE, Venkataramanan R, Klein TE, Altman RB. PharmGKB summary: Cyclosporine and tacrolimus pathways. *Pharmacogenet Genomics*. 2013;23(10):563-585. doi:10.1097/FPC.0b013e328364db84

166. Tacrolimus (marketed as Protopic Ointment) Information | FDA. https://www.fda.gov/drugs/postmarket-drug-safety-information-patients-and-providers/tacrolimus-marketed-protopic-ointment-information. Accessed April 11, 2020.

167. ANNEX I SUMMARY OF PRODUCT CHARACTERISTICS - Glivec. 2006:809-822. https://www.ema.europa.eu/en/documents/product-information/protopic-epar-product-information_en.pdf. Accessed June 4, 2020.

168. Leonardi A. Management of Vernal Keratoconjunctivitis. *Ophthalmol Ther*. 2013;2(2):73-88. doi:10.1007/s40123-013-0019-y

169. Usha SY, Ashish MA. Review on: an Ointment. *Human*. 2015;4(2):170-192. www.ijppr.humanjournals.comwww.ijppr.humanjournals.com. Accessed April 23, 2020.

170. Topical drug dosage forms for eye conditions. *Pharm J*. 2017;2017(May):1-13. https://www.pharmaceutical-journal.com/cpd-and-learning/learning-article/topical-drug-dosage-forms-for-eye-conditions/20202915.article?firstPass=false. Accessed April 23, 2020.

171. Fujita E, Teramura Y, Shiraga T, et al. Pharmacokinetics and tissue

distribution of tacrolimus (FK506) after a single or repeated ocular instillation in rabbits. *J Ocul Pharmacol Ther*. 2008;24(3):309-319. doi:10.1089/jop.2007.0083

172. Kino T, Hatanaka H, Hashimoto M, et al. Fk-506, A Novel Immunosuppressant Isolated From A Streptomyces. *J Antibiot (Tokyo)*. 1987;40(9):1249-1255. doi:10.7164/antibiotics.40.1249
173. Patel P, Patel H, Mehta T, Panchal S. Formulation strategies for drug delivery of tacrolimus: An overview. *Int J Pharm Investig*. 2012;2(4):169. doi:10.4103/2230-973x.106981
174. FDA. RAPAMUNE (sirolimus) ORAL SOLUTION AND TABLETS. 1999:1-46. www.wyeth.com. Accessed July 23, 2020.
175. Sehgal VN, Srivastava G, Dogra S. Tacrolimus in dermatology - Pharmacokinetics, mechanism of action, drug interactions, dosages, and side effects: Part I. *Skinmed*. 2008;7(1):27-30. doi:10.1111/j.1540-9740.2007.06485.x
176. *RAPAMYCIN Product Number R0395 Storage Temperature-20 °C*.
177. Trasi NS, Purohit HS, Wen H, Sun DD, Taylor LS. Non-Sink Dissolution Behavior and Solubility Limit of Commercial Tacrolimus Amorphous Formulations. *J Pharm Sci*. 2017;106(1):264-272. doi:10.1016/j.xphs.2016.09.016
178. Ahmad S, Johnston BF, Mackay SP, et al. In silico modelling of drug-polymer interactions for pharmaceutical formulations. *J R Soc Interface*. 2010;7(SUPPL. 4). doi:10.1098/rsif.2010.0190.focus

179. Bukhari NI. *Quaternary Ammonium Palmitoyl Glycol Chitosan-Based Nano-Doxorubicin Delivery System: Potential Applications for Cancer Treatment and Theranostic 1 MedDocs EBooks*.; 2019. http://meddocsonline.org/. Accessed July 27, 2020.

180. Sahu A, Kasoju N, Goswami P, Bora U. Encapsulation of curcumin in Pluronic block copolymer micelles for drug delivery applications. *J Biomater Appl*. 2011;25(6):619-639. doi:10.1177/0885328209357110

181. Heaton A, Ward MK, Johnston DG, Alberti KG, Kerr DN. Evaluation of glycerol as an osmotic agent for continuous ambulatory peritoneal dialysis in end-stage renal failure. *Clin Sci (Lond)*. 1986;70(1):23-29. doi:10.1042/CS0700023

182. Lech K. High Performance Liquid Chromatography (HPLC). In: *The Encyclopedia of Archaeological Sciences*. Hoboken, NJ, USA: John Wiley & Sons, Inc.; 2018:1-7. doi:10.1002/9781119188230.saseas0303

183. 12.5: High-Performance Liquid Chromatography - Chemistry LibreTexts. https://chem.libretexts.org/Courses/Northeastern_University/12%3A_Chromatographic_and_Electrophoretic_Methods/12.5%3A_High-Performance_Liquid_Chromatography. Accessed July 24, 2020.

184. MALVERN. Zetasizer Nano Series - Performance, Simplicity, Versatility. *Malvern Instruments Ltd*. 2014:20. www.malvern.com. Accessed July 24, 2020.

185. Hoo CM, Starostin N, West P, Mecartney ML. A comparison of atomic force microscopy (AFM) and dynamic light scattering (DLS) methods to characterize nanoparticle size distributions. *J Nanoparticle Res*. 2008;10(SUPPL. 1):89-96.

doi:10.1007/s11051-008-9435-7

186. Stetefeld J, McKenna SA, Patel TR. Dynamic light scattering: a practical guide and applications in biomedical sciences. *Biophys Rev*. 2016;8(4):409-427. doi:10.1007/s12551-016-0218-6

187. Goodhew P. *Electron Microscopy and Analysis*. 2nd ed. London ;;New York: Taylor & Francis; 1988.

188. Harris JR. The future of transmission electron microscopy (TEM) in biology and medicine. *Micron*. 2000;31(1):1-3. doi:10.1016/S0968-4328(99)00059-1

189. Seesaard T, Kerdcharoen T, Wongchoosuk C. Hybrid materials with carbon nanotubes for gas sensing. In: *Semiconductor Gas Sensors*. Elsevier; 2019:185-222. doi:10.1016/B978-0-08-102559-8.00006-9

190. Bello V, Mattei G, Mazzoldi P, et al. Transmission electron microscopy of lipid vesicles for drug delivery. In: *AIP Conference Proceedings*. Vol 1275. ; 2010:166-169. doi:10.1063/1.3505070

191. Rhoades R, Bell DR. *Medical Physiology: Principles for Clinical Medicine (MEDICAL PHYSIOLOGY (RHOADES))*.; 2012. https://books.google.com.sa/books?id=tBeAeYS-vRUC&pg=PA34&dq=The+depression+of+freezing+point+compared+to+pure+water+is+direct+related+to+the+osmotic+concentration&hl=en&sa=X&ved=2ahUKEwjHwrDR5urqAhWIxqQKHewuCFEQ6AEwAnoECAMQAg#v=onepage&q=The depression o. Accessed July 26, 2020.

192. Löser A. Micro-Osmometer. 2018;814:73-90. www.loeser-osmometer.de. Accessed July 21, 2018.

193. Björn A, Segura P, Monja L, Karlsson A, Ejlertsson J, Svensson BH. *Rheological Characterization*. www.intechopen.com. Accessed January 26, 2019.

194. Rheosense. *Accurate, Fast, Microliter Sample Volume Viscometer Accuracy for Wide Dynamic Range*.; 2018. http://cdn2.hubspot.net/hub/55675/docs/m-vroc-brochure.pdf. Accessed December 5, 2018.

195. Bunaciu AA, Udriştioiu E gabriela, Aboul-Enein HY. X-Ray Diffraction: Instrumentation and Applications. *Crit Rev Anal Chem*. 2015;45(4):289-299. doi:10.1080/10408347.2014.949616

196. Nezlin A. *Handbook of Modern Pharmaceutical Analysis*. Vol 56.; 2003. doi:10.1016/s0939-6411(03)00105-x

197. Niazi S. *Stability Testing of New Drug Substances and Products*.; 2003. doi:10.3109/9781420081244-10

198. Pucci N, Caputo R, di Grande L, et al. Tacrolimus vs. cyclosporine eyedrops in severe cyclosporine-resistant vernal keratoconjunctivitis: A randomized, comparative, double-blind, crossover study. *Pediatr Allergy Immunol*. 2015;26(3):256-261. doi:10.1111/pai.12360

199. Chougule M, Padhi B, Misra A. Nano-liposomal dry powder inhaler of tacrolimus: Preparation, characterization, and pulmonary pharmacokinetics. *Int J Nanomedicine*. 2007;2(4):675-688.

200. 4 Benefits of High Pressure Homogenization. https://www.beei.com/blog/4-benefits-of-high-pressure-homogenization. Accessed August 2, 2020.

201. Miller T, Van Colen G, Sander B, et al. Drug loading of polymeric micelles.

Pharm Res. 2013;30(2):584-595. doi:10.1007/s11095-012-0903-5

202. Stetefeld J, McKenna SA, Patel TR. Dynamic light scattering: a practical guide and applications in biomedical sciences. *Biophys Rev*. 2016;8(4):409-427. doi:10.1007/s12551-016-0218-6

203. Gumustas M, Sengel-Turk CT, Gumustas A, Ozkan SA, Uslu B. Effect of Polymer-Based Nanoparticles on the Assay of Antimicrobial Drug Delivery Systems. *Multifunct Syst Comb Deliv Biosensing Diagnostics*. January 2017:67-108. doi:10.1016/B978-0-323-52725-5.00005-8

204. ICH. *ICH Topic Q 2 (R1) Validation of Analytical Procedures: Text and Methodology*.; 2006. http://www.emea.eu.int. Accessed August 17, 2020.

205. Sun M, Si L, Zhai X, et al. The influence of co-solvents on the stability and bioavailability of rapamycin formulated in self-microemulsifying drug delivery systems. *Drug Dev Ind Pharm*. 2011;37(8):986-994. doi:10.3109/03639045.2011.553618

206. Baranowski P, Karolewicz B, Gajda M, Pluta J. Ophthalmic drug dosage forms: Characterisation and research methods. *Sci World J*. 2014;2014:861904. doi:10.1155/2014/861904

207. Kim MS, Kim JS, Park HJ, Cho WK, Cha KH, Hwang SJ. Enhanced bioavailability of sirolimus via preparation of solid dispersion nanoparticles using a supercritical antisolvent process. *Int J Nanomedicine*. 2011;6:2997-3009. doi:10.2147/IJN.S26546

208. Hancock BC, Parks M. What is the True Solubility Advantage for Amorphous Pharmaceuticals? *Pharm Res*. 2000;17(4):397-404.

http://library1.nida.ac.th/termpaper6/sd/2554/19755.pdf.

209. Iyamu E, Enobakhare O. pH and Osmolality of Pre-corneal Tear Film and Commercially Available Artificial Tears. *EC Ophthalmol*. 2019;11:17-25.

210. Banik A SP. A NEW TREND: OCULAR DRUG DELIVERY SYSTEM. 2011;2(3). www.pharmasm.com. Accessed December 5, 2018.

211. Serrano DR, Lalatsa A, Dea-Ayuela MA, et al. Oral particle uptake and organ targeting drives the activity of amphotericin B nanoparticles. *Mol Pharm*. 2015;12(2):420-431. doi:10.1021/mp500527x

212. Barhoum A, García-Betancourt ML, Rahier H, Van Assche G. Physicochemical characterization of nanomaterials: Polymorph, composition, wettability, and thermal stability. In: *Emerging Applications of Nanoparticles and Architectural Nanostructures: Current Prospects and Future Trends*. Elsevier Inc.; 2018:255-278. doi:10.1016/B978-0-323-51254-1.00009-9

213. Strandvik GF. Hypertonic saline in critical care: A review of the literature and guidelines for use in hypotensive states and raised intracranial pressure. *Anaesthesia*. 2009;64(9):990-1003. doi:10.1111/j.1365-2044.2009.05986.x

214. Baenninger PB, Voegeli S, Bachmann LM, et al. Variability of tear osmolarity measurements with a point-of-care system in healthy subjects-systematic review. *Cornea*. 2018;37(7):938-945. doi:10.1097/ICO.0000000000001562

215. Linares-Alba MA, Gómez-Guajardo MB, Fonzar JF, Brooks DE, García-Sánchez GA, Bernad-Bernad MJ. Preformulation studies of a liposomal formulation containing sirolimus for the treatment of dry eye disease. *J Ocul Pharmacol Ther*. 2016;32(1):11-22. doi:10.1089/jop.2015.0032

216. Forrest ML, Won CY, Malick AW, Kwon GS. In vitro release of the mTOR inhibitor rapamycin from poly(ethylene glycol)-b-poly(ε-caprolactone) micelles. *J Control Release*. 2006;110(2):370-377. doi:10.1016/j.jconrel.2005.10.008

217. Baba K, Tanaka Y, Kubota A, et al. A method for enhancing the ocular penetration of eye drops using nanoparticles of hydrolyzable dye. *J Control Release*. 2011;153(3):278-287. doi:10.1016/j.jconrel.2011.04.019

218. Li J, Li Z, Zhou T, et al. Positively charged micelles based on a triblock copolymer demonstrate enhanced corneal penetration. *Int J Nanomedicine*. 2015;10(1):6027. doi:10.2147/IJN.S90347

219. Zhang J, Liu Z, Tao C, et al. Cationic nanoemulsions with prolonged retention time as promising carriers for ophthalmic delivery of tacrolimus. *Eur J Pharm Sci*. 2020;144(January):105229. doi:10.1016/j.ejps.2020.105229

220. Tao C, Huo T, Zhang M, Chen Z, Zhang X, Song H. Evaluation of the stability and absorption of tacrolimus self-microemulsifying drug delivery system: In Vitro/In Vivo Evaluation of FK506-SMEDDS. *J Drug Deliv Sci Technol*. 2020;57:101640. doi:10.1016/j.jddst.2020.101640

221. Ren S, Sun X, Lei T, Wu Q. The effect of chemical and high-pressure homogenization treatment conditions on the morphology of cellulose nanoparticles. *J Nanomater*. 2014;2014. doi:10.1155/2014/582913

222. Westlab. How Does Temperature Affect pH? https://www.westlab.com/blog/2017/11/15/how-does-temperature-affect-ph. Accessed August 26, 2020.

223. Joseph E, Singhvi G. Multifunctional nanocrystals for cancer therapy: A

potential nanocarrier. In: *Nanomaterials for Drug Delivery and Therapy*. Elsevier; 2019:91-116. doi:10.1016/B978-0-12-816505-8.00007-2

224. Awwad S, Mohamed Ahmed AHA, Sharma G, et al. Principles of pharmacology in the eye. *Br J Pharmacol*. 2017;174(23):4205-4223. doi:10.1111/bph.14024

225. Luaces-Rodríguez A, Touriño-Peralba R, Alonso-Rodríguez I, et al. c. *Eur J Pharm Sci*. 2018;120:152-161. doi:10.1016/j.ejps.2018.04.038

226. Molecular Envelope Technology | Nanomerics. http://www.nanomerics.com/molecular-envelope-technology. Accessed June 4, 2020.

227. Peterka TR, Lušin TT, Bergles J, Ham Z, Grahek R, Urleb U. Forced degradation of tacrolimus and the development of a UHPLC method for impurities determination. *Acta Pharm*. 2019;69(3):363-380. doi:10.2478/acph-2019-0025

228. Neves J das, Sarmento B. *Mucosal Delivery of Biopharmaceutical. Biology, Challenges and Strategies*.; 2014. https://books.google.co.uk/books?id=puu3BAAAQBAJ&pg=PA253&dq=Ananthula+HK,+Vaishya+RD,+Barot+M,+Mitra+AK.+Duane%27s+Ophthalmology.+In:+Tasman+W,+Jaeger+EA,+editors.+Bioavailability.+Philadelphia:+Lippincott+Williams+%26+Wilkins;+2009&hl=en&sa=X&ved=0ahUKE. Accessed July 22, 2018.

229. Saha P, Kim KJ, Lee VHL. A primary culture model of rabbit conjunctival epithelial cells exhibiting tight barrier properties. *Curr Eye Res*.

1996;15(12):1163-1169. doi:10.3109/02713689608995151

230. Laksitorini M, Prasasty VD, Kiptoo PK, Siahaan TJ. Pathways and progress in improving drug delivery through the intestinal mucosa and blood-brain barriers. *Ther Deliv*. 2014;5(10):1143-1163. doi:10.4155/tde.14.67

231. Ma Y, Semba S, Khan MRI, et al. Focal adhesion kinase regulates intestinal epithelial barrier function via redistribution of tight junction. *Biochim Biophys Acta - Mol Basis Dis*. 2013;1832(1):151-159. doi:10.1016/j.bbadis.2012.10.006

232. Guttman JA, Finlay BB. Tight junctions as targets of infectious agents. *Biochim Biophys Acta - Biomembr*. 2009;1788(4):832-841. doi:10.1016/j.bbamem.2008.10.028

233. Chiba H, Osanai M, Murata M, Kojima T, Sawada N. Transmembrane proteins of tight junctions. *Biochim Biophys Acta - Biomembr*. 2008;1778(3):588-600. doi:10.1016/j.bbamem.2007.08.017

234. Chen W, Hu J, Zhang Z, et al. Localization and expression of zonula occludins-1 in the rabbit corneal epithelium following exposure to benzalkonium chloride. *PLoS One*. 2012;7(7). doi:10.1371/journal.pone.0040893

235. Ghaffarian R, Muro S. Models and methods to evaluate transport of drug delivery systems across cellular barriers. *J Vis Exp*. 2013;80(80):50638. doi:10.3791/50638

236. Van Tonder A, Joubert AM, Cromarty AD. Limitations of the 3-(4,5-dimethylthiazol-2-yl)-2,5-diphenyl-2H-tetrazolium bromide (MTT) assay when compared to three commonly used cell enumeration assays. *BMC Res Notes*.

2015;8(1). doi:10.1186/s13104-015-1000-8

237. Aslantürk ÖS. In Vitro Cytotoxicity and Cell Viability Assays: Principles, Advantages, and Disadvantages. In: *Genotoxicity - A Predictable Risk to Our Actual World*. InTech; 2018. doi:10.5772/intechopen.71923

238. Mshana RN, Tadesse G, Abate G, Miörner H. Use of 3-(4,5-dimethylthiazol-2-yl)-2,5-diphenyl tetrazolium bromide for rapid detection of rifampin-resistant: Mycobacterium tuberculosis. *J Clin Microbiol*. 1998;36(5):1214-1219. doi:10.1128/jcm.36.5.1214-1219.1998

239. Mosmann T. Rapid Colorimetric Assay for Cellular Growth and Survival: Application to Proliferation and Cytotoxicity Assays. *J ofImmunologicalMethods*. 1983;65:55-63. https://ac-els-cdn-com.libproxy.ucl.ac.uk/0022175983903034/1-s2.0-0022175983903034-main.pdf?_tid=596f7d9d-698c-44b1-a43f-2556109c0cc3&acdnat=1532261640_15237f38897374bd951e3f0ab86e8d46. Accessed July 22, 2018.

240. Borner MM, Schneider E, Pirnia F, Sartor O, Trepel JB, Myers CE. *The Detergent Triton X-100 Induces a Death Pattern in Human Carcinoma Cell Lines That Resembles Cytotoxic Lymphocyte-Induced Apoptosis*. Vol 353.; 1994. https://febs.onlinelibrary.wiley.com/doi/pdf/10.1016/0014-5793%2894%2901023-4. Accessed January 29, 2019.

241. Koley D, Bard AJ. Triton X-100 concentration effects on membrane permeability of a single HeLa cell by scanning electrochemical microscopy (SECM). *Proc Natl Acad Sci U S A*. 2010;107(39):16783-16787.

doi:10.1073/pnas.1011614107

242. Odunze U. Engineering of Polymeric Nanoparticles Based on Structure-Activity Relationships (SARs) for Oral Drug Delivery. *Dr thesis, UCL (University Coll London)*. 2018;(July). http://discovery.ucl.ac.uk/10053406/.

243. López-Dávila V, Magdeldin T, Welch H, Dwek MV, Uchegbu I, Loizidou M. Efficacy of DOPE/DC-cholesterol liposomes and GCPQ micelles as AZD6244 nanocarriers in a 3D colorectal cancer in vitro model. *Nanomedicine*. 2016;11(4):331-344. doi:10.2217/nnm.15.206

244. Brown MD, Schatzlein A, Brownlie A, et al. Preliminary characterization of novel amino acid based polymeric vesicles as gene and drug delivery agents. *Bioconjug Chem*. 2000;11(6):880-891. doi:10.1021/bc000052d

245. Kean T, Roth S, Thanou M. Trimethylated chitosans as non-viral gene delivery vectors: Cytotoxicity and transfection efficiency. *J Control Release*. 2005;103(3):643-653. doi:10.1016/j.jconrel.2005.01.001

246. Wang YD, Su YJ, Li JY, Yao XC, Liang GJ. Rapamycin, a mTOR inhibitor, induced growth inhibition in retinoblastoma Y79 cell via down-regulation of Bmi-1. *Int J Clin Exp Pathol*. 2015;8(5):5182-5188. www.ijcep.com/. Accessed October 5, 2020.

247. Wang YD, Su YJ, Li JY, Yao XC, Liang GJ. Rapamycin, an mTOR inhibitor, induced apoptosis via independent mitochondrial and death receptor pathway in retinoblastoma Y79 cell. *Int J Clin Exp Med*. 2015;8(7):10723-10730.

248. Liu NN, Zhao N, Cai N. Suppression of the proliferation of hypoxia-Induced retinal pigment epithelial cell by rapamycin through the /mTOR/HIF-1α/VEGF/

signaling. *IUBMB Life*. 2015;67(6):446-452. doi:10.1002/iub.1382

249. Katiyar SS, Muntimadugu E, Rafeeqi TA, Domb AJ, Khan W. Co-delivery of rapamycin- and piperine-loaded polymeric nanoparticles for breast cancer treatment. *Drug Deliv*. 2016;23(7):2608-2616. doi:10.3109/10717544.2015.1039667

250. Haeri A, Osouli M, Bayat F, Alavi S, Dadashzadeh S. Nanomedicine approaches for sirolimus delivery: a review of pharmaceutical properties and preclinical studies. *Artif Cells, Nanomedicine Biotechnol*. 2018;46(sup1):1-14. doi:10.1080/21691401.2017.1408123

251. Din TADAAT, Seeni A, Khairi WNM, Shamsuddin S, Jaafar H. Effects of rapamycin on cell apoptosis in MCF-7 human breast cancer cells. *Asian Pacific J Cancer Prev*. 2014;15(24):10659-10663. doi:10.7314/APJCP.2014.15.24.10659

252. Milani BY, Milani FY, Park D wouk, et al. Rapamycin inhibits the production of myofibroblasts and reduces corneal scarring after photorefractive keratectomy. *Investig Ophthalmol Vis Sci*. 2013;54(12):7424-7430. doi:10.1167/iovs.13-12674

253. Highlights of Prescribing Information. FDA. www.fda.gov/medwatch. Published 2010. Accessed April 10, 2020.

254. Uchegbu I. PROJECT LICENCE APPLICATION UNDER THE ANIMALS (SCIENTIFIC PROCEDURES) ACT 1986. 2013;(70):1-51.

255. Rabinovich-Guilatt L, Couvreur P, Lambert G, Dubernet C. Cationic vectors in ocular drug delivery. *J Drug Target*. 2004;12(9-10):623-633.

doi:10.1080/10611860400015910

256. Cho MJ, Thompson DP, Cramer CT, Vidmar TJ, Scieszka JF. The Madin Darby Canine Kidney (MDCK) Epithelial Cell Monolayer as a Model Cellular Transport Barrier. *Pharm Res An Off J Am Assoc Pharm Sci*. 1989;6(1):71-77. doi:10.1023/A:1015807904558

257. Rothen-Rutishauser B, Krämer SD, Braun A, Günthert M, Wunderli-Allenspach H. MDCK cell cultures as an epithelial in vitro model: Cytoskeleton and tight junctions as indicators for the definition of age-related stages by confocal microscopy. *Pharm Res*. 1998;15(7):964-971. doi:10.1023/A:1011953405272

258. Ranaldi G, Seneci P, Guba W, Islam K, Sambuy Y. Transport of the antibacterial agent oxazolidin-2-one and derivatives across intestinal (Caco-2) and renal (MDCK) epithelial cell lines. *Antimicrob Agents Chemother*. 1996;40(3):652-658. http://www.ncbi.nlm.nih.gov/pubmed/8851588. Accessed July 23, 2018.

259. Irvine JD, Takahashi L, Lockhart K, et al. MDCK (Madin-Darby canine kidney) cells: A tool for membrane permeability screening. *J Pharm Sci*. 1999;88(1):28-33. doi:10.1021/js9803205

260. Dey S, Gunda S, Mitra AK. Pharmacokinetics of Erythromycin in Rabbit Corneas after Single-Dose Infusion: Role of P-Glycoprotein as a Barrier to in Vivo Ocular Drug Absorption. *J Pharmacol Exp Ther*. 2004;311(1):246-255. doi:10.1124/jpet.104.069583

261. Tak R V., Pal D, Gao H, Dey S, Mitra AK. Transport of acyclovir ester prodrugs

through rabbit cornea and SIRC-rabbit corneal epithelial cell line. *J Pharm Sci*. 2001;90(10):1505-1515. doi:10.1002/jps.1101

262. Hsu CM, Chiang STH, Chang YY, et al. Lychee flower extract inhibits proliferation and viral replication of HSV-1-infected corneal epithelial cells. *Mol Vis*. 2016;22:129-137. http://www.molvis.org/molvis/v22/129. Accessed December 14, 2018.

263. Hutak CM, Kavanagh ME, Reddy IK, Barletta MA. Growth pattern of SIRC rabbit corneal cells in microwell inserts. *J Toxicol - Cutan Ocul Toxicol*. 1997;16(3):145-156. doi:10.3109/15569529709048892

264. Srinivasan B, Kolli AR, Esch MB, Abaci HE, Shuler ML, Hickman JJ. TEER Measurement Techniques for In Vitro Barrier Model Systems. *J Lab Autom*. 2015;20(2):107-126. doi:10.1177/2211068214561025

265. Ye D, Dawson KA, Lynch I. A TEM protocol for quality assurance of in vitro cellular barrier models and its application to the assessment of nanoparticle transport mechanisms across barriers. *Analyst*. 2015;140(1):83-97. doi:10.1039/c4an01276c

266. Krug SM, Amasheh M, Dittmann I, Christoffel I, Fromm M, Amasheh S. Sodium caprate as an enhancer of macromolecule permeation across tricellular tight junctions of intestinal cells. *Biomaterials*. 2013;34(1):275-282. doi:10.1016/j.biomaterials.2012.09.051

267. Ranaldi G, Islam K, SAMBUYI Y, Nazionale della Nutrizione I. Epithelial Cells in Culture as a Model for the Intestinal Transport of Antimicrobial Agents. *Antimicrob Agents Chemother*. 1992;36(7):1374-1381. http://aac.asm.org/.

Accessed July 23, 2018.

268. Somaiah C, Kumar A, Mawrie D, et al. Collagen Promotes Higher Adhesion, Survival and Proliferation of Mesenchymal Stem Cells. 2015. doi:10.1371/journal.pone.0145068

269. Watson C, Mahe M, Helmrath M. In vivo Fluorescein Isothiocyanate-dextran (FD4) Permeability Assay. *BIO-PROTOCOL*. 2015;5(20). doi:10.21769/BioProtoc.1618

270. Palumbo P, Picchini U, Beck B, Van Gelder J, Delbar N, DeGaetano A. A general approach to the apparent permeability index. *J Pharmacokinet Pharmacodyn*. 2008;35(2):235-248. doi:10.1007/s10928-008-9086-4

271. Lugovtsev VY, Melnyk D, Weir JP. Heterogeneity of the MDCK Cell Line and Its Applicability for Influenza Virus Research. *PLoS One*. 2013;8(9):75014. doi:10.1371/journal.pone.0075014

272. Abelson MB, Udell IJ, Weston JH. Normal Human Tear pH by Direct Measurement. *Arch Ophthalmol*. 1981;99(2):301-301. doi:10.1001/archopht.1981.03930010303017

273. Olejnik A, Marecik R, Skrzypczak M, Czaczyk K, Grajek W. Application of rapid caco-2 cell culture system in the studies on the Bacterial Adhesion and Transepithelial Transport. *Pol J Food Nutr Sci*. 2008;58(3):365-371.

274. Lindmark T, Söderholm JD, Olaison G, Alván G, Ocklind G, Artursson P. Mechanism of Absorption Enhancement in Humans After Rectal Administration of Ampicillin in Suppositories Containing Sodium Caprate. *Pharm Res*. 1997;14:930-935.

275. Stuart R 0, Nigam SK. *Regulated Assembly of Tight Junctions by Protein Kinase C*. Vol 92.; 1995. https://www.ncbi.nlm.nih.gov/pmc/articles/PMC41644/pdf/pnas01489-0320.pdf. Accessed February 2, 2019.

276. Hayashi M, Sakai T, Hasegawa Y, et al. Physiological mechanism for enhancement of paracellular drug transport. *J Control Release*. 1999;62(1-2):141-148. http://www.ncbi.nlm.nih.gov/pubmed/10518645. Accessed February 2, 2019.

277. Kowapradit J, Opanasopit P, Ngawhirunpat T, Rojanarata T, Ruktanonchai U, Sajomsang W. Methylated N-(4-N,N-dimethylaminocinnamyl) chitosan enhances paracellular permeability across Caco-2 cells. *Drug Deliv*. 2010;17(5):301-312. doi:10.3109/10717541003706273

278. Wang L, Ding L, Du Z, Liu J. Effects of hydrophobicity and molecular weight on the transport permeability of oligopeptides across Caco-2 cell monolayers. *J Food Biochem*. 2020;44(5). doi:10.1111/jfbc.13188

279. Artursson P, Lindmark T, Davis SS, Illum L. Effect of chitosan on the permeability of monolayers of intestinal epithelial cells (Caco-2). *Pharm Res*. 1994;11(9):1358-1361. doi:10.1023/A:1018967116988

280. Cheng WP, Gray AI, Tetley L, Hang TLB, Schätzlein AG, Uchegbu IF. Polyelectrolyte nanoparticles with high drug loading enhance the oral uptake of hydrophobic compounds. *Biomacromolecules*. 2006;7(5):1509-1520. doi:10.1021/bm060130l

281. Odunze U. Engineering of Polymeric Nanoparticles Based on Structure-

Activity Relationships (SARs) for Oral Drug Delivery. *Un-published*. 2018;(July).

282. Kaiser M, Pereira S, Pohl L, et al. Chitosan encapsulation modulates the effect of capsaicin on the tight junctions of MDCK cells. *Sci Rep*. 2015;5(1):1-14. doi:10.1038/srep10048

283. Wang J, Kong M, Zhou Z, et al. Mechanism of surface charge triggered intestinal epithelial tight junction opening upon chitosan nanoparticles for insulin oral delivery. *Carbohydr Polym*. 2017;157:596-602. doi:10.1016/j.carbpol.2016.10.021

284. Malatesta M, Grecchi S, Chiesa E, Cisterna B, Costanzo M, Zancanaro C. Internalized chitosan nanoparticles persist for long time in cultured cells. *[European J Histochem*. 2015;59:61-65. doi:10.4081/ejh.2015.2492

285. Thanou M, Kotze A, Scharringhausen T, Lueßen H. Effect of degree of quaternization of N-trimethyl chitosan chloride for enhanced transport of hydrophilic compounds across intestinal Caco-2 cell monolayers. *J Control Release*. 2000;64:15-25. https://ac-els-cdn-com.libproxy.ucl.ac.uk/S0168365999001315/1-s2.0-S0168365999001315-main.pdf?_tid=05d83fa7-1861-474c-a6d9-005e9875fa7a&acdnat=1544795747_571ecea8edb36ae9abbac16afb3c51e4. Accessed December 14, 2018.

286. Hsu L, Ho Y, Chuang E, Chen C, Juang J. Effects of pH on molecular mechanisms of chitosan-integrin interactions and resulting tight-junction disruptions . *Biomaterials*. 2018;34(3):23103155.

doi:10.1016/j.biomaterials.2012.09.082

287. Goskonda VR, Khan MA, Hutak CM, Reddy IK. Permeability characteristics of novel mydriatic agents using an in vitro cell culture model that utilizes Sirc rabbit corneal cells. *J Pharm Sci*. 1999;88(2):180-184. doi:10.1021/js980362t

288. Heino J. The collagen family members as cell adhesion proteins. *BioEssays*. 2007;29(10):1001-1010. doi:10.1002/bies.20636

289. Becker U, Ehrhardt C, Schneider M, et al. A comparative evaluation of corneal epithelial cell cultures for assessing ocular permeability. *ATLA Altern to Lab Anim*. 2008;36(1):33-44. doi:10.1177/026119290803600106

290. Malh Otra & D K M Aj Umdar M. *Permeation through Cornea*. Vol 39. https://pdfs.semanticscholar.org/9225/d9cf2c6a2e3701c8cc498d6d0633084e82ae.pdf. Accessed December 17, 2018.

291. Olivieri M, Cristaldi M, Pezzino S, et al. Phenotypic characterization of the SIRC (Statens Seruminstitut Rabbit Cornea) cell line reveals a mixed epithelial and fibroblastic nature. *Exp Eye Res*. 2018;172(April):123-127. doi:10.1016/j.exer.2018.04.004

292. Tscheik C, Blasig I, Winkler L. Trends in drug delivery through tissue barriers containing tight junctions. *Tissue Barriers*. 2013. doi:10.4161/tisb.24565

293. Sugibayashi K, Onuki Y, Takayama K. Displacement of tight junction proteins from detergent-resistant membrane domains by treatment with sodium caprate. *Eur J Pharm Sci*. 2009;36(2-3):246-253. doi:10.1016/j.ejps.2008.09.011

294. Al-Sadi R, Khatib K, Guo S, Ye D, Youssef M, Ma T. Occludin regulates

macromolecule flux across the intestinal epithelial tight junction barrier. *Am J Physiol Gastrointest Liver Physiol*. 2011;300(6):G1054-64. doi:10.1152/ajpgi.00055.2011

295. Varela-Fernández R, Díaz-Tomé V, Luaces-Rodríguez A, et al. Drug delivery to the posterior segment of the eye: Biopharmaceutic and pharmacokinetic considerations. *Pharmaceutics*. 2020;12(3):1-39. doi:10.3390/pharmaceutics12030269
296. Bochot A, Fattal E. Liposomes for intravitreal drug delivery: A state of the art. *J Control Release*. 2012;161(2):628-634. doi:10.1016/j.jconrel.2012.01.019
297. Patel A, Cholkar K, Agrahari V, Mitra AK. Ocular drug delivery systems: An overview. *World J Pharmacol*. 2013;2(2):47-64. doi:10.5497/wjp.v2.i2.47
298. Kim SH, Lutz RJ, Wang NS, Robinson MR. Transport barriers in transscleral drug delivery for retinal diseases. *Ophthalmic Res*. 2007;39(5):244-254. doi:10.1159/000108117
299. Bourlais CL, Acar L, Zia H, Sado PA, Needham T, Leverge R. Ophthalmic drug delivery systems--recent advances. *Prog Retin Eye Res*. 1998;17(1):33-58. http://www.ncbi.nlm.nih.gov/pubmed/9537794. Accessed December 3, 2018.
300. Rodrigues GA, Lutz D, Shen J, et al. Topical Drug Delivery to the Posterior Segment of the Eye: Addressing the Challenge of Preclinical to Clinical Translation. *Pharm Res*. 2018;35(12). doi:10.1007/s11095-018-2519-x
301. Gwon A. Animal Models in Eye Research. In: *Animal Models in Eye Research*. ; 2008:184-204. doi:10.1016/B978-0-12-374169-1.00013-8
302. US9446026B2 - Ocular formulations for drug-delivery to the posterior segment

of the eye - Google Patents. https://patents.google.com/patent/US9446026B2/en. Accessed April 9, 2020.

303. Platania C, V, Fisichella, A F, F G. Delivery of TGF-β1 to the Back of the Eye: Implications in Age-Related Neurodegenerative Diseases. *Int J Mol Sci*. 2017;18(2076).

304. Earla R, Cholkar K, Gunda S, Earla R, Mitra AK. Bioanalytical method validation of rapamycin in ocular matrix by QTRAP LC–MS/MS: Application to rabbit anterior tissue distribution by topical administration of rapamycin nanomicellar formulation. *J Chromatogr B Anal Technol Biomed Life Sci*. 2012:76-86. doi:10.1111/j.1743-6109.2008.01122.x.Endothelial

305. Benichou G, Sharma A, Casiraghi F, et al. Rapamycin Nano-Micelle Ophthalmic Solution Reduces Corneal Allograft Rejection by Potentiating Myeloid-Derived Suppressor Cells' Function. *Front Immunol | www.frontiersin.org*. 2018;9:2283. doi:10.3389/fimmu.2018.02283

306. Nguyen QD, Merrill PT, Sepah YJ, et al. Intravitreal Sirolimus for the Treatment of Noninfectious Uveitis: Evolution through Preclinical and Clinical Studies. *Ophthalmology*. 2018;125(12):1984-1993. doi:10.1016/j.ophtha.2018.06.015

307. Dejneka NS, Kuroki AM, Fosnot J, Tang W, Tolentino MJ, Bennett J. Systemic rapamycin inhibits retinal and choroidal neovascularization in mice. *Mol Vis*. 2004;10:964-972. http://www.ncbi.nlm.nih.gov/pubmed/15623986. Accessed January 26, 2019.

308. Krishnadev N, Forooghian F, Cukras C, et al. Subconjunctival sirolimus in the treatment of diabetic macular edema. *Graefes Arch Clin Exp Ophthalmol*.

2011;249(11):1627-1633. doi:10.1007/s00417-011-1694-9

309. Shah M, Edman MC, Janga SR, et al. Rapamycin eye drops suppress lacrimal gland inflammation in a murine model of sjögren's syndrome. *Investig Ophthalmol Vis Sci*. 2017;58(1):372-385. doi:10.1167/iovs.16-19159

310. Nguyen QD, Ibrahim MA, Watters A, et al. Ocular tolerability and efficacy of intravitreal and subconjunctival injections of sirolimus in patients with non-infectious uveitis: Primary 6-month results of the SAVE Study. *J Ophthalmic Inflamm Infect*. 2013;3(1):1-15. doi:10.1186/1869-5760-3-32

311. Zhang Z. Retention Time Alignment of LC/MS Data by a Divide-and-Conquer Algorithm. *J Am Soc Mass Spectrom*. 2012;23:764-772. doi:10.1007/s13361-011-0334-2

312. Guideline on bioanalytical method validation. 2012;44(July 2011):1-23.

313. *Bioanalytical Method Validation Guidance for Industry*.; 2018. http://www.fda.gov/Drugs/GuidanceComplianceRegulatoryInformation/Guidances/default.htmand/orhttp://www.fda.gov/AnimalVeterinary/GuidanceComplianceEnforcement/GuidanceforIndustry/default.htm. Accessed November 29, 2020.

314. Kruve A, Kaupmees K. Adduct Formation in ESI/MS by Mobile Phase Additives. *J Am Soc Mass Spectrom*. 2017;28(5):887-894. doi:10.1007/s13361-017-1626-y

315. Guan F, Uboh C, Soma L, Hess A, Luo Y, Tsang DS. Sensitive liquid chromatographic/tandem mass spectrometric method for the determination of beclomethasone dipropionate and its metabolites in equine plasma and urine.

J Mass Spectrom. 2003;38(8):823-838. doi:10.1002/jms.495

316. Mortier K, Zhang G, Peteghem C, Lambert W. Adduct Formation in Quantitative Bioanalysis: Effect of Ionization Conditions on Paclitaxel. *J Am Soc Mass Spectrom*. 2004;15:585-592. https://ac.els-cdn.com/S1044030504000042/1-s2.0-S1044030504000042-main.pdf?_tid=d78676e6-ec9b-4863-9525-7940cd199a23&acdnat=1544533646_1de9895bfd21681c9bdc3ded0366d514. Accessed December 11, 2018.
317. Jurchen JC, Cooper RE, Williams ER. *The Role of Acidic Residues and of Sodium Ion Adduction on the Gas-Phase H/D Exchange of Peptides and Peptide Dimers NIH Public Access*. Vol 14.; 2003.
318. Pierrot-Deseilligny C. Effect of gravity on vertical eye position. In: *Annals of the New York Academy of Sciences*. Vol 1164. Blackwell Publishing Inc.; 2009:155-165. doi:10.1111/j.1749-6632.2009.03864.x
319. Ham BM, Cole RB, Jacob JT. Identification and comparison of the polar phospholipids in normal and dry eye rabbit tears by MALDI-TOF mass spectrometry. *Investig Ophthalmol Vis Sci*. 2006;47(8):3330-3338. doi:10.1167/iovs.05-0756
320. Chrai SS, Patton TF, Mehta A, Robinson JR. Lacrimal and Instilled Fluid Dynamics in Rabbit Eyes. *J Pharm Sci*. 1973;62(7):1112-1121. doi:10.1002/jps.2600620712
321. Toze TN, Rowland M. Introduction to Pharmacokinetics and Pharmacodynamics: The Quantitative ... - Thomas N. Tozer, Malcolm

Rowland - Google Books. Lippincott Williams and Wilkins. https://books.google.co.uk/books?id=DO-7q2Vzz-AC&pg=PA275&dq=area+of+a+trapezoid+rule+malcolm&hl=en&sa=X&ved=0ahUKEwjoyrrH5s7oAhUMilwKHa67BoAQ6AEIKDAA#v=onepage&q=area of a trapezoid rule malcolm&f=false. Published 2006. Accessed April 4, 2020.

322. Valentine JL, Shyu WC, Grossman SJ. The Application of ADME Principles in Pharmaceutical Safety Assessment. In: *Comprehensive Toxicology: Second Edition*. Vol 1-14. Elsevier Inc.; 2010:123-136. doi:10.1016/B978-0-08-046884-6.00106-8

323. Hughes PM, Olejnik O, Chang-Lin JE, Wilson CG. Topical and systemic drug delivery to the posterior segments. *Adv Drug Deliv Rev*. 2005;57(14 SPEC. ISS.):2010-2032. doi:10.1016/j.addr.2005.09.004

324. Emoto C, Fukuda T, Cox S, Christians U, Vinks AA. Development of a physiologically-based pharmacokinetic model for sirolimus: Predicting bioavailability based on intestinal CYP3A content. *CPT Pharmacometrics Syst Pharmacol*. 2013;2(7). doi:10.1038/psp.2013.33

325. Cochereau-Massin I, Bauchet J, Faurisson F, Vallois JM, Lacombe P, Pocidalo JJ. Ocular kinetics of pefloxacin after intramuscular administration in albino and pigmented rabbits. *Antimicrob Agents Chemother*. 1991;35(6):1112-1115. doi:10.1128/AAC.35.6.1112

326. Ahmed I, Patton TF. Importance of the noncorneal absorption route in topical ophthalmic drug delivery. *Investig Ophthalmol Vis Sci*. 1985;26(4):584-587.

327. Kalam MA, Alshamsan A. Poly (D, L-lactide-co-glycolide) nanoparticles for

sustained release of tacrolimus in rabbit eyes. *Biomed Pharmacother*. 2017;94:402-411. doi:10.1016/j.biopha.2017.07.110

328. Kaminer J, Powers AS, Horn KG, Hui C, Evinger C. Characterizing the spontaneous blink generator: An animal model. *J Neurosci*. 2011;31(31):11256-11267. doi:10.1523/JNEUROSCI.6218-10.2011
329. Whittaker AL, Williams DL. Evaluation of Lacrimation Characteristics in Clinically Normal New Zealand White Rabbits by Using the Schirmer Tear Test I. *J Am Assoc Lab Anim Sci*. 2015;54(6):783-787.
330. Ikoma N, Raghav K, Chang G. An Update on Randomized Clinical Trials in Metastatic Colorectal Carcinoma. *Surg Oncol Clin N Am*. 2017;26(4):667-687. doi:10.1016/j.soc.2017.05.007
331. Stanca H, Stanca S, Tabacaru B, Boruga M, Balta F. Bevacizumab in Wet AMD treatment: A tribute to the thirteen years of experience from the beginning of the anti-VEGF era in Romania. *Exp Ther Med*. 2019;18(6):4993-5000. doi:10.3892/etm.2019.7858
332. Prete M, Dammacco R, Fatone MC, Racanelli V. Autoimmune uveitis: clinical, pathogenetic, and therapeutic features. *Clin Exp Med*. 2016;16(2):125-136. doi:10.1007/s10238-015-0345-6
333. Dick AD. Retinal antigen-specific t cells mediate experimental autoimmune uveoretinitis (EAU) in PVG rat a model for tracking antigen-specific CD4+ t cells in the inflamed Eye. *Ocul Immunol Inflamm*. 1995;3(4):261-270. doi:10.3109/09273949509069120
334. Boldison J, Chu CJ, Copland DA, et al. Tissue-Resident Exhausted Effector

Memory CD8 + T Cells Accumulate in the Retina during Chronic Experimental Autoimmune Uveoretinitis. *J Immunol*. 2014;192(10):4541-4550. doi:10.4049/jimmunol.1301390

335. Eskandarpour M, Alexander R, Adamson P, Calder VL. Pharmacological Inhibition of Bromodomain Proteins Suppresses Retinal Inflammatory Disease and Downregulates Retinal Th17 Cells. *J Immunol*. 2017;198(3):1093-1103. doi:10.4049/jimmunol.1600735
336. Agarwal RK, Caspi RR. Rodent models of experimental autoimmune uveitis. *Methods Mol Med*. 2012;900:443-469. doi:10.1007/978-1-60761-720-4_22
337. Gardner PJ, Joshi L, Lee RWJ, Dick AD, Adamson P, Calder VL. SIRT1 activation protects against autoimmune T cell-driven retinal disease in mice via inhibition of IL-2/Stat5 signaling. *J Autoimmun*. 2013;42:117-129. doi:10.1016/j.jaut.2013.01.011
338. Caspi RR. Experimental Autoimmune Uveoretinitis in the Rat and Mouse. *Curr Protoc Immunol*. 2003;53(1). doi:10.1002/0471142735.im1506s53
339. Uy HS, Yu-Keh E, Chan PS. Posterior uveitis. *Dev Ophthalmol*. 2015;55:163-166. doi:10.1159/000438968
340. Luo L, Yang J, Oh Y, et al. Controlled release of corticosteroid with biodegradable nanoparticles for treating experimental autoimmune uveitis. *J Control Release*. 2019;296:68-80. doi:10.1016/j.jconrel.2019.01.018
341. FDA's acceptance of Santen's Opsiria marks a milestone for the company. https://www.pharmaceutical-technology.com/comment/commentfdas-acceptance-of-santens-opsiria-marks-a-milestone-for-the-company-

5802460/. Accessed April 18, 2020.

342. Powell JD, Delgoffe GM. The Mammalian Target of Rapamycin: Linking T Cell Differentiation, Function, and Metabolism. *Immunity*. 2010;33(3):301-311. doi:10.1016/j.immuni.2010.09.002

343. Li J, Kim SG, Blenis J. Rapamycin: one drug, many effects. *Cell Metab*. 2014;19(3):373–379. doi:10.1016/j.cmet.2014.01.001

344. Shanmuganathan VA, Casely EM, Raj D, et al. The efficacy of sirolimus in the treatment of patients with refractory uveitis. *Br J Ophthalmol*. 2005;89(6):666-669. doi:10.1136/bjo.2004.048199

345. Gilbert RM, Zhang X, Sampson RD, et al. Clinical remission of sight-threatening non-infectious uveitis is characterized by an upregulation of peripheral T-regulatory cell polarized towards T-bet and TIGIT. *Front Immunol*. 2018;9(MAY):907. doi:10.3389/fimmu.2018.00907

346. Nida Sen H, Larson TA, Meleth AD, Smith WM, Nussenblatt RB. Subconjunctival sirolimus for the treatment of chronic active anterior uveitis: Results of a pilot trial. *Am J Ophthalmol*. 2012;153(6):1038-1042. doi:10.1016/j.ajo.2011.12.018

347. The Association for Research in Vision and Ophthalmology- Statement for the Use of Animals in Ophthalmic and Vision Research. https://www.arvo.org/About/policies/statement-for-the-use-of-animals-in-ophthalmic-and-vision-research/. Accessed March 21, 2020.

348. Zhang P, Zam A, Pugh EN, Zawadzki RJ. Evaluation of state-of-the-art imaging systems for in vivo monitoring of retinal structure in mice: current

capabilities and limitations. In: *Ophthalmic Technologies XXIV*. Vol 8930. SPIE; 2014:1-9. doi:10.1117/12.2040964

349. Akanni E, Palini A. Immunophenotyping of Peripheral Blood and Bone Marrow Cells by Flow Cytometry. *EJIFCC*. 2006;17:17-21.
350. Flow cytometry immunophenotyping | Abcam. https://www.abcam.com/protocols/flow-cytometry-immunophenotyping. Accessed March 22, 2020.
351. Picot J, Guerin CL, Le Van Kim C, Boulanger CM. Flow cytometry: Retrospective, fundamentals and recent instrumentation. *Cytotechnology*. 2012;64(2):109-130. doi:10.1007/s10616-011-9415-0
352. What is flow cytometry (FACS analysis)? https://www.antibodies-online.com/resources/17/1247/what-is-flow-cytometry-facs-analysis/. Accessed March 23, 2020.
353. Chaim M. Roifman. Interleukin 2 Receptor Gamma - an overview | ScienceDirect Topics. https://www.sciencedirect.com/topics/medicine-and-dentistry/interleukin-2-receptor-alpha. Accessed May 8, 2020.
354. Castro G, Liu X, Ngo K, et al. RORγt and RORα signature genes in human Th17 cells. *PLoS One*. 2017;12(8). doi:10.1371/journal.pone.0181868
355. Sun D, Liang D, Kaplan HJ, Shao H. The role of Th17-associated cytokines in the pathogenesis of experimental autoimmune uveitis (EAU). *Cytokine*. 2015;74(1):76-80. doi:10.1016/j.cyto.2014.12.017
356. Joean O, Hueber A, Feller F, et al. Suppression of Th17-polarized airway inflammation by rapamycin. *Sci Rep*. 2017;7(1):1-13. doi:10.1038/s41598-

017-15750-6

357. Dorfman DM, Hwang ES, Shahsafaei A, Glimcher LH. T-bet, a T cell-associated transcription factor, is expressed in Hodgkin's lymphoma. *Hum Pathol*. 2005;36(1):10-15. doi:10.1016/j.humpath.2004.10.006

358. Shoda H, Yanai R, Yoshimura T, et al. Dietary omega-3 fatty acids suppress experimental autoimmune uveitis in association with inhibition of Th1 and Th17 cell function. Schunck W-H, ed. *PLoS One*. 2015;10(9):e0138241. doi:10.1371/journal.pone.0138241

359. Liu X, Gao N, Li M, et al. Elevated Levels of CD4+CD25+FoxP3+ T Cells in Systemic Sclerosis Patients Contribute to the Secretion of IL-17 and Immunosuppression Dysfunction. *PLoS One*. 2013;8(6). doi:10.1371/journal.pone.0064531

360. Lu Y, Wang J, Gu J, et al. Rapamycin regulates iTreg function through CD39 and Runx1 pathways. *J Immunol Res*. 2014;2014. doi:10.1155/2014/989434

361. Adeegbe DO, Nishikawa H. Natural and induced T regulatory cells in cancer. *Front Immunol*. 2013;4(JUL). doi:10.3389/fimmu.2013.00190

362. Zhao H, Liao X, Kang Y. Tregs: Where we are and what comes next? *Front Immunol*. 2017;8(NOV):1. doi:10.3389/fimmu.2017.01578

363. Jäger A, Kuchroo VK. Effector and regulatory T-cell subsets in autoimmunity and tissue inflammation. *Scand J Immunol*. 2010;72(3):173-184. doi:10.1111/j.1365-3083.2010.02432.x

364. Long SA, Buckner JH. CD4 + FOXP3 + T Regulatory Cells in Human Autoimmunity: More Than a Numbers Game. *J Immunol*. 2011;187(5):2061-

2066. doi:10.4049/jimmunol.1003224

365. Battaglia M, Stabilini A, Migliavacca B, Horejs-Hoeck J, Kaupper T, Roncarolo M-G. Rapamycin Promotes Expansion of Functional CD4 + CD25 + FOXP3 + Regulatory T Cells of Both Healthy Subjects and Type 1 Diabetic Patients. *J Immunol*. 2006;177(12):8338-8347. doi:10.4049/jimmunol.177.12.8338

366. Battaglia M, Stabilini A, Roncarolo MG. Rapamycin selectively expands CD4+CD25+FoxP3 + regulatory T cells. *Blood*. 2005;105(12):4743-4748. doi:10.1182/blood-2004-10-3932

367. Stallone G, Infante B, Lorenzo A Di, Rascio F, Zaza G, Grandaliano G. mTOR inhibitors effects on regulatory T cells and on dendritic cells. *J Transl Med*. 2016;14(1):152. doi:10.1186/s12967-016-0916-7

368. Mérida S, Palacios E, Navea A, Bosch-Morell F. New immunosuppressive therapies in uveitis treatment. *Int J Mol Sci*. 2015;16(8):18778-18795. doi:10.3390/ijms160818778

369. Nguyen QD, Merrill PT, Clark WL, et al. Intravitreal Sirolimus for Noninfectious Uveitis: A Phase III Sirolimus Study Assessing Double-masKed Uveitis TReAtment (SAKURA). In: *Ophthalmology*. Vol 123. ; 2016:2413-2423. doi:10.1016/j.ophtha.2016.07.029

370. Zhang Z, Wu X, Duan J, et al. Low dose rapamycin exacerbates autoimmune experimental uveitis. *PLoS One*. 2012;7(5). doi:10.1371/journal.pone.0036589

371. Singh K, Axelrod S, Bielory L. The epidemiology of ocular and nasal allergy in the United States, 1988-1994. *J Allergy Clin Immunol*. 2010;126(4).

doi:10.1016/j.jaci.2010.06.050

372. Duke RE, Adio A, Oparah SK, Odey F, Eyo OA. Evaluation of a Public Child Eye Health Tertiary Facility for Pediatric Cataract in Southern Nigeria I: Visual Acuity Outcome. *Open Ophthalmol J*. 2016;10(1):119-125. doi:10.2174/1874364101610010119

373. Dogru M, Nakagawa N, Tetsumoto K, Katakami C, Yamamoto M. Ocular surface disease in atopic dermatitis. *Jpn J Ophthalmol*. 1999;43(1):53-57. doi:10.1016/S0021-5155(98)00061-6

374. Thomson AW, Bonham CA, Zeevi A. Mode of action of tacrolimus (fk506): Molecular and cellular mechanisms. *Ther Drug Monit*. 1995;17(6):584-591. doi:10.1097/00007691-199512000-00007

375. Zhai J, Gu J, Yuan J, Chen J. Tacrolimus in the treatment of ocular diseases. *BioDrugs*. 2011;25(2):89-103. doi:10.2165/11587010-000000000-00000

376. Sengoku T, Kishi S, Sakuma S, Ohkubo Y, Goto T. FK506 inhibition of histamine release and cytokine production by mast cells and basophils. *Int J Immunopharmacol*. 2000;22(3):189-201. doi:10.1016/S0192-0561(99)00076-4

377. Ohashi Y, Ebihara N, Fujishima H, et al. A randomized, placebo-controlled clinical trial of tacrolimus ophthalmic suspension 0.1% in severe allergic conjunctivitis. *J Ocul Pharmacol Ther*. 2010;26(2):165-173. doi:10.1089/jop.2009.0087

378. Fukushima A, Ohashi Y, Ebihara N, et al. Therapeutic effects of 0.1% tacrolimus eye drops for refractory allergic ocular diseases with proliferative

lesion or corneal involvement. *Br J Ophthalmol*. 2014;98(8):1023-1027. doi:10.1136/bjophthalmol-2013-304453

379. Kheirkhah A, Zavareh MK, Farzbod F, Mahbod M, Behrouz MJ. Topical 0.005% tacrolimus eye drop for refractory vernal keratoconjunctivitis. *Eye*. 2011;25(7):872-880. doi:10.1038/eye.2011.75
380. Shoughy SS, Jaroudi MO, Tabbara KF. Efficacy and safety of low-dose topical tacrolimus in vernal keratoconjunctivitis. *Clin Ophthalmol*. 2016;10:643-647. doi:10.2147/OPTH.S99157
381. Takamura E, Uchio E, Ebihara N, et al. Japanese guidelines for allergic conjunctival diseases 2017. *Allergol Int*. 2017;66(2):220-229. doi:10.1016/j.alit.2016.12.004
382. Talymus Product Information Sheet. https://www.rad-ar.or.jp/siori/english/kekka.cgi?n=1714. Published 2014. Accessed August 8, 2020.
383. Ebihara N, Ohashi Y, Fujishima H, et al. Blood level of tacrolimus in patients with severe allergic conjunctivitis treated by 0.1% tacrolimus ophthalmic suspension. *Allergol Int*. 2012;61(2):275-282. doi:10.2332/allergolint.11-OA-0349
384. Tacrolimus (FK506) [104987-11-3] Generon. https://www.generon.co.uk/other-products-186/tacrolimus-fk506-104987-11-3-182005040.html. Accessed April 4, 2020.
385. Siegl C, König-Schuster M, Nakowitsch S, et al. Pharmacokinetics of topically applied tacrolimus dissolved in Marinosolv, a novel aqueous eye drop

formulation. *Eur J Pharm Biopharm*. 2019;134(July 2018):88-95. doi:10.1016/j.ejpb.2018.11.015

386. Nourry H, Viard C, Cambourieu C, Warnet J. A relevant choice for corticoid eye drops: solution or suspension? *J Fr Ophtalmol*. 2011;34(10):691-696. https://www.ncbi.nlm.nih.gov/pubmed/22001623. Accessed April 5, 2020.
387. Taylor PJ, Jones A, Balderson GA, Lynch S V., Norris RLG, Pond SM. Sensitive, specific quantitative analysis of tacrolimus (FK506) in blood by liquid chromatography-electrospray tandem mass spectrometry. *Clin Chem*. 1996;42(2):279-285.
388. Robles-Piedras AL, González-López EH. Tacrolimus levels in adult patients with renal transplant. *Proc West Pharmacol Soc*. 2009;52:33-34. http://www.ncbi.nlm.nih.gov/pubmed/22128417. Accessed February 21, 2019.
389. Lebwohl M, Gower T. A safety assessment of topical calcineurin inhibitors in the treatment of atopic dermatitis. *MedGenMed Medscape Gen Med*. 2006;8(4):8. /pmc/articles/PMC1868387/?report=abstract. Accessed December 1, 2020.
390. Elias PM. An appropriate response to the black-box warning: Corrective, barrier repair therapy in atopic dermatitis. In: *Hong Kong Journal of Dermatology and Venereology*. Vol 17. ; 2009:104-105.
391. Hecq J, Siepmann F, Siepmann J, Amighi K, Goole J. Development and evaluation of chitosan and chitosan derivative nanoparticles containing insulin for oral administration. *Drug Dev Ind Pharm*. 2015;41(12):2037-2044. doi:10.3109/03639045.2015.1044904

392. Kanwal U, Bukhari NI, Rana NF, et al. Doxorubicin-loaded quaternary ammonium palmitoyl glycol chitosan polymeric nanoformulation: Uptake by cells and organs. *Int J Nanomedicine*. 2019;14:1-15. doi:10.2147/IJN.S176868

393. Carlisle RT, Digiovanni J. Differential diagnosis of the swollen red eyelid. *Am Fam Physician*. 2015;92(2):106-112.

394. Toshida H, Nguyen DH, Beuerman RW, Murakami A. Neurologic evaluation of acute lacrimomimetic effect of cyclosporine in an experimental rabbit dry eye model. *Investig Ophthalmol Vis Sci*. 2009;50(6):2736-2741. doi:10.1167/iovs.08-1880

395. Bentivoglio AR, Bressman SB, Cassetta E, Carretta D, Tonali P, Albanese A. Analysis of blink rate patterns in normal subjects. *Mov Disord*. 1997;12(6):1028-1034. doi:10.1002/mds.870120629

396. Maurice D. The effect of the low blink rate in rabbits on topical drug penetration. *J OculPharmacolTher*. 1995;11(1080-7683):297-304. doi:10.1089/jop.1995.11.297